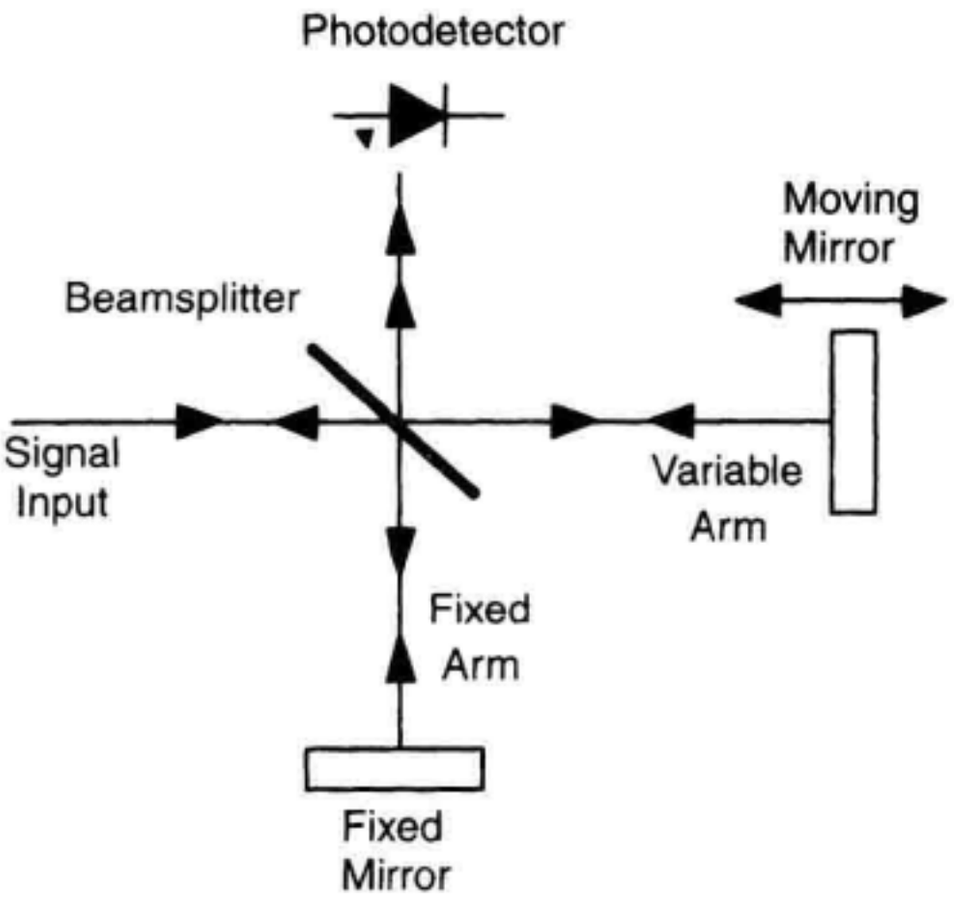

Figure 4.1 Block diagram of a Michelson interferometer.

terference effects between the two paths of the interferometer. Through the analysis of these interference patterns, the wavelength of light can be calculated. There are two alternate but equivalent viewpoints useful in analyzing the interferometer operation. The two beams can be analyzed in terms of light interfering as the path length in the interferometer changes. This will be referred to as the fringe-counting description of wavelength-meter operation. This approach will be discussed first in the next section. Alternately, if one arm of the interferometer is moved at a constant rate, the frequency of the light in the moving arm is Doppler-frequency shifted. The detector then mixes (see Chapter 5) the light from the Doppler-shifted and unshifted arms. The beat frequency between these two signals will be used to calculate the unknown frequency of the input signal.

4.2.1 Fringe-Counting Description of Wavelength Meter Operation

The light reflected from the two mirrors is interfered where it is combined at the detector. In order for interference to occur, the light from the two arms must overlap in space and be identical in polarization. As an example, assume that the light from the input beam has a well-defined input wavelength such as that from a DFB laser. The form for the photocurrent generated from the interferometer detector is:

$$I(\Delta L) = 1 + \cos((2\pi\Delta L)/\lambda_u) + \phi \tag{4.2}$$

where I is the photodetector photocurrent, ΔL is the optical path length difference between the two interferometer arms, λ_u is the unknown wavelength of the light in the medium of the interferometer, and ϕ is a phase-shift difference for equal path length delays between the two arms. Note that the path-length difference, ΔL, is twice the mirror-movement distance because of the double transit through each interferometer arm. This interference between two light beams coming from a signal source is called homodyne interferometry. Homodyne analysis is studied extensively in Chapter 5.

If the path-length difference, ΔL, is an integer multiple of the wavelength of light in the medium of the interferometer, the light will constructively interfere. All of the input light will be incident on the detector. If the path-length difference results in destructive interference at the photodetector, all of the light will go back out the input port.

In wavelength meter measurement operation, the position of the variable length arm is scanned. Figure 4.2a shows the scanned interferometer output measurements for a 1550 nm DFB laser. The result of a measurement of photocurrent versus mirror position will be referred to as an interferogram. The interferogram shows the detector signal alternating from dark to light as the variable position mirror is scanned. The plot of Figure 4.2a shows only a small segment of the interferogram over a 25 μm window. Figure 4.2b shows the optical spectrum for the same laser. For a narrow spectral width signal (10 MHz linewidth) such as the DFB shown in Figure 4.2b, the interference signal will remain strong for interferometer delays of many meters.

Figure 4.3a shows the interferogram measurement for a 1550 nm LED. Figure 4.3b shows the power versus wavelength for the 1550 nm LED as measured with a grating-based OSA. The interferograms for the LED and DFB are very different. Strong interference is found over a wide path-length difference range for the DFB of Figure 4.2. Interference patterns are found only near zero path-length difference for the LED. The difference between the two interferograms is caused by the difference in coherence properties of a source. For a DFB laser, the two signals arriving at the photodetector have a well-defined phase relationship resulting in a strong interference signal even for wide ranges of the variable mirror position. For the LED source, the phase relationship between the two signals starts to become random as the path-length difference increases. This randomness in the phase relationship is caused by the LED having a less well-defined wavelength due to the source's wide spectral width. For a broadband source with a Gaussian power versus wavelength distribution, the photocurrent interferogram function is given as:

$$I(\Delta L) = 1 + \exp^{-\left(\frac{\pi}{4\sqrt{2}}\left(\frac{4\Delta L\Delta\lambda_{pulse}}{\lambda^2-\Delta\lambda_{pulse}^2}\right)^2\right.}\cos\left(\frac{2\pi\Delta L}{\lambda}\right) \tag{4.3}$$

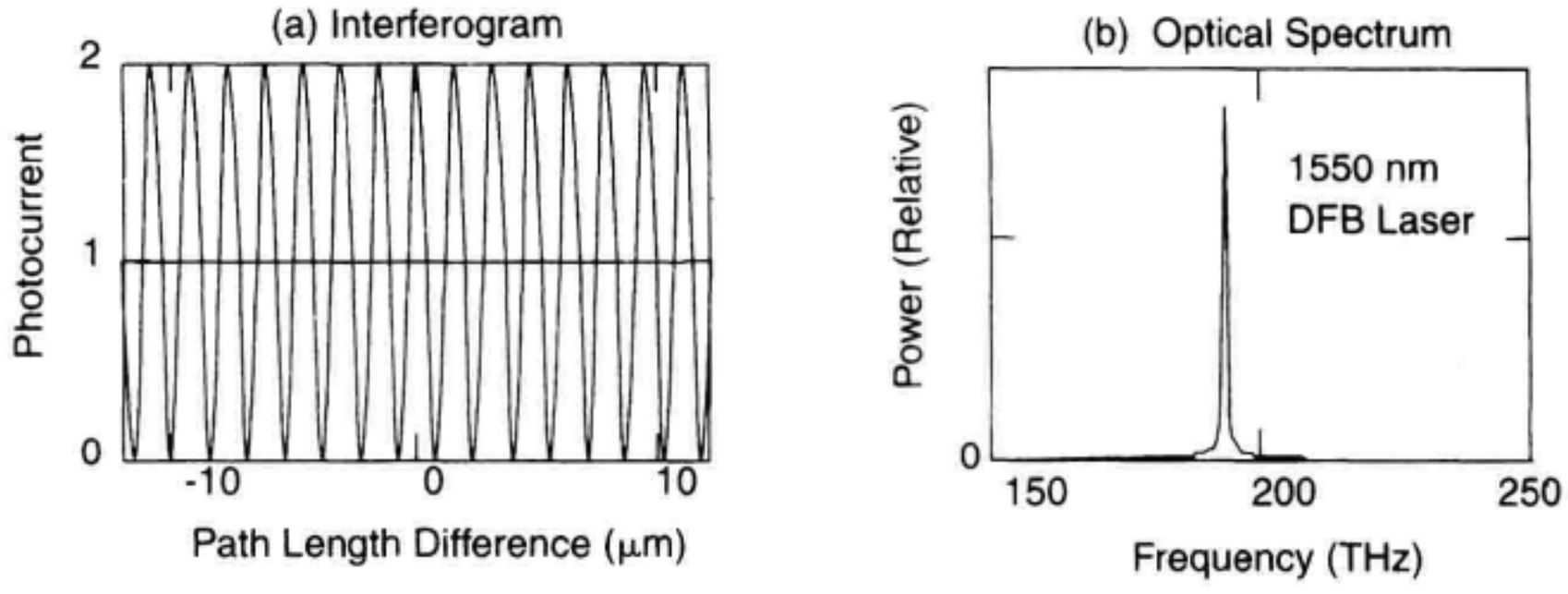

Figure 4.2 (a) Interferogram for a 1550 nm DFB laser. (b) Optical spectrum of the 1550 nm DFB laser.

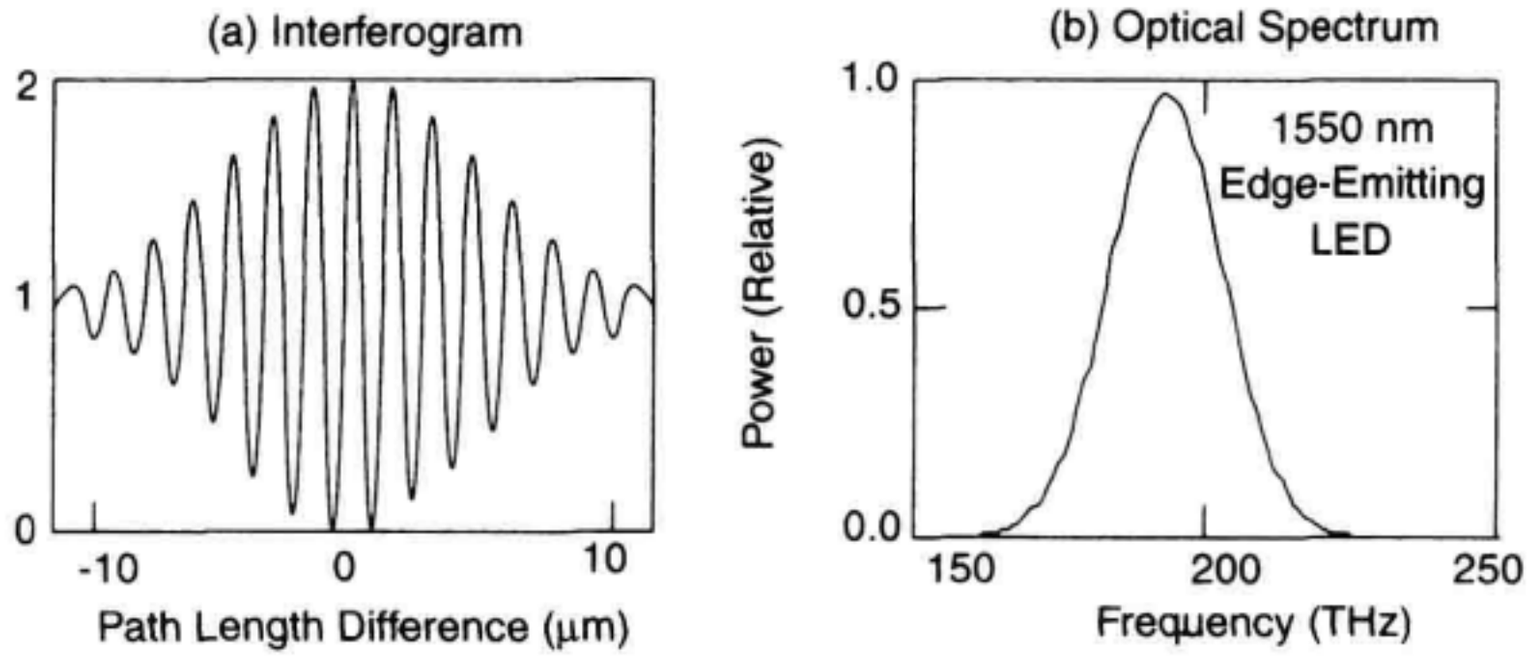

Figure 4.3 (a) Interferogram for a 1550 nm LED. (b) Optical spectrum of the 1550 nm LED.

where $\Delta\lambda_{pulse}$ is the spectral width of the LED at half power points, λ is the center wavelength of the LED, and ΔL is the optical path-length difference.

Figures 4.2 and 4.3 demonstrate that the Michelson interferometer can distinguish between wide and narrow spectral-width signals. The degree of complete constructive and destructive interference in the interferogram is referred to as fringe visibility. The fringe visibility becomes poor for the LED example of Figure 4.3 for path-length differences away from zero. The interferogram for the LED starts to reduce away from zero path-length delay because the phase fluctuations of the two delayed arms are uncorrelated for large path-length differences. Michelson interferometers with low coherence sources inputs can be used for high-resolution reflectometry (Chapter 10).

Let's take a moment to define some of the terminology associated with the spectral width of a signal. The terms linewidth, spectral width, coherence length, and coherence time all refer to the same basic property of a signal. The coherence length of a signal is directly measured in the interferogram examples of Figures 4.2 and 4.3. The coherence length, L_c, is defined as the distance where the coherence function drops to $1/e$ of its maximum value. There are several related functions to the coherence length. The coherence time, τ_C, is the time associated with propagating the coherence length distance.

$$\tau_C = \frac{L_c}{\text{velocity}} \tag{4.4}$$

The spectral width of a signal (full-width at half of maximum), $\delta f_{1/2}$ (in GHz), is also related to the coherence length and coherence time.

$$\delta f_{\frac{1}{2}} = \frac{1}{\pi\tau_C} \tag{4.5}$$

The DFB has a well-defined wavelength and therefore would be considered a highly coherent signal. The LED in contrast is more incoherent because it does not have nearly as well defined of center wavelength.

For the example of Figure 4.3, the LED would have an approximate coherence length of 16 μm, and a coherence time of 0.06 ps for a spectral width of 50 nm (6 THz). Let's contrast this to a DFB laser with an unmodulated linewidth of 10 MHz. The coherence length would be 10 meters and the coherence time would be 32 ns. It would not be practical to build a variable length arm into a Michelson interferometer to directly measure the coherence length of an unmodulated DFB laser.

Unknown Wavelength Calculation. Now that we have spent some time understanding how interferograms are formed in a Michelson-interferometer scan, it is time to see how this information can be used to measure the wavelength of the input signal. The principle of wavelength measurement is very simple. The distance between peaks in the interferograms of Figures 4.3 and 4.4 gives the wavelength. If the interferometer is in a vacuum, λ_{vac} is measured. If the interferometer is in air, λ_{air} is measured.

Let us first assume that one can measure the position of the movable mirror with perfect accuracy and therefore ΔL is a known variable. The measurement of wavelength is then found by moving the variable-length mirror a known amount of distance and then counting the number of interference fringes that appear at the detector. If the mirror movement distance is Δx, the path length change is $\Delta L = 2\Delta x$. The number of counted fringes in the length ΔL is N. The unknown wavelength in the medium of the interferometer, λ_u, will be:

$$\lambda_u = \left(\frac{\Delta L}{N}\right) \tag{4.6}$$

It is important to note that the unknown wavelength is the wavelength measured in the medium of the interferometer. If the interferometer is located in a vacuum, the parameter, λ_u, will be the vacuum wavelength. If the interferometer is located in an air environment, λ_u will be the wavelength for that particular air environment. On first assumption, one can assume that the index of refraction of air is 1.00027. The index of refraction of air will be examined in detail in Section 4.4.2.

So far two limitations have been introduced to the measurement of wavelength:

1. The position of the mirror must be known very accurately.
2. The index of refraction of the interferometer environment has to be known accurately.

These limitations will be addressed in sections 4.2.3 and 4.2.4. Before going on to these discussions, it is useful to view the operation of the interferometer from a Doppler-shift point of view.

4.2.2 Doppler-Shift Approach to Understanding Wavelength Meter Operation

In this approach let us assume that the adjustable mirror is moved at a constant velocity through the zero path-length difference position. The moving mirror will cause a Doppler frequency shift on the light in the moving arm. The Doppler frequency shift will be:

$$\Delta f = (2v_m f_0/(v_i)). \tag{4.7}$$

where Δf is the Doppler frequency shift, v_m is the mirror velocity, f_u is the optical frequency of the signal, and v_i is the speed of light in the medium of the interferometer. What might be a typical Doppler frequency shift? For a mirror velocity of 1.5 m/s and a center frequency of 193.5 THz, (1550 nm light), the Doppler frequency shift would be 1.93 MHz.

The light incident on the photodetector is of two slightly different center frequencies in the moving interferometer case studied here. The detector will measure the beat frequency between the fixed and moving arm paths. If the detector is measuring the beat-frequency signal for the time period, T, the number of zero crossings, N, measured during the period, T, will be:

$$N = \Delta f T \tag{4.8}$$

The unknown frequency of the input signal can then be measured as:

$$f_0 = (v_i N/(2v_m T)) \tag{4.9}$$

In this measurement, accurate knowledge of mirror velocity and a time period are required. This is equivalent to knowing the total distance moved as is analyzed in the fringe-counting method since velocity multiplied by time gives a total distance.

4.2.3 Accurate Measurement of Distance, Velocity, and Time

In Section 4.2.1, it was shown that it is critical to have accurate position measurements of the moveable mirror. One must either know the absolute mirror position accurately, or know the velocity and sample period accurately.

It is interesting to note that Michelson interferometers are often used as accurate distance-measurement tools. If the wavelength of the input laser, λ_{known}, is already a well-known number, Equation 4.4 can be rewritten so that distance is the quantity being measured.

$$\Delta L = \lambda_{known} N \tag{4.10}$$

The key to accurate wavelength measurement therefore is to include a very accurate laser reference in the same interferometer as the unknown input. Figure 4.4 shows a wavelength meter that uses the Michelson interferometer with two input beams. One interferometer uses a well-known laser wavelength standard at its input to measure the mirror motion accurately. The other path measures the interferogram of the unknown input. The implementation shown in Figure 4.4 has the known and unknown signals making equivalent but noncoincident paths through the interferometer. Alternately, the two beams are placed coincident to each other with dichroic (wavelength-separating) filters used to separate the reference and unknown signals at the detector. By comparing the outputs of the reference photodetector and the unknown photodetector, very accurate wavelength

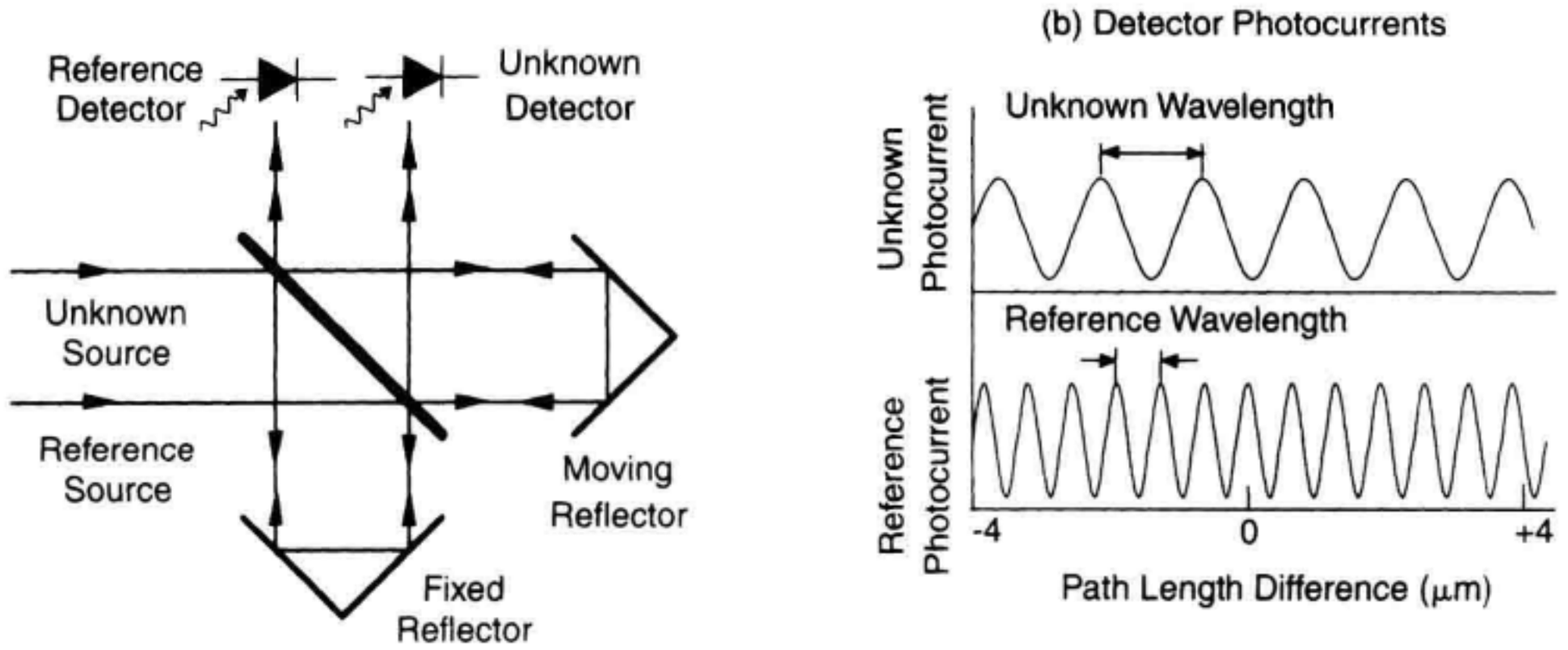

Figure 4.4 (a) Michelson interferometer with an added wavelength reference input added. (b) Example photocurrent values versus optical path length difference.

measurements can be made. An analysis of the interferometer with the laser wavelength standard will now be made.

4.2.4 Wavelength Measurement with Respect to a Wavelength Standard

The interferogram of the unknown signal is compared to that of the known standard. If the mirror is moved over a specified scan length, the interference fringes in both the reference and unknown arms are counted. The wavelength of the unknown signal can then be calculated by comparing the fringe counts in the unknown and the reference signal paths and taking the ratio of counts.

$$\lambda_u = (N_r/N_u)(n_u/n_r)\lambda_r \tag{4.11}$$

where λ_u is the unknown wavelength, λ_r, is the reference wavelength, n_r is the index of refraction at the reference wavelength, n_u is the index of refraction at the unknown wavelength, N_r is the number of reference counts over a distance L, and N_u is the number of unknown wavelength detector counts over distance L. The equation requires that an accurate ratio of the index of refraction at the reference wavelength to the index at the unknown wavelength be known. Section 4.4.2 explores how accurately this ratio can be determined for an air environment interferometer. It is this relationship between the fringe counting at the reference frequency and the unknown frequency that allows accurate wavelength measurements. Figure 4.4b shows an example of the photocurrents that are measured in the reference arm and the unknown arms for a reference wavelength of 633 nm and an unknown arm wavelength of 1550 nm. Equation 4.11 compares the interferogram period of the two signals and takes into account the index of refraction at both the reference and the unknown wavelengths.

4.2.5 Summary of Michelson-Interferometer Wavelength-Meter Operation

1. The reference laser and the unknown laser signals must take identical path lengths for the measurement to be valid. In the case of Figure 4.4, the lasers do take identical path lengths, but in opposite directions. The alignment of the optics to make these two paths identical will affect wavelength meter accuracy.
2. The accuracy of the measurement is limited by the wavelength accuracy of the reference laser. Section 4.4.3 addresses this question.
3. It is important to know the ratio of the index of refraction between the measurement wavelength and the known wavelength. The absolute index of refraction is not needed, just the ratio. Section 4.4.2 shows that the index-of-refraction ratio is relatively independent of air temperature, pressure, and humidity if some simple corrections are made.
4. The coherence of a source affects the shape of the interferogram. Wide spectral-width sources show interference only over a narrow range of path-length differences in the interferometer.

This section has dealt exclusively with analyzing situations where a single optical source is connected to the measurement instrument. It will be shown that simple fringe counting is of limited usefulness if many different input wavelengths are present simultaneously. The following section will show that by using Fourier transform techniques, multiple signal environments can also be characterized with a Michelson interferometer.

4.3 WAVELENGTH METERS IN MULTIPLE SIGNAL ENVIRONMENTS

Figure 4.2 shows the interferogram that results when a single wavelength signal is applied to a Michelson interferometer. What happens if two or more separate laser sources are combined together into the wavelength meter input? This situation is very common since WDM systems are installed for telecommunications. Figure 4.5 shows the interferogram

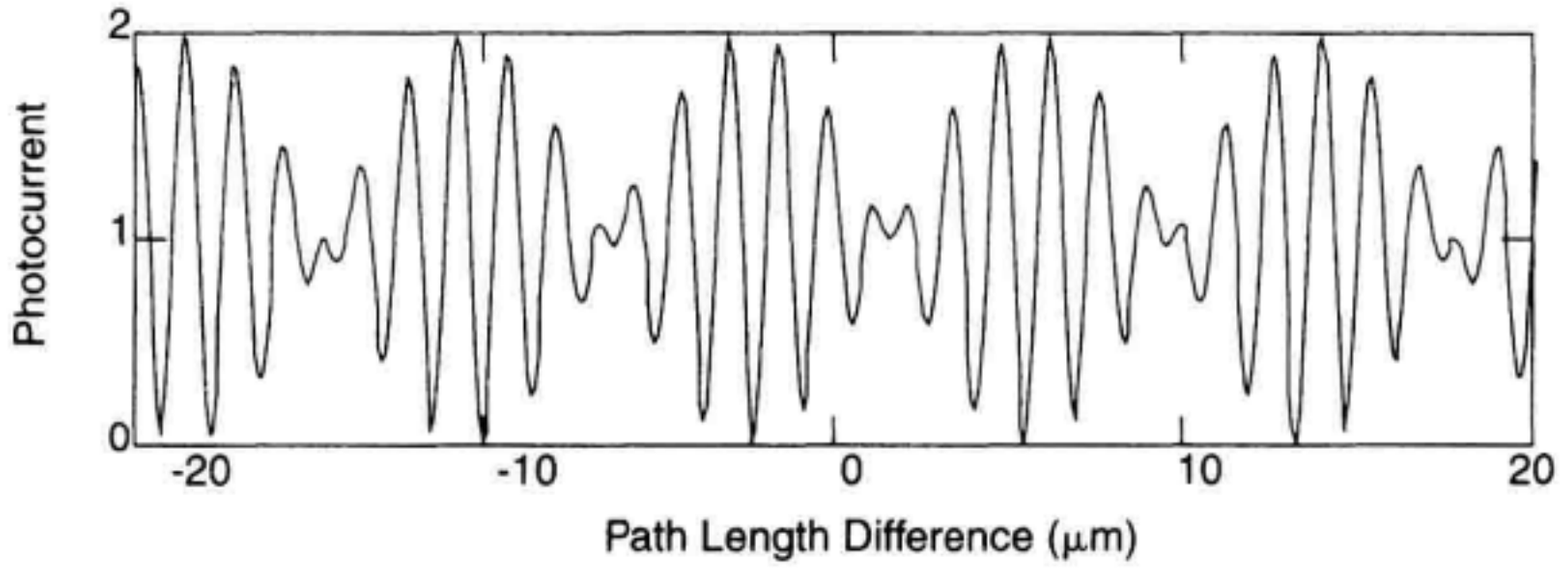

Figure 4.5 The input signal for this interferogram includes a DFB laser at 1300 nm and 1550 nm with equal powers.

that results when 1300 nm and 1550 nm sources are combined and applied to a Michelson-interferometer wavelength meter. The interferogram does not show the regular period of Figure 4.2. In some portions of the interferogram, the interference signal amplitude is also very small. With the simple fringe-counting methods of Section 4.2, it would be difficult to correctly calculate the wavelength of the input signal. The algorithm of Equation 4.11 would produce an average wavelength value between 1300 nm and 1550 nm. This example illustrates the limitation of fringe-counting wavelength meters. With a little more complicated analysis involving Fourier transforms, it will be found that one can display the power versus wavelength for multiple signal environments.

Figure 4.6 illustrates the operation of a Fourier-transform Michelson-interferometer wavelength meter.[5,6] Figure 4.6a shows the interferogram result for an input signal containing a 1300, 1550, and 1650 nm laser with equal powers. This complicated interferogram can be thought of as the sum of three separate interferograms similar to that of Figure 4.2. The single wavelength interferograms of the individual 1300, 1550, and 1650 nm lasers add to produce the complicated pattern of Figure 4.6a.

Let us consider what would result if a Fourier-transform operation were done on the photocurrent versus distance function that makes up the interferogram of Figure 4.6a. The Fourier transform will produce a plot of the photocurrent magnitude versus spatial fre-

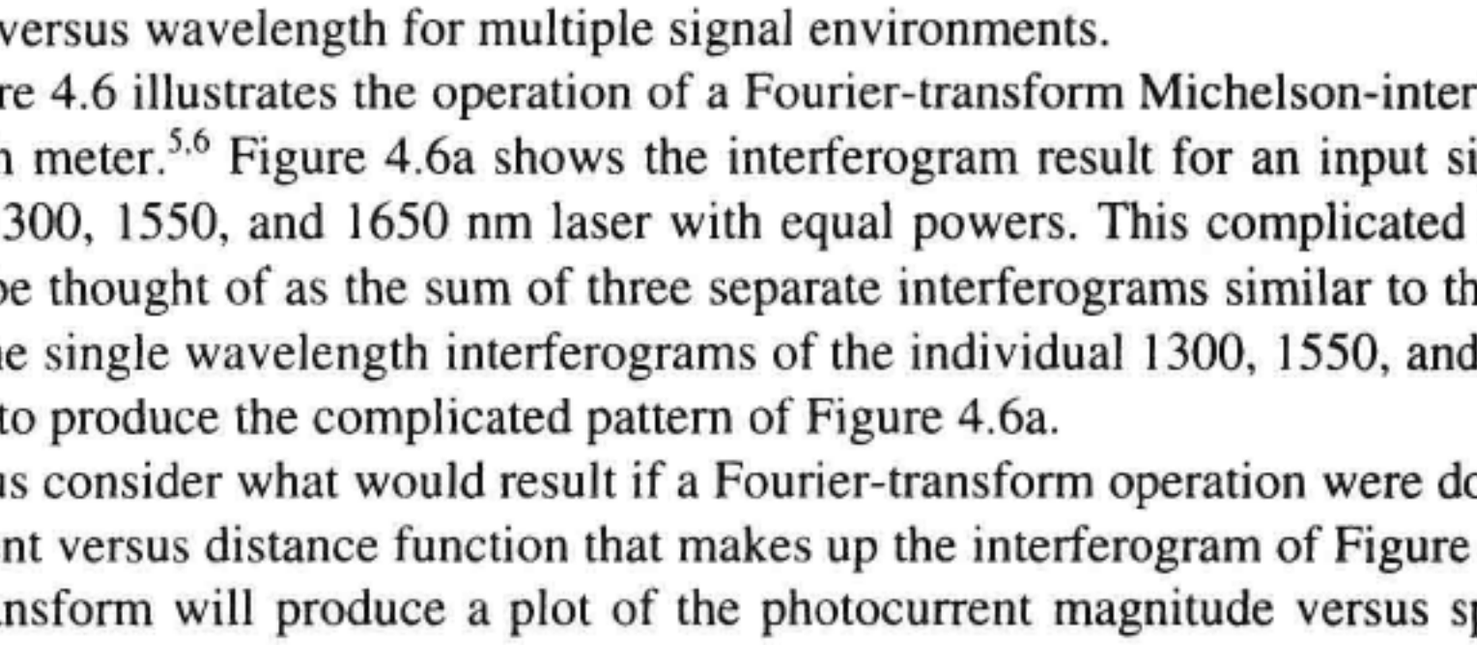

Figure 4.6 (a) The interferogram for a combined 1300, 1550, and 1650 nm signal with equal power. (b) Results of a Fourier transform operation on the interferogram data.

quency, σ (measured in cycles per meter), of the interferogram. Figure 4.6b illustrates the results of performing a Fourier-transform operation on the data of Figure 4.6a. The temporal frequency shown in the plot (cycles per second) is obtained by multiplying by the speed of light in the medium. The Fourier-transform operation on the interferogram allows the wavelength of the signals to be separated and measured individually. Here each of the input signals is individually resolved both in frequency and in power. The Fourier-transform operation does not compromise the wavelength accuracy of the measurement when compared to fringe-counting methods.

In performing the Fourier transform of the data presented in Figure 4.6a, the unknown signal interferogram is sampled at regular distance intervals. The distance spacing between interferogram samples controls the maximum spatial frequency that can be displayed in the result. Using the Nyquist sampling theorem, the maximum spatial frequency that can be measured without aliasing effects is

$$\sigma_{max} = \frac{1}{2\,(\text{distance between samples in the interferogram})} \tag{4.12}$$

Here σ_{max} is the maximum spatial frequency in cycles per meter. Spatial frequency is also referred to as the wavenumber. The maximum temporal frequency of the signal is found by multiplying Equation 4.12 by the speed of light for the interferometer. A convenient sampling interval for the system is the zero crossings of the reference photocurrent. Figure 4.7 illustrates the general method used to process the interferogram data by Fourier techniques.

The discrete Fourier-transform operation on the interferogram data will produce discrete data points in the frequency domain that have a frequency step related to the total interferogram scan distance. The spacing between these frequency points is

$$\sigma_{step} = \frac{1}{\text{total distance of the interferogram}} \tag{4.13}$$

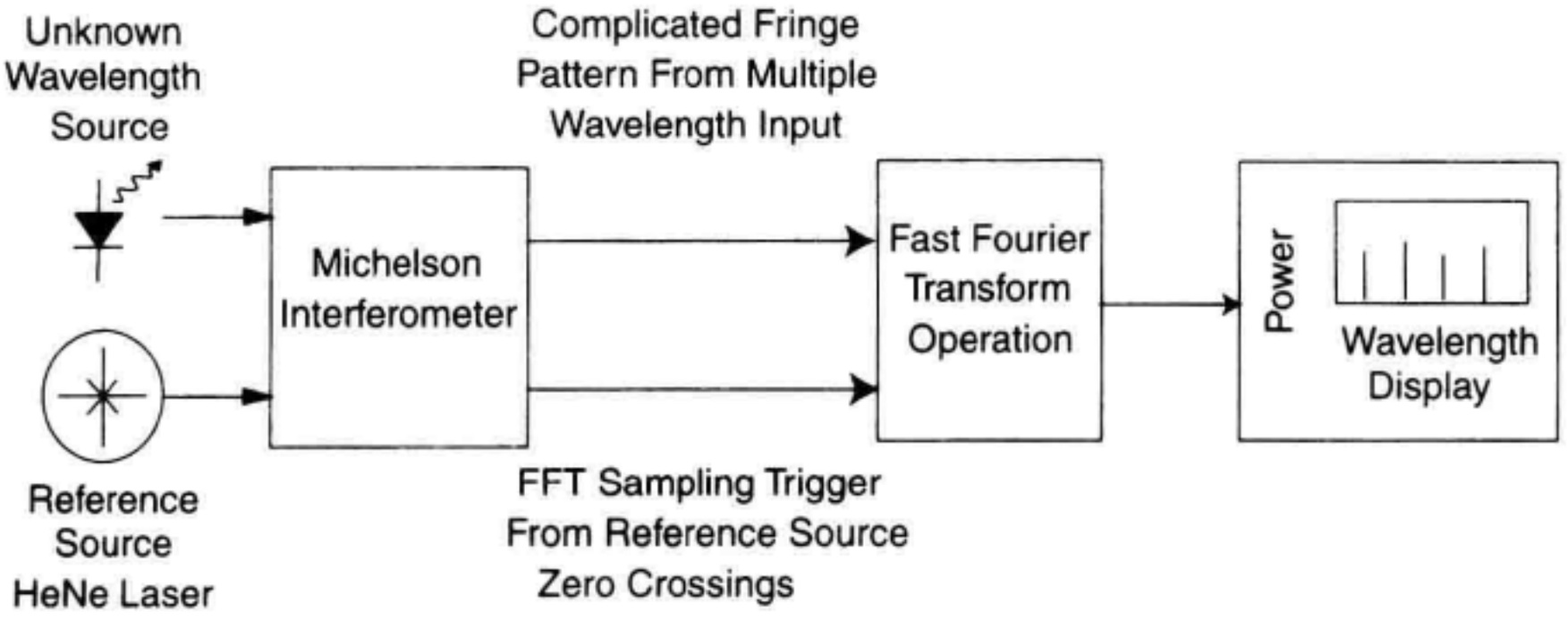

Figure 4.7 The signal processing block diagram of a Fourier-transform wavelength meter.

The temporal frequency step of the signal is found by multiplying Equation 4.13 by the speed of light for the interferometer. For maximum wavelength resolution, it is important to have a small Fourier-transform frequency step. Long interferogram distances are desirable to obtain good wavelength resolution. For ease of processing, the interferometer trace is broken up into 2^n data points so that efficient fast-Fourier-transform algorithms can be used. The raw interferogram data of Figure 4.6a is often multiplied by a windowing function so that the data does not abruptly terminate at the ends of the scan. Abrupt termination of the interferogram data would result in ringing and the introduction of spurious signals in the Fourier transform domain. Specialized digital signal processor chips can be used to accomplish fast-Fourier-transforms quickly. With Fourier-transform capability, the Michelson-interferometer wavelength-meter provides a display very similar to the grating-based OSAs discussed in Chapter 3.

An example calculation is given here to illustrate the use of the equations above. Assume that a helium-neon ($\lambda = 0.633$ μm) reference laser was used and samples were taken at every zero crossing of the HeNe fringe. The maximum frequency that can be displayed without aliasing effects would be 475 THz based on the Nyquist theorem which requires two samples per period at the maximum desired frequency (Equation 4.12). This frequency range is adequate for operation in the fiber-optic communication bands. For a ±30 mm sweep range, the frequency spacing of the data points in the Fourier domain will be 5 GHz (Equation 4.11). The resolution of the system is defined as two Fourier transform data point intervals or in this case 10 GHz. Frequency resolution of 10 GHz is adequate for WDM communication systems spaced at 100 GHz.

Fourier transform wavelength meters are very useful for WDM communication system measurements. Figure 4.8 shows an example measurement of a four-channel WDM source using a Fourier-transform wavelength meter. The frequency spacing between lasers in this example is 100 GHz on average. The Fourier-transform wavelength meter provides accurate measurement of the wavelength, power, and signal-to-noise ratio for WDM communication systems.

4.4 ABSOLUTE WAVELENGTH ACCURACY CONSIDERATIONS FOR MICHELSON-INTERFEROMETER WAVELENGTH METERS

Here are some of the important variables that influence wavelength meter accuracy.

1. Maximum path-length change in the variable arm of the interferometer. The longer the interforometer path-length difference, the better the accuracy. Related to this subject is the ability to count fractional fringes. If one has to round to the nearest integer number of interference fringes and throw away the remainder, valuable wavelength information is being thrown away. There are innovative ways to count down to a fraction of a fringe.
2. Knowledge of the ratio of the index of refraction at the reference wavelength to the index of refraction at the unknown wavelength. The index of refraction in air is a function of humidity, temperature, gas content, etc. How big of an error would re-

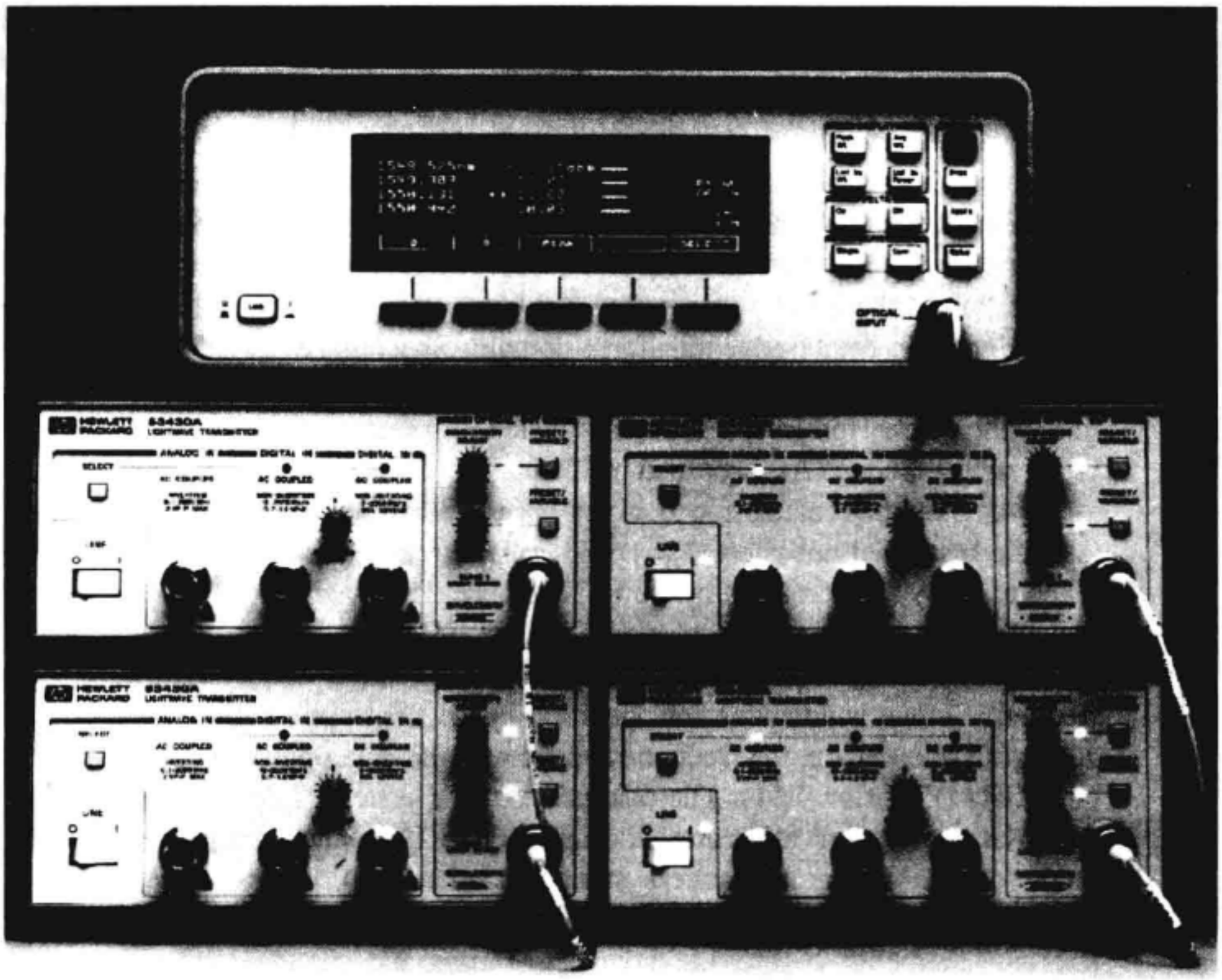

Figure 4.8 A wavelength meter measurement of 4 DFB lasers sources located on the 100 GHz spacing dense WDM grid.

sult if this were ignored? Should one immerse the interferometer in a known environment (nitrogen or a vacuum)?

3. The wavelength accuracy of the reference source will ultimately limit the accuracy of the measurement of the unknown.

4.4.1 The Ability to Count Many Fringes and to Count Them Accurately

The simple wavelength meter as described in Section 4.2 counts the number of fringes that occur in a given path length for both the unknown signal and the reference signal. In order to get accurate wavelength measurements, it is desirable to make a very long path-length difference interferometer to maximize the number of fringe counts. Long sweep distances require increased measurement time. From Equation 4.11, the calculation of an unknown wavelength involves ratioing the fringe counts at the reference wavelength to fringe counts at the unknown wavelength. An entire mirror sweep will probably not result in an integer number of interference fringes at both the reference and unknown wavelengths. Rounding to the nearest integer will degrade measurement accuracy.

It is common to use electronic zero-crossing counters to measure the number of fringes at both the signal and reference wavelengths. In this implementation of a wavelength meter, the fraction of a fringe found at the beginning and end of sweep will be ignored. If this fractional fringe information is not used, the accuracy of the interferometer measurement will be degraded. Here is an example of the magnitude of error for dropping fractional fringes. An interferometer is scanned over a 3 cm range with an input wavelength of exactly 1550 nm; 38709.68 fringes should be counted. If the 0.68 fringe fraction is not counted, the wavelength meter would measure 1550.027 nm. This represents a 17.4 ppm error which is unacceptable for many applications. Improved accuracy can be obtained by increasing the scanning distance or devising methods for fractional fringe counting. In modern wavelength meter designs, methods of fractional fringe counting have led to dramatic improvements in accuracy. Figure 4.9 illustrates a frequency multiplying method of fractional fringe counting. If the variable length arm of the interferometer is scanned at a uniform rate, the output from the detector will be a sinusoidal signal. This signal is then multiplied by a nonlinear electronic circuit to a harmonic of the input frequency. Frequency multiplication up to 100 times has been achieved.[7–9] The multiplied signal is then counted with an electronic counter. If a 10 times multiplication is used, an effective fringe resolution of 1/10 of the unmultiplied fringe period is achieved. Other methods use phase-locked loop techniques for locking a higher frequency oscillator to the output of the detector.

Folding of the optical path allows the path-length difference to be increased for a given mirror motion.[1] This allows for a more compact optical design and increased measurement accuracy.

4.4.2 Index of Refraction and Dispersion of Air

Equation 4.11 showed that the ratio of the index of refraction at the unknown signal wavelength to the index at the reference wavelength is important for accurate wavelength measurements. The wavelength of a signal in air can be appreciably different from the

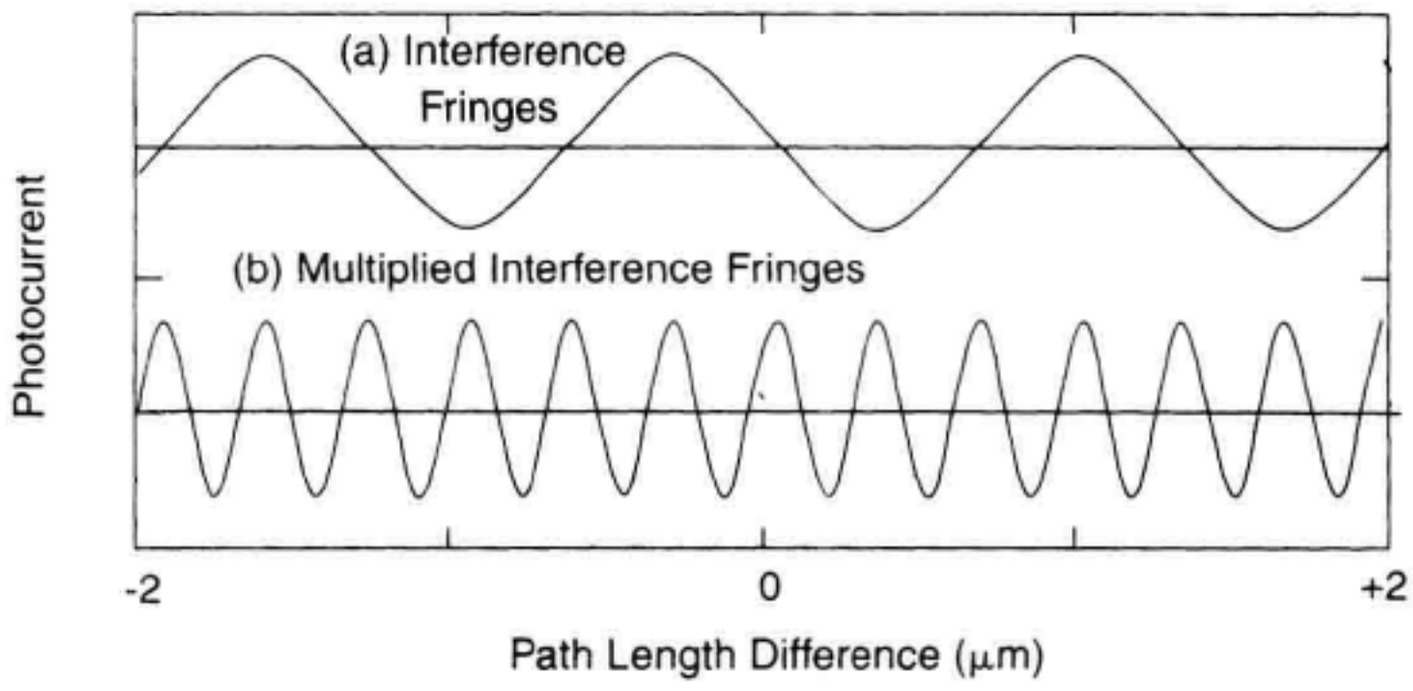

Figure 4.9 The fringe counting capability of a wavelength meter can be increased by using fractional fringe counting techniques: (a) raw photocurrent signal. (b) photocurrent signal multiplied by 4.

index of refraction in a vacuum. Recall that the wavelength in a vacuum and the wavelength in air are related by the equation

$$\lambda_{vac} = n_{air}\lambda_{air} \tag{4.14}$$

where λ_{vac} is the vacuum wavelength and λ_{air} is the wavelength in air, and n_{air} is the index of refraction of air. Michelson interferometers most often make measurements in an air environment. Because of the variability in the index of refraction of air with respect to environmental conditions, it is important to have a set of standard conditions that can be used to clearly state the wavelength. The two most common ways of stating wavelength are the wavelength in a vacuum and the wavelength in standard dry air. The wavelength in a vacuum is self-explanatory. Standard dry air is defined to have pressure of 760 Torr and temperature of 15 C and no water vapor. The index of refraction of air has been extensively studied and accurate models have been developed.[10,11] The use of these models in wavelength meter calculations can improve the accuracy of the wavelength measurement. The index of refraction is a function of temperature, pressure, and gas composition. A useful result is given by Edlen.[10] The wavelength dependence of the index of refraction for standard dry air is given as:

$$n_s = 1 + 10^{-8}\left(8342.13 + \frac{2406030}{130 - \frac{1}{\lambda^2}} + \frac{15997}{38.9 - \frac{1}{\lambda^2}}\right). \tag{4.15}$$

Here the wavelength, λ, is in microns. Figure 4.10 shows a plot of how the index of refraction depends on wavelength for the standard dry-air conditions.

A number to remember is 1.000273 for the telecommunication wavelength areas near 1300 nm and 1550 nm. Equation 4.15 can be corrected for temperature and pressure using the following correction equation:

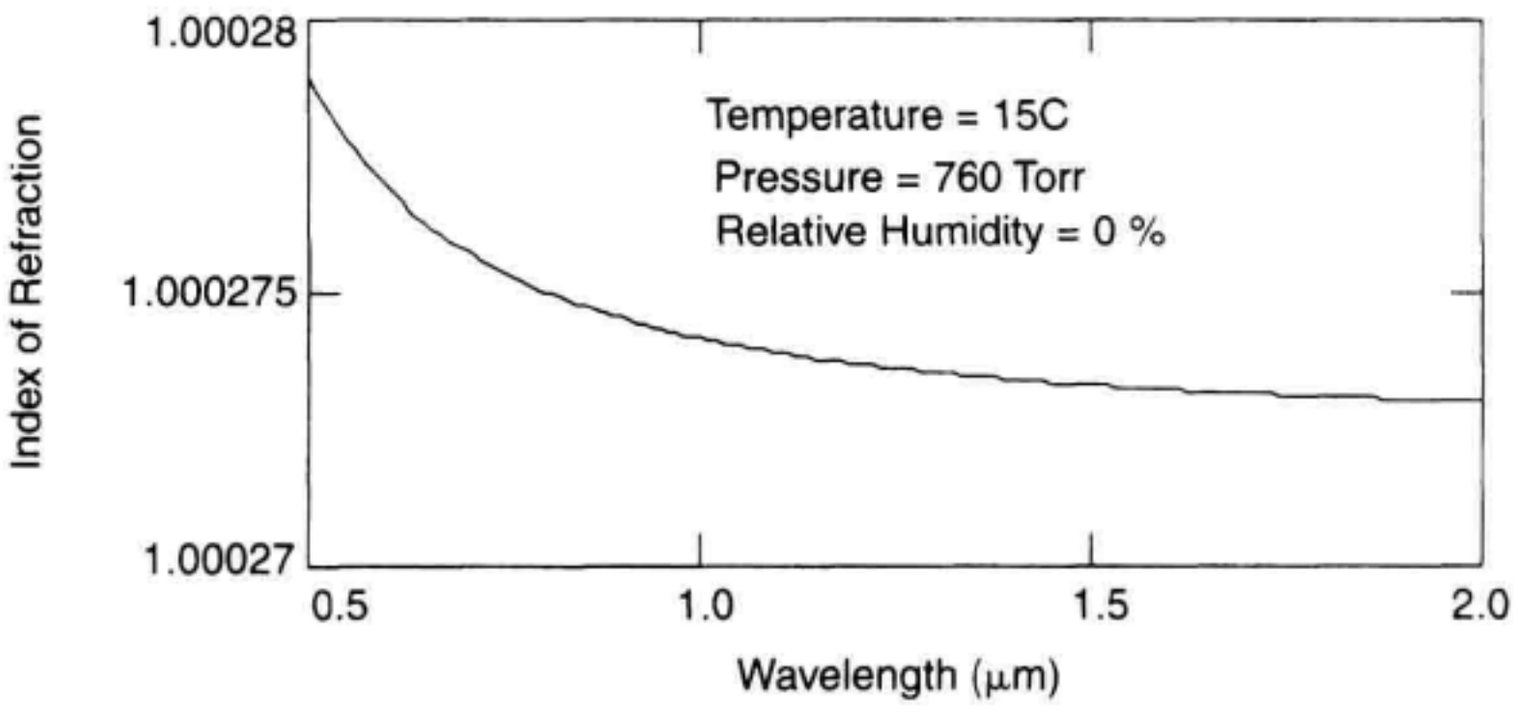

Figure 4.10 The index of refraction versus wavelength for standard dry air.

$$n(T, P) = 1 + \frac{(n_s - 1)(0.00138823)P}{1 + (0.003671)T} \tag{4.16}$$

Here pressure, P, is in Torr and temperature, T, is in Celcius. A further correction can be made to the index for water vapor content in the air.

$$n(T, P, h) = n(T, P) - h^*\left(5.722 - \frac{0.0457}{\lambda^2}\right) 10^{-8} \tag{4.17}$$

Here h is the partial pressure of water vapor in Torr. Equation 4.17 is most accurate for visible light with degraded accuracy at infrared wavelengths. A more everyday measure of water vapor content is relative humidity. The partial water vapor pressure for a 100% relative-humidity day would be approximately 4.3 Torr, 22.6 Torr, and 112 Torr for a temperature of 0, 25, and 55C respectively.

It is useful to see how the index of refraction varies as a function of the three most common variables: pressure, temperature, and humidity. Figure 4.11a shows how the index of refraction changes as a function of wavelength for three values of temperature.

Figure 4.11b, c, and d show variability of the index of refraction at the wavelength of 1550 nm. Figure 4.11b shows a plot of the index versus temperature with 760 Torr pressure and 0% relative humidity. Figure 4.11c shows a plot of index versus pressure with 25C temperature, and 0% relative humidity. Figure 4.11d shows a plot of index versus relative humidity with 25C temperature and pressure of 760 Torr. From these three graphs, it is seen that pressure variations have the largest effect on the index of refraction for reasonable values of the environmental variables. The average atmospheric pressure can vary from 760 Torr at sea level down to 400 Torr at a height of 5000 m.

It is fortunate that the Michelson-interferometer wavelength-meter measurement does not directly depend on absolute value of the index of refraction in air. The only important parameter is how the ratio of indexes at the reference and unknown wavelengths changes with respect to an atmospheric variable of air (see Equation 4.11). The ratio of the index of refraction at the reference and unknown wavelengths is quite insensitive to atmospheric variables. The conditions that tend to raise the index of refraction at the unknown wavelength also raise the index of refraction at the known wavelength, keeping the ratio very constant. Figure 4.12a shows the index of refraction at 633 nm and 1550 nm as a function of temperature. The two curves track each other very closely.

Figure 4.12b shows how the ratio of the index of refraction between 0.633 (HeNe reference laser) and 1.55 μm (unknown signal wavelength) changes versus temperature with a 760 Torr pressure and 0% relative humidity. It may be possible for a wavelength meter to be exposed to temperatures as low as –40C and as high as 45C in an outdoor environment. This temperature-range excursion would cause the ratio of the index of refractions to change by up to 1 ppm. For laboratory or manufacturing environments where the temperature excursions may only be ±10C, temperature corrections would probably not be necessary. For outdoor measurements in extreme conditions, temperature will affect accuracy.

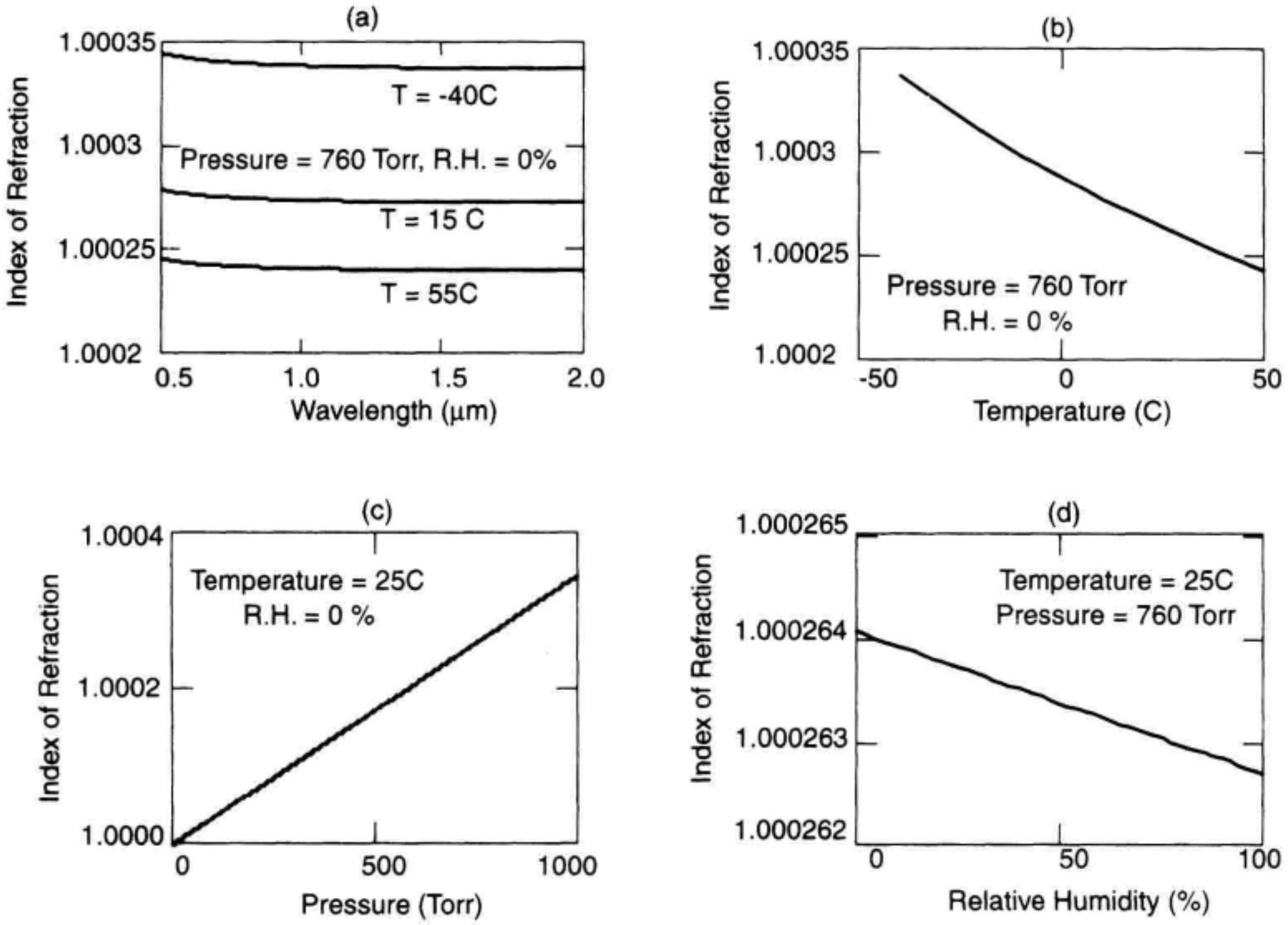

Figure 4.11 (a) The index of refraction as a function of wavelength for 3 different temperatures. (b) Index of refraction as a function of temperature at 1550 nm. (c) Index of refraction as a function of pressure at 1550 nm. (d) Index of refraction as a function of relative humidity at 1550 nm.

Figure 4.12c shows how the ratio of the index of refraction between 0.633 μm to that at 1.55 μm changes versus pressure with a 25C temperature and 0% relative humidity. For a Michelson interferometer in an air environment, a worst case comparison would be to compare a result on top of a 5000 m mountain at a pressure of 400 Torr with that at sea level of 760 Torr. This condition would give a wavelength measurement error of up to 2 ppm. This factor is large enough so that many wavelength meters allow entry of the instrument's air pressure conditions.

Figure 4.12d shows how the ratio of the index of refraction between 0.632 and 1.55 μm changes versus relative humidity with the temperature at 25C and pressure held constant at 760 Torr. In going from 0 to 100% humidity, the ratio changes by only 0.02 ppm. The error will increase for higher temperatures since the water holding content of air increases rapidly with temperature. In general, the effects of humidity may be neglected except that it would be convenient to keep water from condensing on the interferometer optics!

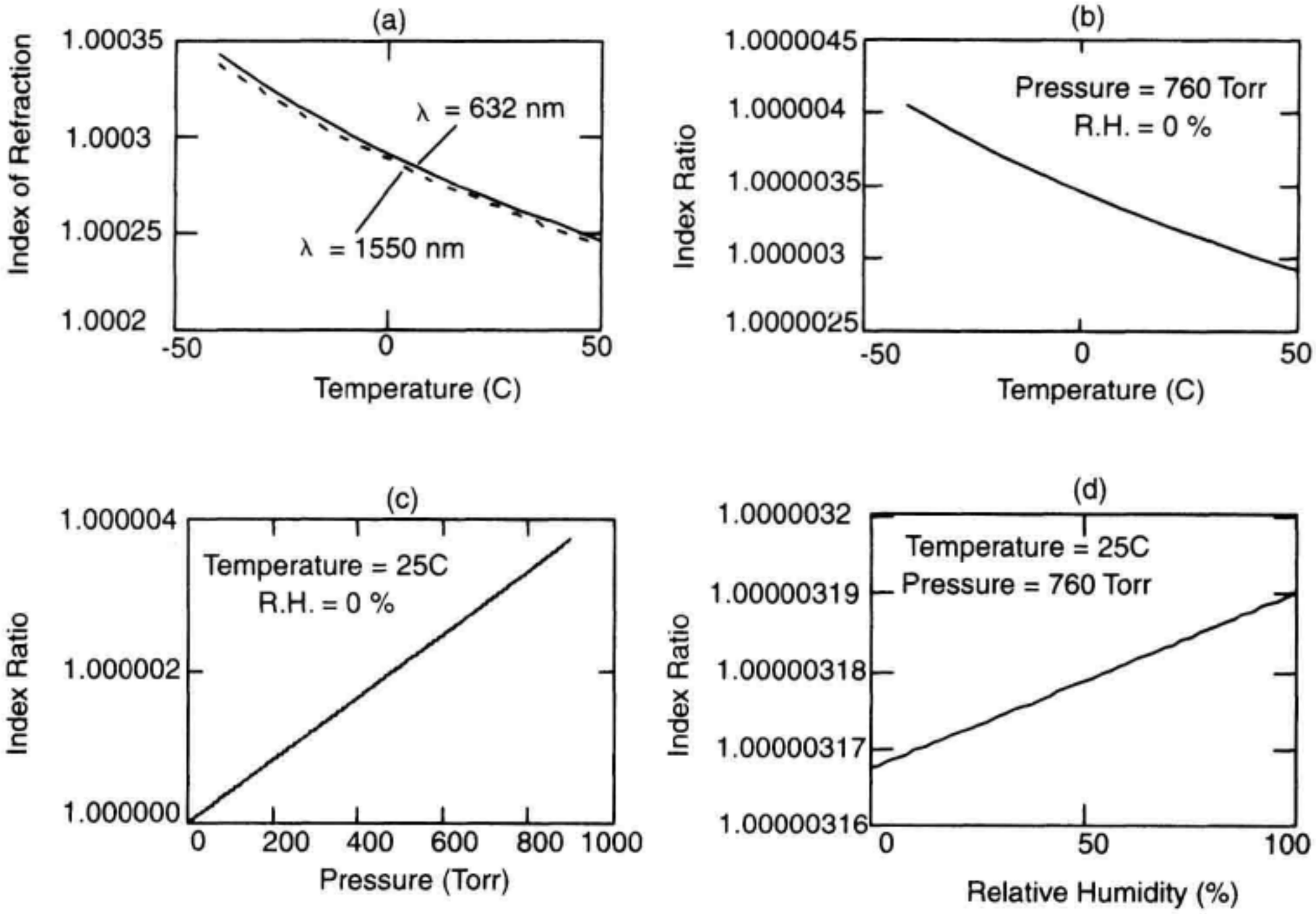

Figure 4.12 (a) Index of refraction as a function of temperature for two different wavelengths. (b) 632 to 1550 nm refractive index ratio as a function of temperature. (c) 632 to 1550 nm refractive index ratio as a function of pressure. (d) 632 to 1550 nm refractive index ratio as a function of relative humidity.

A formula that has been used successfully to take into account the effects of the ratio of the index of refraction on pressure conditions is as follows.

$$f_u = f_{\text{vacuum}}\left[1 + \left(\frac{n_r}{n_u} - 1\right)\left(1 - \frac{\text{Elevation in m}}{500}\right)(0.05)\right] \tag{4.18}$$

where n_r is the index of refraction at the reference wavelength and n_u is the index of refraction at the unknown wavelength. This model only takes into account pressure variations and ignores effects of temperature and humidity. The term $(n_r/n_u - 1)$ is put into memory in tabular form. The second term corrects for elevation dependence of the ratio.

With accurate knowledge of the effects of the index of refraction of air on the measurement, extremely accurate wavelength meter measurements can be made without the use of built-in atmospheric monitoring sensors or by immersing the interferometer in a vacuum chamber. When temperature and pressure are corrected for, environmental effects on the index of refraction limit wavelength accuracy only by several tenths of a part per million.

Table 4.1 Reference Laser Data

Parameter	Wavelength (nm)	Frequency (THz)	Wavenumber cm^{-1}
Helium-Neon	632.99076(2)	473.612692(12)	15798.0189(4)
Helium-Neon	730.6805(11)	410.289572(60)	13685.7870(20)
Helium-Neon	1152.59050(13)	260.103184(30)	8676.1083(10)
Helium-Neon	1523.48761(19)	196.780372(25)	6563.8867(8)
DFB Laser (semiconductor)	800–1600	187–1600	6250–12500

4.4.3 Accuracy of the Reference-Laser Wavelength

Table 4.1 lists several possible choices for a reference laser.[12–15] The numbers listed in parentheses are the standard deviation uncertainties in the last digits of the quoted value. The quoted wavelength values are for lasers set to the center of their gain versus wavelength curve. The actual laser design can reduce reference laser accuracy. The speed of light is taken as $2.99792458(1) \times 10^8$ m/s in these conversions. Helium-Neon (HeNe) gas lasers are the most common choice for reference lasers. There are several choices of wavelength, but the 633 nm line is the most common. It is also very useful that HeNe lines are available in the infrared spectrum to check accuracies of wavelength meters. HeNe tubes have a finite lifetime on the order of 30,000 h of continuous usage. The internal filaments deposit metal on the output mirrors causing the reflectivity to drop, eventually stopping the lasing. The DFB laser example provides a flexible alternative that would allow laser lifetimes approaching 10^6 h. If the wavelength stability of the DFB is accurately characterized, it should be an acceptable laser reference for a telecommunications application wavelength meter. Alternately, the semiconductor laser can be locked to other frequency standards to maintain long-term stability.[15]

633 nm HeNe Laser Wavelength Accuracy. The accuracy of the reference laser wavelength depends on laser construction and on knowledge of some of the details of the energy levels in the laser. The gain versus wavelength of the HeNe line has a center-vacuum wavelength of 632.99076 nm. The Doppler-broadened gain versus wavelength function for the HeNe-optical amplifier has a spectral width of 1.5 GHz.

A major consideration for a HeNe laser reference is how close the laser emits to the center of the gain versus wavelength curve. This situation is given pictorially in Figure 4.13. The length of a typical compact FP resonator for a HeNe laser is typically 15 cm. This means that the longitudinal mode spacing (0.5 × velocity/laser length) of the laser will be approximately 1 GHz. Figure 4.13 shows an example situation of the location of the longitudinal modes with respect to the peak of the gain curve. The accuracy of the source for wavelength-meter applications depends on the power-weighted average of the longitudinal mode wavelength locations. The best possible situation would occur if the longitudinal modes are placed symmetrically around the gain center. In the worst case alignment, the average wavelength would be off by half of the longitudinal mode

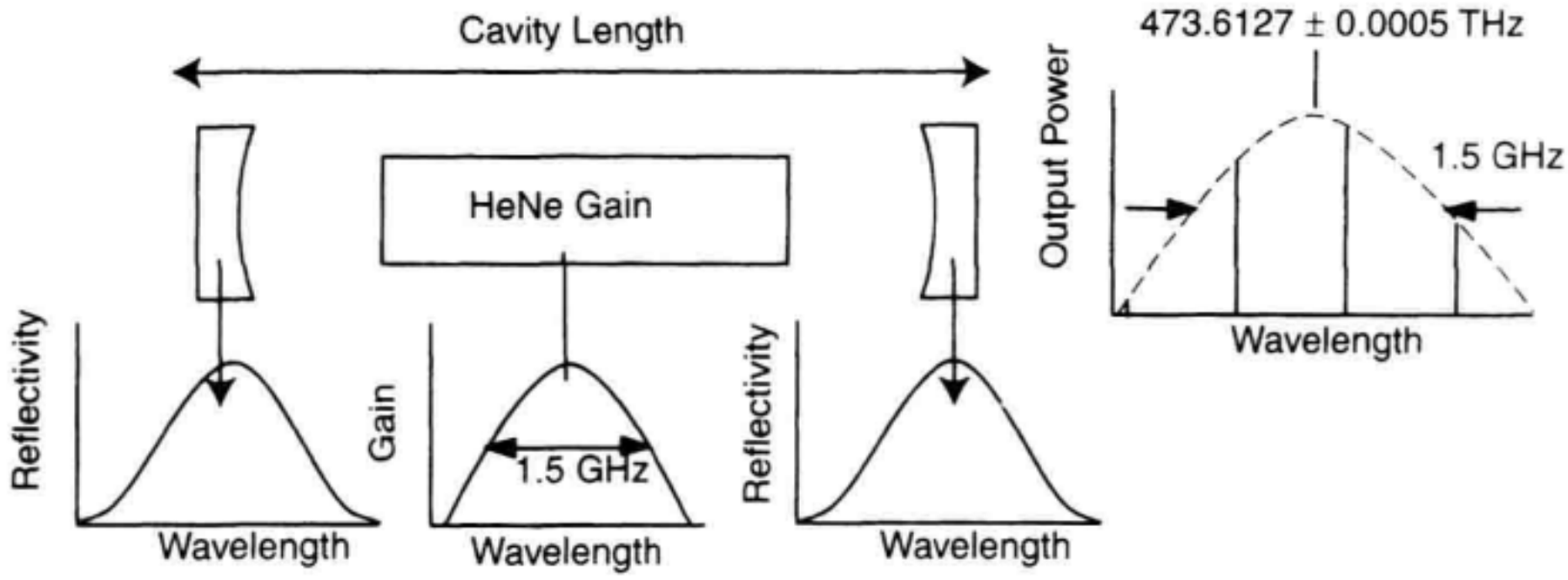

Figure 4.13 Gain peak width and longitudinal mode spacings for Helium Neon lasers.

spacing or 0.5 GHz in this 15 cm cavity length example. For a 15 cm cavity length, this results in a potential 1 ppm error in wavelength. This error will be temperature dependent since the length of the laser resonator is temperature dependent causing the longitudinal mode position to shift. An alternate strategy would be to use a HeNe laser with finely spaced longitudinal modes so that the laser has a multiple longitudinal mode output with the average wavelength being very constant. The accuracy can be significantly improved by using HeNe lasers that have the longitudinal mode position locked to the center of the gain versus wavelength curve. However, this stabilization results in an appreciable increase in the cost of the laser. A gain-center-locked HeNe laser is capable of wavelength errors of less than 0.1 ppm. Further refinements in HeNe laser accuracy are also possible but are not necessary for fiber optic applications.[1]

Other Wavelength References. HeNe lasers with similar wavelength accuracies are available at 730.6 nm, 1152.6 nm, and 1523.5 nm. The considerations illustrated in Figure 4.13 apply to these wavelengths also except for differences in the width of the gain peak and the spacing of the longitudinal modes. These other wavelengths offer lower gain per unit length requiring a significantly longer laser tube. Without stabilization of the longitudinal modes to the line center, accuracies of less than 1 ppm are achievable at these HeNe wavelengths.

Standards organizations have refined very accurate wavelength standards. The use of these elaborate standards is probably not justified for the accuracies required in fiber-optic communications systems. The commercially available HeNe lasers shown in Table 4.2 can be used to verify accuracy of wavelength meters intended for fiber optic applications.

4.4.4 Dependence on the Signal Spectral Width

Figure 4.3 showed the interferogram for a relatively incoherent source. The broad spectral content of the LED caused the fringe visibility to decrease to zero for offsets far from zero path-length difference. The distance over which fringes are visible is a measurement of

the coherence length of a source. For a 1550 nm LED with a 60 nm spectral width, the coherence length is only 20 μm. Away from zero delay, the fringe visibility becomes severely degraded. The fractional fringe-counting techniques of Section 4.4.1 are only useful if the fringes are extremely stable in time. In the poor fringe-visibility region there is a phase-measurement uncertainty that is related to the linewidth of the signal.[1]

Measurement of low coherence signals can cause calculation problems for fringe counting wavelength meter implementations. If the wavelength meter is scanned over a range of ±3 cm range, only a small number of fringes will be counted over the central portion of the scan for the LED example of Figure 4.2. If the wavelength meter doesn't take into account the fact that fringes don't exist away from zero path-length differences, incorrect wavelength measurement values will be displayed.

The Fourier-transform techniques of Section 4.3 are more tolerant to measuring incoherent sources. The Fourier-transform operation will record the characteristic periods that are within the interferogram, even if the fringes are not visible over the entire scan length. Since fewer fringes are involved in the comparison, the center wavelength of the LED will not be measured with a large accuracy. However, this reduced measurement accuracy for an LED is justified because the LED does not have a well-defined center wavelength.

4.4.5 Optical Alignment Issues

It is important that the path lengths be identical between the known and the unknown arms of the interferometer. If the two arms are not well-aligned, the reference laser will not accurately measure the path-length difference for the unknown signal-interference pattern. Alignment errors often enter only second order to the wavelength accuracy. A 1 ppm accuracy requires the input beam to be aligned to a reference beam and/or the instrument optical axis to the order of 10^{-3} radians.[16] Singlemode fiber-optic input-wavelength meters are convenient because the alignment of the input beam to the optical axis of the interferometer is fixed by the fiber launch optics. Wavelength meters that accept open optical beams must be careful so that the input signal is well-aligned to the optical axis of the measurement instrument. A multimode fiber input to a wavelength meter can have an error associated with mode excitation. The distribution of light at the output of multimode fiber can be variable depending on how the fiber optic cable is wiggled. This variability in the excitation conditions leads to wavelength errors due to the uncertainty in the launch conditions into the interferometer as compared to the reference source.

4.4.6 Diffraction Effects

Collimated light slowly diverges according to the mathematics of Gaussian optics. The smaller the diameter of the collimated beam, the wider the divergence cone. Since the two beams of a Michelson interferometer often travel different distances to the receiving detector, the wavefront curvature for these beams will be slightly different. This limitation on fringe counting is illustrated in Figure 4.14. This presents an ultimate limit to the fraction of a fringe that can be counted as described in Section 4.4.1. If the two Gaussian

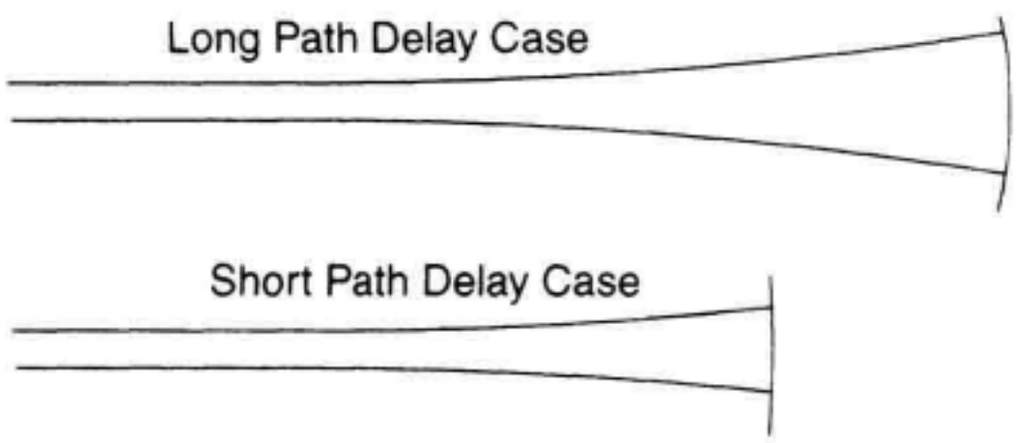

Figure 4.14 Wavefront curvature comparison for non-equal length interferometer arms.

beams travel the same distance, the constant-phase wavefronts perfectly align with each other. If the wavefronts are not perfectly matched, the interference effect will be reduced. The fringe visibility will be reduced as the mirror scan is increased away from equal path delay. For the purpose of fiber-optic communications measurements, this term is very small.[17]

4.4.7 Summary of Wavelength Accuracy Factors

Table 4.2 lists factors that affect wavelength accuracy and comments about each. If all of the factors are taken into account, it is possible to achieve less than 1 ppm accuracy in an air-measurement environment. This would require the use of a HeNe reference laser stabilized to the gain peak, and corrections for temperature and pressure variations.

4.5 MICHELSON WAVELENGTH-METER MEASUREMENT CONSIDERATIONS

In the following section, some of the measurement capabilities of Fourier-transform Michelson-interferometers will be discussed. The areas of discussion are:

1. Wavelength resolution
2. Wavelength coverage
3. Sensitivity, measurement range, dynamic range, and signal to noise

Table 4.2 Comparison of factors that affect wavelength accuracy.

Parameter	Uncertainty Contribution	Comments
Fractional fringe counting error	0.17 ppm	Assumes a 1/10 fringe resolution in 600,000 sample inteferogram
Index of refraction dispersion vs. wavelength	0.2 ppm	Assumes that elevation is known and temp is stabilized ±10C
Reference laser accuracy	0.1 ppm–1 ppm	Depends on wavelength stabilization of HeNe laser

4. Amplitude accuracy
5. Multimode fiber considerations
6. Pulsed signal measurements.

4.5.1 Relative Wavelength Resolution

Figure 4.8 showed the result of a multiple-signal wavelength measurement for a WDM system. This section intends to answer the question, How close can the signals be and still be individually resolved?

The major factor affecting relative wavelength resolution is the length of scan in the Michelson interferometer. This may best be illustrated by an example: An interferometer with a 40.45 mm (±20.225 mm) path delay is taken. The reference fringe period is every $\lambda_{reference}/2$ of mirror translation ($\lambda_{reference}$ = 0.633 μm for a HeNe reference laser). This would yield a total of 131072 samples during one scan. If these samples are put into a fast-Fourier-transform operation, there will be 65535 ($2^{17}/2$) real and 65,535 imaginary frequency bins produced. Each frequency domain point will be spaced by 7.227 GHz (see Equation 4.13) in this example. A single, pure optical frequency input will generate a peak that is 2 bins wide (full-width at half of maximum). In this example the resolution would be 14.454 GHz. The resolution is independent of wavelength. At 1310 nm it would be 0.083 nm and at 1550 nm it would be 0.116 nm. The resolution capability of a Fourier-transform Michelson wavelength-meter is thus given as

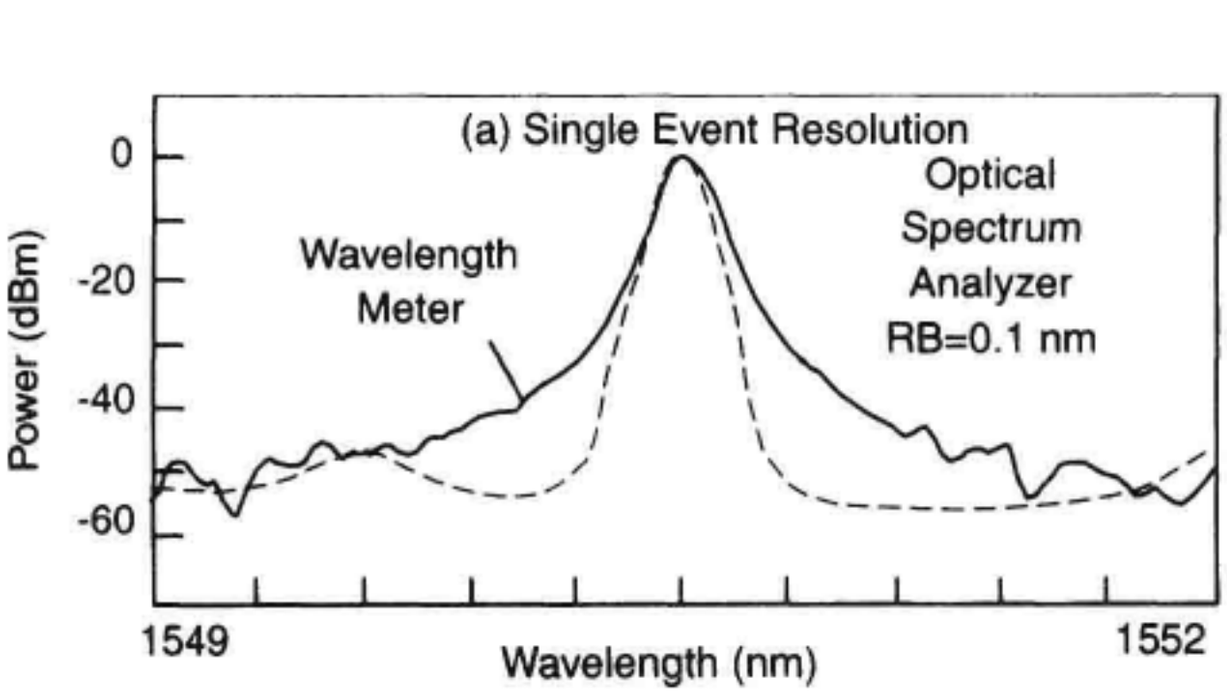

Figure 4.15 (a) Single-event resolution of a DFB laser. (b) Two-event resolution of DFB lasers spaced by 0.2 nm. The wavelength meter results are contrasted with a double-pass grating-based optical spectrum analyzer measurement of the same sources.

$$\text{Resolution (Hz)} = \frac{\text{speed of light}}{\text{total distance of the interferogram}}. \tag{4.19}$$

Figure 4.15a shows the measurement of single-event resolution for a wavelength meter with a mirror scan length of ±20 mm. The effective resolution for this measurement from Equation 4.19 is about 15.6 GHz (0.13 nm). Figure 4.16a shows a measurement of the two-event resolution for two DFB lasers signals separated by 0.2 nm. The two signals are resolved in this case. The plot also shows the results of these two signals as measured by a double-pass diffraction-grating-based OSA. The resolution capability of both instruments is similar near the signal peaks. The OSA has superior resolution 0.2 nm off of the signal peak.

In a FP laser, it is often desirable to know the relative locations of all of the longitudinal modes. Figure 4.16 shows a plot of the modes of an FP laser as measured with a ±20 mm mirror scan length. The modes are nearly uniformly spaced in frequency step. Dispersion and gain-shape effects in the semiconductor cause the modes to have a slight frequency step nonuniformity. These nonuniformities can be used to measure material dispersion. This measurement requires very accurate relative measurements of wavelength. The spacing between modes is approximately 35 GHz in this example.

4.5.2 Wavelength Coverage

The wavelength coverage is limited fundamentally by the wavelength coverage of the photodetectors. InP/InGaAs photodetectors with thin InP-layers above the absorbing region are capable of operating over the 0.6 μm to 1.7 μm wavelength range. The input fiber also has a specified wavelength range over which it operates in a single transverse mode. Multiple transverse-mode operation of the input fiber will decrease wavelength accuracy.

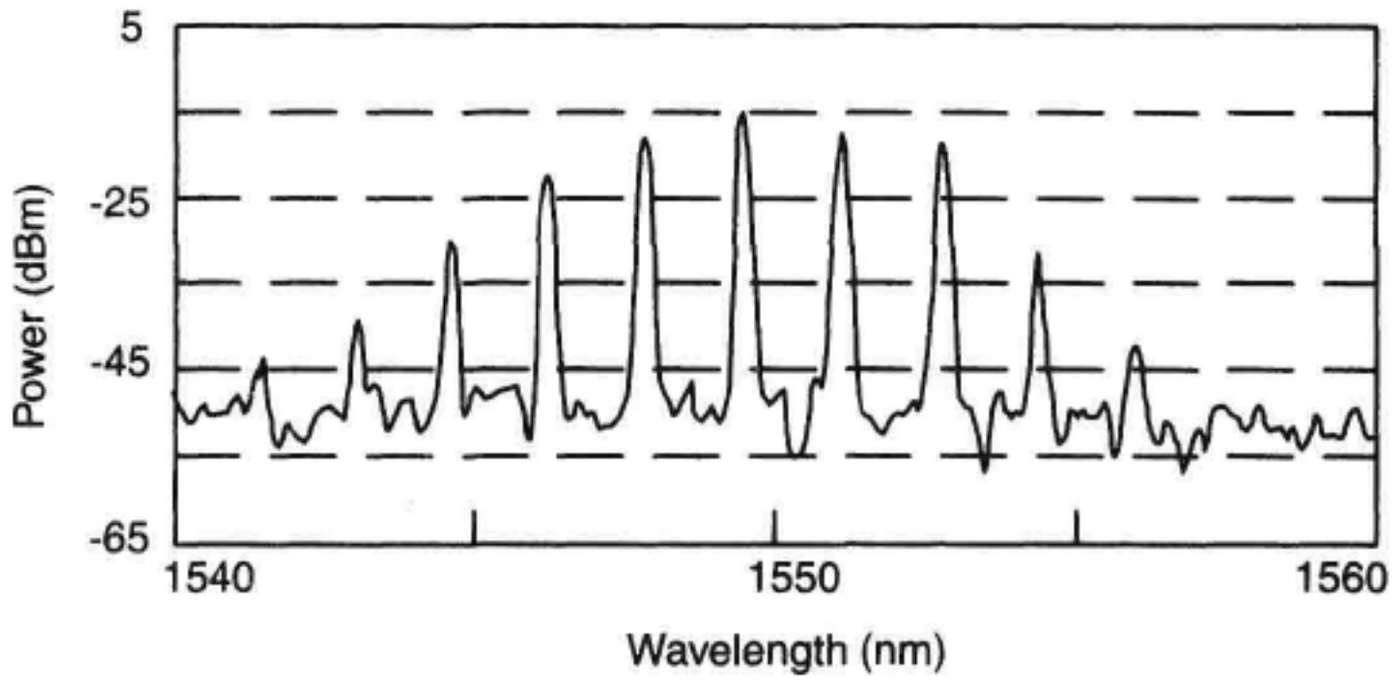

Figure 4.16 A Fabry-Perot laser spectrum measured on a Michelson interferometer wavelength meter.

4.5.3 Sensitivity and Measurement Speed, Measurement Range, and Dynamic Range

Sensitivity and Measurement Speed. Sensitivity refers to the smallest signal that can be measured with a wavelength meter. The sensitivity of a wavelength meter is best demonstrated using a design example.

Example

Assume that a wavelength meter has a mirror scan of ±20 mm and a desired measurement speed of 0.1 s. Let us assume that the wavelength meter has the block diagram as shown in Figure 4.7. The ±20 mm span will produce approximately 2^{17} samples in the 0.1 s interval. This corresponds to a data rate of 1.3 MHz. Let us assume that the optical receiver uses a 10 MHz bandwidth. For a 10 MHz bandwidth, a high-performance optical receiver can use a transimpedance value of 10,000 ohms. The achievable sensitivity of such a receiver can be found from Table A.1 in Appendix A as –80 dBm assuming a photodetector responsivity of 0.5Amp/Watt including Michelson interferometer losses. It takes at least a 15 dB signal-to-noise ratio to make a reasonably accurate wavelength measurement (for example, 3 ppm wavelength accuracy). The resulting sensitivity in this example is therefore –65 dBm.

The example above shows that the sensitivity of a wavelength meter is worse than that of the grating-based OSAs studied in Chapter 3. It is important to compare the two instruments in a similar measurement condition. Let's assume that the goal of a measurement is to find the wavelength and power of a signal known to have a wavelength near 1550 nm. For the OSA, a narrow 10 nm wavelength sweep would be adequate to find the wavelength of the signal. The optical receiver in the OSA can use a narrow detection bandwidth of 100 Hz. From Table A.1 in Appendix A, assuming a 100,000 ohm transimpedance and a detector responsivity of 0.02 Amp/Watt (includes monochromater loss), a sensitivity of –90 dBm should be achievable. The OSA should have a signal-to-noise ratio of 10 dB to make an accurate wavelength measurement. This would result in a sensitivity of –80 dBm to compare with the –64 dBm sensitivity of the wavelength meter. The biggest difference between the two instruments sensitivities is the large detection bandwidth required to achieve a fast measurement speed in the wavelength meter. The wavelength meter always needs to make a full scan over the desired path length delay to achieve good wavelength resolution independent of knowledge of the approximate signal wavelength. If compromises are made in measurement speed or in the desired wavelength range of the wavelength meter, sensitivities comparable to OSAs can be achieved.

Measurement Range. Measurement range compares the largest signal that can be measured to the sensitivity of the instrument. The largest signal that can be handled is limited by power-handling limitations of the interferometer optics or the photodetector and is typically around 10 dBm. The sensitivity of a wavelength meter in the example above was –64 dBm. The resulting measurement range in this example would be 74 dB. This would compare to a grating based OSA measurement range of 90 dB for the above example.

Dynamic Range. Dynamic range refers to the ability to measure small signals in the presence of large signals. OSAs and wavelength meters have significantly different dynamic-range capabilities. The skirts of the filter in an OSA limit the dynamic range of a double-pass grating OSA to about 70 dB.

The wavelength meter has a dynamic range limited by the large amount of shot noise that is present in the optical receiver. This dynamic range limitation is shown by an example.

Example

The conditions from the wavelength-meter sensitivity calculation above will again be used. Let's assume that an input signal with 1 mW of average power is input to the wavelength meter. For a detector responsivity of 1 Amp/Watt, 1 mA of photocurrent will be produced in the detector. This large input signal will generate a significant amount of shot noise in the receiver. Assuming a 10 MHz receiver bandwidth, Table A.2 in Appendix A shows that the current shot noise value is 57 nA for a 10 MHz bandwidth. This 57 nA of shot noise is 42 dB lower than the average current of 1 mA. The dynamic range of the wavelength meter in this example would be 42 dB.

This dynamic range limitation is illustrated in the FP laser measurement example in Figure 4.16. The wavelength meter used for this measurement has similar parameters as in the above example. There appears to be a noise floor in the measurement that is about 37 dB lower than the peak of the spectrum. This noise floor is due to shot-noise generation in the optical receiver. If the DFB signal were removed from the wavelength meter, the displayed noise floor would drop by over 30 dB. In an OSA, the optical receiver receives a large shot-noise contribution only when the signal falls within the passband of the OSA filter. A typical double-pass grating-based OSA may have a dynamic range of over 70 dB.

Signal-to-Noise Ratio Measurement. Michelson interferometers with Fourier-transform capability can be used to make signal-to-noise ratio measurements on the signal input. Signal-to-noise measurements are very important for optically amplified WDM systems. The amplified spontaneous emission noise from erbium-doped fiber amplifiers is added to the signal power. If the signal-to-noise ratio become significantly worse than 20 dB (0.1 nm noise bandwidth), bit-error ratio problems will occur.

For wavelength meters, the signal-to-noise ratio measurement capability is limited by the dynamic range of the measurement system as described in the last section. For closely spaced WDM channels, the selectivity of the wavelength meter is another factor that can limit the capability to measure signal-to-noise ratio. The measurement effectiveness is improved by taking long interferometer sweeps and by using a slow measurement speed. The effective filter width of the noise measurement must also be taken into account when calculating noise power. The effective filter width is approximately equal to the resolution given by equation 4.19.

4.5.4 Amplitude Accuracy

Traditional power meters need the wavelength of the light entered before accurate power measurements can be made because of the change in detector responsivity with wavelength. Since wavelength meters automatically calculate wavelength, one does not need to

enter wavelength to accurately measure power. The amplitude accuracy of multiple-wavelength Fourier-transform measurements is more complicated to achieve. Amplitude accuracy of the instrument can be calibrated while operating with the data in the frequency domain.

4.5.5 Singlemode and Multimode Fiber Input Considerations for Wavelength Meters

The use of a singlemode fiber optic input for a wavelength meter greatly simplifies the use and the accuracy of the instrument. With a fixed-position fiber input to the interferometer, the alignment of the input signal to the optical axis of the interferometer is well-defined and repeatable. This avoids wavelength errors due to optical axis misalignment.

A wavelength meter using a multimode-fiber input will have reduced performance when compared to a singlemode fiber input in terms of wavelength accuracy. When a narrow spectral width source is coupled into multimode-fiber, a speckle pattern appears in the fiber cross-section because of interference between the multiple paths through the fiber. The optics of the Michelson interferometer images the input fiber-speckle pattern to the detector through each arm of the interferometer. The speckle pattern features must be placed identically on top of each other at the detector in order for interference to occur. This means that the alignment of the interferometer optics to accommodate multimode fiber inputs is as critical as for singlemode fiber inputs. The fringe visibility of the wavelength meter is also degraded compared to a singlemode input. The fringe visibility will also vary with the exact nature of the speckle pattern of the input. This causes the instrument sensitivity to vary with movement of the input fiber.

Multimode fiber also may produce a slightly different wavelength readout depending on how well all of the modes within the fiber are excited. If the waveguide is excited off of the center axis of the multimode fiber, the effective angle of the input beam may be misaligned with respect to the reference laser beam resulting in a path length mismatch and resulting wavelength error.

4.5.6 Measurement of Pulsed Signals

The scanning Michelson-interferometer analysis done up to this point made the assumption that unmodulated signals are present at the input. Wavelength-meter designs based on movement in time of an interferometer arm will not make correct measurements on lasers with very low repetition-rate intensity-modulation or frequency modulation. In fiber optic systems, it is common to measure signals that have intensity modulation. The SONET transmission standard has modulation spectral content that extends down to 8 kHz. Pseudorandom binary-sequence modulated signals can have frequency content at even lower modulation rates. Even cw lasers can have instabilities that can lead to erroneous data in a wavelength measurement.

What are the limitations for measuring modulated or pulsed lasers with a Michelson interferometer? If the modulation period is short compared to the measurement time of the instrument, accurate measurements can be made. If the modulation period is too long, significant wavelength measurement errors can result. Fringe-counting wavelength meters

are especially prone to producing erroneous results with low-frequency modulation signals present. However, averaging of the wavelength measurement over many measurements may improve the accuracy of the reading.

Fourier transform wavelength meters are more tolerant of pulsed input waveforms than are fringe-counting wavelength meters. When a periodic low-frequency modulation signal is present on the interferogram, the Fourier transform of that signal will produce modulation sidebands around the actual signal wavelength. The extra sidebands caused by the low frequency modulation will appear as spurious signals in the display that are suppressed from the main signal. The wavelength value of the main signal is still accurately displayed in the pulsed condition.

4.6 ALTERNATE WAVELENGTH METER TECHNIQUES

In this section, some alternate techniques for accurate wavelength measurement are made. The coverage is not complete, but it does discuss some important considerations that may not be well-covered by Michelson-interferometer wavelength-meter designs. The four configurations to be discussed are the FP filter, the static FP interferometer, static Fizeau interferometer, and wavelength discriminator. The static interferometer techniques are excellent for pulsed-laser measurements. Wavelength discriminator techniques have limited accuracy, but have simplicity and low cost.

4.6.1 Fabry-Perot Filters

The first part of this chapter discussed the use of a Michelson interferometer. There are other configurations that can be used to interfere light. The FP interferometer is shown in Figure 4.17. FP filters are also referred to as etalons. In an FP interferometer, light is incident on an optical component with two reflecting surfaces. The light that exits the interferometer consists of a direct path added to a large number of reflected paths through the interferometer.

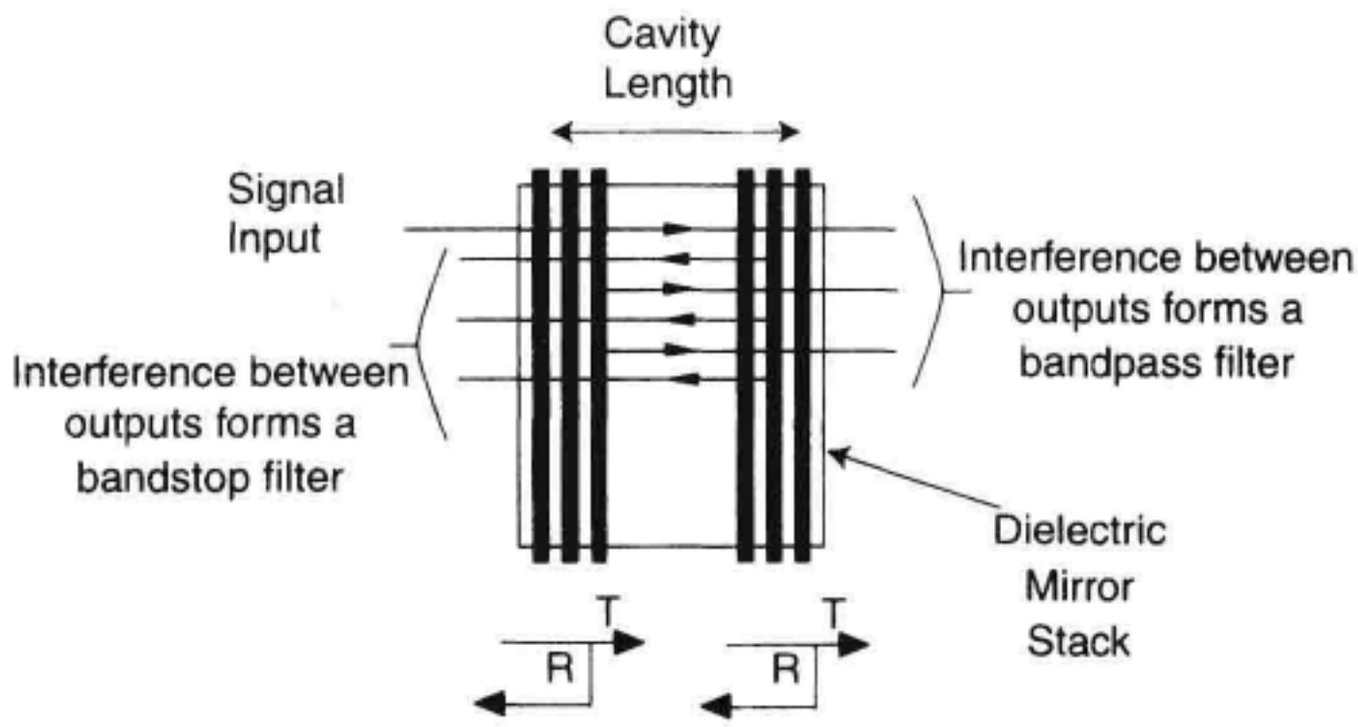

Figure 4.17 A Fabry-Perot interferometer.

The outputs add constructively or destructively depending on the wavelength of light. A similar interference occurs on the reflected signals from the interferometer. The FP interferometer is most commonly used as a tunable filter. The filter applications make use of the fact that the transmission loss through the filter is very wavelength selective. The passband of the filter can be adjusted by changing the angle of the incident light or by varying the spacing between the two reflections. The FP configuration can also be used as a fringe-counting wavelength meter. In the fringe-counting application, a diverging beam is applied to the interferometer. A detector array is then used to measure the distance between interference fringes that are found at the output of the interferometer. This section concentrates on a discussion of the FP interferometer in the filter application. Sections 4.6.2 and 4.6.3 will describe static fringe-counting configurations.

An analysis of the lossless FP interferometer will aid in the understanding of this type of wavelength meter. There are many excellent books that describe in detail the mathematics of an FP filter,[18–20] the results of the analysis are presented here. The filtering function of the interferometer is accomplished by interfering the initially transmitted signal with many delayed versions of the input signal. The maximum tran mission occurs when the delayed signals add-in phase with the first transmitted signal. The transmission function through a FP interferometer is given as[19]

$$\text{Transmission} = \frac{(1-R)^2}{(1-R)^2 + 4R\sin^2\left(\dfrac{2\pi Ln\cos\theta}{\lambda_{vac}}\right)}. \tag{4.20}$$

In this equation, it is assumed that both mirrors have equal mirror power reflectivity, R. The index of refraction between the mirrors is n, the mirror spacing is L, and the angle of the input light with respect to the perpendicular is θ.

Figure 4.18 shows an example filter function for a mirror spacing of 50 μm and mirror reflectivities of 0.9, 0.95, and 0.99. The most obvious characteristic of the filter is the repeated passband. There are several terms used to describe the characteristics of an FP interferometer passband. The frequency spacing between the repeated transmission peaks of Figure 4.18 is

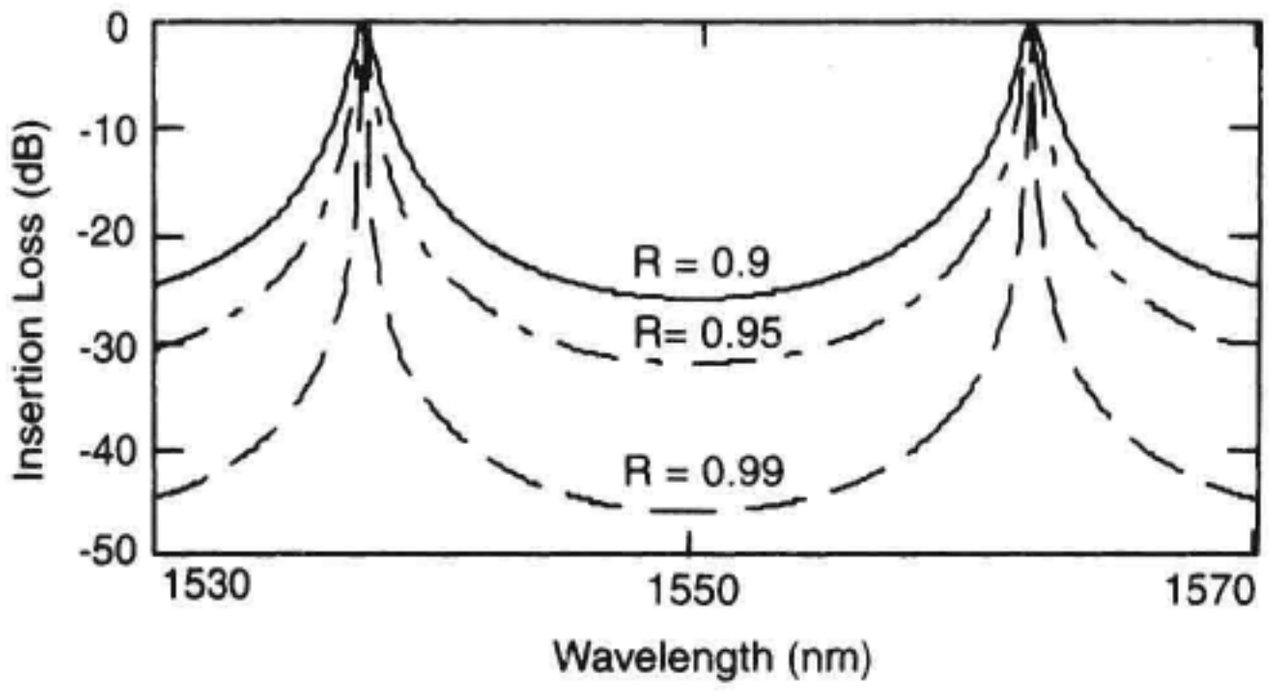

Figure 4.18 Fabry-Perot filter transmission versus wavelength for a mirror spacing of 50 μm and mirror reflectivities of 0.9, 0.95 and 0.99.

$$\Delta f = \frac{c}{2nL\cos\theta}. \tag{4.21}$$

The free spectral range (FSR) is another term that describes the transmission peak spacing in terms of wavelength spacing:

$$|\Delta\lambda| = \frac{\lambda^2\cos\theta}{2nL} \tag{4.22}$$

The width (full-width at half of maximum) of the transmission peak is given as:

$$\delta f_{\frac{1}{2}} = \frac{(1-R)c}{2\pi\, nL\sqrt{R}\cos\theta} \tag{4.23}$$

The width of the transmission peaks in Figure 4.18 would be 100 GHz, 49 GHz, and 9.6 GHz for the 0.9, 0.95, and 0.99 mirror reflectivity cases shown.

The larger the mirror reflectivity, the narrower the transmission response. The term finesse describes the sharpness of the transmission peak in comparison to the width between repeated passbands.

$$\text{Finesse} = \frac{\Delta f}{\delta f_{\frac{1}{2}}} \tag{4.24}$$

Finesse values of several hundred are easily obtainable with values of up to several thousand being practical.

Repeated Passband Limitation on Narrow Spectral-Width Filters. An FP filter can have an extremely narrow passband. With a very narrow passband, it is possible to accurately locate the wavelength of a signal in a wavelength-meter implementation where the FP filter is followed by a power meter. Narrow-width passbands can be accomplished with either very high values of mirror reflectivities or with wide mirror spacings. A major limitation of FP filters is the repeated nature of the passband. The repeated passband introduces uncertainty in the actual center wavelength measurement because one does not know which passband is being used in the repeated filter response. The repeated passband effect can be reduced by introducing mirrors that have a wavelength dependent reflectivity.[18] Figure 4.19 shows the measured passband of an FP filter that has many of the repeated passbands eliminated with special mirror coatings. This bandpass filter has a single with a very narrow (1 nm wide) passband. All of the repeated passbands are suppressed in this case out to 1400 nm.

Filter Wavelength Tuning. The FP filter can be used as a tunable filter to locate the wavelength of an unknown signal in a manner similar to that of the diffraction grating in Chapter 3. FP filters are tuned by adjusting the angle of the incoming light with respect to the mirror or by adjusting the spacing between the mirrors. Equations 4.20 to 4.24 describe how the center-wavelength and filter-width changes with respect to mirror spacing and angle.

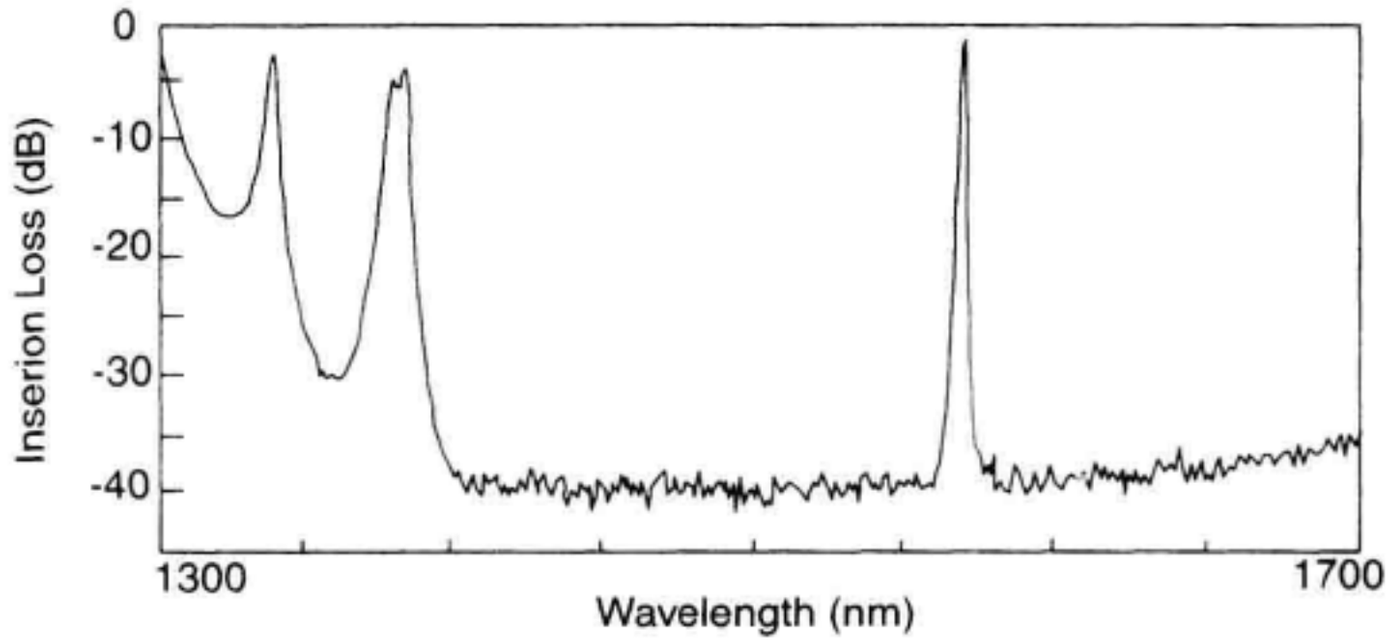

Figure 4.19 Transmission response of a Fabry-Perot filter with mirror coatings to reduce repeated passbands.

As the angle of the filter is changed, the width of the passband degrades. The multiple-reflection light beams do not completely overlap with the initially transmitted beam reducing the magnitude of interference. The maximum tuning range is limited by the range of acceptable filter-passband characteristics. This method of wavelength adjustment has the advantage of stability and simplicity. A disadvantage of angle tuning is that the transmission through the filter becomes polarization sensitive.

Length tuning suffers from the mechanical complexity of keeping the mirrors perpendicular with respect to length change. The free spectral range and filter width are also changing as the FP filter length is adjusted.

4.6.2 Static Fabry-Perot Interferometer Wavelength Meter

The first part of this section emphasized the use of the FP filter as a bandpass filter that can be wavelength tuned. The FP filter can also be used in a static fringe-counting mode of operation.[21] Static FP wavelength meters can measure the wavelength of individual laser pulses as well as cw beams because the measurements are obtained spatially. The word static in the title of this section emphasizes that there are no moving parts in the design. This is in contrast to the Michelson interferometer applications where a mirror is scanned in time to make a wavelength measurement.

The generation of interference fringes in a static FP etalon is illustrated in Figure 4.20. The Fabry-Perot etalon is illuminated with a diverging light beam. A bull's-eye concentric-ring pattern of interference fringes is produced. The spacing between the interference fringes is used to calculate the wavelength of the unknown signal. The wavelength meter is calibrated by comparing the interference pattern of the unknown signal to that produced by an accurate reference wavelength source such as a HeNe laser. Care must be taken so that both the reference and unknown wavelengths illuminate the FP etalon identically. Many of the wavelength accuracy considerations discussed in Section 4.4 of this chapter apply to static FP designs. The wavelength accuracy of the HeNe laser is important, the index of refraction dispersion must be considered, and fractional fringe-counting is important for high accuracy measurements.

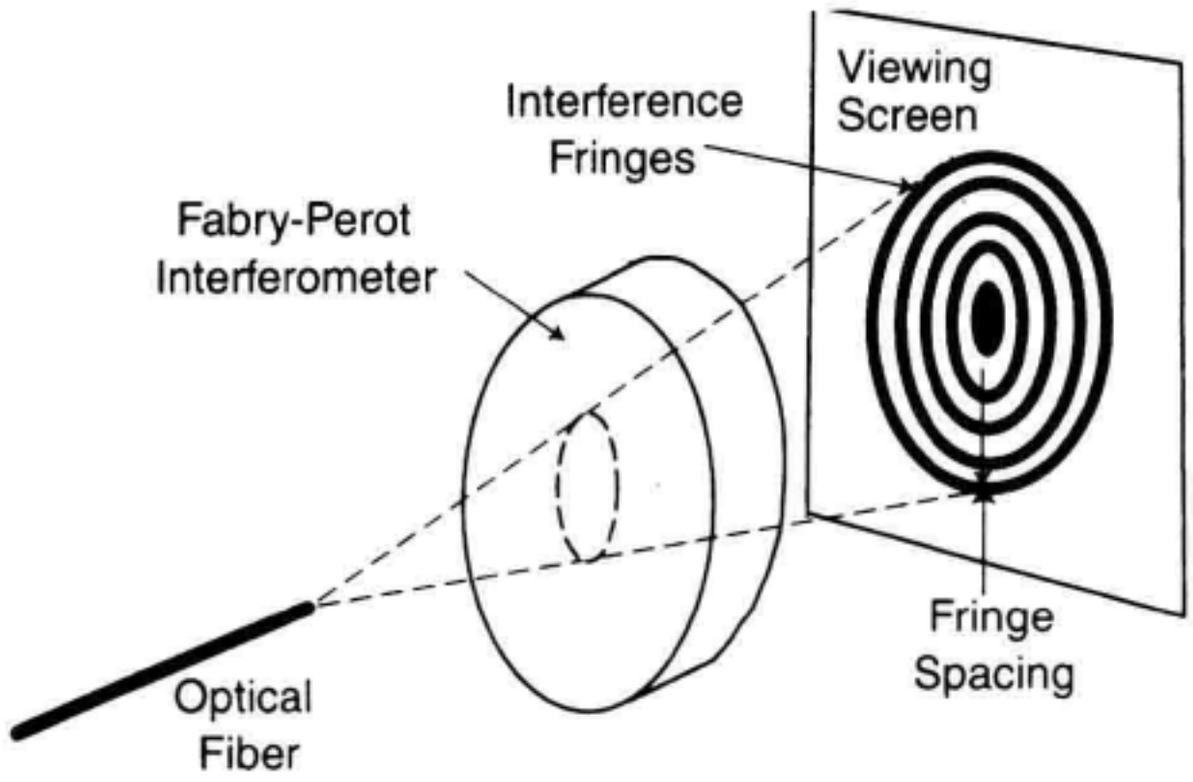

Figure 4.20 Static Fabry-Perot interferometer interference fringes.

4.6.3 Static Fizeau Interferometer Wavelength Meter

The Fizeau interferometer is similar to an FP interferometer except that the two reflecting surfaces form a wedge instead of being parallel. Fizeau wavelength meters are very important for accurate measurements of pulsed and modulated signals. Figure 4.21 shows a block diagram of a Fizeau interferometer[22–25] wavelength meter. The Fizeau interferometer wedge can be considered as a collection of FP interferometers with slightly different mirror spacings. The Fizeau wavelength meter uses reflections off of the front and back surfaces of the wedge to introduce interference. The two surfaces of the wedge have relatively low values of reflectivity so that only two dominant waves are being interfered. The reflected light from the wedge is then imaged on to a detector array where the interference pattern is recorded.

It is the measurement of the period of the interference fringes that allows the unknown wavelength of the signal to be measured. A calibration of the unknown fringe period can be made by comparing it to the fringe period of a reference laser signal. By com-

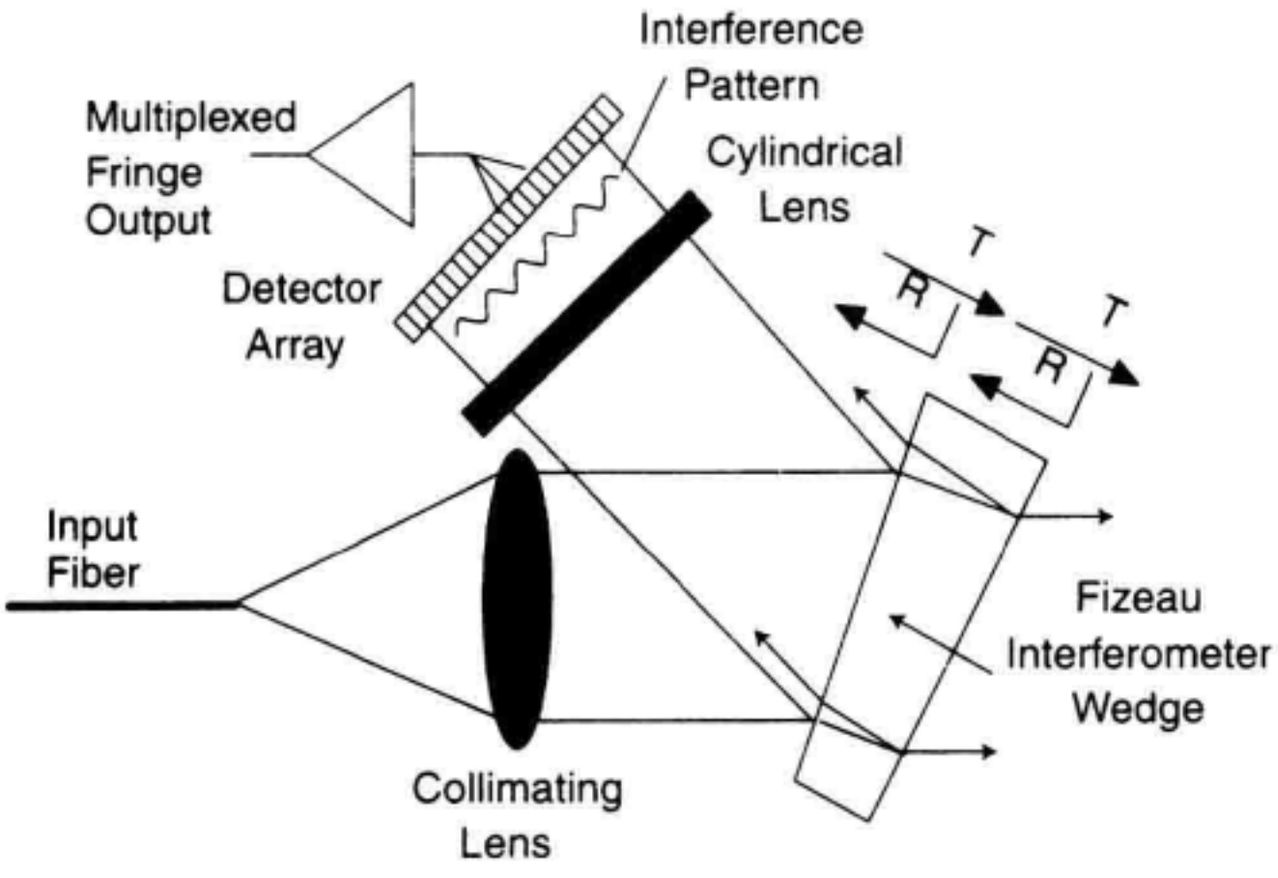

Figure 4.21 Static Fizeau interferometer wavelength meter diagram.

paring the period of the reference fringes to the period of the unknown fringes, the wavelength of the unknown can be accurately measured. The frequency of the unknown signal, λ_u, can be compared to the frequency of the known signal, λ_r, by the equation:

$$\lambda_u = (N_r/N_u)(n_u/n_r)\lambda_r \tag{4.25}$$

In this case, the definition of N_r and N_u are slightly different than for the Michelson interferometer case of Equation 4.11. N_r and N_u refer to the number of fringes that are measured over the length of the photodetector array. As was the case for the Michelson interferometer wavelength meter, n_r and n_u are the index of refraction in the medium of the interferometer which is often air or glass. The number of fringes that are counted on the detector array has the same wavelength accuracy implications as the number of fringes that are measured in one scan of a Michelson interferometer. More interference fringes will be measured if the slope of the wedge in Figure 4.21 is increased or if the length of the detector array is increased. The slope cannot be increased to very large values though because the fringe visibility decreases and the detector array has a finite density of detector elements.

It is the spatial interference pattern on the detector array that is one of the key features of the design. In a scanning Michelson wavelength meter, measurement inaccuracy can result if the amplitude or spectral characteristics of the input signal change over the duration of an interferogram scan. This limitation on measurement of pulsed signals was described in Section 4.5.6 for Michelson wavelength meters. The Fizeau wavelength meter does not require any physical motion to measure wavelength. Instead of adjusting the mirror spacing, the Fizeau interferometer has a built-in scanning function since the signal is simultaneously applied to the entire Fizeau wedge. This makes the Fizeau-wavelength meter design superior for measurements on optical sources with low frequency modulation or instabilities. The use of a detector array is often a cost barrier for use in the telecommunication wavelengths of 1100 to 1700 nm. Low-cost silicon detector arrays are not available at these wavelengths. Arrays of InGaAs/InP detector arrays are available though and the cost should decrease to make commercial products more practical. The Fizeau interferometer also suffers from poor sensitivity. The design of Figure 4.21 uses 4% reflectors to induce the interference pattern on the detector array. This means that 92% of the input power is unused. The power from the source is also distributed among a large number of array elements.

4.6.4 Wavelength Discriminators

A wavelength discriminator uses a filter that has its insertion-loss versus wavelength well-characterized. Figure 4.22 shows an example of a discriminator-based wavelength meter. An input signal is applied to the wavelength meter beam splitter. Figure 4.22 shows the transmission and reflection characteristics versus wavelength for an example discriminator element. A fraction of the power reaches detector 1 and another portion reaches detector 2. If most of the photocurrent is found on detector 1 and very little on detector 2, then it is evident that the signal wavelength must be on the short end of the wavelength range. Thus by ratioing the photocurrents and comparing to a previously measured

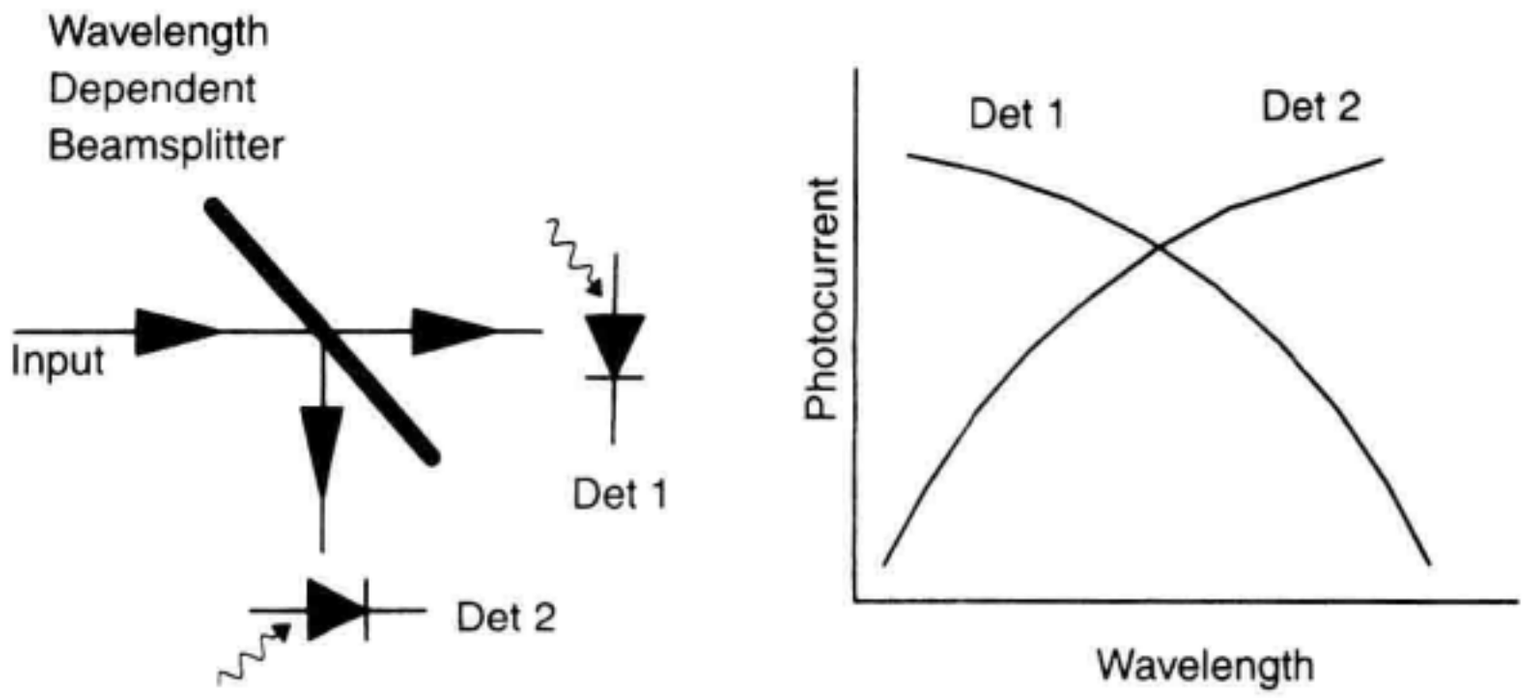

Figure 4.22 Wavelength discriminator.

calibration table, the wavelength of the input as well as the power of the signal can be measured. Absorption filters using doped glass are one method to achieve the change in transmission versus wavelength. This type of wavelength meter is very simple and may be adequate for many applications. Most optical power meters require the user to enter the wavelength of the incoming signal. With the wavelength discriminator, this problem can be solved with simultaneous knowledge of the wavelength and photocurrent.

The method has moderate wavelength accuracy capabilities when compared to interferometer-based wavelength meters. If the discriminator function changes rapidly with wavelength, better wavelength accuracy will be achievable at the expense of wavelength coverage. Typical accuracy for this type of wavelength meter is 650 ppm for a unit that can cover a single telecommunication wavelength band. Wavelength meters of this type cannot distinguish individual signals from a multiple signal environment.

4.7 SUMMARY

Comparison of Wavelength Meter Techniques. Table 4.3 provides a comparison of the Michelson wavelength meter methods discussed in this chapter with the OSA techniques discussed in Chapter 3. This comparison is made for instruments that are optimized to make measurements with a comparable measurement update rate. The most dramatic difference between the two techniques is the achievable dynamic range for Michelson interferometer wavelength meters. The shot noise generated in the optical receiver is the limiting factor for the Michelson design.

This chapter discussed the accurate measurement of wavelength, concentrating on a Michelson interferometer approach. After reading this chapter, there are several important points that should be highlighted.

1. It is important to state the conditions for a wavelength measurement. Vacuum wavelength numbers and standard dry air wavelengths are most often quoted.

Table 4.3 Comparison of Michelson interferometer wavelength meter with a grating-based optical spectrum analyzer

Parameter	Michelson Interferometer Wavelength Meter	Grating-Based Optical Spectrum Analyzer
Absolute wavelength accuracy	1 ppm	150 ppm < 30 ppm with calibrator
Sensitivity for 1-s update rate	-65 dBm	-80 dBm
Wavelength resolution	0.1 nm (12 GHz at 1550 nm) depends on scan length	0.1 nm (12 GHz at 1550 nm) depends on number of illuminated grating lines
Dunamic range	40 dB limited by shot noise	70 dB limited by filter stopband rejection
Wavelength range	All fiber optic wavelengths	All fiber optic wavelengths

2. The Michelson interferometer is the most common platform used for accurate wavelength measurements. This method compares the wavelength of an unknown signal to that of a highly accurate laser wavelength reference.
3. Wavelength meters for the telecommunication bands can achieve less than ±1 ppm error in absolute wavelength accuracy.
4. Wavelength meters are capable of individually resolving multiple signal inputs simultaneously using Fourier transform techniques.
5. Fabry-Perot filters are useful alternatives to diffraction-grating based OSAs.
6. Static (no moving parts) Fabry-Perot and Fizeau interferometer designs can be optimized to measure the wavelength of sources with low frequency modulation.
7. Wavelength discriminators offer a low-cost approach to wavelength measurement with reduced performance.

REFERENCES

General Michelson Interferometer Wavelength Meter References

1. Obarski, G.E. 1990. Wavelength measurement system for optical fiber communications. Boulder, CO: *NIST Technical Report NIST/TN-1336.*
2. Snyder, J.J. 1982. *Laser wavelength meters. Laser Focus:* 18(1), 55–61.
3. Lawrence, M. 1984. Continuous wave laser wavelength measurement using the travelling michelson interferometer. *Opt. Laser Tech:* 137–140.
4. Monochalin, J.P., M.J. Kelly, J.E. Thomas, N.A. Kumit, A. Szoke, P.H. Lee, and A. Javan. 1981. Accurate laser wavelength measurement with a precision two-beam scanning Michelson interferometer. *Applied Optics* 20, No. 5: 736–757.

Fourier Transform Spectroscopy

5. Thorne, A.P. 1988. *Spectrophysics,* London: Chapman and Hall, pp. 185–201.
6. Junttila, M.L., B. Stahlberg, E. Kyro, T. Veijola, and K. Kauppinen. 1987. Fourier transform wavemeter. *Review of Scientific Instruments* 58, No. 7: 1180–1184.

References on Fractional Fringe Counting

7. Hall, J.L., and S.A. Lee. 1976. Interferometric real-time display of cw dye laser wavelength with sub-doppler accuracy. *Appl. Phys. Lett.* 29 (6): 367–369.
8. Bennett, S.J., and P. Gill. 1980. A digital interferometer for wavelength measurement. *J Phys. E.* 13, 174–177.
9. Ishakawa, J., I. Nobujiko, and K. Tanaka. 1986. Accurate wavelength meter for cw lasers. *Appl. Optics.* 25, No. 5: 639–643.

Reference on Standard Dry Air and the Index of Refraction of Air

10. Edlen, B. 1966. The refractive index of air. *Metrologia* 2, No. 2: 71–80.
11. Peck, E.R., and K. Reeder. 1972. Dispersion of Air. *Journal of the Optical Society of America* 62, No. 8: 958–962.

HeNe Laser Wavelength Accuracy

12. Melles-Griot Product Catalog, 1996. Fundamentals of Helium-Neon Lasers. 1770 Ketterling Street, Irvine, CA., 92714.
13. Jennings, D.A., F.R. Peterson, and K.M. Evenson. 1979. Frequency measurement of the 260-THz (1.15 μm) HeNe laser. *Optics Letters* 4, No. 5: 129–130.
14. Moore, C.E. 1971. *Atomic Energy Levels as Derived from the Analysis of Optical Spectra: Vol 1,* Boulder, CO: NSRDS-NBS 35, Vol 1 (COM-72-51282): 77.
15. Tetu, M. 1997. Absolute Wavelength Stability Ions. Optical Fiber Communications Conference. Dallas, TX: Optical Society of America, Tutorial FE1: 167–220.

Beam Misalignment

16. Kowalski, F.V., R.T. Hawkins, and A.L. Schawlow. 1976. Digital Wavemeter for cw Lasers. *J. Opt. Society of America* 66, No. 9: 965–966.

Diffraction Limits on the Beam

17. Bonsch, G. 1985. Simultaneous wavelength comparison of Iodine-stabilized lasers at 515 nm, 633 nm, and 640 nm. *IEEE Trans. Instrum. Meas.* Vol. IM-34, No. 2: 248–251.

Fabry-Perot Filter References

18. Macleod, H.A. 1989. *Thin-Film Optical Filters* 2nd ed. New York: McGraw-Hill.
19. Haus, Herman. 1984. *Waves and Fields in Optoelectronics.* Englewood Cliffs, NJ: Prentice Hall.
20. Born, M., and E. Wolf. 1970. *Principles of Optics.* Oxford: Pergamon Press.

Static Fabry-Perot Interferometer

21. Byer, R.L., J. Paul, and M.D. Duncan in *Laser Spectroscopy III,* editors J.L. Hall and J.L. Carlsten, Springer-Verlag, Heidelberg, 1977.

Fizeau Interferometer Wavelength Meters

22. Morris, M.B., T.J. McIlrath, and J.J. Snyder. 1984. Fizeau wavemeter for pulsed laser wavelength measurement. *Applied Optics* 23: 3862–3868.
23. Gardner, J.L. 1985. Compact Fizeau wavemeter, *Applied Optics,* Vol. 24: 3570–3573.
24. Gray, D.F., K.A. Smith, and F.B. Dunning. 1986. Simple compact Fizeau wavemeter. *Applied Optics* 25: 1339–1343.
25. Gardner, J.L. 1986. Wavefront curvature compensation in a Fizeau wavemeter. *Applied Optics* 25: 3799–3800.

CHAPTER

5

High Resolution Optical Frequency Analysis

Douglas M. Baney, Wayne V. Sorin

5.1 INTRODUCTION

The intensity and frequency dynamics of optical sources are key characteristics in determining the performance of optical systems. These characteristics determine, for example, the effects of fiber-group-velocity-dispersion on the transmitted signal, channel spacings in wavelength division multiplexed (WDM) systems, and the impact of fiber nonlinearities such as stimulated Brillouin scattering.[1] Measurement of the intensity dynamics is relatively straightforward using a photodetector and an appropriate electronic receiver (see Chapter 6 for more coverage). On the other hand, optical phase noise and frequency chirp, which have substantial impact on the optical power spectrum and the quality of transmitted signals, are not detectable with simple optical power detection. Using the optical mixing and interference techniques described in this chapter, the phase noise and frequency dynamics of optical sources are readily measured. This chapter focuses on the following topics:

- laser linewidth and phase noise (without modulation);
- optical power spectrum of a modulated source;
- time-domain chirp measurement of an optical carrier;
- frequency-domain FM measurement of an optical carrier.

The semiconductor laser is the workhorse optical source for telecommunications. It can be mass-produced in wafer form and efficiently coupled to the singlemode optical fiber that forms high-speed optical links. The light output from these lasers can be modulated to transmit information by varying their injection current. The unmodulated laser ex-

hibits both intensity and phase noise which affects its performance in communications links. When modulation is applied, the optical source spectrum may be broadened (chirped) beyond the limits set by the information bandwidth. The spectral broadening due to chirp combines with wavelength dispersion in optical fiber to erode the shape of the transmitted pulses. This can lead to increased error rates in communications systems. The broadened spectrum of the modulated optical source also limits the proximity of channels in WDM systems. This chapter is aimed at methods to characterize linewidth, power spectrum, and chirping in optical sources. With these tools, a better understanding of the optical sources and ultimately the system performance can be obtained.

The linewidth of a typical single-frequency semiconductor laser is of the order of 10 MHz. To measure this linewidth, a typical grating-based OSA (see Chapter 3) would need about a thousand times improvement in resolution. Other optical filter-based methods such as scanning FP filters and interference filters are not covered in this chapter, the reader is referred to Chapters 3 and 4 for more information on these techniques. In general, these scanning filter methods are not able to achieve the measurement resolutions afforded by the methods presented in this chapter. The measurement techniques discussed in this chapter not only attain the required frequency resolution, but also allow measurement of the frequency response and frequency dynamics of optical signals. As a reference, the following matrix is provided which helps with the task of matching the desired measurement to a specific characterization technique. In Table 5.1, the column labeled *difficulty* refers to the ease with which the measurement can be set up and operated. The section column refers the reader to the appropriate chapter section.

In Section 5.2, basic concepts concerning laser dynamics and interferometry are discussed that will aid in understanding the measurement concepts presented later on. Section 5.3 discusses various methods of linewidth characterization. High-resolution measurement of the power spectrum of a modulated optical signal is examined in Section 5.4.

Table 5.1 Measurement Technique Comparisons

Measurement	Technique/Comments	Difficulty	Section
Linewidth (unmodulated)	Heterodyne: high-resolution, sensitive	low	5.3.1
	Delayed self-heterodyne: ~10 kHz-1 GHz range	low	5.3.2
	Delayed self-homodyne: ~10 kHz-1 GHz range	very low	5.3.3
	Discriminator: phase noise and jitter	moderate	5.3.5
Optical spectrum	Heterodyne: measure any spectrums	low	5.4.1
	Gated delayed self-homodyne: symmetrical spectrum	low	5.4.2
Frequency chirp measurement	Coherent discriminator: oscilloscope	moderate	5.5
Swept FM measurement	Coherent discriminator: network analyzer	moderate	5.6

Sections 5.5 and 5.6 concern the measurement of time-domain laser chirp and frequency domain FM response.

5.2 BASIC CONCEPTS

Measurement Assumptions

Prior to delving deeper into the subject, it is worthwhile to discuss some constraints with respect to the measurement methods presented here. The lasers under test are assumed to operate in a single-longitudinal mode (SLM). This is another way of saying that all the resonant frequencies of the laser cavity are suppressed with the exception of a single-mode. Properly designed DFB and DBR lasers operate in a singlemode. An illustration of a laser spectrum (no modulation) is shown in Figure 5.1. The laser lineshape typically has a Lorentzian-shaped central peak,[2,3] small sidebands caused by relaxation oscillations, and small sidemodes (cavity frequencies) located further away. Many of the measurement techniques presented in this chapter are only valid in the SLM regime. Optical mixing or interference (see Section 5.5.5) plays a key role in the measurement methods presented here. To obtain efficient interference, the following conditions are required between the interfering beams:

- polarization alignment
- spatial overlap

All of the optical fiber in the circuits discussed in this chapter are singlemode. Singlemode fiber insures good spatial overlap of the optical waves that are combined in the measurement setups. Often, the optical fiber used in the measurement setups allow the po-

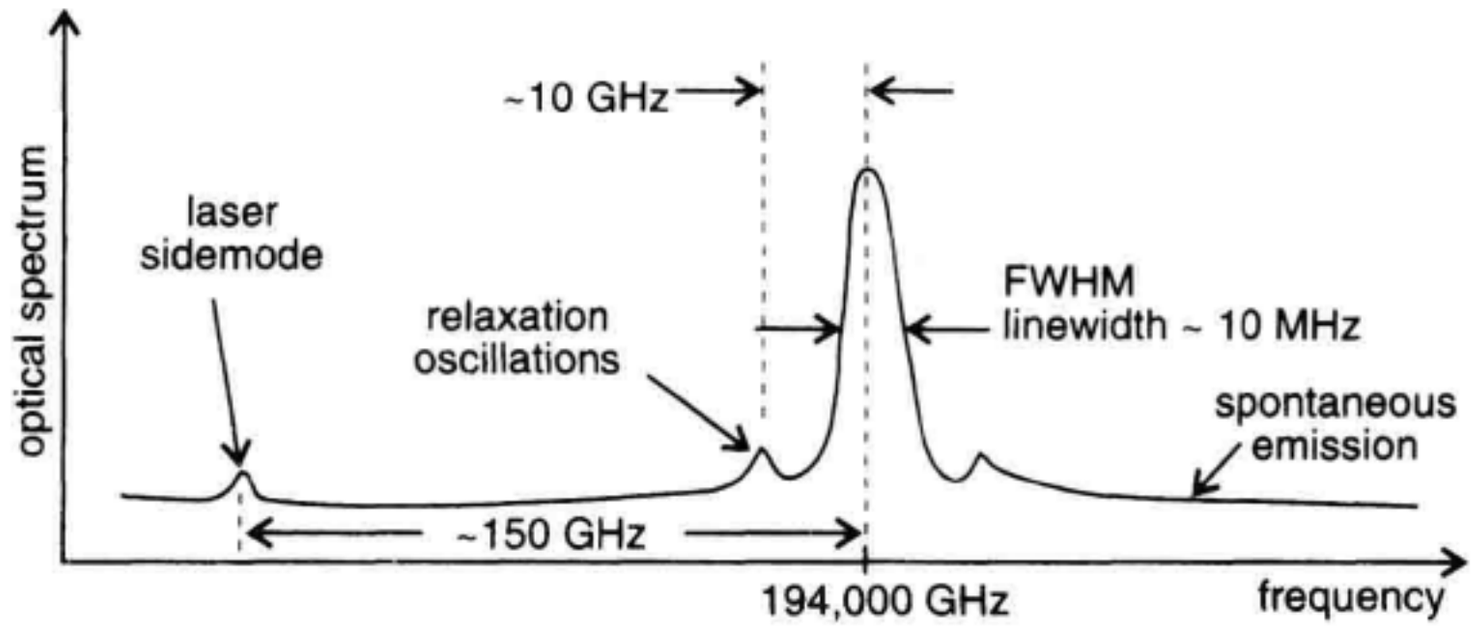

Figure 5.1 Laser spectrum with central peak, relaxation oscillation peaks, laser side-modes, and spontaneous emission.

larization states of the propagating light to freely evolve without any control. To overcome this problem, polarization state controllers are often placed in the measurement circuits to permit polarization alignment.

Coherence Time

The coherence time, τ_c, of a laser is a measure of the spectral purity of the laser frequency over time. In two-path interferometers, the degree to which an optical wave interferes with a time-delayed portion of itself depends on the coherence time of the wave with respect to the optical delay. Coherence time is reduced by random events, such as spontaneous emission in the laser cavity, which alter the phase or frequency of the laser-output field. This is illustrated in Figure 5.2. In Figure 5.2(a), the coherence time is longer since the phase is predictable during the interval of time T_1–T_2. In Figure 5.2b random phase changes cause an uncertainty in the phase relation between time T_1 and time T_2. The coherence time, τ_c, varies inversely with laser linewidth, $\Delta\upsilon$. It is defined for spectra with Lorentzian lineshapes as

$$\tau_c = \frac{1}{\pi\Delta\nu} \tag{5.1}$$

Thus as the source linewidth increases, the coherence time decreases. The related concept of coherence length, L_c, is also used in discussions on interferometry. The coherence length is simply the coherence time multipled by the velocity of light: $v_g = c/n_g$, where n_g, the group velocity index, is approximately 1.47 in optical fiber

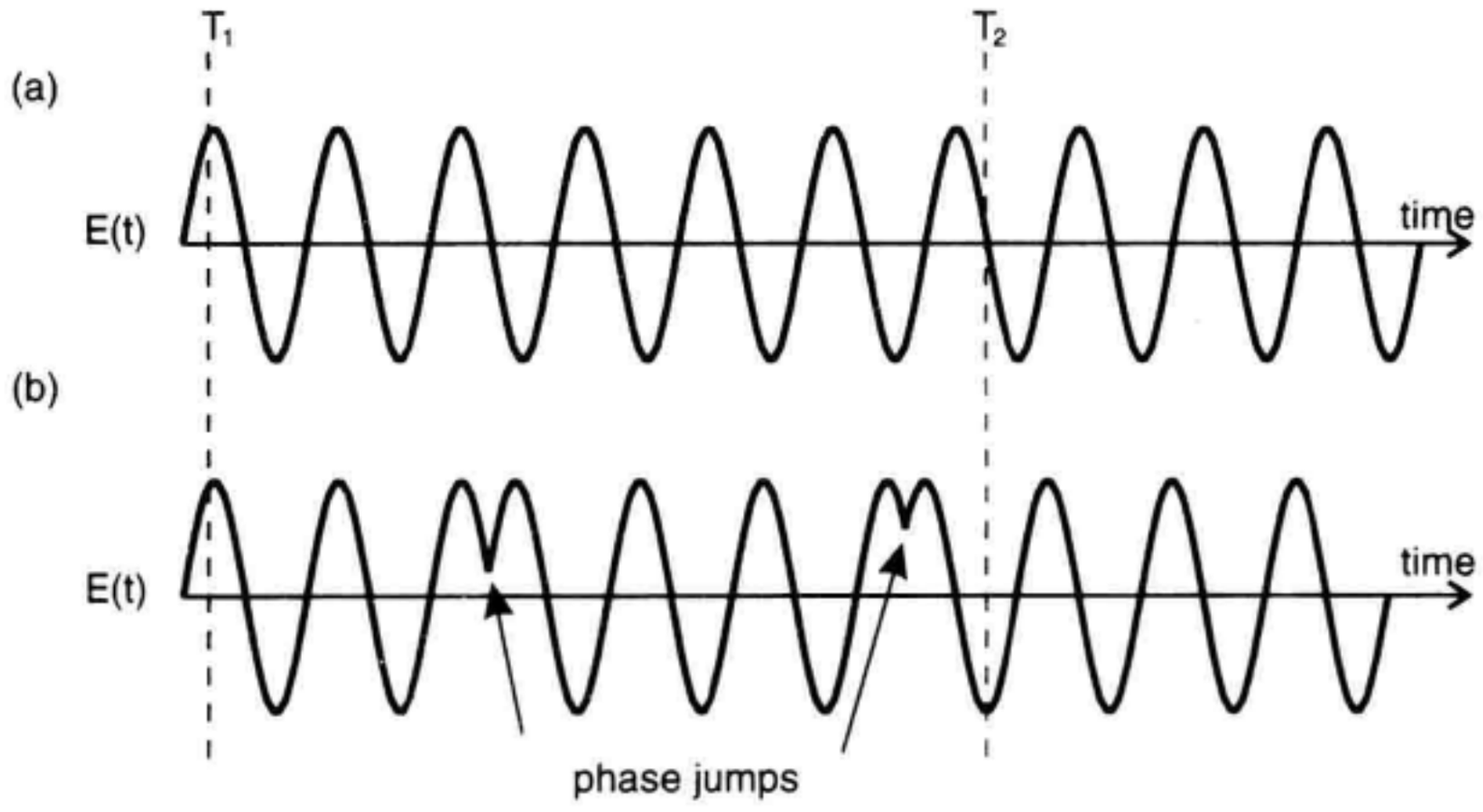

Figure 5.2 Concept of coherence time. (a) Coherent light: across the time interval the phase of the optical field is predictable. (b) Short coherence: random phase jumps cause the phase of the optical field to be uncertain across the time interval.

$$L_c = \nu_g \tau_c \tag{5.2}$$

As an example, consider a laser with a linewidth of 10 MHz. The coherence time and coherence length from Equations 5.1 and 5.2 are 32 ns and 6.5 m respectively.

5.2.1 Linewidth and Chirp

The two dominant causes of spectral broadening in single-longitudinal-mode lasers are phase noise and frequency chirp. Random phase noise is created when spontaneous-emission, originating in the laser cavity gain media, changes the phase of the freerunning laser frequency. This process is magnified by physical effects within the laser cavity. The magnification is quantified by the laser's effective amplitude-phase coupling factor, α_{eff}. A large value of α_{eff} results in increased laser linewidth. More generally, α_{eff} represents the link between power changes in the laser cavity to phase changes of the emitted light. The result is a broadening of the laser spectral linewidth. Another laser process, known as relaxation oscillations, (see Figure 5.1) causes subsidiary peaks centered around the central mode of the laser. These peaks generally lie within 20 GHz of the carrier and are much smaller in amplitude than the main peak.

Laser frequency chirp results in significant spectral broadening when the laser injection current is modulated.[4] The unwanted frequency modulation, or chirp, can broaden the laser spectrum well beyond the freerunning optical linewidth. The magnitude of the chirp is proportional to the amplitude-phase coupling factor α_{eff}. Material and structural properties of the laser contribute to the value of α_{eff}, hence the resulting chirp. Laser chirp (without intensity modulation) is illustrated in Figure. 5.3. The sweeping of the optical phase is due to the presence of frequency modulation or chirp on the optical carrier. A laser undergoing intensity modulation at 2.5 Gbit/s can occupy more than 25 GHz of optical spectrum caused by laser chirp. More detail on laser linewidth, relaxation oscillations, and chirp can be found in Agrawal,[3] Henry,[5] and references therein.

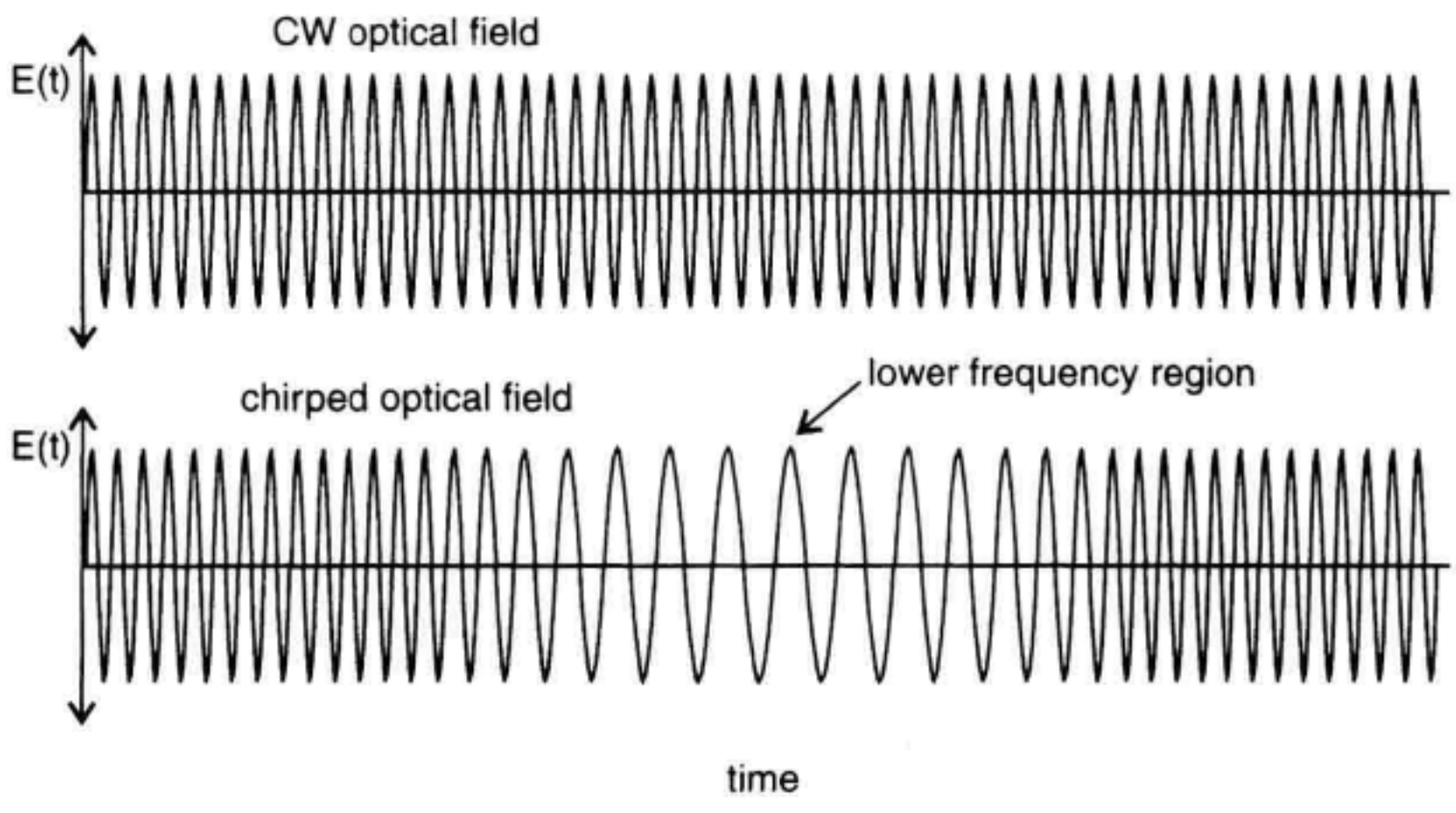

Figure 5.3 Optical field with and without frequency chirp.

Some relations for estimating the laser linewidth, the relaxation resonance frequency, and the chirp of a semiconductor laser are given here. These relations are pertinent to the measurement process since it is important to note relevant experimental conditions when making measurements. The equations below, while not complete, will help indicate some of the dependencies. The variables and constants are defined in Table 5.2.

Static Linewidth

$$\Delta\nu_1 = \frac{1}{4\pi P} n_{sp} (1 + \alpha_{\text{eff}}^2) h\nu \frac{\log(1/R)}{\tau_p \tau_{rt}} \tag{5.3}$$

Small Signal Chirp

$$\Delta\nu_{\max} = \frac{\alpha_{\text{eff}} m f_m}{2} \tag{5.4}$$

Large Signal Chirp

$$\Delta\nu_c = \frac{\alpha_{\text{eff}}}{4\pi} \left(\frac{1}{P} \frac{\partial P}{\partial t} \right) \tag{5.5}$$

Table 5.2 Variable Definitions

Symbol	Description	Typical Range of Values
$\Delta\nu$	FWHM optical linewidth (without modulation)	0.01–100 MHz
P	optical output power	0.1–500 mW
n_{sp}	spontaneous emission factor	~2.5
α_{eff}	effective amplitude-phase coupling coefficient	−1–10
h	Planck's constant	6.634×10^{-34} J-s
ν	optical frequency	193 THz@λ = 1.55 μm
R	laser facet reflectivity	~ 0.30
τ_p	cold cavity photon lifetime	1 ~ 2 ps
τ_{rt}	laser cavity round-trip delay	~ 0.5 ps
m	intensity modulation index	0–1
f_m	frequency of sinudoidal intensity modulation	0–20 GHz
$\Delta\nu_c$	transient frequency chirp (with modulation)	~1 to 100 GHz
$\frac{\partial P}{\partial t}$	rate of change with time of the optical intensity	W/s

Example

A laser has an effective amplitude-phase coupling factor, $\alpha_{eff} = 5$. If the laser, undergoing 2.5 Gb/s intensity modulation has an intensity slope of 5 mW/30 ps at 4 mW average output, estimate the transient frequency chirp.

Solution

Using Equation 5.5 and $\frac{\partial P}{\partial t} = 1.67 \times 10^8\ W/s$
the chirp $\Delta\nu \gtrsim_c$ is estimated to be approximately 20 GHz.

5.2.2 Interference between Two Optical Fields

In this section, we examine some of the basics of interference between two optical fields. The concept of interference will be central to the measurement techniques of this chapter. The heterodyne case will be discussed first. This case uses a local oscillator laser as a measurement reference to measure a second signal source with unknown spectral characteristics. Interference of a wave with a delayed version of itself will also be examined. In both cases, we shall see that interference between waves causes intensity variations that are detectable using a photodiode. When the photocurrent is analyzed with electronic instrumentation, information on the optical carrier variations can be obtained. In this chapter, frequency will be denoted by both f and ν. f will represent frequencies below ~100 GHz and υ will denote frequencies above ~100,000 GHz.

Heterodyne: Interference between Two Fields. Consider the two optical fields incident on the photodetector after passing through the combiner as shown in Figure 5.4:

$$E_s(t) = \sqrt{P_s(t)}\, e^{j(2\pi\nu_s t + \phi_s(t))} \tag{5.6}$$

$$E_{LO}(t) = \sqrt{P_{LO}}\, e^{j(2\pi\nu_{LO} t + \phi_{LO}(t))} \tag{5.7}$$

These two fields are scaled such that their magnitudes squared are optical powers (in other words, $P(t) = |E(t)|^2$). The optical field frequencies and phases are designated by ν and $\phi(t)$. If either field were separately detected on a photodetector, the resulting photocurrent would follow only the power variations, $P(t)$, and all phase information would be lost. The optical phase $\phi(t)$ takes into account any laser-phase noise or optical frequency modulation. The value of υ at a wavelength of 1.55 μm is 194,000 GHz. Thus the

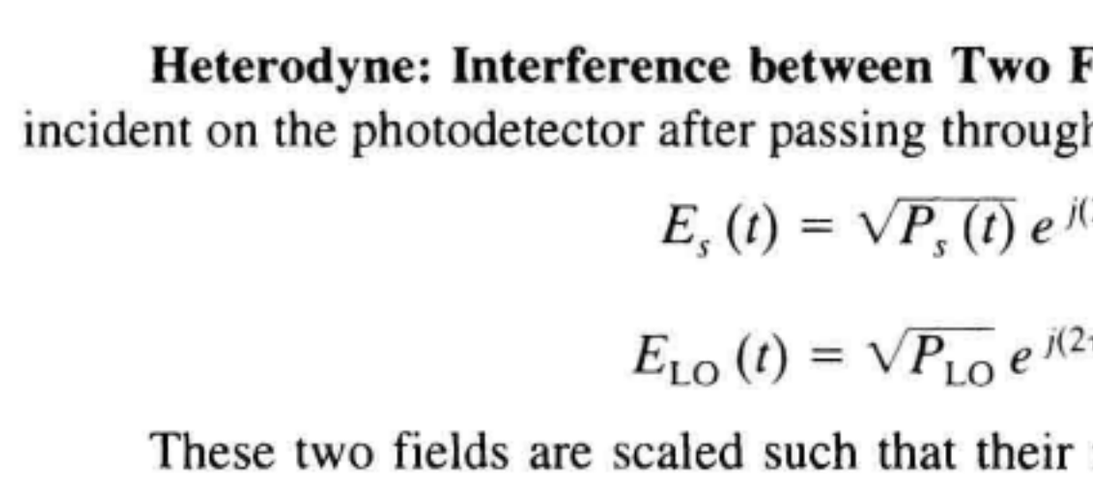

Figure 5.4 Setup for interfering two optical fields. The electrical spectrum analyzer display is proportional to the photocurrent power spectrum.

total phase, $2\pi\nu t + \phi(t)$ of each optical field, changes at a rate much too fast for electronic instrumentation to respond. The optical spectrum corresponding to the two fields is shown in Figure 5.5a. Here the local oscillator has constant power and the signal laser has a small intensity modulation index of m. To obtain the correct spectral display, the local oscillator frequency is set to a lower optical frequency than the signal under study. The optical combiner delivers the spatially overlapped optical fields to the photodetector where interference is detected. The total field $E_T(t)$ at the photodetector is:

$$E_T(t) = E_s(t) + E_{\text{LO}}(t) \tag{5.8}$$

Since power is detected (in other words, $P(t) = |E_T(t)|^2$), and not the optical field itself, photodetection is nonlinear with respect to the optical field. This fortunate situation allows us to detect interference between fields. The photocurrent generated in the detector is proportional to the squared magnitude of the field.

$$i(t) = \mathcal{R}|E_T(t)|^2 \tag{5.9}$$

where $\mathcal{R}$ is the detector responsivity given by

$$\mathcal{R} = \frac{\eta_d q}{h\nu} \ [A/W] \tag{5.10}$$

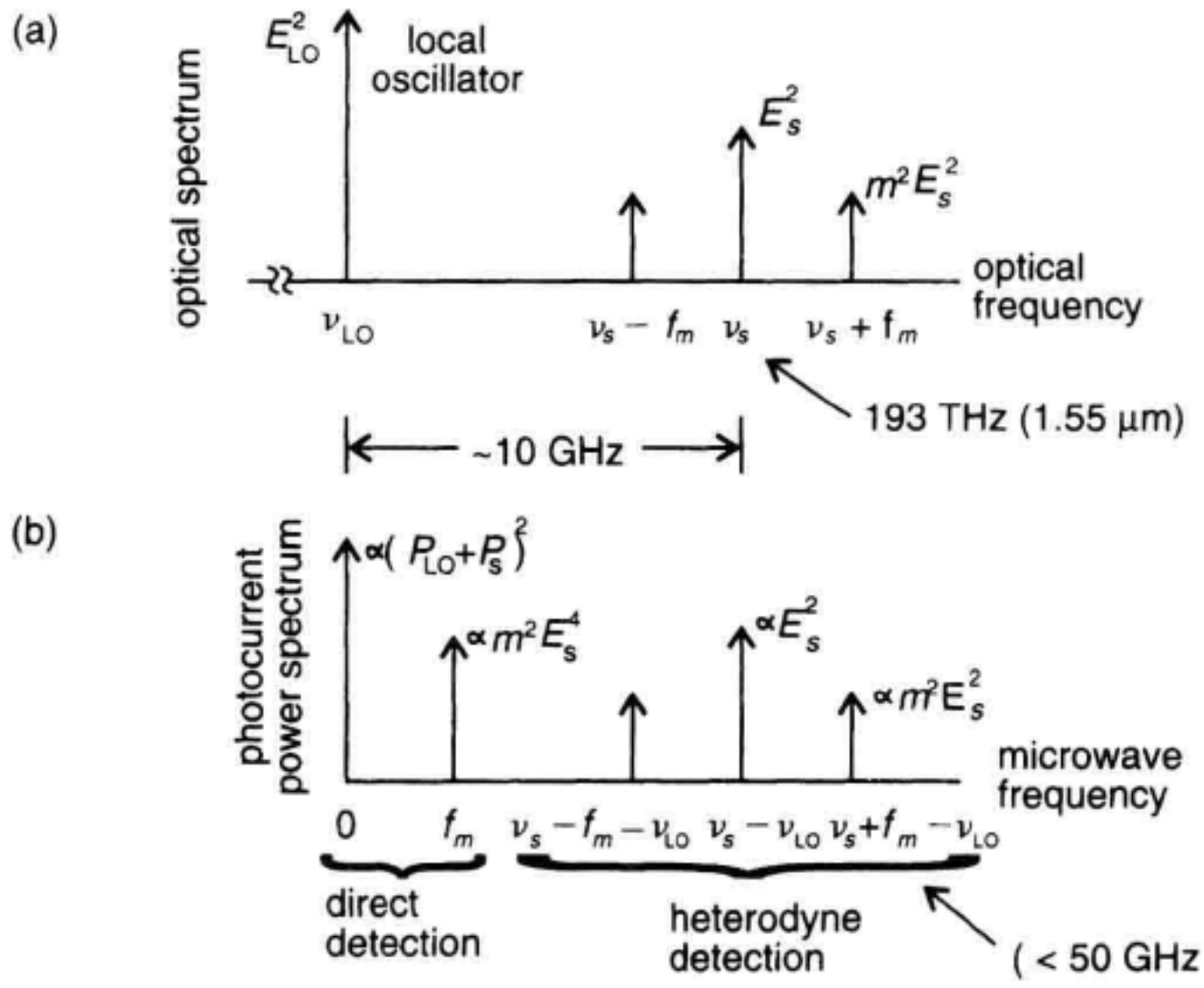

Figure 5.5 (a) Optical spectrum of modulated light. (b) Photocurrent spectrum after heterodyne translation of the optical spectrum to low frequencies for electronic analysis.

where η_d ($0 < \eta_d \leq 1$) is the detector quantum efficiency, a measure of the conversion efficiency of incident photons into electrical charge. The parameters q and $h\upsilon$ are electronic charge (1.6021×10^{-19}C) and photon energy ($h = 6.6256 \times 10^{-34}$ J, $\nu = c/\lambda$) respectively. Substituting Equation 5.6, 5.7, and 5.8 into 5.9 we obtain using $f_{IF} = \nu_s - \nu_{LO}$ and $\Delta\phi(t) = \phi_s(t) - \phi_{LO}(t)$:

$$i(t) = \mathcal{R}[P_s(t) + P_{LO} + 2\sqrt{P_s(t)P_{LO}}\cos(2\pi f_{IF}t + \Delta\phi(t))] \tag{5.11}$$

The first two terms correspond to the direct intensity detection of $E_s(t)$ and $E_{LO}(t)$. The third term is the important heterodyne mixing term. Note that the actual optical frequency is gone and only the difference frequency is left. Thus the heterodyne method is able to shift spectral information from high optical frequencies to frequencies that can be measured with electronics as shown in Figure 5.5b. In the heterodyne method, the local oscillator serves as a reference, with known frequency, amplitude, and phase characteristics. Thus the signal spectrum, including both intensity and frequency contributions can be obtained. Equation 5.11 will be used later on in Section 5.3 in the discussions on optical heterodyne.

Self-Homodyne: Interference between a Field and a Delayed Replica. Next we will consider the case where one of the two interfering optical fields is a delayed version of the other. This condition can be created by a variety of two-path optical circuits such as the Mach-Zehnder and Michelson interferometers (see Chapter 4) as well as Fabry-Perot interferometers. A Mach-Zehnder interferometer is shown in Figure 5.6a. The input field is split and routed along two paths with unequal lengths. Time τ_o is the differential time delay between the two fields traversing the two arms of the interferometer. The photocurrent generated at the detector is found in a similar way as with the heterodyne case

$$i(t) = \mathcal{R}[P_1(t) + P_2(t) + 2\sqrt{P_1 P_2}\cos(2\pi\nu_o\tau_o + \Delta\phi(t,\tau_o))] \tag{5.12}$$

where $P_1(t)$ and $P_2(t)$ are the powers delivered to the photodetector from each interferometer path. The average phase-setting of the interferometer is given by $2\pi\nu_o\tau_o$ and $\Delta\phi(t,\tau_o) = \phi(t) - \phi(t - \tau_o)$ is the time-varying phase difference caused by phase or frequency modulation of the input signal, and the interferometer delay τ_o. The interferometer free-spectral range (FSR) is defined as the change in optical frequency, to obtain a phase shift of 2π between the two combining fields. In other words, it is the frequency difference between the two peaks shown in Figure 5.6b. Obviously, from Equation 5.12, the FSR is the reciprocal of the net interferometer differential delay, τ_o.

Assuming $\Delta\phi(t, \tau_o)$ is small, varying the interferometer delay or the average optical frequency can cause the photocurrent to swing from minimum to maximum as shown in

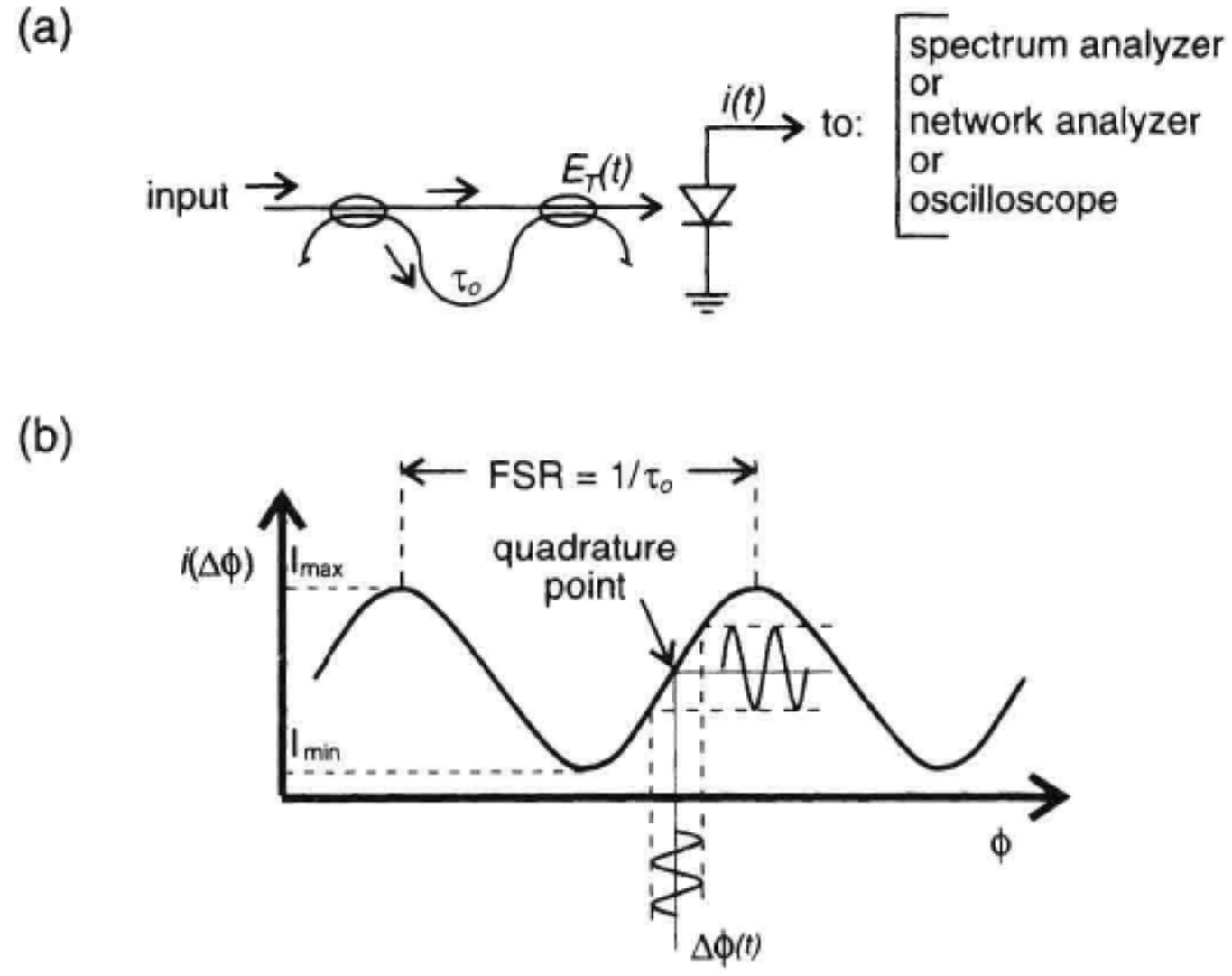

Figure 5.6 (a) Mach-Zehnder interferometer with optical detection and instrumentation for analysis of photocurrent. (b) Dependence of interferometer output on the phase difference between the interfering fields. FSR = free spectral range.

Figure 5.6b. Limitations to the minimum and maximum current swings can be caused by a lack of polarization alignment between the fields, mismatch between path losses through the interferometer, or the limited coherence time of the optical source.

If the average phase $2\pi\nu_o\tau_o$ is equal to $\pi/2$, or more generally, equal to $\pi(2n + 1/2)$, $n = 0, 1, 2, \ldots$, the interferometer is biased in quadrature. This point is indicated in Figure 5.6b. When an interferometer is biased at quadrature, it can linearly transform small optical-phase excursions $\Delta\phi(t,\tau_o)$ into photocurrent variations. This is because the cosine characteristic varies linearly for small changes, $\Delta\phi(t, \tau_o)$ about the quadrature point. Thus the interferometer can function as a frequency discriminator as long as operation is confined to the approximately linear part of the interferometer transfer characteristic. At the quadrature point, Equation 5.12 becomes:

$$i(t) = \mathcal{R}[P_1(t) + P_2(t) + 2\sqrt{P_1(t)P_2(t)}\sin(\Delta\phi(t, \tau_o))] \tag{5.13}$$

If $\Delta\phi(t, \tau_o)$ is small such that the approximation $\sin(\Delta\phi(t, \tau_o)) \approx \Delta\phi(t, \tau_o)$ is valid, then the discriminator acts as a linear transducer converting phase or frequency modulation into power variations that can be measured with a photodetector:

$$i(t) = \mathcal{R}[P_1(t) + P_2(t) + 2\sqrt{P_1(t)P_2(t)}\,\Delta\phi(t, \tau_o)] \tag{5.14}$$

The first two terms correspond to simple direct detection, the third term is the useful interference signal. In Sections 5.3.5, 5.5, and 5.6, the application of the interferometer as a discriminator to measure laser-phase noise, time-domain chirp, and FM response is pre-

sented. In these applications, the interferometer delay, τ_o, must be smaller than the source coherence time τ_c to maintain good interferometer contrast, which is a measure of the difference between I_{max} and I_{min} in Figure 6b.

5.3 LASER LINEWIDTH CHARACTERIZATION

In this section, several methods for linewidth characterization of freerunning (unmodulated) singlemode lasers are discussed. Linewidth is often defined in terms of the full-width half-maximum (FWHM) of the optical field power spectrum. Grating-based optical spectrum analyzers (OSAs) don't offer the measurement resolution required for laser linewidth measurement, so alternative characterization methods must be used. The alternative methods brought forth here include the optical heterodyne method, the delayed self-heterodyne method, the delayed self-homodyne method, and an optical discriminator technique. These methods are capable of obtaining the extremely high resolution required for laser linewidth measurements. Understanding the advantages and limitations of each of the methods will aid in deciding which method is best in a particular application. At the end of this section the strengths and weaknesses of the various methods are generalized.

5.3.1 Heterodyne Using a Local Oscillator

Heterodyne analysis is the only technique presented in this chapter capable of characterizing nonsymmetrical spectral lineshapes. Not only will the heterodyne method provide linewidth data, it also is used to measure the optical power spectrum of an unknown optical signal. This method offers exceptional sensitivity and resolution. The key component required for these measurements is a stable, narrow linewidth reference laser.

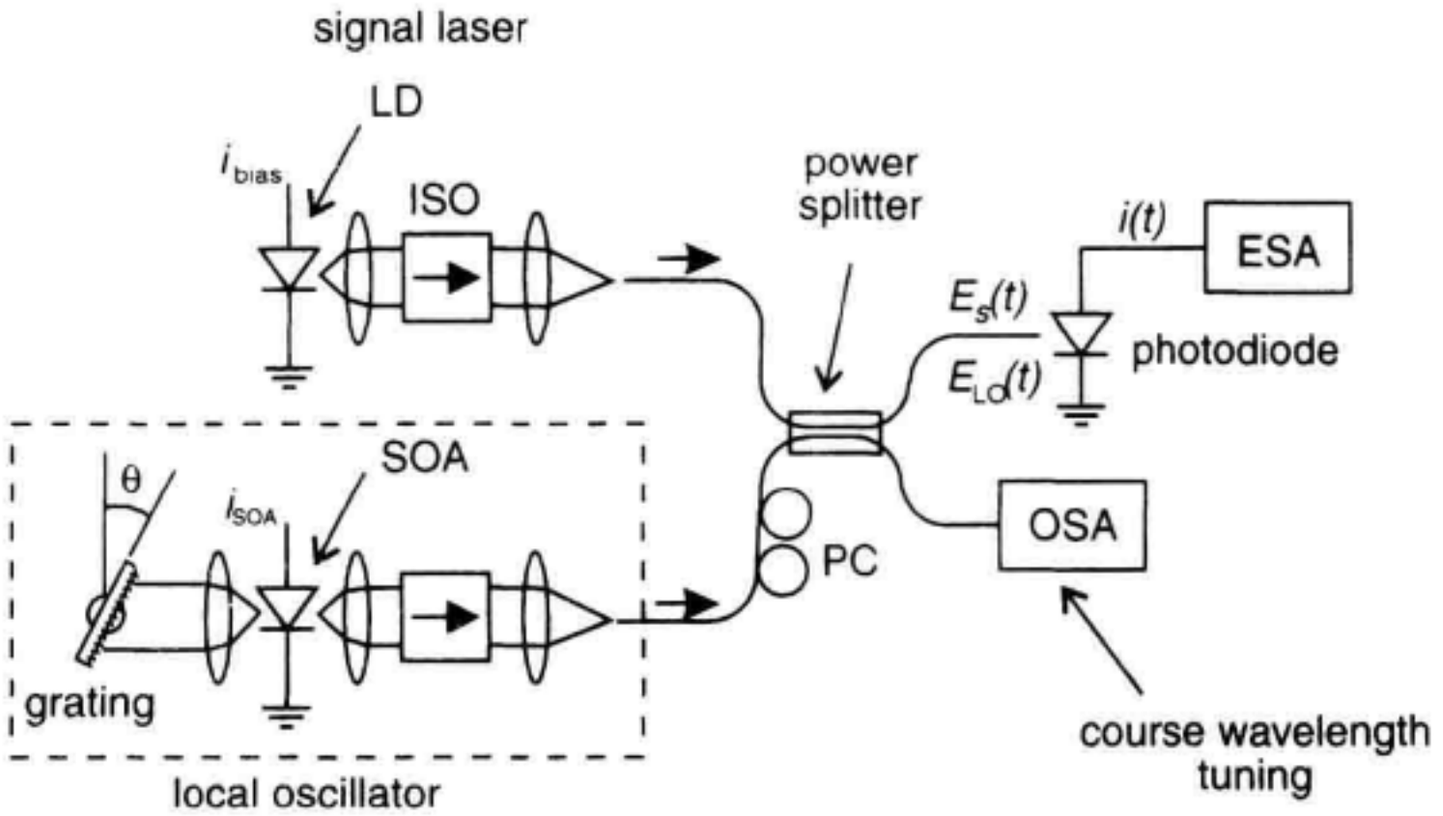

Figure 5.7 Optical heterodyne setup for measuring laser linewidth using an external cavity laser for local oscillator. SOA = semiconductor optical amplifier, ISO = optical isolator, LD = semiconductor laser diode, PC = polarization state controller.

The setup for optical heterodyne discussed here is illustrated in Figure 5.7. In this setup, the reference laser (local oscillator) is tuned appropriately and then its optical frequency is fixed during the measurement. This is possible because of the wide analysis bandwidth offered by electrical spectrum analyzers. An alternative way would be to have a narrow bandwidth electrical detection and a swept local oscillator. This alternative method[6] sets stringent requirements on the tuning fidelity of the local oscillator and will not be discussed further here. In Figure 5.7, light from the local oscillator (LO) is combined with the signal laser under test. A grating-tuned external cavity diode laser is used as the LO in this example. Polarization state converters are placed in the LO path to align the polarization state of the local oscillator to that of the signal under test. The coupler combines the two fields, delivering half the total power to each output port. One port leads to a photodetector which detects the interference beat tone, converting it to an electrical tone. Note that the local oscillator laser frequency must be tuned close to the signal laser frequency to allow the mixing product to fall within the bandwidth of typical detection electronics. A course alignment of the local oscillator wavelength is performed using an OSA or a wavelength meter. The local oscillator frequency is tuned to a frequency just lower than the average frequency of the laser under study. This creates a heterodyne beat tone between the LO and each of the frequency components in the signal spectrum as indicated in Figure 5.8. Thus each frequency component is translated to a low-frequency interference term described by:

$$i(t) = \mathcal{R}[P_s(t) + P_{LO} + 2\sqrt{P_s(t)P_{LO}}\cos(2\pi(\nu_s - \nu_{LO})\,t + \Delta\phi(t))] \qquad (5.15)$$

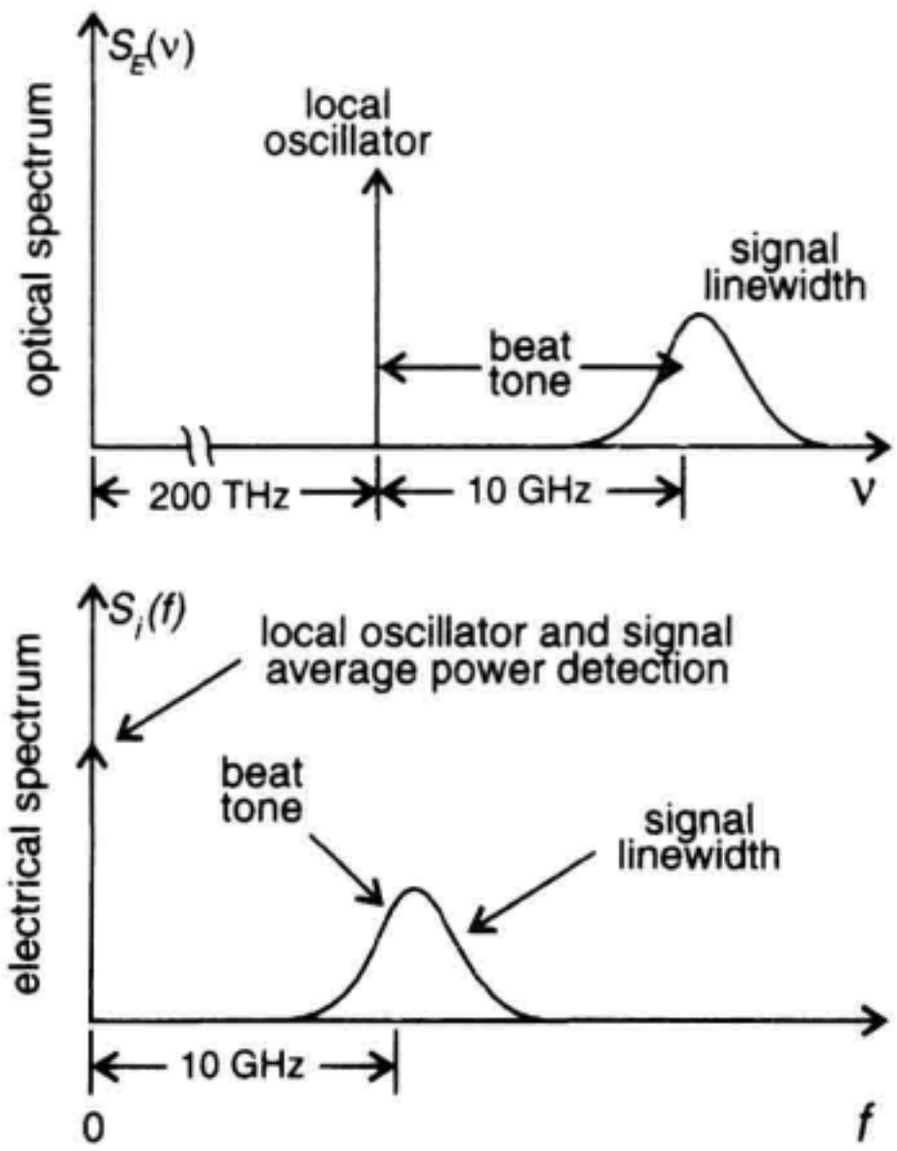

Figure 5.8 The mixing process in terms of beat-tone slices mixed down to low frequencies that can be analyzed with electronic instrumentation.

If the local-oscillator phase noise is small with respect to the test laser, the beat tone will be broadened primarily by the phase noise $\Delta\phi(t) \sim \phi_s(t)$ of the laser under study. The beat frequencies due to signal phase noise are measured using an ESA.

Heterodyne Power Spectrum. The ESA display is proportional to the power spectrum of the photodetector current which contains products of optical heterodyne mixing as well as direct detection terms[7,8]

$$S_i(f) \approx \mathcal{R}^2 \{S_d(f) + 2[S_{LO}(\nu) \otimes S_s(-\nu)]\} \tag{5.16}$$

(ESA $\Rightarrow$ direct detection + heterodyne spectrum)

$S_d(f)$ is the ordinary direct detection that could be measured with just a photodetector and ESA. The second term is the useful heterodyne mixing product which is the convolution of the local oscillator spectrum $S_{LO}(\nu)$ with the signal spectrum $S_s(\nu)$. The convolution originates from the multiplication of the time-varying local oscillator field with the signal field in the photodetector. Multiplication in the time domain is equivalent to convolution in the frequency domain. The lineshape of the laser, including any asymmetries, is replicated at a low frequency set by the optical frequency difference between the two lasers. The convolution given in Equation 5.16 is illustrated in Figure 5.9. As the convolution scans the LO lineshape (Dirac-Δ function as shown) from negative infinity, it passes to zero at ν_{LO}, traces out the test-laser lineshape and continues to positive infinity. The net result is a translation of the test-laser lineshape to the average difference frequency between the LO and the test laser. Note from Equation 5.15 that as the LO linewidth broadens, its linewidth can dominate the photocurrent spectrum and decrease the frequency resolution of the heterodyne measurement.

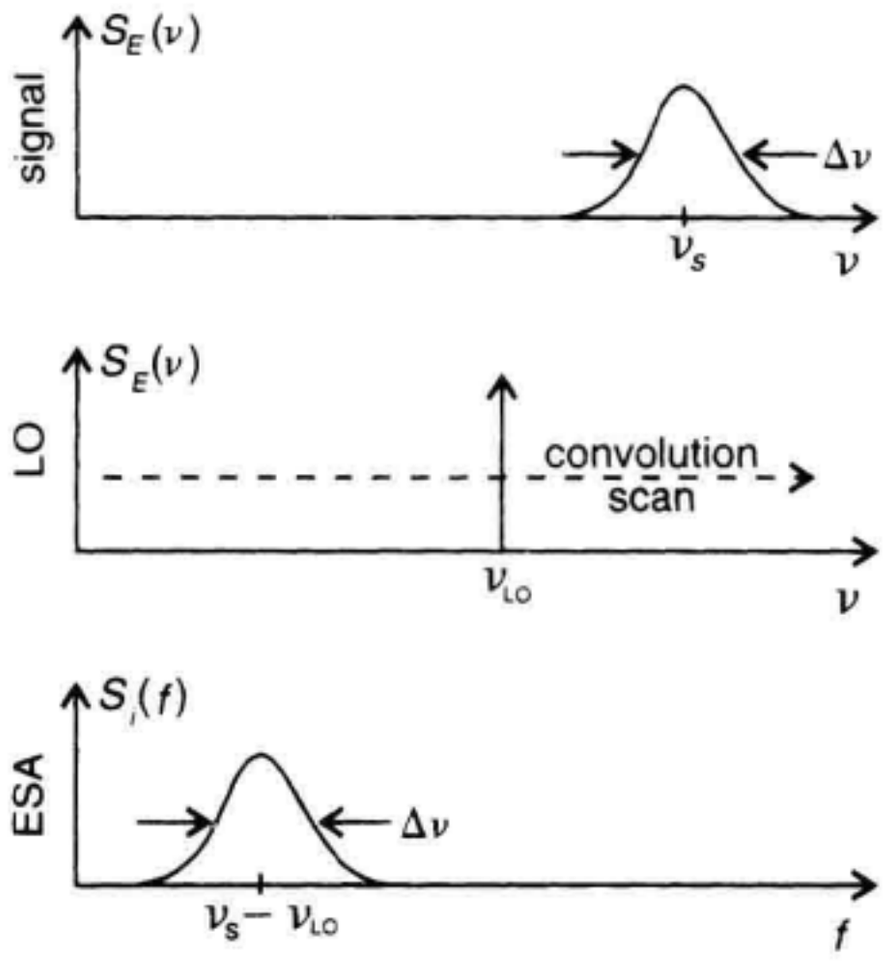

Figure 5.9 Convolution of narrow linewidth laser translates signal spectrum to low frequencies.

If the LO laser linewidth is small compared to the laser under test, the lineshape spectrum of the local oscillator, $S_{LO}(\nu)$ is approximated with a Dirac-Δ function: P_{LO} $\delta(\nu - \nu_{LO})$. Thus from Equation 5.16 the ESA will display:

$$S_i(f) \approx 2\mathcal{R}^2 P_{LO} S_s(\nu - \nu_{LO}) \tag{5.17}$$

Thus the ESA gives a measure proportional to the actual laser power spectrum $S_s(\upsilon)$ translated to low frequencies accessible to electronics. The key to the exceptional sensitivity of the heterodyne method is evident in Equation 5.17 where the detected spectrum strength increases with local oscillator power, P_{LO}. Large local oscillator power translates to better sensitivity.

Signal-to-Noise Ratio. The measurement signal-to-noise ratio, SNR, is the ratio of the detected heterodyne signal to all of the noise contributions. These noise contributions include the receiver thermal noise, local oscillator RIN, and interference noise. Interference noise is due to optical reflections in the measurement setup that convert laser phase noise into intensity noise which is detected at the receiver (see Section 5.3.3). The best performance is achieved when the dominant noise contribution is the shot noise from the local oscillator. In this case, the detection is said to be quantum-limited or shot-noise limited. The SNR for this case is:

$$\left(\frac{S}{N}\right)_{\text{shot noise limit}} = \frac{\mathcal{R} P_s}{q B_e} \tag{5.18}$$

where P_s is the optical-signal power incident on the photodetector and B_e is the electrical bandwidth of the ESA. Note that this shot-noise limited sensitivity is independent of the local oscillator power and the minimum detectable power is approximately equal to a single photon within the electrical detection response time.

Example

Estimate the minimum detectable signal for the case of heterodyne detection with a $B_e = 100$ kHz electrical bandwidth and a strong local oscillator power.

Solution

The minimum detectable signal is estimated by setting the signal-to-noise ratio to unity. Using $q = 1.602 \times 10^{-19}$ and solving for P_s we obtain:

$$P_s \simeq 2 \times 10^{-14}\, W \text{ or } -107 \text{ dBm}.$$

Frequency Resolution. Several effects contribute to the net frequency resolution of the linewidth measurement. The measured spectrum is a convolution (see Equation 5.16) of the signal-field power spectrum with that of the local oscillator laser. This sets the minimum spectral resolution equal to the linewidth of the local oscillator. The linewidth of typical tunable external cavity semiconductor lasers is typically of the order of 100 kHz. However, in practice, the effective linewidth can be much greater due to fre-

quency jitter or 1/f frequency noise. Frequency jitter is the random change in the operating frequency of the laser over time. It is usually caused by environmentally-induced changes in the laser cavity. The time scales for frequency jitter are slow, typically less than a microsecond, but they can still be faster than the integration time of the electronic spectrum analysis. When the measurement averaging time takes a few seconds, the effective linewidth of an external cavity laser can easily be a factor of ten greater (several MHz). Another contributing factor to frequency resolution is the resolution bandwidth of the electrical spectrum analyzer. The resolution bandwidth filter should be set so as not to limit the desired measurement resolution.

Experiment. The beat spectrum of two semiconductor lasers separated in optical frequency by 8.3 GHz is shown in Figure 5.10. The full-width half-maximum, FWHM, linewidth of a laser is often measured with respect to an assumed Lorentzian spectral shape. The displayed FWHM response is the sum of the laser linewidth and the local oscillator linewidth. Therefore, a narrow LO linewidth is desirable to clearly resolve the laser-under-test linewidth. Often there is frequency jitter as discussed earlier. The effect of frequency jitter is to widen the displayed lineshape. The effects of frequency jitter on the linewidth measurement can be reduced by measuring further down on the displayed lineshape as shown in Figure 5.10. The measured result is then transformed into the correct FWHM linewidth. The advantages of measuring further down on the lineshape can be understood by considering the effect of frequency jitter, on the power spectrum. The Lorentzian-optical power spectrum centered at ν_o has a functional form given by:

$$S_E(\nu) \sim \frac{1}{1 + \left[\frac{\nu - \nu_o}{\Delta\nu/2}\right]^2} \tag{5.19}$$

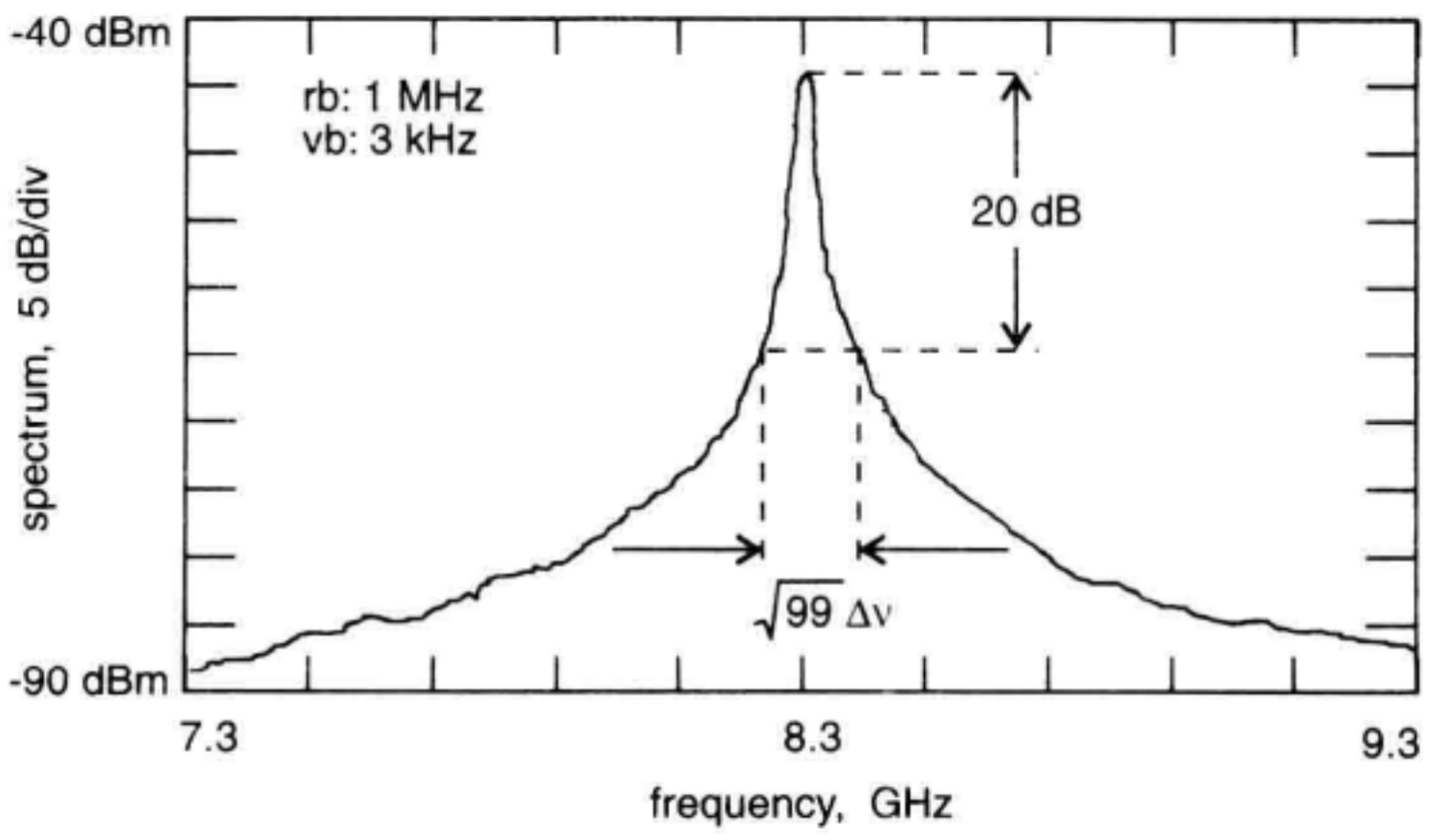

Figure 5.10 Laser linewidth measurement using optical heterodyne method.

Where $\Delta\nu$ is the FWHM linewidth and ν is optical frequency. When $\nu - \nu_o$ is zero, $S_E(\nu)$ is maximum. As $\nu - \nu_o$ increases, the magnitude falls off in a way characteristic of the Lorentzian function. If frequency jitter $\delta\nu(t)$ is present the spectrum "jitters around" in time:

$$S_E(\nu, t) \sim \frac{1}{1 + \left[\dfrac{\nu - \nu_o + \delta\nu(t)}{\Delta\nu/2}\right]^2} \tag{5.20}$$

When $\nu - \nu_o$ is small, on the order of $\delta\nu$, variations in $\delta\nu$ cause significant changes in the amplitude of $S_E(\nu)$ and hence the measured FWHM linewidth. As $\nu - \nu_o$ increases, relative to $\delta\nu$, the magnitude of the function depends more on the value of $\nu - \nu_o$ and less on the effects of $\delta\nu$. Thus the error due to frequency jitter decreases as the measurement is made further down the skirt of the lineshape, as long as the measurement SNR is adequate and the laser lineshape follows a known functional form.

For the usual case of a Lorentzian-shaped spectrum, the correspondence between the measured full-width at a specific power and the FWHM linewidth is shown in Table 5.3.

Experiment. In this experiment, the dependence of the test laser's optical frequency on bias current is characterized. The measurement setup consists of a wavelength-tunable external cavity laser and the test laser (DFB-LD) as shown in Figure 5.7. The grating-based OSA allows setting of the local oscillator to a slightly longer wavelength than that of the test-laser wavelength. The heterodyne beat frequency was set to a baseband frequency of 1.75 GHz by fine-tuning the local oscillator wavelength. The spectrums for three bias currents are shown in Figure 5.11. The DFB was initially biased at 70 mA. Decreasing the DFB laser current to 62 mA increased the DFB laser frequency, caused by thermal heating in the semiconductor cavity. This resulted in a 9.43 GHz separation between the local oscillator and the test-laser frequencies. When the injection current was set to 54 mA, the frequency difference increased to 16.73 GHz. From this data the DFB's optical frequency change, $\Delta\nu_o$ with bias current is:

$$\frac{\Delta\nu_o}{\Delta i} \approx -1\ \text{GHz/mA} \tag{5.21}$$

Table 5.3 Heterodyne Technique Linewidth Relations

Measured Full-Width Point	Corresponding Width
−3 dB	$\Delta\upsilon$
−10 dB	$\sqrt{9}\ \Delta\upsilon$
−20 dB	$\sqrt{99}\ \Delta\upsilon$
−30 dB	$\sqrt{999}\ \Delta\upsilon$

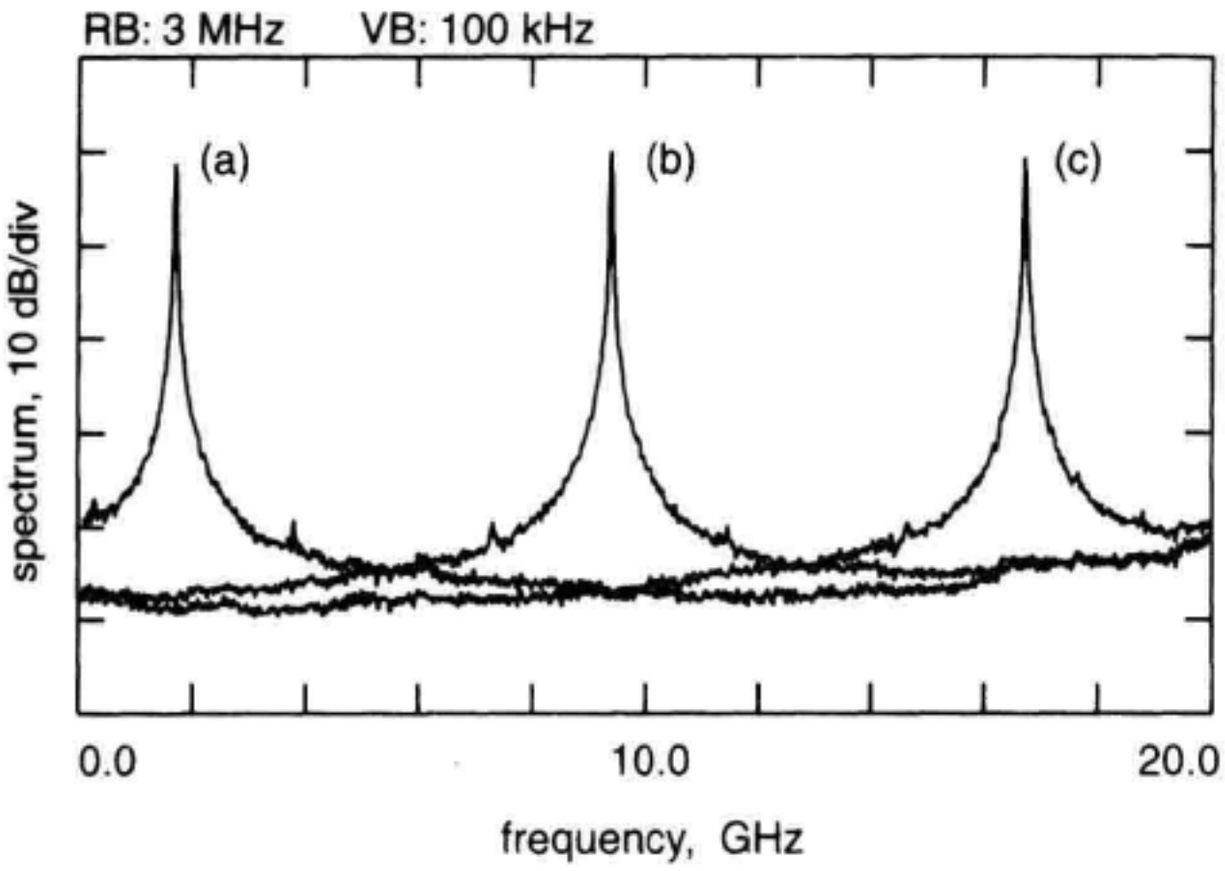

Figure 5.11 Optical heterodyne power spectrums of a DFB laser biased at a current of (a) 70 mA, (b) 62 mA, (c) 54 mA.

5.3.2 Delayed Self-Heterodyne

The delayed self-heterodyne technique provides a simple way to perform linewidth measurements without the requirement of a separate local oscillator laser. Taking advantage of the large optical delays attainable with optical fiber, Okoshi and co-workers demonstrated that linewidth measurements could be performed with a simple optical interferometer.[9] The delayed self-heterodyne concept is shown in Figure 5.12a. Incident light is split into two paths by the interferometer. The optical frequency of one arm is offset with respect to the other. If the delay, τ_o of one path exceeds the coherence time, τ_c of the source, the two combining beams interfere as if they originated from two independent lasers offset in frequency by $\delta\nu$ as shown in Figure 5.12b. Thus the system performs similarly to optical heterodyne. The beat tone produced is displaced from 0 Hz by the frequency shift by $\delta\nu$. An electrical spectrum analyzer displays the beat tone which is broadened by the laser linewidth. The translation of linewidth information from optical frequencies to low frequencies where electronics instrumentation operate is shown in Figure 5.13. As with the optical heterodyne case, the spectrum on the ESA is a convolution of the individual power spectrums of the interfering waves.

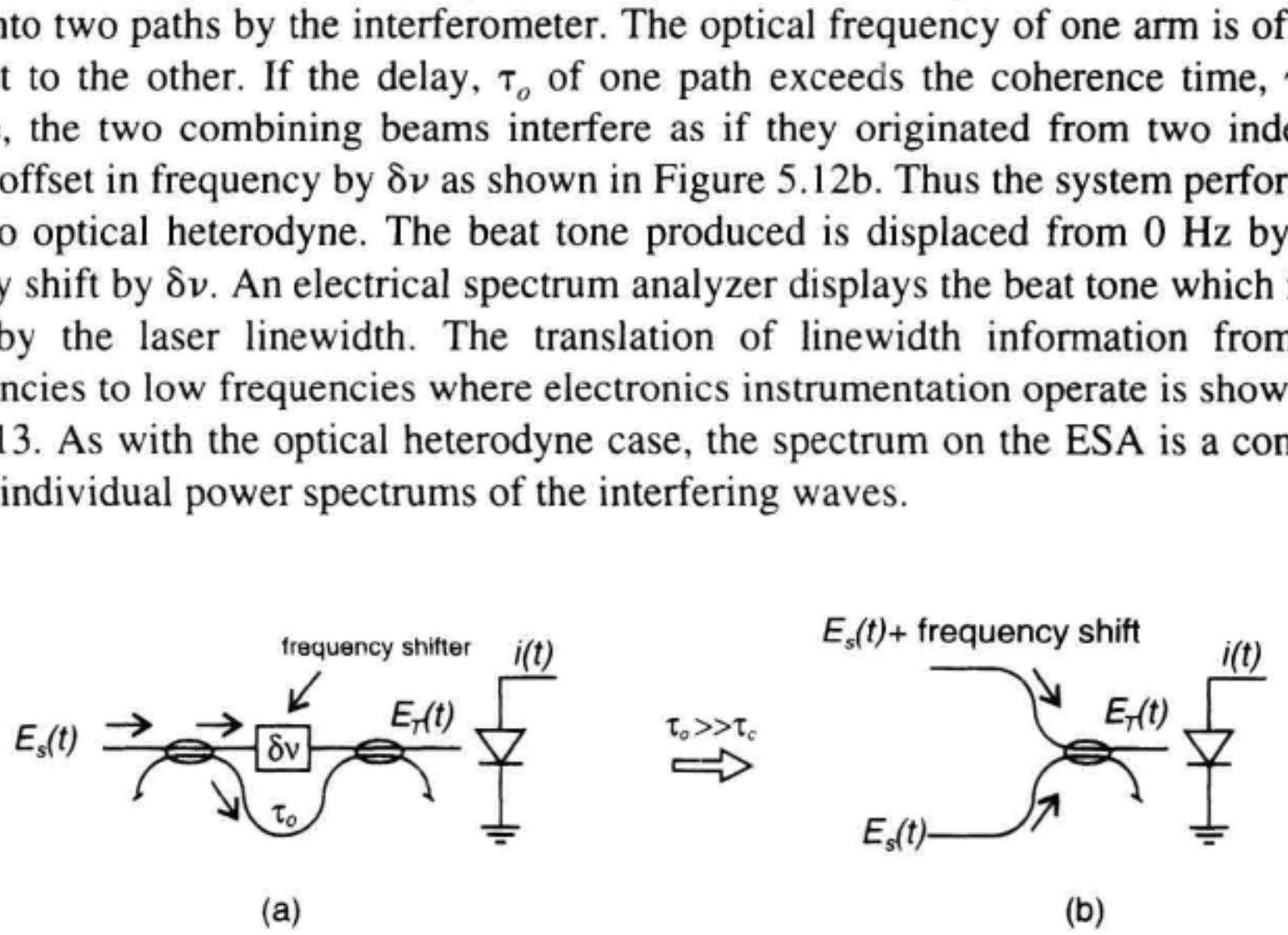

Figure 5.12 Delayed self-heterodyne method: (a) optical measurement setup, (b) equivalent circuit when the interferometer delay time is larger than the signal coherence time.

The requirement for incoherent mixing sets a minimum delay requirement of the interferometer with respect to the laser's linewidth:

$$\tau_o \geqslant \frac{1}{\Delta\nu} \tag{5.22}$$

When this condition is satisfied, the mixing becomes independent of the phases of the interfering light, leading to a more stable measurement. In Section 5.3.4, a more detailed analysis of the effects of laser coherence is given. For a linewidth of 10 MHz, the minimum required differential time delay will be about 100 ns. This corresponds to approximately 20 m of singlemode optical fiber. Note that given the large optical delays afforded by low-loss singlemode optical fiber, linewidth measurements below 10 kHz are possible.

Photocurrent Spectrum. Similar to the case of optical heterodyne, the delayed self-heterodyne photocurrent spectrum consists of direct detection as well as the desired mixing product:

$$\begin{gathered} S_i(f) \approx \mathcal{R}^2 \{S_d(f) + 2[S_s(\nu - \delta\nu) \otimes S_s(-\nu)]\} \\ (\text{ESA} \Rightarrow \text{direct direction} + \text{self-heterodyne spectrum}) \end{gathered} \tag{5.23}$$

$\delta\nu$ is the shift frequency applied to the field traversing one arm of the interferometer and $\mathcal{R}$ is the usual detector responsivity. Since the mixing term is essentially the test laser spectrum convolved with itself (see Figure 5.13) and displaced in frequency by $\delta\nu$ the displayed lineshape will always be symmetrical, even if the original lineshape had important asymmetries.

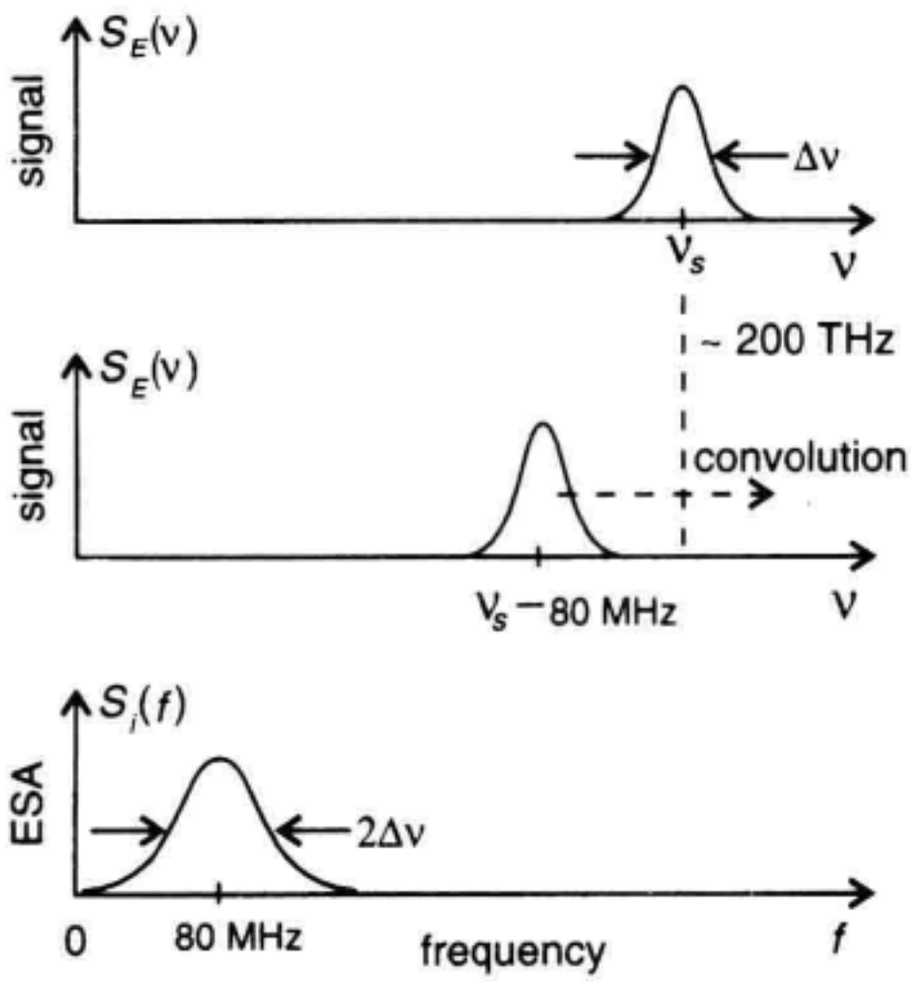

Figure 5.13 The delayed self-heterodyne mixing of the laser field with a frequency shifted replica.

Linewidth Interpretation. For the case of a Lorentzian-shaped laser field spectrum, the displayed lineshape will be twice that of the actual linewidth as shown in Figure 5.13. Shifting the beat frequency from DC is useful to avoid instrumental limitations such as the DC response, the low-frequency noise, and the local-oscillator feedthrough in electrical spectrum analyzers. The optical lineshapes of semiconductor lasers are typically Lorentzian-shaped. Fortunately the Lorentzian and Gaussian lineshapes retain their form during conversion from the optical spectrum to the electrical domain through the delayed self-heterodyne process. Gaussian lineshapes have a FWHM photocurrent spectrum larger by a factor of $\sqrt{2}$ than the original optical lineshape. The more common Lorentzian lineshape has a FWHM detected lineshape larger by a factor of two.

Laser sources exhibiting frequency jitter or 1/f noise will yield larger measured linewidths in a similar way as the heterodyne technique. In this case, the measured linewidth will vary with the interferometer delay.[10] A larger delay yields a larger linewidth. For Lorentzian lineshapes, the 3 dB linewidth must be inferred from measurements taken further down on the displayed lineshape as with the heterodyne case. Table 5.4 indicates the correspondence between the measured full-width at a specific level and the FWHM linewidth assuming a Lorentzian profile.

Frequency Shifters. The frequency shift in delayed self-heterodyne linewidth measurements can be obtained with a variety of devices including acousto-optic frequency shifters, phase modulators, and intensity modulators. The use of small signal-injection current modulation on the test laser has also been demonstrated to displace the beat spectrum from 0 Hz.[11] Frequency shifting the light in one arm of the interferometer by 2.37 GHz using a semiconductor amplifier has also been demonstrated.[12] An arrangement using an acousto-optic Bragg-frequency shifter is shown in Figure 5.14. It is important that the frequency shift be larger than the spectral content of the laser under study, if not, foldover effects near zero frequency will distort the observed spectrum.

Experiment. An acousto-optic frequency shifter provided an 80 MHz shift frequency for a delayed self-heterodyne linewidth measurement as shown in Figure 5.14. An interferometer with a delay, τ_o, of 3.5 μs was used in the experiment. This corresponded to about 715 m of spooled fiber. A polarization controller was used to align the polarizations of the combined fields. The preamplifier following the photodiode provided high gain (~30 dB) to reduce the effects of the ESA noise on the sensitivity of the electronic

Table 5.4 Self-Heterodyne Linewidth Relations

Measured Full-Width Point	Displayed Width
−3 dB	$2\Delta\nu$
−10 dB	$2\sqrt{9}\,\Delta\nu$
−20 dB	$2\sqrt{99}\,\Delta\nu$
−30 dB	$2\sqrt{999}\,\Delta\nu$

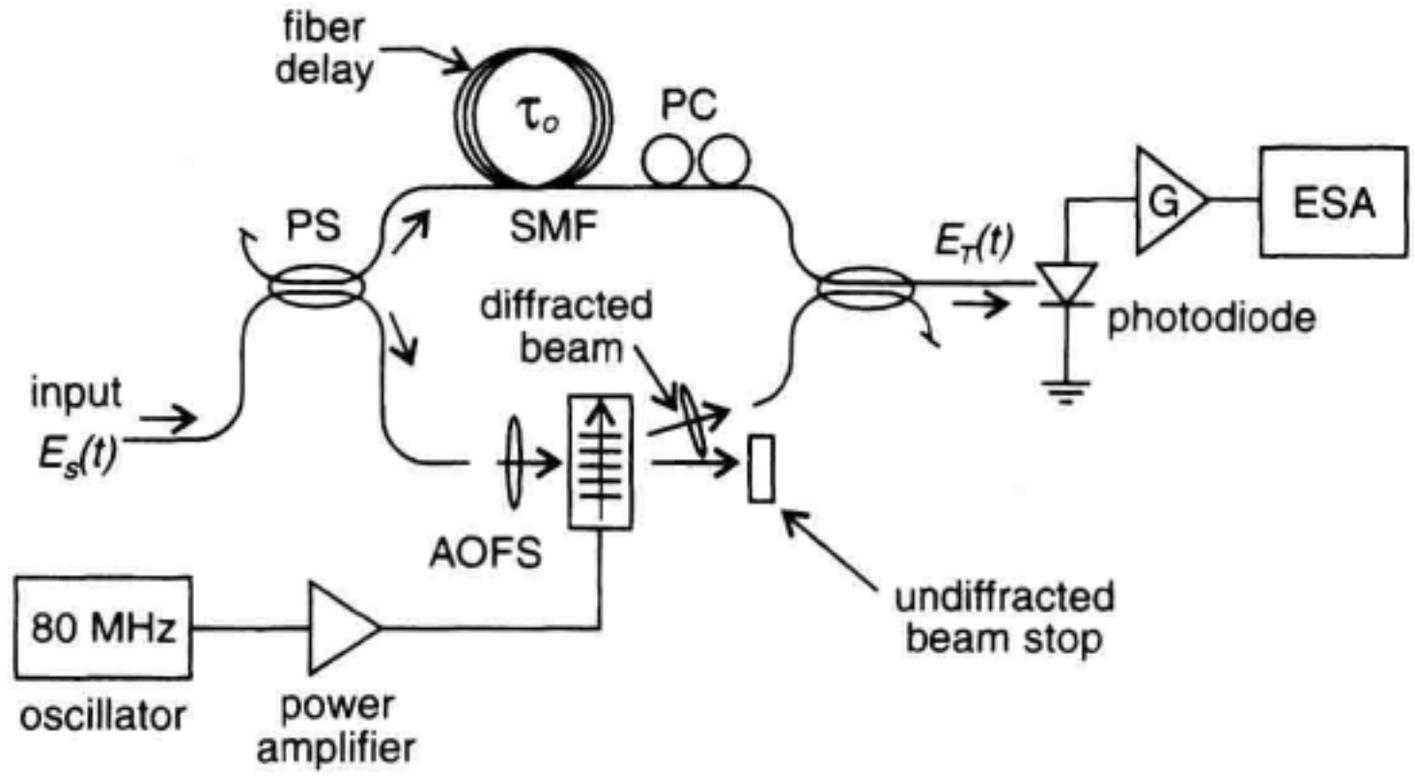

Figure 5.14 Optical self-heterodyne setup for laser linewidth measurement. AOFS = acousto-optic frequency shifter.

spectrum analysis. The optical linewidth measurement is shown in Figure 5.15. A close-in view of the linewidth measurement is shown in the inset. The displayed linewidth is 33.2 MHz which yields a laser linewidth of 16.6 MHz.

5.3.3 Delayed Self-Homodyne

The delayed self-homodyne technique offers a very simple means to measure the linewidth of an unmodulated laser.[9,13,14] Except for the presence of an optical frequency

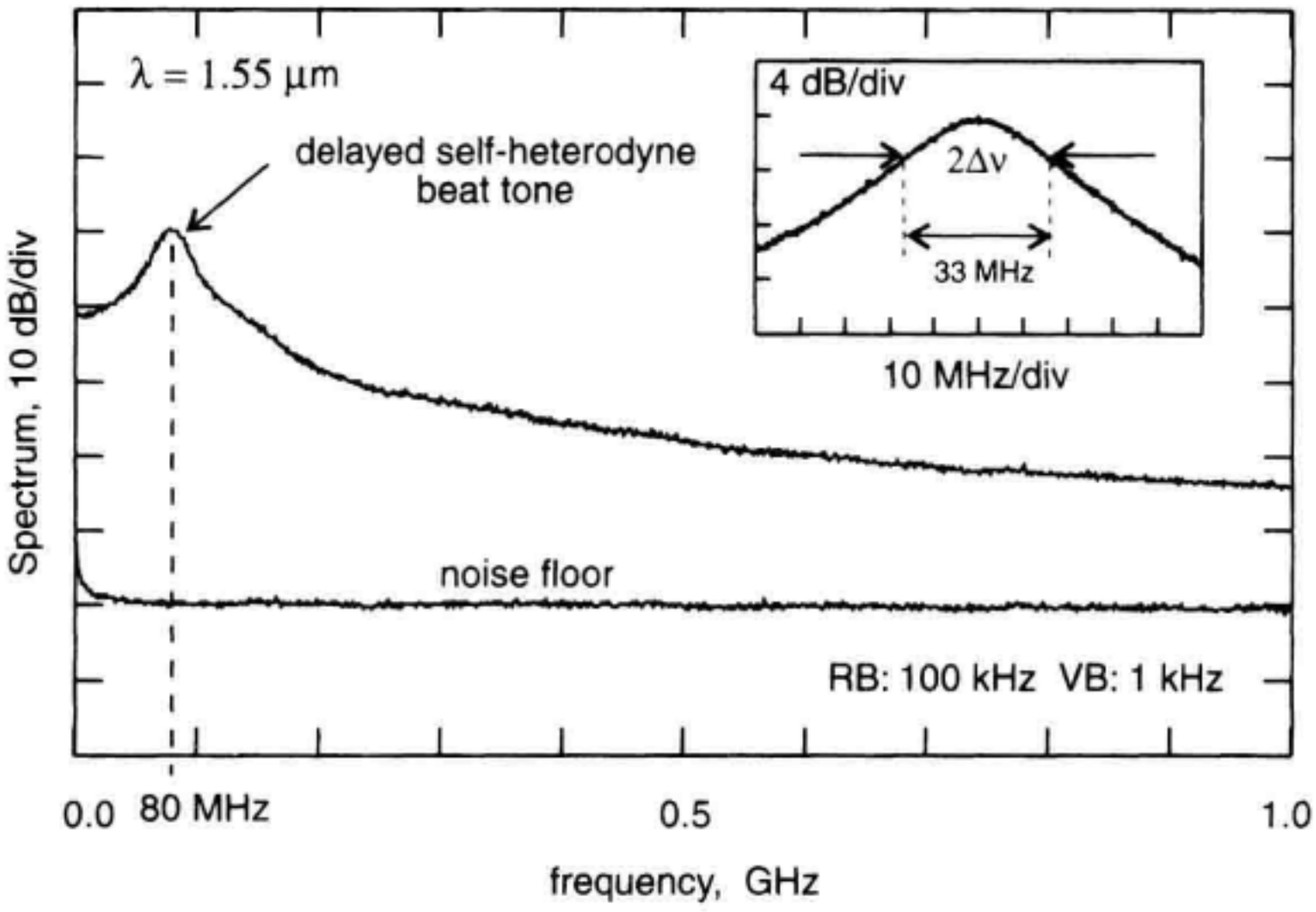

Figure 5.15 Measurement of DFB laser linewidth using optical delayed self-heterodyne technique. Inset shows close-in view of the spectrum.

shifter in the delayed self-heterodyne case, the self-homodyne and self-heterodyne techniques are the same. This method, like the delayed self-heterodyne technique, is well-suited for linewidth measurements because of the extremely high resolution afforded by using optical interferometers with low-loss fiberoptic delays. As with the delayed self-heterodyne method, any frequency jitter of the laser frequency will broaden the measured linewidth. To reduce this effect, the measurements can be performed further down the displayed lineshape. Table 5.4 may be used to infer the correct FWHM linewidth for a Lorentzian lineshape.

Several optical circuit implementations for the delayed self-homodyne method are shown in Figure 5.16. The optical circuit must deliver to the photodetector two fields, one being a delayed replica of the other. The requirement on coherence is satisfied if the differential delay τ_o of the interferometer satisfies Equation 5.22. The reasons for this delay requirement are similar to the delayed self-heterodyne case discussed in Section 5.3.2. More detail on the effect of laser coherence will be presented in Section 5.3.4.

Photocurrent Spectrum. The photocurrent spectrum for the delayed self-homodyne technique consists of direct detection as well as the desired mixing product but without the frequency shift:

$$S_i(f) \approx \mathcal{R}^2 \{S_d(f) + 2[S_s(\nu) \otimes S_s(-\nu)]\} \tag{5.24}$$

(ESA $\Rightarrow$ direct detection + self-homodyne spectrum)

where $\mathcal{R}$ is the detector responsivity. Since the mixing term is essentially the test-laser spectrum convolved with itself, the displayed lineshape will always be symmetrical, even if the original lineshape had important asymmetries. Note that Equations 5.23 and 5.24 are nearly identical except for the frequency shift used in the delayed self-heterodyne method.

The translation of linewidth information from the optical spectrum to the electrical spectrum is illustrated in Figure 5.17. For the case of laser lineshapes described by Lorentzian or Gaussian functions, the displayed electrical power spectrum will have identical functional shapes to the actual optical spectrum. The reason for this is that the shape of these functions are preserved through the autocorrelation operation. The lineshapes of semiconductor lasers are often approximated by a Lorentzian-shaped profile.

The relationship between the measured self-homodyne FWHM linewidth and the actual optical field linewidth is the same as for the delayed self-heterodyne technique given in Table 5.4. Note that since the delayed self-homodyne method centers the mixing spectrum at 0 Hz, only half of the symmetrical spectrum is viewed (see Figure 5.17). Thus the laser FWHM linewidth corresponds to the measured –3 dB frequency point.

5.3.4 Photocurrent Spectrum: Coherence Effects

In this section, the interplay of the laser coherence time, τ_c and the interferometer differential delay, τ_o is presented in more detail. The reader may jump to the experiment at the end of Section 5.3.4 if a more detailed knowledge of the delay requirements is not desired. This type of analysis, along with actual experiments, provides the basis for the in-

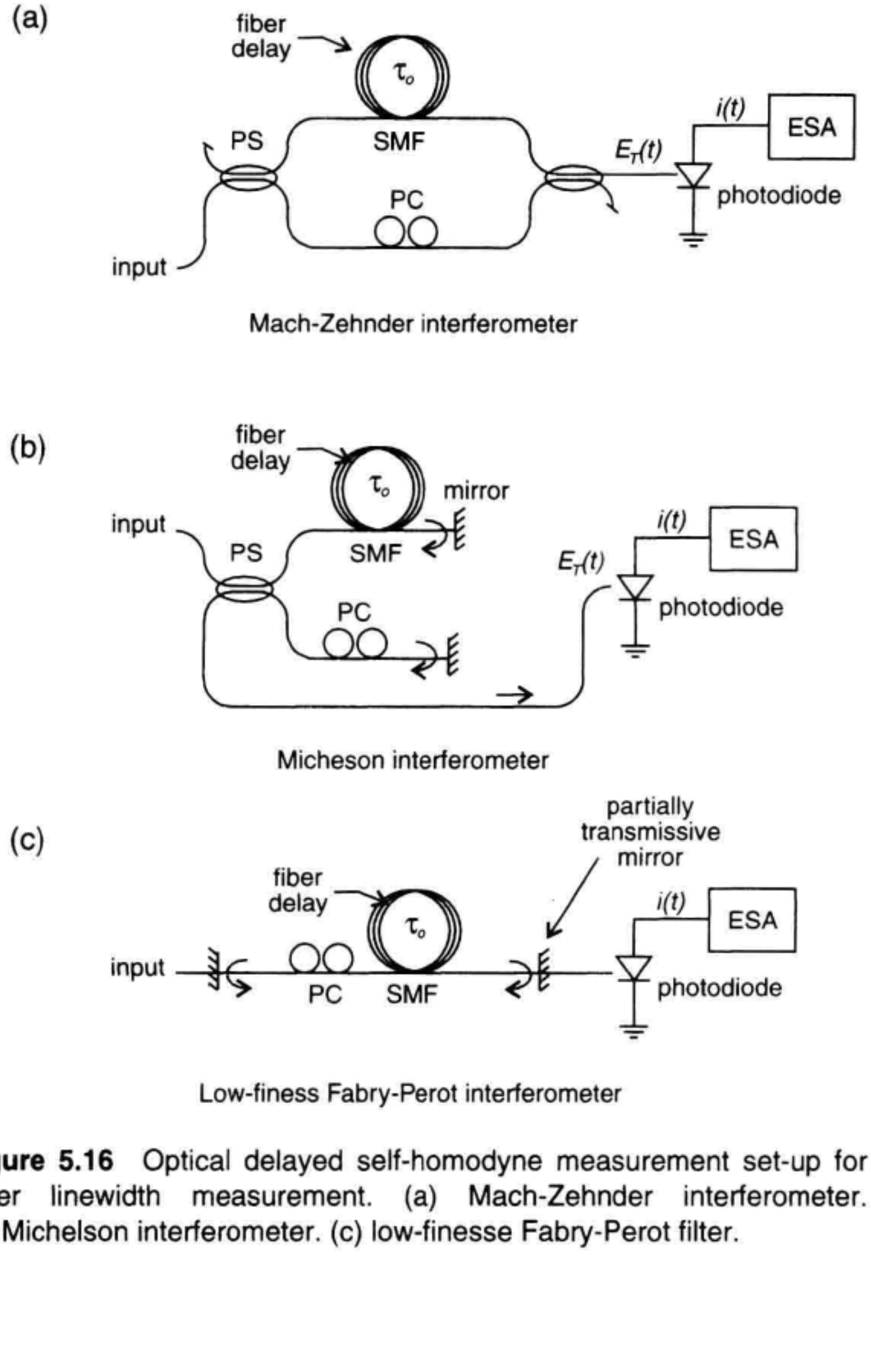

Figure 5.16 Optical delayed self-homodyne measurement set-up for laser linewidth measurement. (a) Mach-Zehnder interferometer. (b) Michelson interferometer. (c) low-finesse Fabry-Perot filter.

terferometer delay requirements set forth by Equation 5.22. It also applies to the delayed self-heterodyne technique since the physical basis is much the same as with the delayed self-homodyne case.[14] This section is supplemental to the basic linewidth measurement methods. The information provided here, however, can find application in a wide variety of interferometric problems ranging from the linewidth measurement techniques described here to problems of phase noise to intensity noise conversion in optical amplifiers and communications systems.

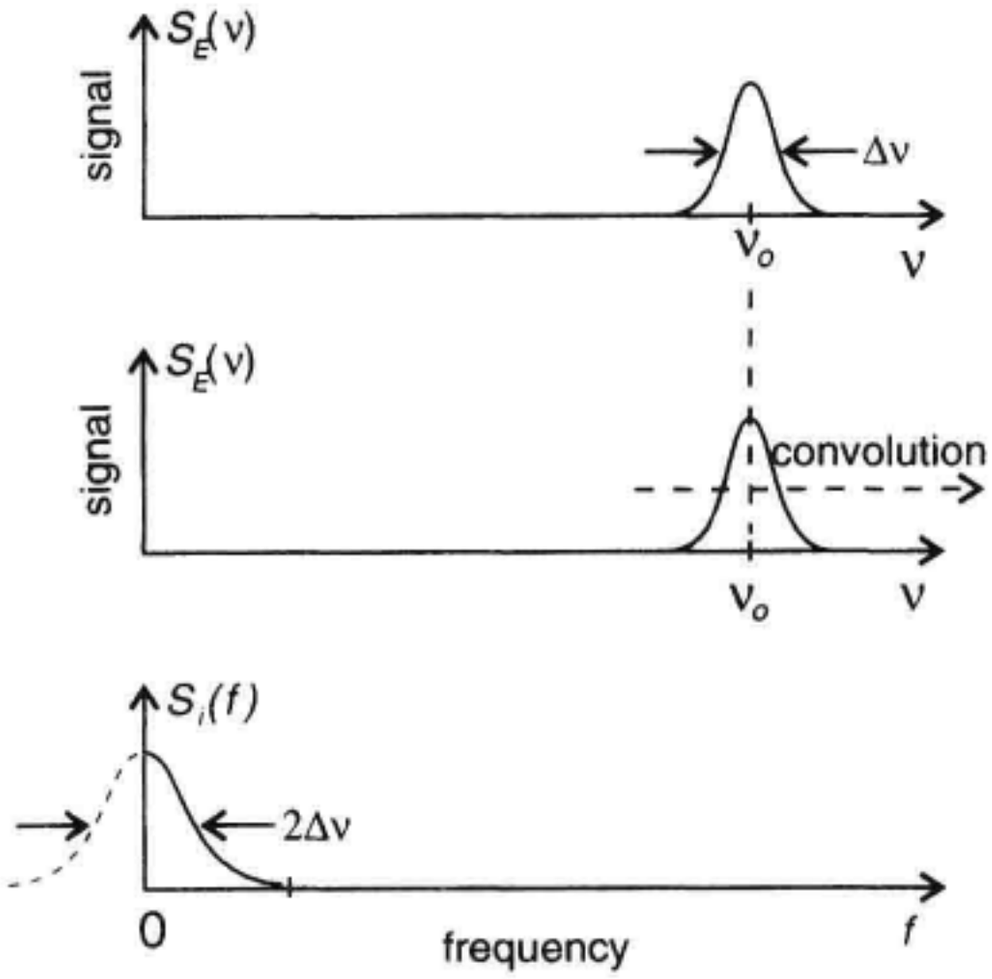

Figure 5.17 The delayed self-homodyne mixing of the laser field with itself.

In this section, we will examine the relationship between the photocurrent power spectrum displayed on the ESA, the laser linewidth, $\Delta\nu$ and the interferometer delay τ_o. The end result is an equation which predicts the photocurrent power spectrum for any degree of correlation between the combined fields. From this equation it is possible to determine the interferometer delay requirement in terms of a linewidth measurement error. The end result is quite broad and can be applicable in a variety of interferometric problems in any regime of coherence. The foregoing premise is that the laser lineshape can be approximated by the usual Lorentzian function (see Equation 5.19).

Analysis. The ESA display is proportional to the photocurrent spectral density by way of the standard resistance, 50 ohms, and any gains or losses in the system. The photocurrent spectrum can be evaluated through a computation of the currents induced by the total incident field at the photodetector. This calculation is quite tedious and is only briefly outlined here to give the reader an idea of the sequences involved. The total complex field at the photodetector, $E_T(t)$ has two contributions, one from each interferometer path.

$$E_T(t) = \sqrt{P_1}\, e^{j(2\pi\nu_o t + \phi(t))} + \sqrt{P_2}\, e^{j(2\pi\nu_o (t+\tau_o) + \phi(t+\tau_o))} \tag{5.25}$$

The random-phase noise process of the laser is described by $\phi(t)$. This phase noise leads to a phase jitter, $\phi(t) - \phi(t+\tau)$, that is assumed to have a zero-mean Gaussian probability distribution. By virtue of the Weiner-Khintchine theorem, the photocurrent power spectrum (displayed by the ESA) is the Fourier transform of the photocurrent autocorrelation function, $R_i(\tau)$ defined as:

$$R_i(\tau) = \Re q G_E^{(1)}(0)\delta(\tau) + \Re^2 G_E^{(2)}(\tau) \tag{5.26}$$

where $G_E^{(1)}(0)$ and $G_E^{(2)}(\tau)$ are the first- and second-order optical field autocorrelations defined as

$$G_E^{(1)}(0) = [E_T(t)E_T^*(t)] \tag{5.27}$$

$$G_E^{(2)}(\tau) = [E_T(t)E_T^*(t)E_T(t+\tau)E_T^*(t+\tau)] \tag{5.28}$$

and τ is the autocorrelation scanning variable. The brackets indicate either ensemble averaging or time-averaging since the optical field is described by a stationary and random process. Considering that $E_T(t)$ is composed of two fields, one a delayed version of the other, Equation 5.28 becomes somewhat tedious. Once Equation 5.26 is calculated, a Fourier-transform operation (Weiner-Khintchine theorem) is performed to obtain the photocurrent power spectral density, $S_i(f)$

$$S_i(f) = \int_{-\infty}^{\infty} R_i(\tau)e^{-j2\pi f\tau}\,d\tau \tag{5.29}$$

The calculated power spectrum is valid for any degree of correlation between the combined fields. The polarization states of the combined fields are assumed to be aligned to achieve maximum interference. The three contributions (ignoring thermal noise) to the single-sided photocurrent spectrum are the direct detection, $S_{dc}(f)$, the shot noise $S_{\text{shot}}(f)$ and the sought after mixing term, $S_{\text{mix}}(f)$.[14]

$$S_i(f) = S_{dc}(f) + S_{\text{shot}}(f) + S_{\text{mix}}(f) \tag{5.30}$$

where
$$S_{dc}(f) = \delta(f)\mathcal{R}^2[P_1 + P_2 + 2\sqrt{P_1P_2}\cos(2\pi\nu_o\tau_o)e^{-\pi\Delta\nu\tau_o}]^2$$

$$S_{\text{shot}}(f) = 2q\mathcal{R}[P_1 + P_2 + 2\sqrt{P_1P_2}\cos(2\pi\nu_o\tau_o)e^{-\pi\Delta\nu\tau_o}]$$

$$S_{\text{mix}}(f) = \frac{8\,\mathcal{R}^2\,P_1P_2\,\pi^{-1}\,\Delta\,\nu^{-1}e^{-2\pi\Delta\nu\tau_o}}{1+\left(\frac{f}{\Delta\nu}\right)^2}[\cosh(2\pi\Delta\nu\tau_o) - \cos(2\pi f\tau_o)$$

$$+ \cos^2(2\pi\Delta\nu\tau_o)\left\{\cos 2\pi f\tau_o - \frac{\Delta\nu\sin 2\pi f\tau_o}{f} - e^{-2\pi\Delta\nu\tau_o}\right\}]$$

The equation variables are summarized in Table 5.5.

The important self-homodyne mixing term, $S_{\text{mix}}(f)$ appears unwieldy, but simplifies in certain limits. It can be visualized by plotting its value for various settings of $\Delta\nu\tau_o$. This product is proportional to the ratio of the interferometer delay τ_o to the coherence time, τ_c of the laser. Figure 5.18 plots this in terms of relative intensity noise (RIN). Recall that RIN is the ratio of the intensity-noise spectral density to the average power squared. RIN is convenient to use because it normalizes the display with respect to average power. The linewidth was fixed to 30 MHz. When the product $\Delta\nu\tau_o$ is unity, the shape of the spectrum is approximately that of the original Lorentzian laser lineshape but with twice the spectral width. As the product $\Delta\nu\tau_o$ is reduced below 1, the effects of phase between the interfering waves becomes more significant and ripple appears in the spec-

Table 5.5 Variable Definitions

Symbol	Definition
$\delta(f)$	Dirac-Δ function, $\delta(f=0)=1$, $\delta(f\neq 0)=0$
$\mathcal{R}$	detector responsivity [A/W]
P_1	power delivered to detector from path 1 of interferometer [W]
P_2	power delivered to detector from path 2 of interferometer [W]
$\Delta\nu$	laser FWHM optical linewidth [Hz]
ν_o	average optical frequency [Hz]
τ_o	interferometer delay [s]
f	display frequency [Hz]

trum. The spectrum here corresponds to the quadrature case where the efficiency of phase noise to intensity noise conversion is maximum. Also note that the first null in the spectrum appears at a frequency of $1/\tau_o$.

In terms of frequency resolution, these results can be interpreted as follows: For large $\Delta\nu\tau_o$, the resolution is determined by the linewidth of the test laser. In the other extreme, when the product $\Delta\nu\tau_o$ becomes small compared to unity, the resolution is limited by the differential time-delay of the interferometer. In the regime of partial coherence, the resolution is a blend of the interferometer resolution and the laser linewidth. Curve fitting Equation 5.30 with $\Delta\nu$ as a fitting parameter to the measured data can also be used in the regime of partial coherence in order to estimate the laser linewidth.[15] This may be useful

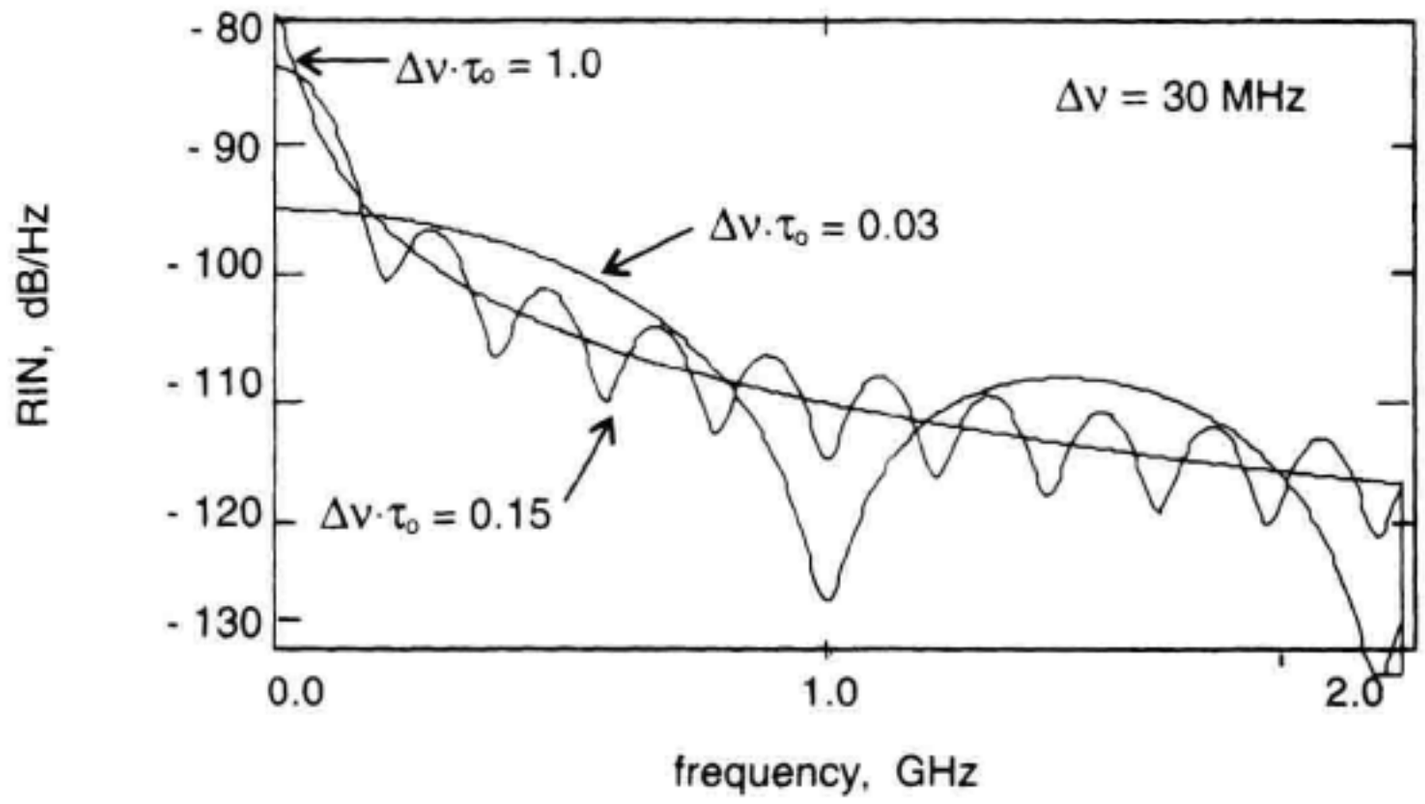

Figure 5.18 Relative intensity noise spectrum for various values of the $\Delta\upsilon\tau_o$ product.

when this technique is applied to very narrow linewidth lasers and long fiber delays are not available to insure incoherent mixing.

Incoherent Regime: $\Delta\nu\tau_o \geq 1$. As the product of linewidth and delay, $\Delta\nu\tau_o$ in Equation 5.30 becomes large, the mixing term, $S_{mix}(f)$ tends to a Lorentzian function centered at zero frequency with a FWHM twice that of the original linewidth. In this regime the electrical spectrum is a scaled version of the actual laser lineshape:

$$S_i(f) \approx \mathcal{R}^2 [P_1 + P_2]^2 \delta(f) + \mathcal{R}^2 P_1 P_2 \frac{4/\pi\Delta\nu}{1 + \left(\frac{f}{\Delta\nu}\right)^2} \tag{5.31}$$

The shot-noise term has been dropped, but the DC term was kept since it is useful for the computation of RIN. The effects of interferometric losses and linewidth on the strength of the delayed self-homodyne beat tone are readily determined from Equation 5.31.

Error Due to Partial Coherence: $\Delta\nu\tau_o \leq 1$. Equation (5.30) provides the theoretical basis for determining the measurement error that would result when there is insufficient delay, τ_o. The theoretical linewidth measurement overestimate, as a function of $\Delta\nu\tau_o$, is shown in Figure 5.19a.[8] Thus the minimum delay, τ_o, can be determined based on the acceptable error caused by the partial coherence. Additionally, Figure 5.19a can be used to correct for measurements performed in the partially coherent regime. In Figure 5.19b the minimum fiber delay length is plotted as a function of laser linewidth. The lower limit for the incoherent range is defined here by the $\Delta\nu\tau_o = 1$ boundary. This corresponds to a linewidth error for the worst-phase condition of approximately 3%. A fiber group index of 1.47 and a Mach-Zehnder topology (see Figure 5.16) were assumed for the calculation.

Experiment. A delayed self-homodyne linewidth measurement for a DFB laser biased above its threshold current is shown in Figure 5.20. In the experiment, the 30 dB isolator in the DFB laser package was inadequate and an additional isolator with 60 dB isolation was added. The laser output was connected to a fiber Mach-Zehnder interferometer which had a differential time delay between the two interferometer paths of 3.5 μs. The interferometer output was detected by a photodetector-preamplifier combination whose signal was analyzed by an ESA. The measured linewidth was 47 MHz when the laser was biased at a current of 40 mA. As a check to see if Equation 5.22 is satisfied, we note that the product $\Delta\nu\tau_o \approx 164 >> 1$. Thus the assumption of incoherent mixing is satisfied.

5.3.5 Coherent Discriminator Method

This section deals with characterizing the optical carrier variations and linewidth of a cw (continuous wave) laser using an interferometric optical FM discriminator.[16,17] These types of measurements are important in characterizing sources such as tunable external cavity lasers, local oscillators for coherent detection, and externally modulated FSK (frequency shift keyed) communications lasers. Since we are assuming that the laser runs cw,

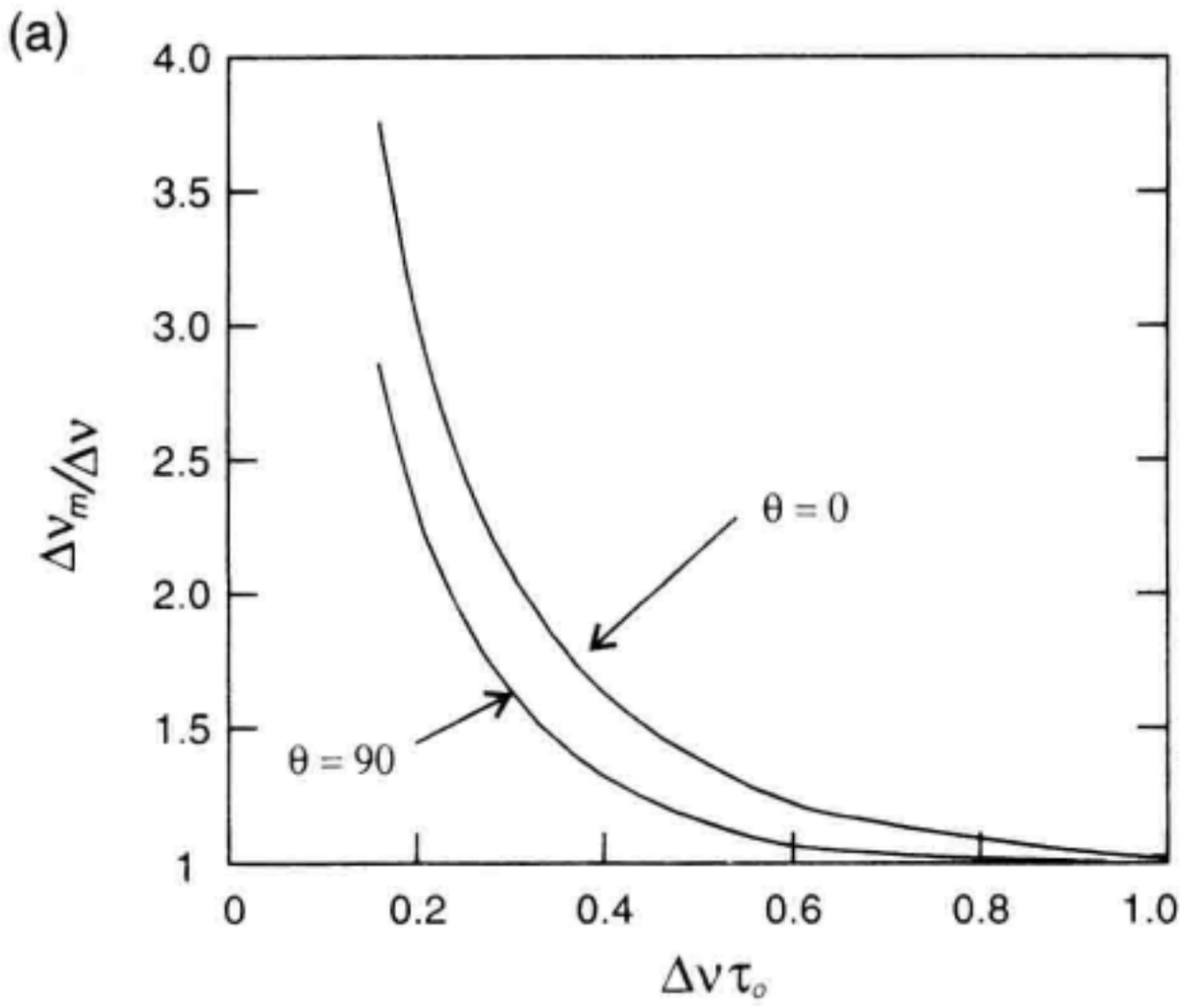

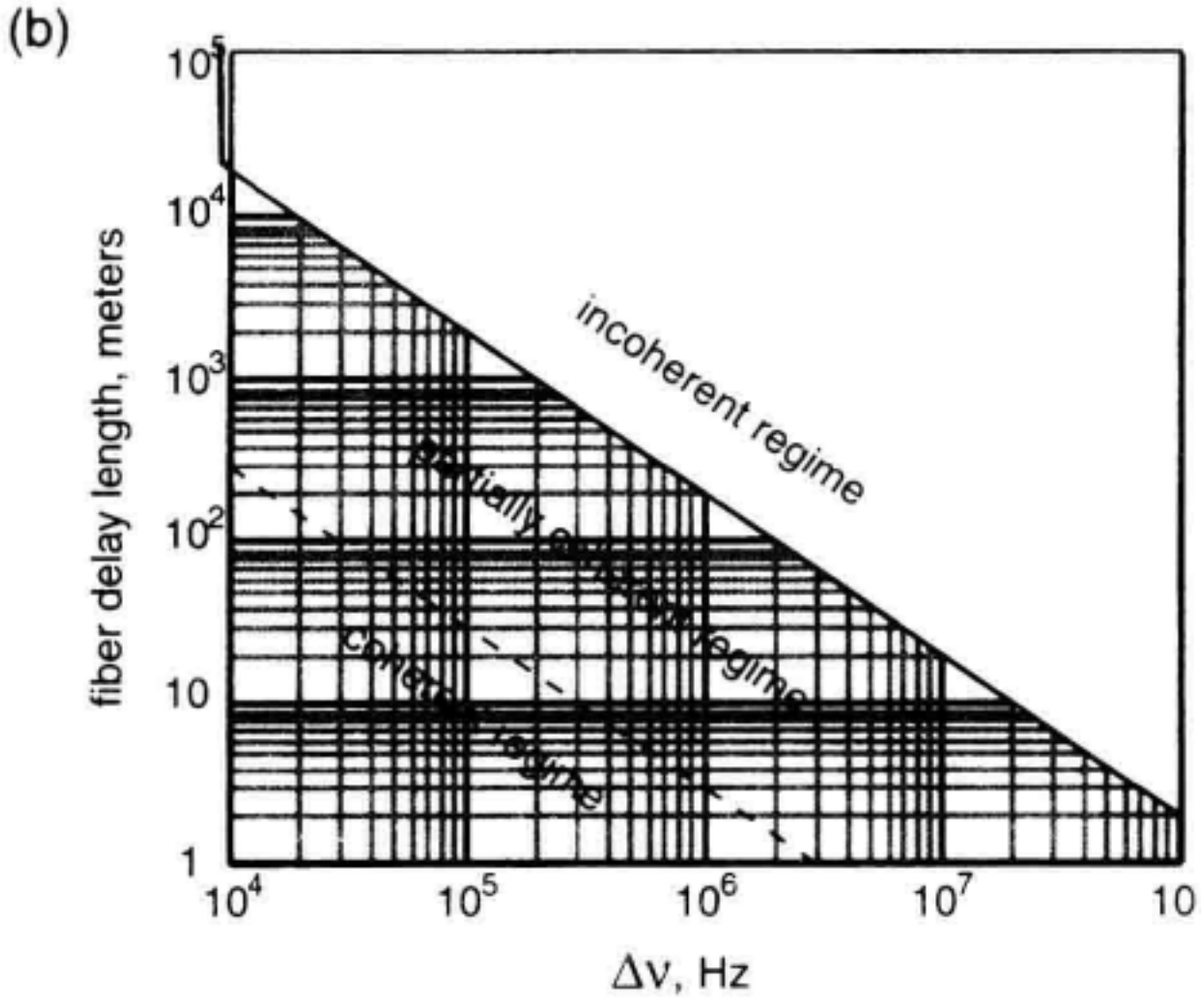

Figure 5.19 (a) Ratio of measured FWHM linewidth to actual laser linewidth for various values of the $\Delta\nu\tau_o$ product. (b) Minimum interferometer delay versus laser linewidth.

its intensity will be constant and variations will occur only in its optical frequency or phase. The case for combined frequency and intensity variations will be covered in Sections 5.5 and 5.6.

The purpose of an optical FM discriminator is to convert optical carrier fluctuations into intensity variations that can then be measured directly. There are many interferometric configurations available to construct such a discriminator, for example, a Michelson interferometer, a Mach-Zehnder interferometer, or an optical resonator could be used (see for example Figure 5.16). This section will use a Mach-Zehnder interferometer to describe the discriminator operation. This type of interferometer is shown in Figure 5.21a.

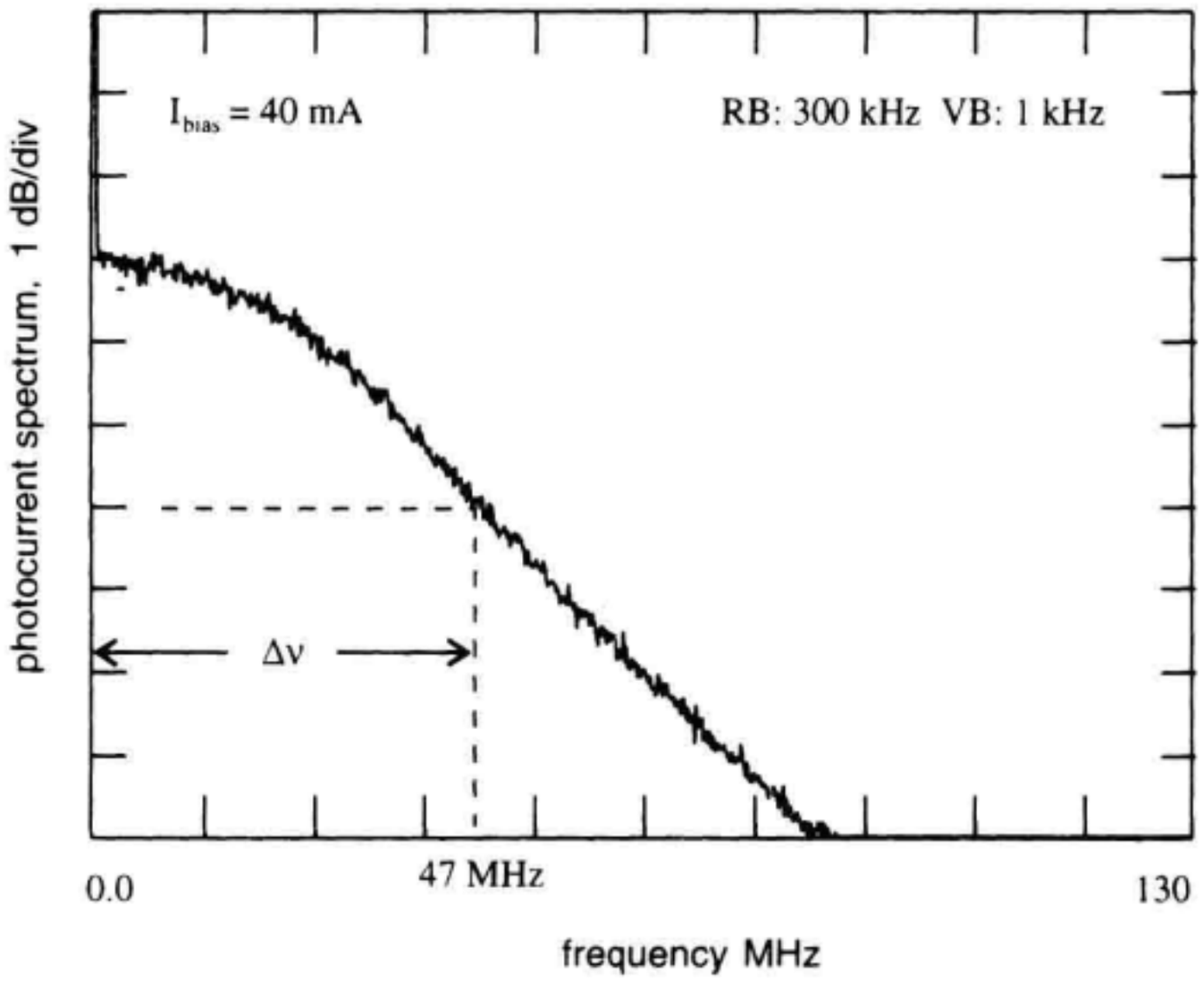

Figure 5.20 Linewidth measurement using delayed self-homodyne technique.

The main parameter that characterizes this type of discriminator is the differential optical time delay, τ_o, between the two paths through the interferometer. A fiber-optic phase modulator and feedback circuit are used to hold the interferometer in the quadrature position where optical frequency variations can be linearly converted into intensity variations. A polarization controller (PC) is added to one arm to avoid orthogonal polarization states for the two interfering signals.

The variations on the laser frequency can be described by using the instantaneous frequency of the optical carrier as

$$\nu(t) = \nu_o + \delta\nu(t) \tag{5.32}$$

where ν_o is the average optical frequency and $\delta\nu(t)$ describes the smaller frequency variations about the large average offset frequency. Without the feedback circuit activated, optical interference results in a photocurrent approximated by

$$i(t) \cong i_o + \Delta i \cos(2\pi\nu_o\tau_o + 2\pi\delta\nu(t)\,\tau_o) \tag{5.33}$$

where τ_o represents the differential time delay through the interferometer and Δi is equal to the maximum amplitude of the photocurrent variations due to optical interference. Equation 5.33 is illustrated in Figure 5.21b. In obtaining Equation 5.33, certain constraints are assumed when relating the optical phase to the instantaneous frequency variations. These constraints will be discussed later.

With the feedback circuit activated, the phase modulator is used to stretch one of the fiber arms to keep the interferometer in quadrature. The quadrature position is shown

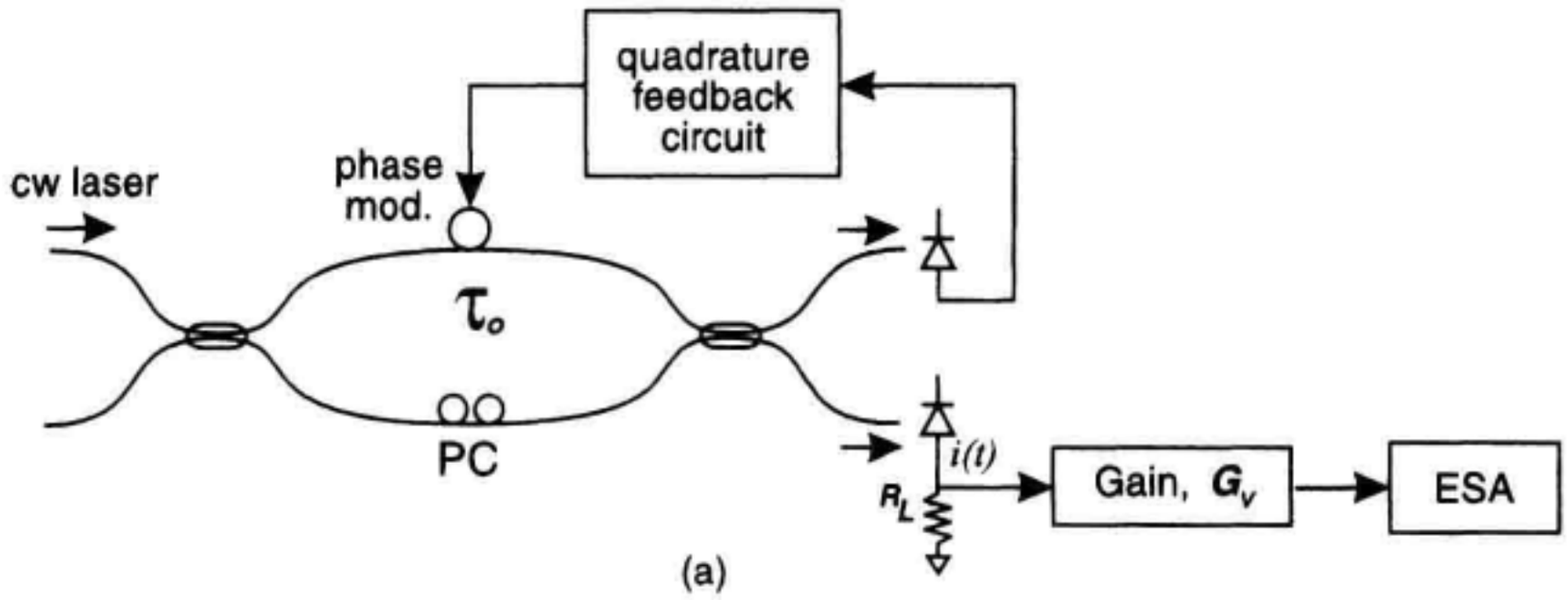

Figure 5.21 Optical frequency discriminator for linewidth measurement.

in Figure 5.21b. The feedback circuit is used to compensate for slow drifts in the average optical frequency and in the fiber lengths of the interferometer. At the quadrature position, small current variations are linearly proportional to the optical frequency fluctuations. Assuming some restrictions on the magnitude of $\delta\nu$ compared to τ_o, Equation 5.33 can be approximated to give

$$\frac{\delta i}{\delta \nu} \cong 2\pi\tau_o\Delta i \tag{5.34}$$

where $\delta i/\delta\nu$ represents the discriminator slope which describes the conversion of optical frequency variations into photocurrent variations. The factor $2\pi\tau_o\Delta i$ is sometimes referred to as the discriminator constant. The constraints used in obtaining Equation 5.34 will be addressed below. Equation 5.34 gives an important result, it states that we can get a direct measurement of the optical carrier variations even though they are centered at several hundreds of terahertz. It also shows that only two experimental parameters are required to calibrate the FM discriminator. These two parameters are the differential time delay τ_o and the peak current variations, Δi, due to the interference effect. In practice, the differential time delay can be measured in several ways. For example, by using a high-resolution optical reflectometer (see Chapter 10) or by probing the interferometer with a

frequency-scanned intensity-modulated source (for example, a component analyzer as described in Chapter 7). The peak current variations, Δi, can be easily measured by sending a ramp voltage to the fiber phase modulator. When performing a discriminator measurement, matched polarization states for the two interfering signals is not required. But it is important that the polarization states remain constant throughout the measurement and that the interference signal is large enough to achieve adequate signal sensitivity.

Linearity Assumptions. For the approximations used in Equations 5.33 and 5.34 to be valid, some constraints need to be set for the relationship between $\delta\nu(t)$ and τ_o. These constraints can be stated mathematically as

$$\Delta\phi(t) = 2\pi\int_{t}^{t+\tau_o} \delta\nu(t)dt \cong 2\pi\delta\nu(t)\tau_o << 1 \tag{5.35}$$

where this expression describes the phase difference between the optical signals from the two arms of the discriminator. Another way of stating this constraint is that the optical frequency should not change much during the time delay τ_o. This keeps the phase variations in Equation 5.33 small so the approximation $\sin(\theta) \sim \theta$ is valid at the quarature position. A slightly more subtle constraint is that $\delta\nu(t)$ should not contain any high-frequency modulation components (in other words, $f_{\max} << 1/\tau_o$). These faster frequency fluctuations can experience more attenuation than the lower frequency fluctuations causing a distortion from the linear relationship given in Equation 5.34. The above constraints can usually be satisfied since the delay, τ_o, can be made arbitrarily small.

Now we will address some of the details involved in measuring the frequency content of the optical carrier fluctuations. These measurements can be important. For example, external cavity tunable lasers often have mechanical resonances due to the design and dimensions of its physical structure. These resonant frequencies typically occur in the kilohertz range and can be easily identified by sending the output of an FM discriminator into an electrical spectrum analyzer (ESA). It is also possible to measure the fundamental laser linewidth (due to spontaneous emission) from the power spectral density of the output signal, $\delta i(t)$. When discussing frequency domain measurements using an FM discriminator, confusion can occur between the optical frequency and the frequency fluctuations that the optical frequency possesses. In order to minimize this confusion, the symbol for optical frequency will be υ and the frequency variations of the optical carrier will be described using f.

Since the optical frequency variations for a cw laser tend to be somewhat random, it is convenient to measure the power spectral density (PSD), $S_\nu(f)$, of the optical frequency fluctuations. Using the linear relationship given in Equation 5.34, the PSD of the measured photocurrent, $S_i(f)$, is related to the optical frequency variations by the relation

$$S_i(f) \cong (2\pi\tau_o\Delta i)^2 S_\nu(f) \tag{5.36}$$

which is valid for $2\pi\delta\nu\tau_o << 1$ and $f << 1/\tau_o$. By making a more rigorous analysis, the constraint $f << 1/\tau_o$ can be removed if one uses the more accurate expression of

$$S_i(f) \cong (2\pi\tau_o\Delta i)^2 \,\mathrm{sinc}^2(\tau_o f)\, S_v(f) \tag{5.37}$$

where $\mathrm{sinc}(x) = \sin(\pi x)/(\pi x)$. The only remaining constraint required for Equation 5.37 is that $2\pi\delta\nu\tau_o << 1$, so that the $\sin\theta \sim \theta$ approximation used for Equation 5.34 remains valid.

As mentioned earlier, the fundamental laser linewidth (linewidth without any external perturbations on the laser) can be determined from the PSD of the optical frequency. For a cw laser with a Lorentzian linewidth of $\Delta\nu$, the PSD of the optical frequency caused by the effects of spontaneous emission is given by

$$S_v(f) = \frac{\Delta\nu}{\pi} \tag{5.38}$$

which states that the PSD is a constant, independent of frequency. For actual lasers experiencing external perturbations, this result will usually not be accurate at low frequencies. Depending on the specifics of the laser and the sensitivity of the measurement setup, it is often possible to find a frequency range where the flat spectral characteristics given by Equation 5.38 is valid.

Typically an ESA measures electrical power from which a power spectral density (PSD) can be estimated. The relationship between the output of the ESA and the PSD of the input voltage is given by

$$P_{\mathrm{ESA}}(f) = \frac{R_L^2\, G_v^2\, B_e}{R_c}\, S_i(f) \tag{5.39}$$

where $P_{\mathrm{ESA}}(f)$ is the electrical power measured on the ESA, R_L is the effective load resistance of the receiver that converts the photocurrent into a voltage, G_v is the voltage gain between the receiver and the ESA, B_e is the effective noise bandwidth for the bandpass filter setting of the ESA and R_c is the characteristic impedance of the ESA (usually $R_c = 50\ \Omega$). The following example will be used to illustrate the use of some of the above equations.

Experiment. This experiment will be used to illustrate a measurement of the fundamental linewidth of a DFB laser using a fiber-optic Mach-Zehnder FM discriminator. The experimental setup shown in Figure 5.21 will be used to perform the measurement. First, the time delay of the FM discriminator is measured using a component analyzer (see Chapter 7). By measuring the transmission of optical intensity modulation as a function of the modulation frequency, a sinusoidal pattern is obtained with a period of 1 GHz. Since the interferometer differential time delay is equal to the inverse of this period, we get $\tau_o = 1$ nsec. Next, the DFB laser source is connected to the input of the discriminator and a ramp voltage is sent to the fiber phase modulator. The peak-to-peak variations in the photocurrent due to the interference is measured to be $2\Delta i = 20\ \mu\mathrm{A}$. From the above two measurements, the discriminator constant is calculated to be $2\pi\tau_o\Delta i = 6.28 \times 10^{-2}\ \mu\mathrm{A/MHz}$. Next the ramp voltage is removed and the phase modulator is connected to the locking circuit which biases the FM discriminator in quadrature.

Before reaching the spectrum analyzer, the photocurrent first passes through a transimpedance amplifier ($R_L = 10\ \mathrm{K}\Omega$) and then an AC-coupled voltage amplifier ($G_v = 100$). A flat spectral density, as predicted by Equation 5.38, is observed on the spec-

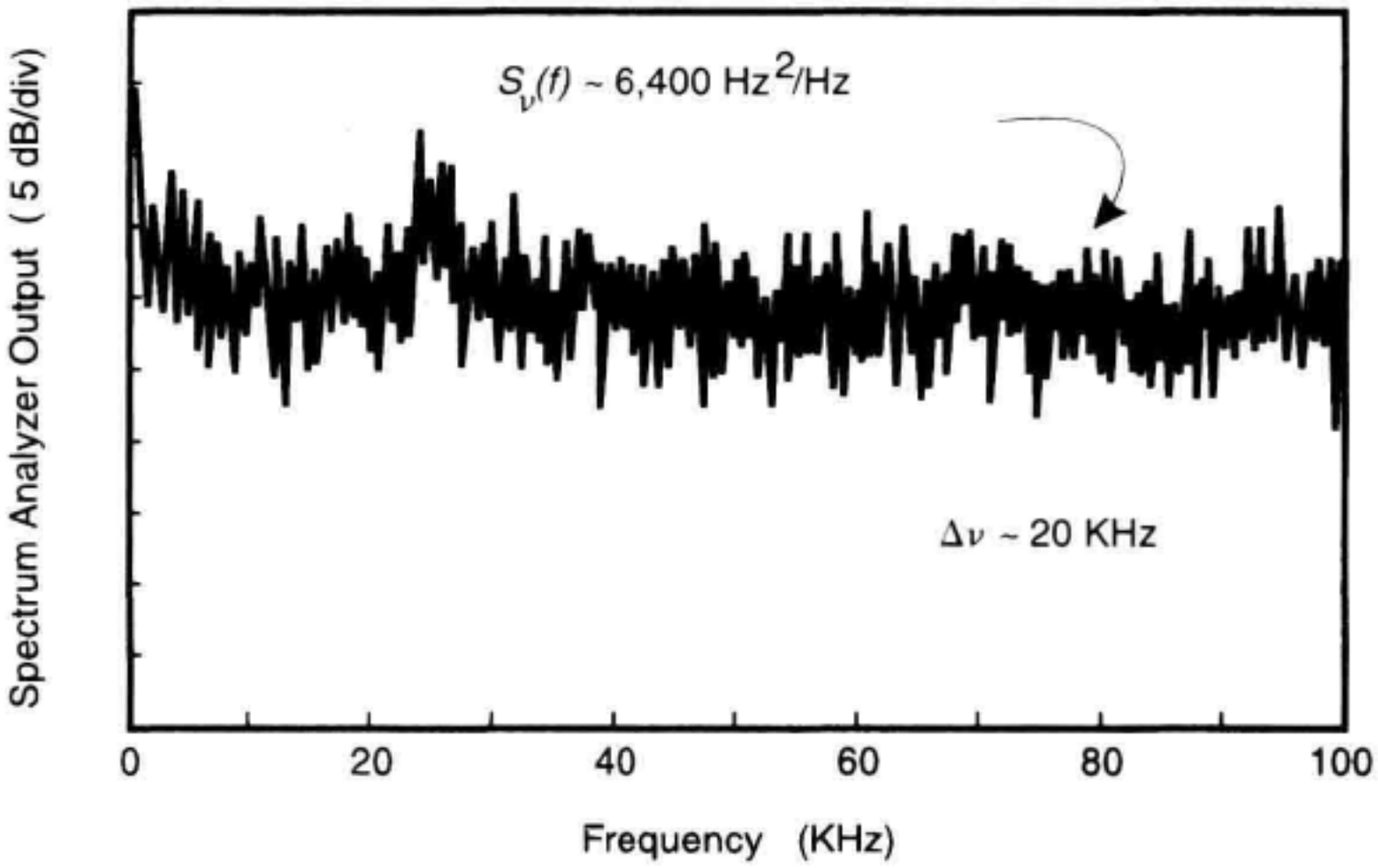

Figure 5.22 Measurement of the optical frequency spectral density of an external cavity laser using an optical discriminator.

trum analyzer. The electrical power in a resolution bandwidth of $B_e = 100$ KHz is measured to be −16 dBm (in other words, $P_{ESA} = 2.5 \times 10^{-5}$ watts). Given that the characteristic impedance of the ESA is $R_c = 50\ \Omega$, we now have enough information to calculate the PSD for the measured photocurrent. Putting the above values into Equation 5.39 we get a value of $S_i(f) = 1.25 \times 10^{-20}$ A^2/W. Using this value and the earlier calculated discriminator constant, Equation 5.36 gives a PSD for the instantaneous frequency of $S_\nu(f) = 3.2 \times 10^6$ Hz^2/Hz. From Equation 5.38, we can now calculate the linewidth of the laser, which is $\Delta\nu = 10$ MHz. Although this example yielded only a single laser parameter, the measurement of the power spectral density of the optical frequency provides additional information concerning low frequency noise effects due to electrical pump current noise and the strength of any relaxation oscillations.

Other optical arrangements besides a Mach-Zehnder interferometer can be used to realize an FM discriminator. For example, a fiber ring resonator biased on the edge of a resonance peak can be used to convert optical carrier variations into intensity changes. Figure 5.22 shows an experimental measurement using a fiber ring resonator as a FM discriminator.[16] A feedback circuit is used to lock to the side of the resonator resonance. The discriminator constant (slope of current vs. frequency) is much steeper than the previous example, being approximately 21 μA/MHz. The source being measured was an external cavity laser whose linewidth is much narrower than that of a DFB laser. For this reason, the discriminator constant was chosen to be much larger. For this measurement, the power spectral density for the external cavity laser was determined to be about $S_\nu(f)$ ~ 6,400 Hz^2/Hz, which corresponds to a fundamental linewidth of 20 KHz. From observing Figure 5.22, the PSD of the carrier frequency is reasonably flat as predicted by theory for a

laser with a Lorentzian lineshape. The increase in noise at about 26 KHz is an artifact caused by a resonance in the PZT phase modulator used in the locking circuit. For frequencies below about 5 KHz, the spectral density becomes larger as environmentally induced frequency jitter becomes more dominant.

5.3.6 Comparison of Techniques

In Section 5.3, four different linewidth measurement techniques were described. There is some overlap in capability between the techniques as well as differences in the measurement implementations. The useage of any particular method depends on how well it matches the measurement goals.[17] One aspect of linewidth measurement that quickly differentiates the heterodyne technique from the other methods is asymmetry. If the measurement requires characterization of asymmetries in the lineshape of the laser under study, the heterodyne technique is the only possibility. The delayed self-heterodyne, the delayed self-homodyne, and the discriminator methods do not yield information on linewidth asymmetry. In terms of measurement simplicity, the delayed self-homodyne and delayed self-heterodyne methods are the easiest to implement. The delayed self-heterodyne method is slightly more difficult than the delayed self-homodyne method because of the requirement of an optical frequency shifter. The discriminator method does not directly yield linewidth, therefore the interpretation of the data is more difficult. Another advantage of the delayed self-heterodyne/homodyne methods is the auto-wavelength tracking. Since the local oscillator signal in these measurements is provided by the laser under test, slow drifts in wavelength are tolerated. This is extremely useful when the laser linewidth is characterized with bias current or laser temperature as a parameter. The discriminator method is well-adept to characterizing sources of perturbation such as acoustic resonances that cause frequency jitter. It can also perform narrower linewidth measurements than the delayed self-homodyne and delayed self-heterodyne techniques. The delayed self-heterodyne, the delayed self-homodyne, and the discriminator linewidth measurement methods are based on the usual approximation that the laser exhibits a Lorentzian lineshape. This assumption is usually valid, but should be considered beforehand for any particular laser.

The principle characteristics of the methods covered in this section are outlined here as an aid in determining which method is most suitable to a particular measurement requirement:

Optical Heterodyne

Advantages

- highest sensitivity
- measures extremely narrow linewidths (limited by LO linewidth)
- measures asymmetric lineshape and non-Lorentzian characteristics
- characterizes optical frequency jitter.

Disadvantages

- may require an OSA to match LO wavelength with signal wavelength
- local oscillator needs to have low frequency jitter and linewidth compared to linewidth of laser under test
- requires wavelength tracking if test laser wavelength changes because of changes in temperature, optical feedback, or injection current

Delayed Self-Heterodyne/Self-Homodyne

Advantages

- simple experimental setup
- less sensitive to slow wavelength drift
- measures narrow linewidth lasers $\Delta\nu \sim 5$ kHz (fiber delay dependent)

Disadvantages

- does not measure asymmetric lineshape
- self-heterodyne: limited on maximum linewidth measurement by frequency shifter
- linewidth overestimate due to frequency jitter (can be corrected)

Coherent Discriminator

Advantages

- measures phase-noise frequency spectrum
- measures laser jitter spectrum
- measures extremely narrow laser linewidths

Disadvantages

- more complicated experimental setup and calibration

5.4 OPTICAL SPECTRAL MEASUREMENT OF A MODULATED LASER

Knowledge of the optical spectrum of a modulated laser is critical to determine the viability of a laser source in a telecommunications system. The broadened spectrum places limits on channel spacings due to cross-talk and creates pulse broadening due to dispersion in the optical fiber. Accurate modeling of laser and modulator performance requires spectral measurements on actual lasers for validation and determination of laser parameters. Typical grating-based OSAs (see Chapter 3) are excellent tools for studying laser side-mode structure but they usually lack the necessary spectral resolution for measurements of the modulation spectrum imparted onto the optical carrier.

Intensity modulation, laser chirp and phase and intensity noise all contribute to the laser's optical spectrum. The spectral broadening during modulation of the laser output

power is primarily due to the direct intensity modulation and the resulting frequency chirp. The time-varying optical field is composed of three basic parts: the magnitude, $\sqrt{P(t)}$, which describes the power variation with time, the average operating frequency, ν_o and the phase variations of the carrier, $\phi(t)$:

$$E_s(t) = \sqrt{P_s(t)}\, e^{j(2\pi\nu_o t + \phi(t))} \tag{5.40}$$

The corresponding single-sided optical field spectrum is a convolution of the power spectrum of the modulation envelope, $S_m(f)$ with the carrier frequency centered at ν_o:

$$S_s(\nu) = S_m(f_\nu) \otimes < P_s(t) > \delta(\nu - \nu_s) \tag{5.41}$$

where the bracket < > denotes a time averaged value.

Ideally, $S_m(f)$ would correspond to the power spectrum of the amplitude modulation used to impart signals onto the optical carrier, however, the effects of laser chirp and linewidth are included in $S_m(f)$.

The measurement methods of this section are geared towards finding the power spectrum of $S_m(f)$. We are less concerned about precise determination of the carrier frequency since this information is readily obtainable from such instruments as wavelength meters or OSAs. In this section two measurement methods will be discussed which allow for high-resolution characterization of $S_m(f)$. The first method, optical heterodyne, allows measurement of arbitrarily shaped power spectrums by using a second laser to serve as a local oscillator. The second approach, the gated delayed self-homodyne (GDSH) technique does not require an additional laser to serve as a local oscillator. It does require access to the modulation input applied to the laser under test. The GDSH technique is most useful in situations where the optical spectrums are approximately symmetric about the optical carrier (predominantly FM broadened). Another method, the scanning FP filter, may also be used for characterization of the optical power spectrum. FP filters are covered in Chapter 4.

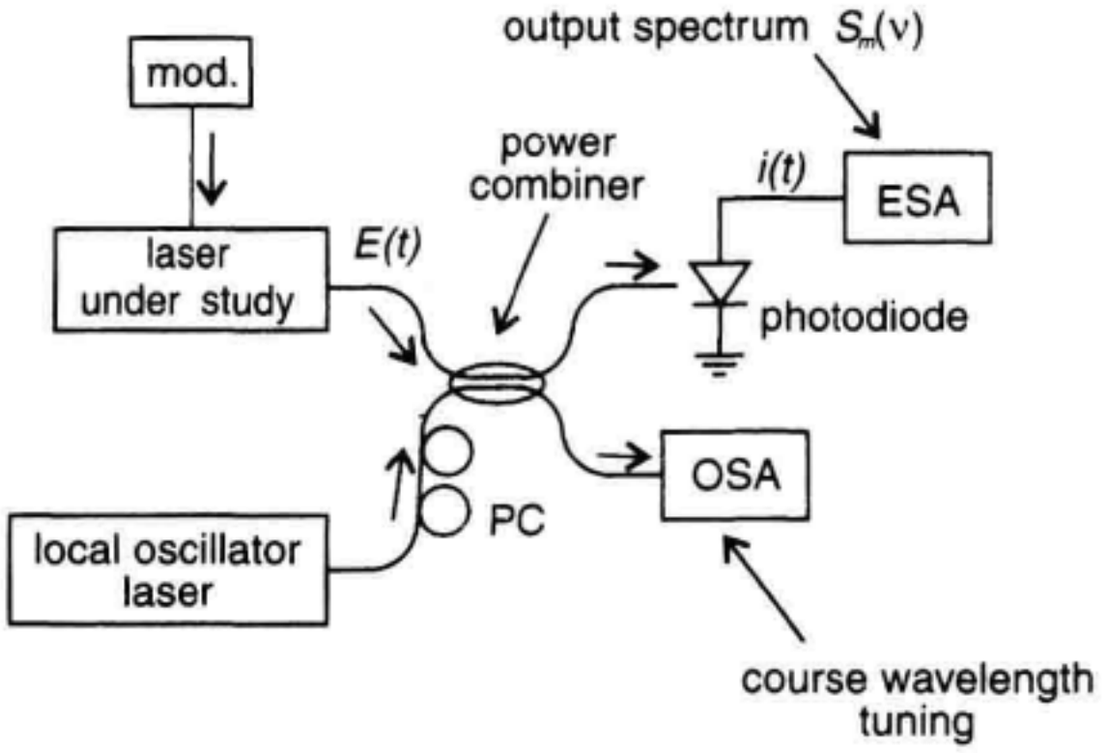

Figure 5.23 Optical heterodyne setup for modulated laser power spectrum measurement. PC = polarization state controller.

5.4.1 Heterodyne Method

The heterodyne approach for measuring the modulated laser spectrum is based on the same principles discussed previously for laser linewidth measurements. The reader is referred to Section 5.3.1 for background information. An optical heterodyne setup is shown in Figure 5.23. The modulated laser signal is combined with the local oscillator signal using a fused fiber directional coupler. The OSA provides course frequency (wavelength) alignment of the local oscillator with respect to the signal laser. The alignment must be precise enough to place the heterodyne beat tone within the bandwidth of the photodiode and ESA. Polarization controllers optimize the signal-to-noise ratio of the displayed spectrum. An electrical preamplifier after the high-speed photodiode improves the system sensitivity by reducing the effect of the thermal noise contributed by the ESA. The desired preamplifier gain is typically of the order of 30 to 40 dB. In this type of heterodyne measurement, the local oscillator is fixed and the optical spectrum is traced out with a broadband ESA. The local oscillator has a narrow linewidth for maximum resolution, therefore for stable measurements, optical reflections must be minimized. Fusion-spliced connections or angled connector interfaces should be used in the measurement setup.

Amplitude and Frequency Scaling. The amplitude scaling displayed on the ESA corresponds to an actual optical spectrum, thus the relative heights of the spectral sidebands are preserved. The display will have a one-to-one frequency correspondence with the actual optical field spectrum, the spectrum is simply translated to a low frequency that can be measured with electronic instrumentation. The bandwidth of the ESA typically places limitations on the extent of the observable power spectrum to less than 100 GHz. The displayed spectrum, which is proportional to the photocurrent spectral density, $S_i(f)$ depends on the local oscillator spectrum $S_{LO}(\nu)$ and the optical spectrum of the modulated laser as well as any direct detection intensity components

$$S_i(f) \approx \mathcal{R}^2 \{S_{dc}(f) + 2S_s(\nu) \otimes S_{LO}(-\nu)\} \quad (5.42)$$
$$(\text{ESA} = \text{direct detection} + \text{mixing})$$

When the local oscillator linewidth is narrow compared to the modulated laser linewidth, its lineshape can be approximated with the Dirac-Δ function. The convolution in Equation 5.42 is straightforward and the observed display on the ESA is the actual optical spectrum frequency translated to within the operation range of the ESA

$$S_i(f) \approx \mathcal{R}^2\{S_{dc}(f) + 2 < P_s > < P_{LO} > S_m(f) \otimes \delta(f - \nu_s + \nu_{LO})\} \quad (5.43)$$
(narrow local oscillator linewidth)

A comparison of Equations 5.41 and 5.43 indicates that the heterodyne technique measures the power spectrum of the optical field modulation about the difference frequency between the LO and the signal.

The local oscillator frequency, ν_{LO}, should be set with respect to the signal frequency, such that the average frequency difference places the heterodyne products above the highest spectral extent of the direct intensity detection. This helps avoid confusion between the direct detection spectrum, $S_{dc}(f)$ and the optical field power spectrum, $S_m(f)$.

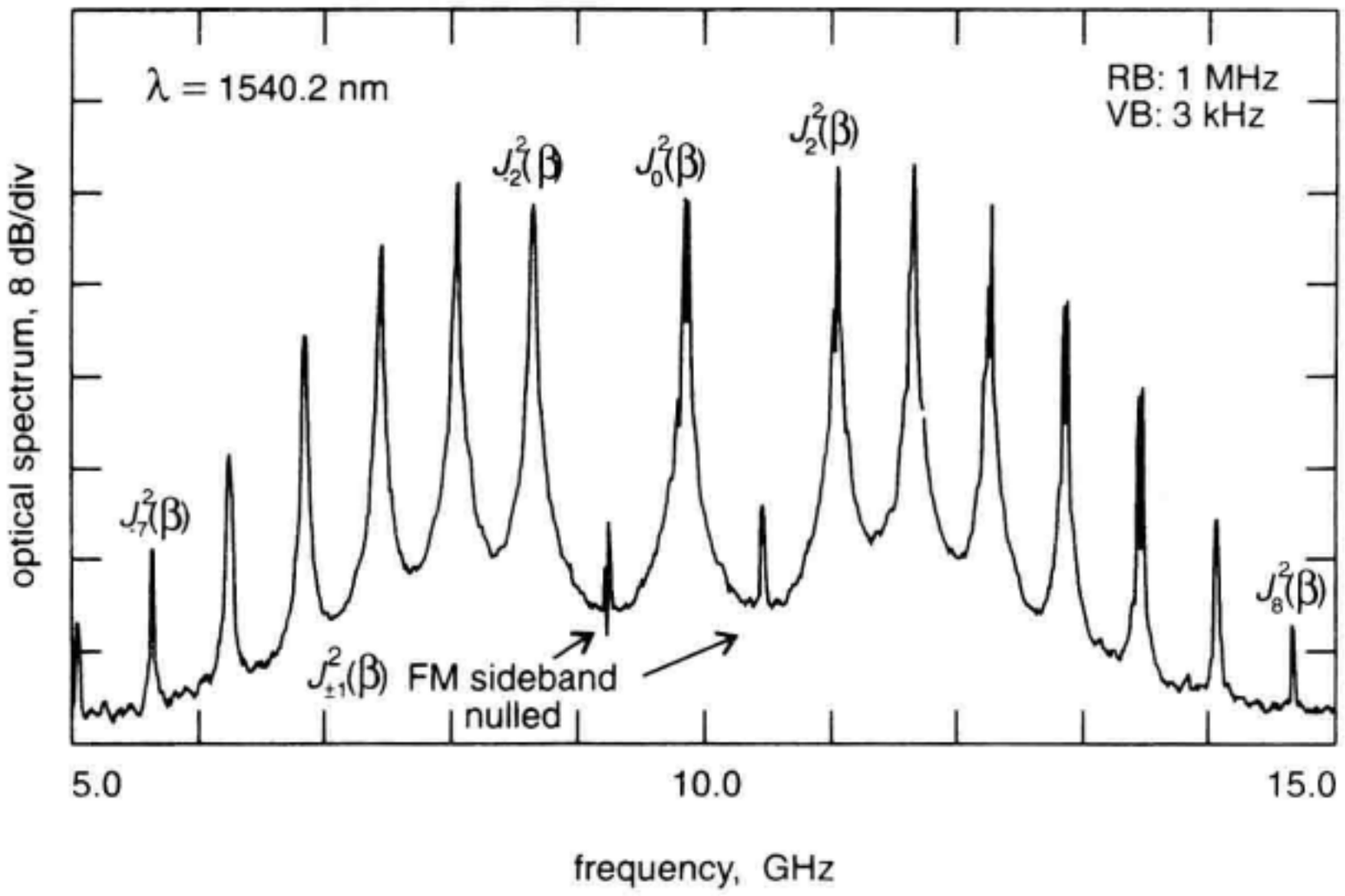

Figure 5.24 Optical heterodyne power spectrum measurement of current modulated DFB laser. Modulation rate is 600 MHz.

Experiment. An optical heterodyne measurement result is shown in Figure 5.24 using the experimental setup shown in Figure 5.23. The signal source was a DFB semiconductor laser undergoing sinusoidal current modulation at a 600 MHz rate. The local oscillator consisted of a tunable external cavity laser which was set at a frequency approximately 5 GHz less than the DFB optical frequency. The DFB current modulation resulted in frequency chirp yielding a predominantly FM-broadened spectrum as shown. Accurate measurements of the FM index (β) can be obtained by nulling one of the FM sideband pairs. Here, the first-order Bessel function sidebands, $J_{\pm1}(\beta)$ were nulled yielding an FM index, $\beta = 3.84$. Decreasing the current modulation frequency to 10 MHz resulted in a continuous spectrum as the individual lines were joined due to the spreading effects of the DFB laser linewidth.

5.4.2 Gated-Delayed Self-Homodyne

The optical power spectrum of a modulated laser can be measured using a simple arrangement consisting of an interferometer, and an optical receiver followed by an electrical spectrum analyzer. This measurement method, called the gated-delayed self-homodyne (GDSH) technique[18] makes optical spectrum analysis possible without the requirement of an additional laser to serve as a local oscillator. It is particularly useful for FM-dominated optical spectrums where the optical field spectrum is approximately symmetric with respect to the carrier frequency. An advantage of this method compared to the heterodyne method is the automatic wavelength tracking. For example, if the laser's average wavelength drifts because of temperature changes, the modulated power spectrum will still be displayed since the laser serves also as a local oscillator. For the same reasons, an OSA is

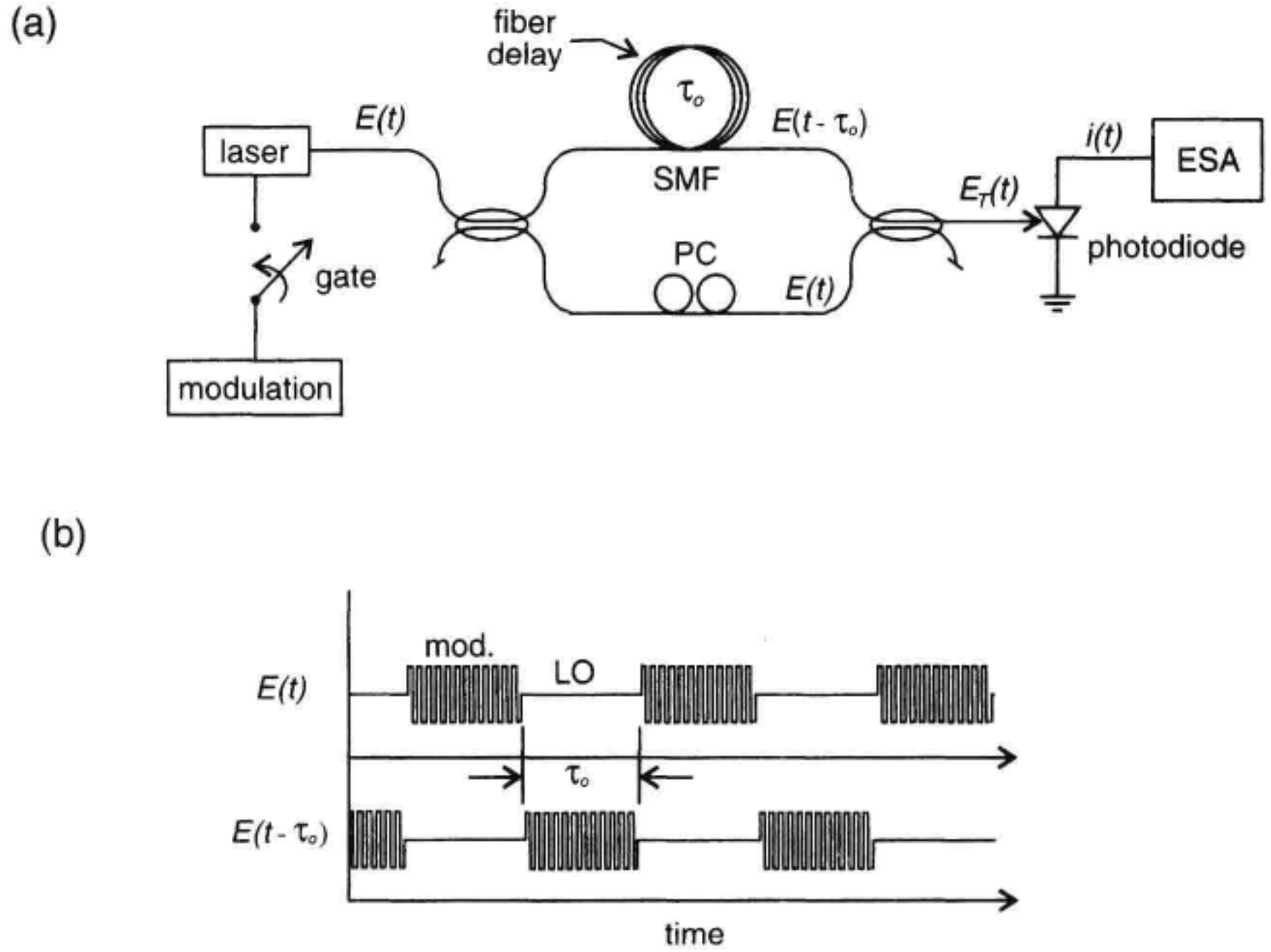

Figure 5.25 Gated-delayed self-homodyne measurement of optical spectrum. (a) Measurement set-up. (b) Timing diagram for signals through interferometer paths.

not required for frequency alignment making the measurement quicker and easier to implement.

The GDSH method setup is shown in Figure 5.25a. As with the optical heterodyne method discussed earlier, the measured spectrum is observed on an ESA. The underlying requirement for this method is that the laser can be operated in two temporally sequential states as shown in Figure 5.25b. In one state, the laser is in its freerunning mode with no modulation applied. This state is called the local oscillator state. The second state is the modulated state with a corresponding optical spectrum to be measured. The differential time delay, τ_o, between the two interferometer paths, results in temporal alignment of a modulated laser state with the local oscillator laser state at the power combiner near the photodetector. To achieve the required temporal alignment, the gate frequency must satisfy:

$$f_g = \frac{1}{2\,\tau_o} \tag{5.44}$$

The system behaves much in the same way as with the heterodyne technique, but with a spectral display about 0 Hz instead of some intermediate frequency. The displayed photocurrent power spectrum on the ESA is the optical spectrum of the modulated laser,

as long as the spectrum is symmetric. The optical spectrums will be symmetric if the laser spectral output is dominated by either FM or AM effects.

Photocurrent Power Spectrum. The analysis of the displayed ESA spectrum and how it relates to the actual optical field spectrum requires calculation of the photocurrent power spectrum.[19] It turns out that the most useful operation is in the incoherent regime where

$$\tau_o > \frac{1}{\Delta\nu} \tag{5.45}$$

is satisfied. Under this condition, the optical field phases of the two temporal states are uncorrelated allowing the unmodulated state to act as an independent local oscillator. This is the same requirement as with the delayed self-homodyne and delayed self-heterodyne measurement of laser linewidth. The expression for the ESA spectrum in the incoherent case is:

$$S_i(f) \approx R^2\{S_I(f) + 2S_m(\nu) \otimes S_{\mathrm{LO}}(-\nu)\} \tag{5.46}$$

Thus, as with the heterodyne case, the ESA display has two main components, the filtered direct intensity detection, $S_I(f)$, and the product of the mixing of the laser in its local oscillator state with the modulated state. Since this method is a homodyne technique, it folds the optical spectrum about the LO frequency, therefore it only accurately measures spectras that are symmetrical. A complete theoretical analysis of the technique is given in Baney and Gallion.[19] If there is a shift in the average optical frequency between the local oscillator state and the modulated state, the spectral components below 0 Hz will not align with the positive frequencies when folded about 0 Hz. In practice, this results in the appearance of two FM sidebands in place of one. Using this effect, the GDSH method can accurately measure shifting of the average carrier wavelength between the modulated and unmodulated laser states.

Experiment. A spectral measurement of a modulated DFB laser using the GDSH technique is shown in Figure 5.26. The measurement setup is shown in Figure 5.25a. The interferometer differential delay, τ_o, was 3.5 μs, thus from Equation 5.44 the required gate frequency was 143 kHz. A separate pulse generator provided a gate signal for the microwave synthesizer. The synthesizer put out 600 MHz cw when the gate signal was high, and nothing when the gate signal was low. This pulsed sinusoidal modulation was applied to the current input of the DFB laser through a bias tee. The DFB was well isolated (~ 60 dB) to reduce the effects of system reflections. The interferometer differential delay, τ_o, was 3.5 μs which along with the DFB laser linewidth (tens of MHz) placed the system in the desirable incoherent regime of operation (see Equation 5.45). Polarization control improved the polarization state matching to increase the displayed SNR. A preamplifier following the photodiode provided approximately 30 dB of gain to overcome the large noise figure of the ESA. The RF power was set to null the first FM sideband (FM index, β, of 3.84) as seen in the figure.

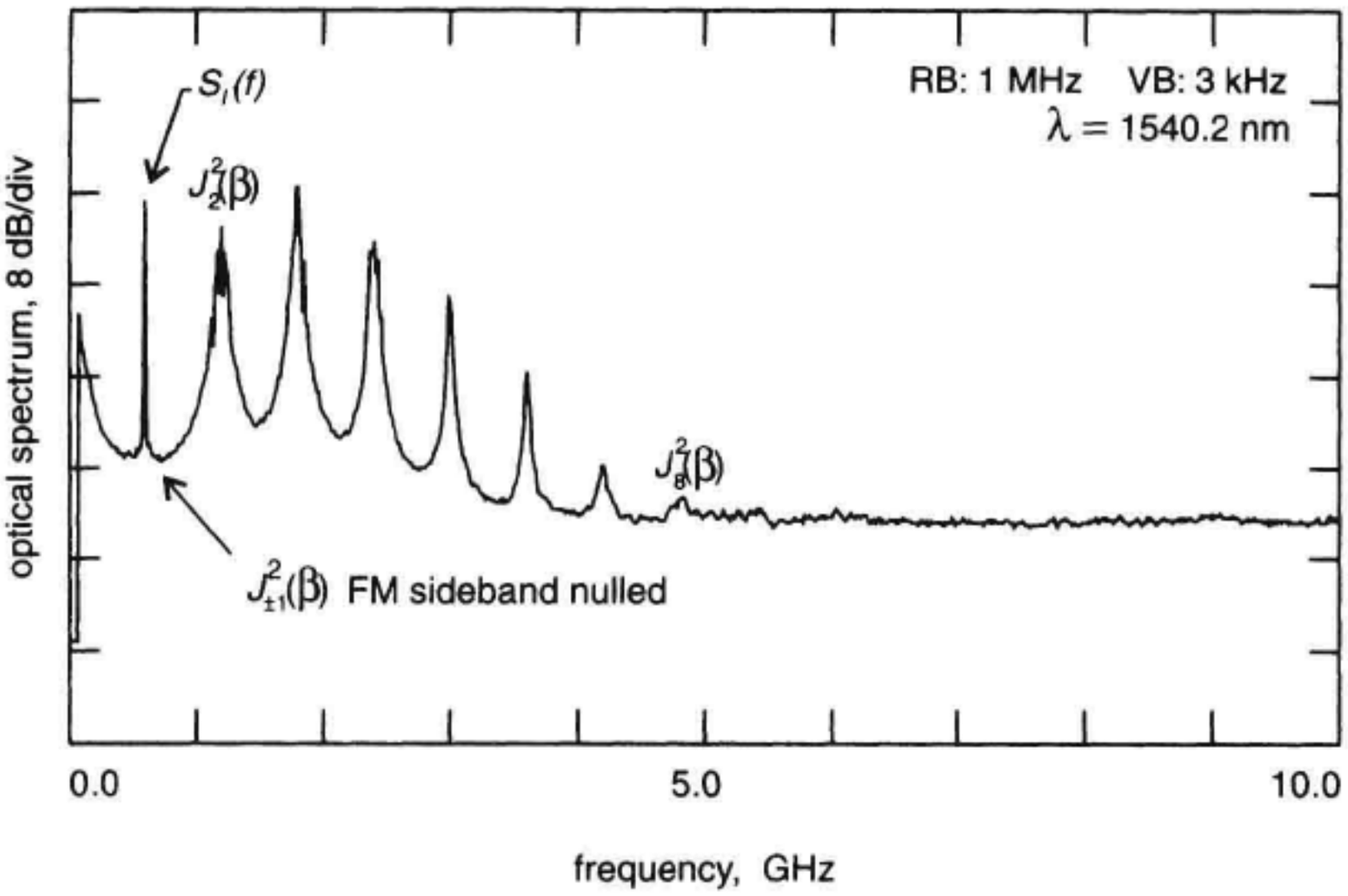

Figure 5.26 Optical power spectrum of current modulated DFB laser using gated-delayed self-homodyne method. Modulation rate = 600 MHz.

Comparison of Heterodyne and GDSH. In Section 5.4, we discussed the heterodyne and GDSH methods for measurement of the power spectrum of a modulated laser. Both techniques offer high resolution characterization of the optical spectrum. In the heterodyne method, frequency resolution is limited by the linewidth of the local oscillator while the GDSH method is limited by the linewidth of the laser under study. The heterodyne method also offers significantly higher sensitivity. This is because of the narrow linewidth local oscillator, more efficient optics and, of course, the heterodyne gain (see Equation 5.17). The heterodyne case is thus preferred over the GDSH technique except when a separate local oscillator laser is not available, or if wavelength tracking between the local oscillator and the laser under test becomes an issue. As a comparison to the scanning FP filter method, suppose we wish to perform high resolution spectrum analysis over the EDFA gain region from 1520 to 1570 nm. This is readily accomplished with either the heterodyne method (since commercially available lasers tune over 100 nm) or the GDSH technique. The FP filter would need a 50 nm free spectral range. To attain the same resolution as the heterodyne technique (assume 1 MHz local oscillator linewidth) the FP filter would require a finesse of 6 million!

5.5 LASER CHIRP MEASUREMENT

In the previous sections, heterodyne and interferometric techniques for characterization of optical source linewidth and power spectrum were discussed. A related measurement is the time domain measurement of the chirp (see Figure 5.3) of a modulated optical source

such as a laser or modulator. Measurement of chirp provides valuable information concerning the dynamics of the laser frequency excursions during intensity modulation. Since the velocity of light through optical fiber varies with frequency, and chirped pulse would be expected to spread out over time. Sources exhibiting a large amount of chirp will experience more rapid pulse-spreading, leading to intersymbol interference in high-speed digital links. Generally, the more rapid the optical power variations, the greater the chirp, as predicted in Equation 5.5.

The time dependence of frequency chirp can be characterized using optical discriminators. The purpose of the discriminator is to convert optical frequency variations into detectable intensity variations. Optical slope discriminators may be realized using optical filters, interferometers, or even heterodyne techniques. In principle, any linear optical component with wavelength-dependent transmission characteristics may serve as a discriminator. While we will examine in detail the Mach-Zehnder discriminator,[20] it is noted that other two path interferometers are similar in operation. In fact, a variety of optical circuits have been configured into discriminators; these include birefringent crystals, optical fibers, FP filters, and Michelson interferometers in bulk-optic or fiber form, to name a few.[16,21,22]

Conversion of Chirp to Intensity Variations. An interferometer circuit for measuring laser chirp is shown in Figure 5.27. Modulated light from the source, in this case a laser diode, enters the Mach-Zehnder interferometer as shown in Figure 5.27a. The differential time of flight between the two interferometer paths is denoted by τ_o. The light is recombined in the output coupler which directs half of the light from each path to the photodetectors. One photodetector provides both average power detection as well as high-speed measurement of intensity variations caused by the discriminated optical frequency variations. The second detector is used for measuring only the average power. When the average powers from each of the two interferometer output ports are equal, the interferometer is in quadrature. This enables conversion of optical frequency chirp into intensity changes via the linear discriminator slope characteristic shown in Figure 5.27b.

A feedback circuit maintains quadrature by adjusting the delay τ_o. The required delay adjustment is small, on the order of an optical wavelength. This delay can be realized using piezo-electric (PZT) devices. The quadrature feedback circuit should respond quickly to environmental factors affecting the interferometer path delay. The measurement apparatus uses a sampling oscilloscope which is triggered by the laser modulation source. This enables the comparison of several measured time records, each for a specific interferometer state, to calculate chirp. The three interferometer states are:

- Quadrature: both shutters open;
- Shutter A closed, shutter B open;
- Shutter A open, shutter B closed.

From an analysis of the photocurrent time records corresponding to the three interferometer states, the chirp is calculated.

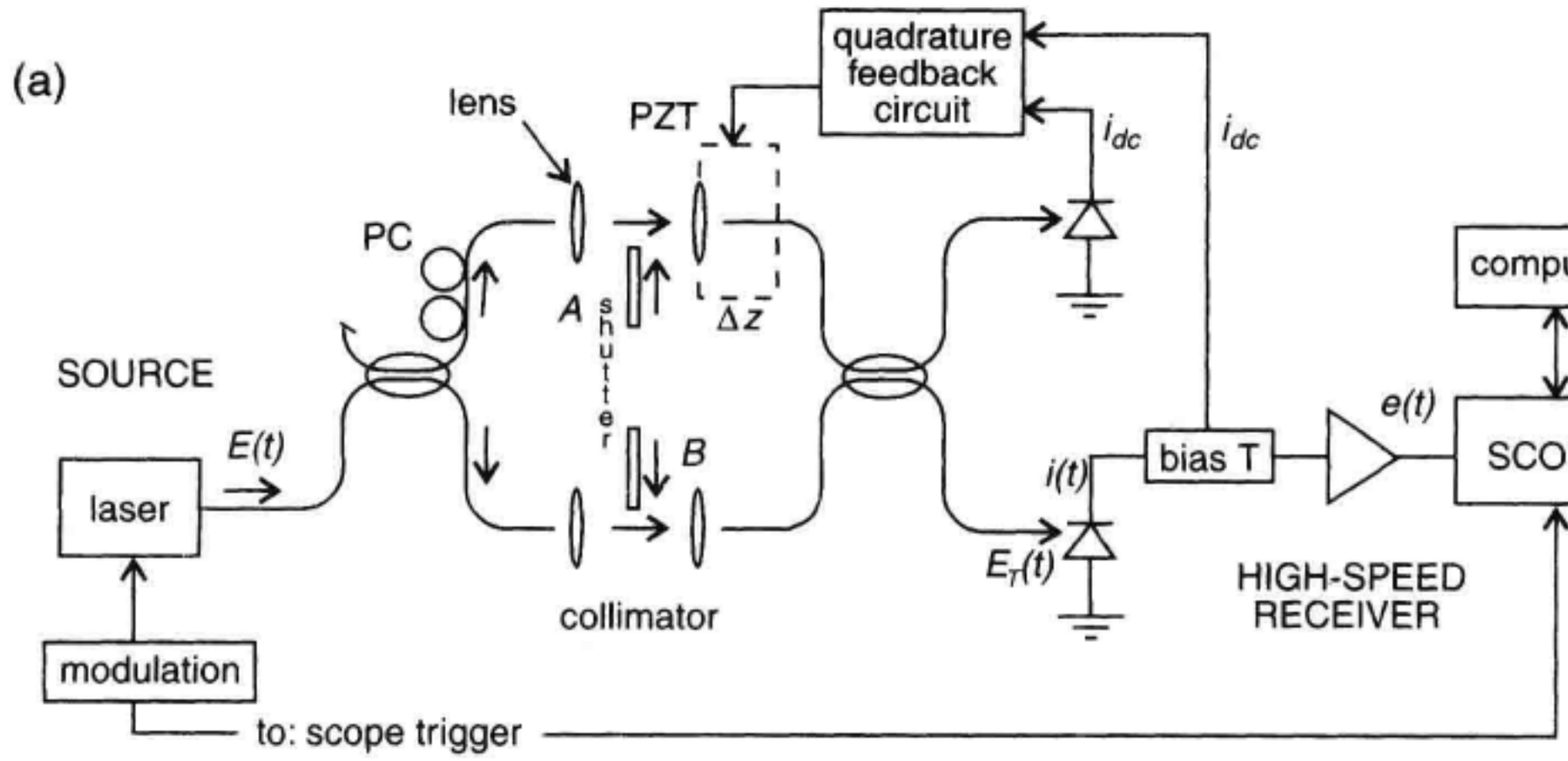

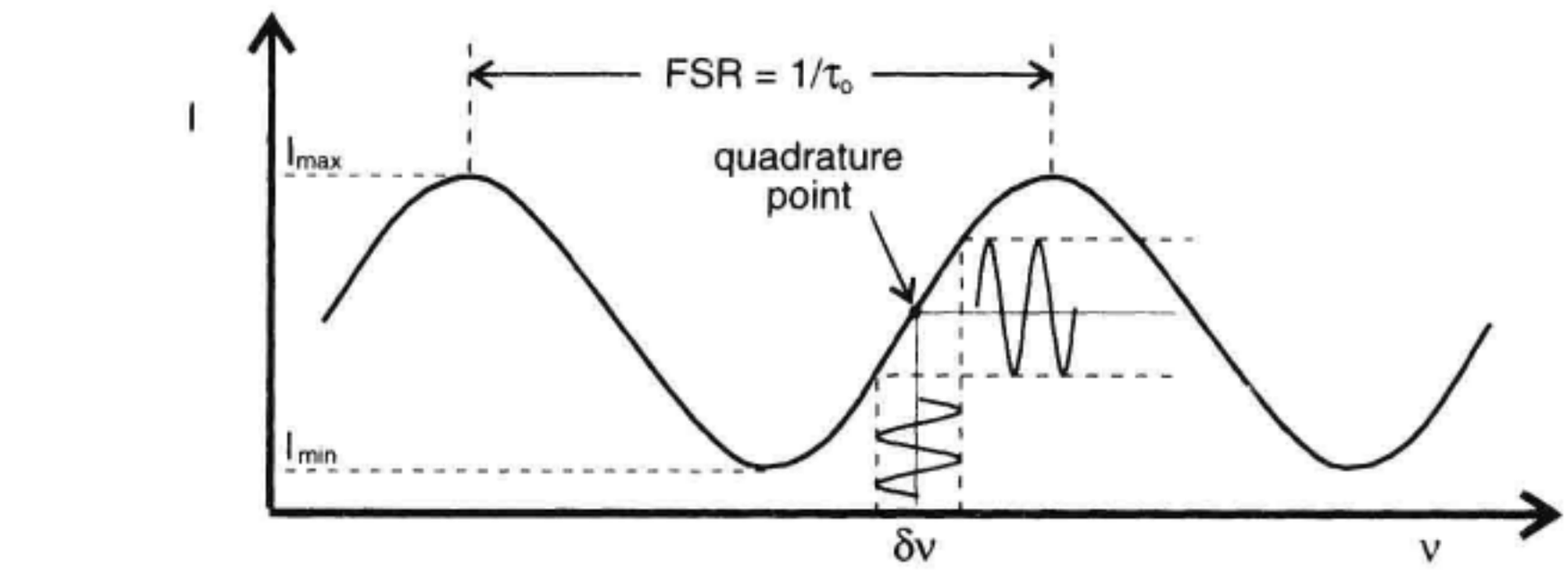

Figure 5.27 (a) Time-domain laser chirp measurement using a Mach-Zehnder interferometer followed by a high-speed receiver. (b) Interferometer discriminator characteristic.

Analysis. For the class of discriminators that consist of interferometers with two optical paths, the average output power from one port of the interferometer is the sum of the path power contributions and an interference term (see Equation 5.12):

$$P_o(t) = P_1(t) + P_2(t) + 2\sqrt{P_1(t)P_2(t)}\cos(\Delta\phi(t, \tau_o) + 2\pi\nu_o\tau_o) \qquad (5.47)$$

where ν_o is the average optical carrier frequency and τ_o is the differential interferometer delay. In the absence of any frequency modulation, $\Delta\phi(t)$ is zero. However any changes in the frequency of the signal at the interferometer input will create a change in phase between the combined signals at the interferometer output. We will use the interferometer output intensity in the following analysis, but since the current or voltage in the electronic receiver is proportional to optical intensity, they can be substituted in place of intensity.

To maintain coherent interference between the light beams in Figure 5.27a, the interferometer delay, τ_o, should satisfy:

$$\tau_o \ll \frac{1}{\Delta\nu} \tag{5.48}$$

Satisfying the quadrature biasing experimentally is equivalent to requiring a relationship between the average optical frequency, ν_o, and the interferometer delay:

$$2\,\pi\,\nu_o\,\tau_o = \frac{\pi}{2} + 2\,n\,\pi \tag{5.49}$$

where $n = 0, 1, 2, \ldots$. Note that there are really two quadrature points in Figure 5.27b having opposite slopes. Here we restrict operation to the quadrature point with positive slope.

The instantaneous frequency deviations, $\delta\nu(t)$ of the optical carrier is the time derivative of the phase:

$$\frac{\Delta\phi(t)}{\Delta\tau} \approx 2\pi\delta\nu(t) \tag{5.50}$$

Equation 5.50 can be approximated when delay τ_o is small compared to the fastest modulation periods:

$$\Delta\phi(t,\ \tau_o) \approx 2\pi\tau_o\,\delta\nu(t) \tag{5.51}$$

Substitution of Equations 5.49 and 5.51 into 5.47 leads to

$$P_Q\,(t) = P_1\,(t) + P_2\,(t) + 2\,\sqrt{P_1\,(t)\,P_2\,(t)}\,\sin(2\,\pi\,\tau_o\,\delta\nu(t)) \tag{5.52}$$

where $P_Q\,(t)$ is the discriminator output when the interferometer is set at quadrature. To determine $\delta\nu(t)$, we need to measure $P_1(t)$ and $P_2(t)$. These two time records are easily found by alternately blocking each of the interferometer paths.[20] In Figure 5.27a, a shutter is placed in the collimators. Note that the concept of a discriminator constant does not apply here since the discrimination slope depends on the input power which is now changing as a function of time. The direct detection $P_1\,(t) + P_2\,(t)$ and the power dependence of the discriminator characteristic, $\sqrt{P_1(t)P_2(t)}$ is used to calculate the chirp $\delta\upsilon\,(t)$

$$\delta\nu(t) = \frac{1}{2\pi\,\tau_o}\,\arcsin\left(\frac{P_Q\,(t) - P_1\,(t) - P_2\,(t)}{2\sqrt{P_1\,(t)\,P_2\,(t)}}\right) \tag{5.53}$$

The delay τ_o may be measured by connecting a white light source (ASE from an EELED or EDFA for example) to the interferometer and observing the nulls in the interferometer output spectrum with an OPS. For larger delays, an optical component analyzer or narrow pulse source and high-speed oscilloscope are used to measure τ_o.

Interferometer Delay Requirement. To maintain unambiguous chirp measurement, the peak frequency excursion $\delta\nu_{peak}$ (see Figure 5.26) must be less than one-fourth the interferometer free-spectral range. Preferably, the maximum chirp is confined to the

approximately linear region of the interferometer characteristic to reduce the effects of noise on the chirp measurement

$$\delta\nu_{\text{peak}} \leqslant \frac{\text{FSR}}{8} = \frac{1}{8\,\tau_o} \tag{5.54}$$

The approximation given by Equation 5.51 concerns the validity of the derivative approximation as the delay τ_o increases. The delay must be small compared to the inverse of the highest frequency components, f_m, of interest in the measurement.

$$\tau_o \ll \frac{1}{f_m} \tag{5.55}$$

Experiment. An example of a time domain measurement of frequency chirping is shown in Figure 5.28.[8] The experimental arrangement was similar to that shown in Figure 5.27. A DFB laser diode was current modulated at a 1 Gb/s rate which resulted in simultaneous power and frequency variation. A high-speed InGaAs photodetector with an integrated traveling-wave GaAs microwave amplifier fed the demodulated signal to a high-speed sampling oscilloscope for analysis. Three measurements were performed as indicated by Equation 5.53. The adjustable delay τ_o was first set to zero using the ASE

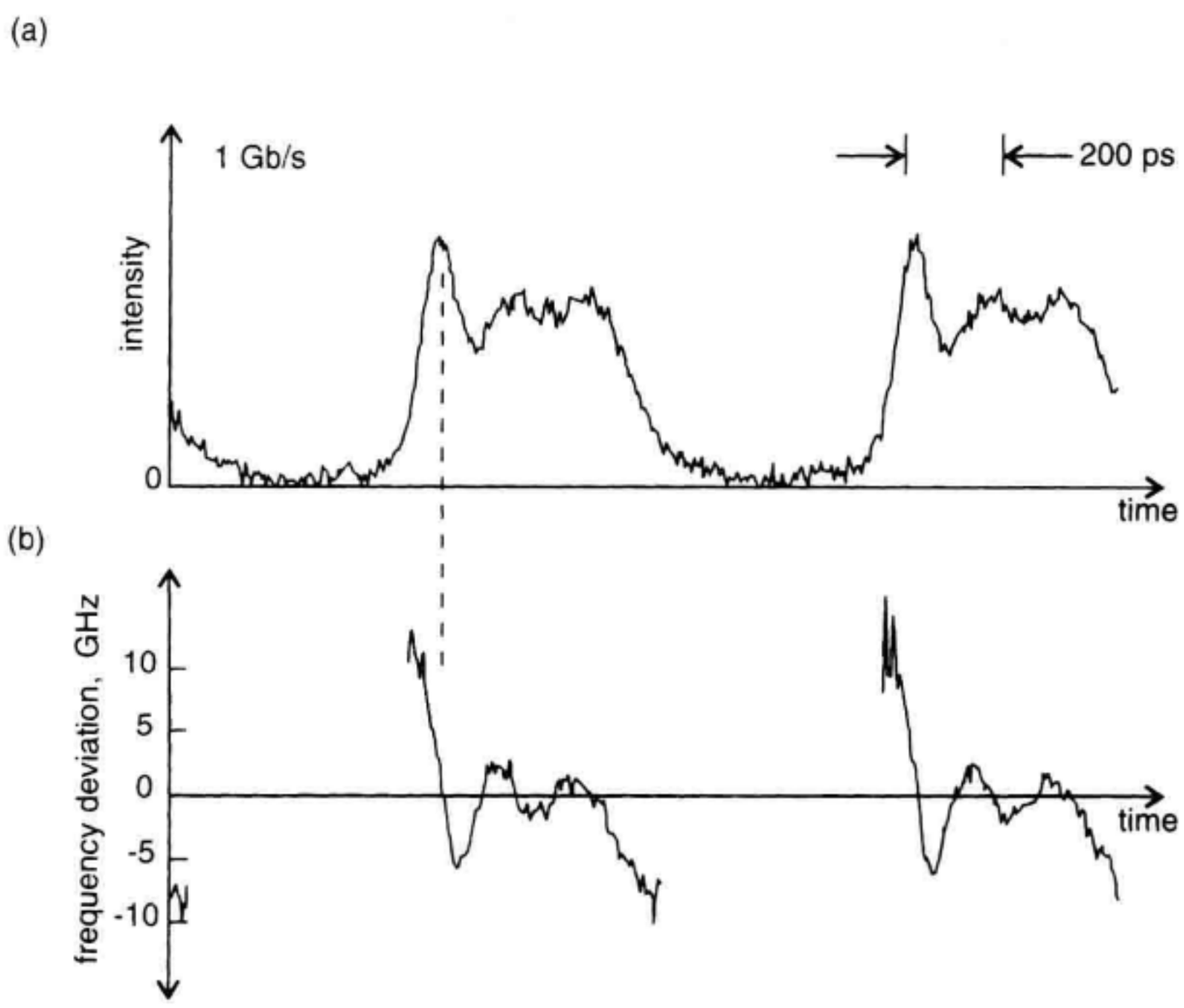

Figure 5.28 Optical discriminator used to measure DFB laser. (a) Intensity modulation. (b) Frequency chirp. Laser current was modulated at a 1 Gb/s rate.

from the DFB laser biased near its threshold current and an OSA to observe the interference nulls. Adjustment of a micrometer controlling the free-space path of one of the collimators fixed the delay τ_o. Polarization controllers were used to align the polarizations of the interfering beams of light. The intensity overshoot in the top trace is due to relaxation oscillations. The rise time was approximately 30 ps. The bottom trace is the measured dynamic frequency chirp. At the beginning of the pulse, the optical frequency chirps over 15 GHz.

Using the technique described in this section, the frequency chirp of a laser or optical modulator can be characterized even in the presence of 100% amplitude modulation. Since the measurement is made in the time domain, both the magnitude and the phase of the amplitude and frequency modulation are measured. In addition to the measurement of the time-domain FM response, this technique can also be applied towards frequency domain measurements of the FM response by characterising laser FM response as a function of modulation frequency applied to the laser.

5.6 FREQUENCY MODULATION MEASUREMENT

This section will discuss a frequency domain technique for characterizing both the AM and FM responses of an optical modulator[8,21,23] using a coherent interferometer. A measurement technique using an interferometer operated in the incoherent regime has been used to measure the FM response versus frequency.[24,25] This method won't be discussed further here since it measures just the magnitude of the FM response and not the phase. The coherent technique presented here consists of a stimulus/response measurement which allows the simultaneous measurement of both the AM and FM imparted onto the optical signal. This type of measurement is useful for characterizing devices such as DFB lasers, $LiNbO_3$ amplitude or phase modulators, and semiconductor electro-absorption modulators.

As discussed in Section 5.5 for the time-domain coherent-discriminator technique, the presence of amplitude modulation can lead to corruption of the measured FM due to the amplitude-dependent discrimination slope of optical interferometers. The direct intensity modulation can be removed from the interference data by making two measurements, each on an opposite slope of the FM discriminator. With these two measurements, the AM and FM responses can be determined. This separation, which requires the measurement of the amplitude and phase at each modulation frequency, can be accomplished using a vector network analyzer.

Figure 5.29 shows a fiber Mach-Zehnder FM discriminator used to perform the frequency domain measurement. The input to the FM discriminator originates from the optical modulator (DFB, $LiNbO_3$, etc.) to be tested. An electrical network analyzer provides the sinusoidal stimulus to the modulator and measures the resulting response (both amplitude and phase) from the discriminator output. Two separate frequency domain measurements are taken, one with the discriminator locked onto the positive slope and the other locked to the negative slope. Since the AM signal is in-phase for both measurements and

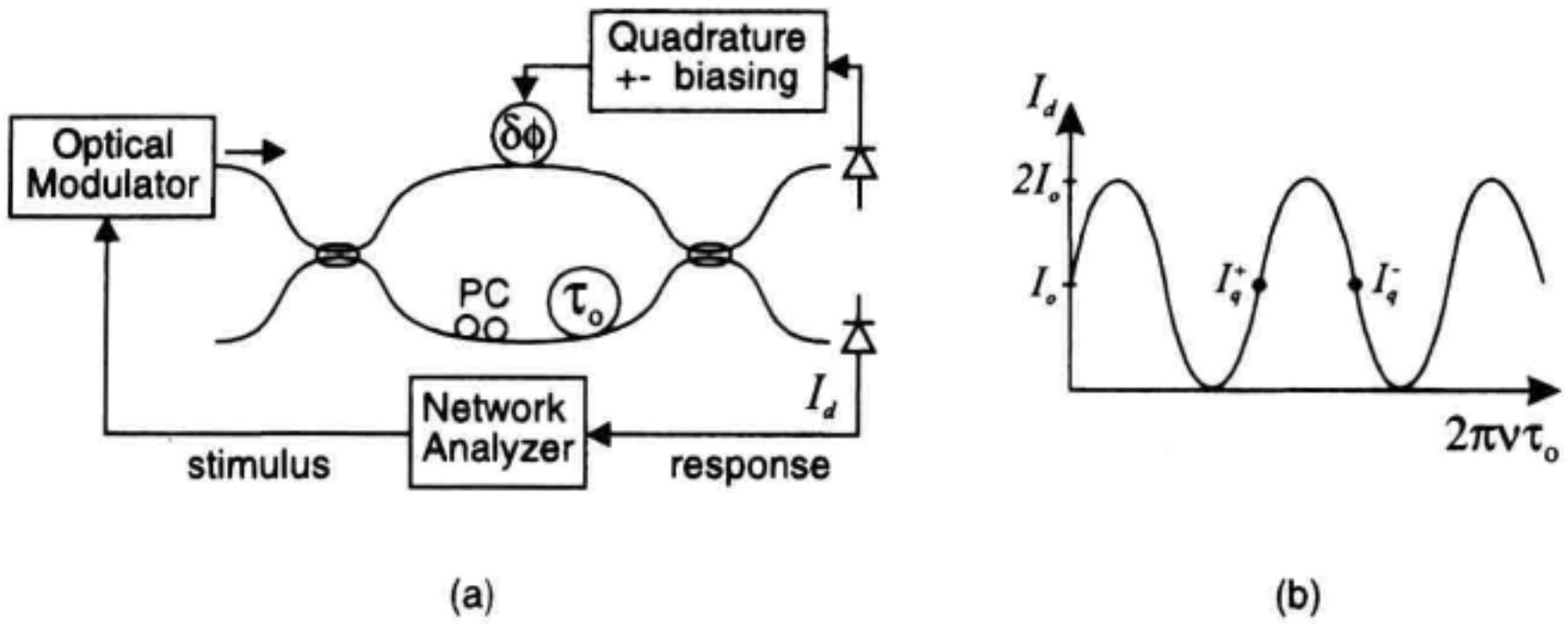

Figure 5.29 Optical FM discriminator used to measure the AM and FM response of an optical modulator.

the FM signal is 180 degrees out-of-phase, by either adding or subtracting the two measurements, the AM and FM responses can be separated. At each frequency, both a magnitude and phase is recorded, therefore the addition and subtraction involves the computation of complex numbers. To better understand this process, the following definitions and equations will be introduced. A more complete analysis can be found in Sorin and coworkers.[23]

Let the complex optical electric field generated by the optical modulator be described by

$$E(t) = \sqrt{P(t)}\, e^{j(2\pi\nu_o t + \phi(t))} \tag{5.56}$$

where ν_o is the average optical frequency and $\phi(t)$ describes the frequency or phase deviations away from the optical carrier. Since the network analyzer delivers a sinusoidal stimulus to the modulator, the response for the optical power can be described by

$$P(t) = P_o[1 + Re\{\tilde{m}(f)e^{j2\pi ft}\}] \tag{5.57}$$

where f is the modulation frequency generated by the network analyzer and P_o is the average optical power. The complex intensity modulation index $\tilde{m}\,(f)$ represents both the amplitude and phase with respect to the driving stimulus from the network analyzer. The operation Re{ } denotes taking only the real part of the complex expression.

Assuming that the optical modulator operates in a linear regime, the resulting optical phase modulation can be described by

$$\phi(t) = \mathrm{Re}\{\tilde{\phi}(f)e^{j2\pi ft}\} \tag{5.58}$$

where $\tilde{\phi}(f)$ is the complex phase modulation index. As with the intensity modulation, the optical phase modulation has a relative amplitude and phase with respect to the driving signal from the network analyzer.

Sometimes it is more convenient to describe the optical carrier variations in terms of an optical frequency modulation as opposed to a phase modulation. Since optical fre-

quency is related to optical phase through a time derivative, the relationship for sinusoidal modulation can be expressed as

$$\phi(t) = 2\pi\int \nu(t)dt = Re\left\{\frac{\tilde{\nu}(f)}{jf}\, e^{j2\pi ft}\right\} \tag{5.59}$$

where $\tilde{\nu}(f)$ is the complex optical frequency modulation at the driving frequency f delivered by the network analyzer. $\tilde{\nu}(f)$ contains both a relative magnitude and phase with respect to the stimulus from the network analyzer.

By sending the modulated optical field described by Equations 5.56 to 5.59 into the FM discriminator, interference signals can be calculated for the two quadrature locking positions. For the positive and negative slope positions, the complex quantities $\tilde{I}_q^+(f)$ and $I_q^-(f)$ represent the measured amplitude and phase of the output photocurrent at the modulation frequency f. The complex intensity modulation index $\tilde{m}(f)$ is related to the sum of these two measurements by

$$\tilde{I}_{AM}(f) = \tilde{I}_q^+(f) + \tilde{I}_q^-(f) = 2I_o \cos(\pi f \tau_o) e^{-j\pi f\tau_o}\, \tilde{m}(f) \tag{5.60}$$

where I_o is the interference amplitude of the photocurrent and τ_o is the differential time delay through the FM discriminator. The term $\cos(\pi f\tau_o)e^{j\pi f\tau_o}$, describes the filtering effect caused by the Mach-Zehnder interferometer on the input optical intensity. By performing calculations, as described by Equation 5.60, the amplitude and phase of the intensity modulation index can be determined as a function of the stimulus frequency.

The optical phase modulation on the input signal can be calculated in a similar manner by using the difference between the two measured photocurrents. This relationship is given by

$$\tilde{I}_{PM}(f) = \tilde{I}_q^+(f) - \tilde{I}_q^-(f) \approx 4jI_o \sin(\pi f \tau_o) e^{-j\pi f\tau_o}\, \tilde{\phi}(f) \tag{5.61}$$

where the approximation sign is used to account for the fact that the discriminator slope, see Figure 5.29b, is not perfectly linear. By keeping $|\tilde{\phi}(f)| < 0.1$ rad, this nonlinearity error can be kept below 1%. Another potential error represented by the approximation sign occurs when the input intensity modulation becomes large. This error occurs due to second-order mixing effects between the intensity modulation and the nonlinearly generated higher harmonics of the phase modulation. This error is less than 10% for modulation indices below $|\tilde{m}(f)| \leq 50\%$.[23]

If one wishes to express the optical carrier deviations in terms of a frequency modulation, Equation 5.59 can be inserted into Equation 5.61 to give

$$\tilde{I}_{FM}(f) = \tilde{I}_q^+(f) - \tilde{I}_q^-(f) = 4\pi\tau_o\, I_o \,\mathrm{sinc}(f\tau_o) e^{-j\pi f\tau_o}\, \nu(f) \tag{5.62}$$

where $\mathrm{sinc}(x) = \sin(\pi/\pi x)/\pi x$. As in Equation 5.61, to keep the approximation reasonably valid, the constraints of $|\tilde{\nu}(f)| \leq 0.1/\tau_o$ and $|\tilde{m}(f)| < 0.5$ should be observed.

Experimental Results. To illustrate the use of the above analysis, two experimental examples will be discussed. The first consists of measuring the frequency domain response of a current modulated 1300 nm DFB laser.[23] This measurement was performed by using a HP 8703A optical component analyzer to modulate the pump current of the

DFB laser. With the FM discriminator locked on the positive slope, a frequency measurement from 130 MHz to 10 GHz was performed to generate the data array, $\tilde{I}_q^+(f)$. The polarity to the locking element was then reversed, causing the bias position to change to a negative slope, and the array $\tilde{I}_q^-(f)$ was measured. This data was then inserted into Equations 5.60 and 5.62 to generate the results shown in Figure 5.30. These results were also normalized by the amplitude of the modulated pump current injected into the laser. The differential time delay for the discriminator was set ($1/\tau_o = 17.1$ GHz) to avoid loss of the high-modulation frequencies caused by the filtering effects of the interferometer. The peak response in Figure 5.30, at about 2.7 GHz, is due to relaxation oscillations within the laser. At this modulation frequency, the intensity modulation index was 5%/mA and the optical frequency deviation was about 650 MHz/mA.

The next example consists of measuring the residual phase modulation produced by a $LiNbO_3$ amplitude modulator.[23] Because of its push-pull electrode configuration, the modulator should theoretically impart only intensity modulation and no phase modulation. However, in practice, residual-phase modulation exists due to the nonideal construction of the device. Figure 5.31 shows the photocurrent difference as calculated by Equations 5.60 and 5.61. This measurement is different in nature to that for the DFB laser since the interferometer time delay was made much larger. The inverse of the time delay was $1/\tau_o = 273$ MHz, which is relatively small compared to the 5 GHz measurement range. For this reason the filtering effects of the discriminator are present, as seen by the periodic response in the measured data. It is interesting to note that the peaks in the periodic response correspond to locations where the filtering effects of the discriminator are removed. At these points, the modulation index and phase index can be read directly from

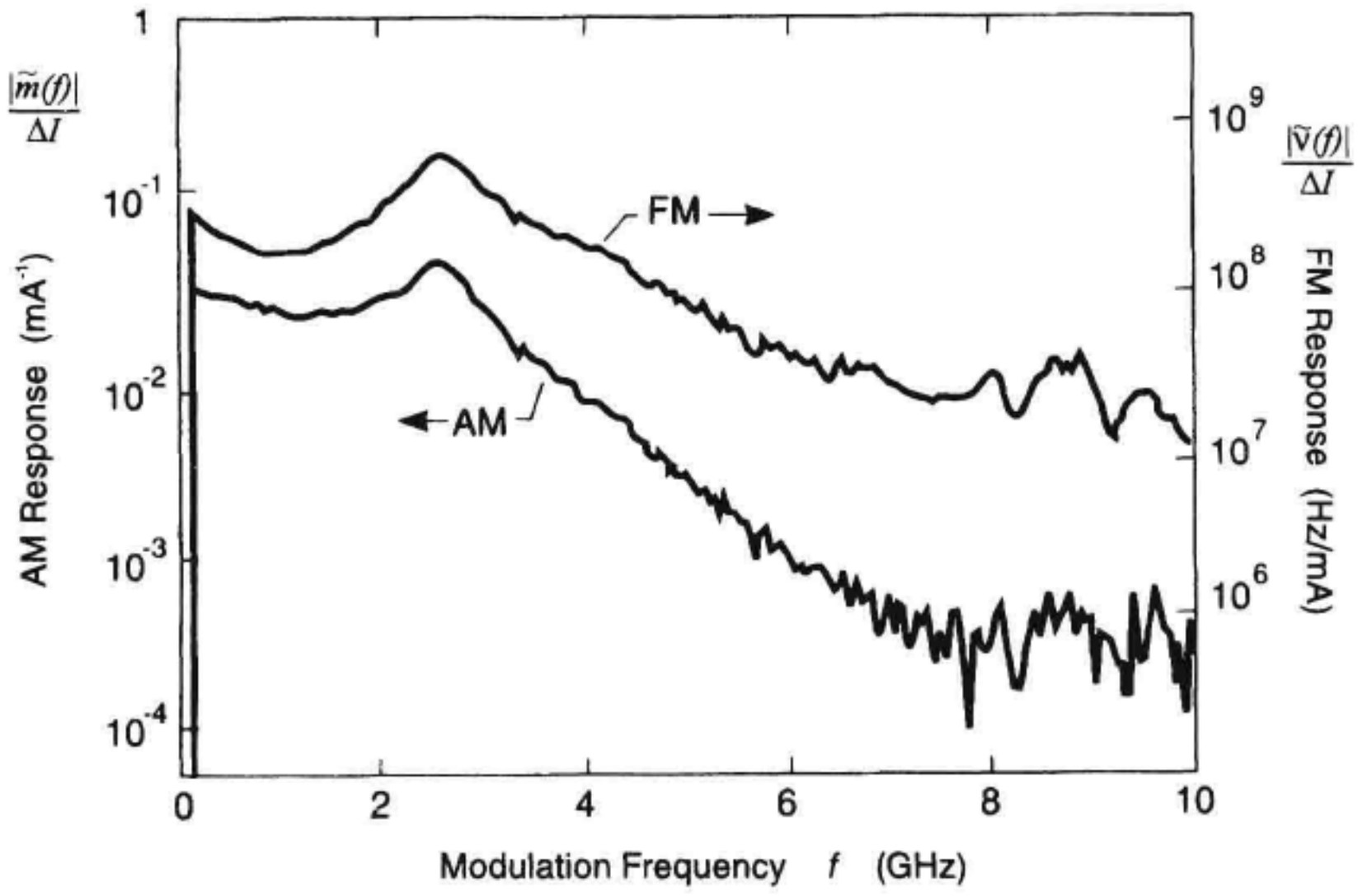

Figure 5.30 AM and FM response versus frequency for a current modulated DFB laser.

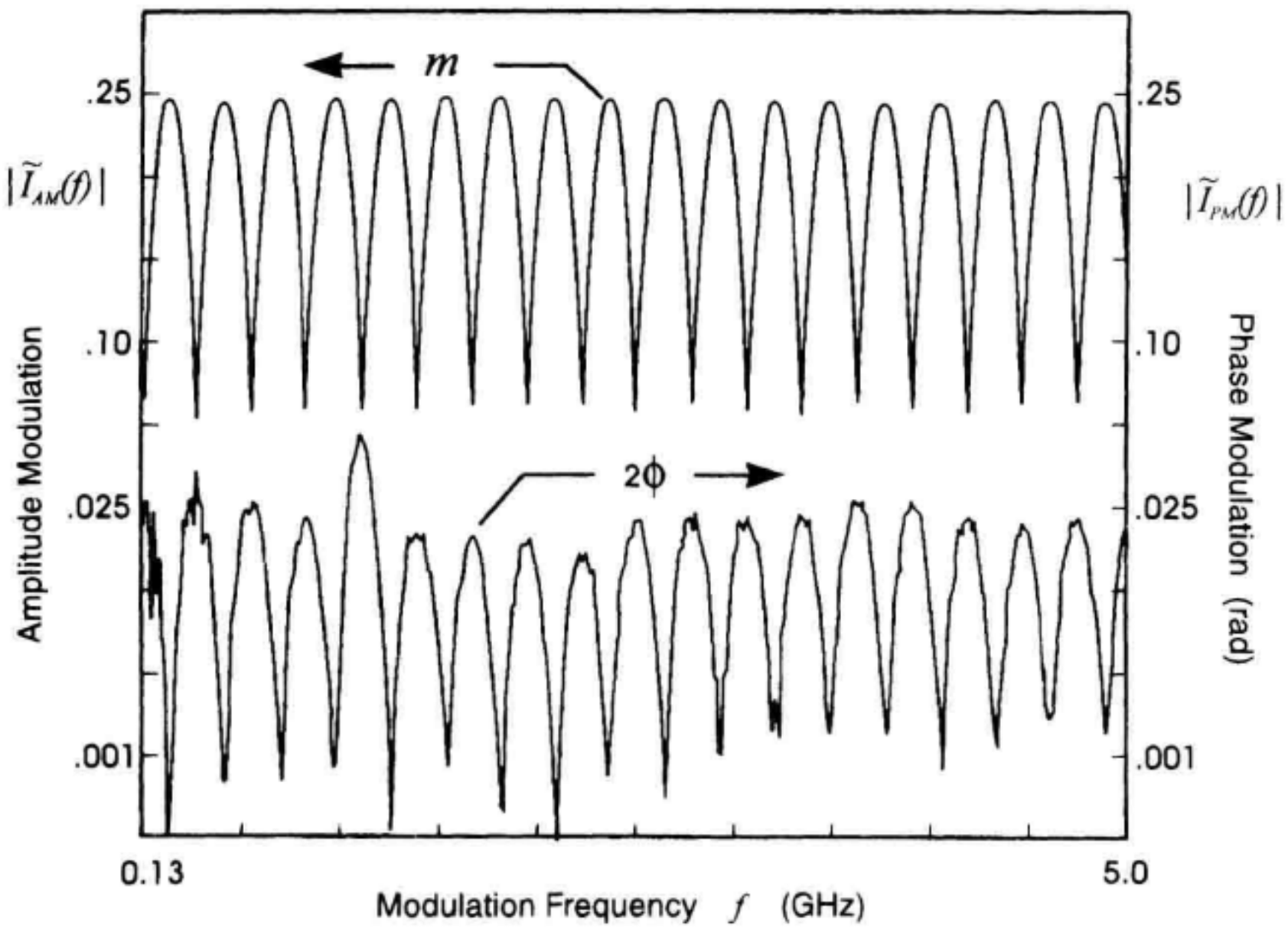

Figure 5.31 Frequency domain measurement of the intensity modulation (m) and phase modulation (2ϕ) response of a $LiNbO_3$ intensity modulator.

the plot in Figure 5.31. For this particular $LiNbO_3$ modulator, the phase modulation was about $2\phi = 0.025$ rad for an intensity modulation of $m = 0.25$. The ratio of these two numbers yields the modulator's amplitude-phase coupling factor α (see Section 5.2.1) of $2\phi/m = 0.1$. This figure of merit represents the ratio of the FM to AM sidebands on the electric field of the modulated optical carrier.

Using the technique described in the above section, the frequency domain response of an optical modulator can be characterized. This technique allows for an accurate measurement of the FM frequency response, even in the presence of some accompanying intensity modulation. Both the magnitude and phase, relative to a sinusoidal stimulus, is measured for the generated intensity and optical frequency modulation. Assuming the modulator is operated in its linear region, this frequency domain data can be used to predict time-domain responses.

5.7 SUMMARY

This chapter covered a variety of techniques for high-resolution measurement of laser linewidth, modulated power spectrum, frequency chirp, and FM response. The measurement techniques have, as a common theme, the concept of interference. The interference allows normally undetectable phase or frequency modulation to be measured with a high-

speed photodetector. The signal from the photodetector is then analyzed with either an electrical spectrum analyzer, oscilloscope, or network analyzer. The heterodyne, delayed self-heterodyne, delayed self-homodyne, and coherent discriminator techniques were discussed for linewidth measurements. The heterodyne and the gated-delayed self-homodyne techniques were discussed for their application to measurement of the power spectrum of a modulated laser. In the latter part of this chapter, two important topics were considered: the time domain measurement of laser or modulator chirp, and the FM response of a laser or modulator. Both of these techniques were based on coherent interference to convert phase or frequency modulation into measurable intensity changes.

REFERENCES

1. Agrawal, G.P. 1995. *Nonlinear Fiber Optics.* 2nd ed. San Diego, CA: Academic Press.
2. Hinkley, E.D. and Freed, C. 1969. Direct observation of the Lorentzian line shape as limited by quantum phase noise in a laser above threshold. *Phys. Rev. Lett.* 23(6): 277–280.
3. Agrawal, G.P. 1986. *Long-wavelength semiconductor lasers.* NY: Van Nostrand Reinhold Co. Inc.
4. Koch, T.L. and J.E. Bowers 1984. Nature of wavelength chirping in directly modulated semiconductor lasers. *Electron. Lett.* 20(25): 1038–1039.
5. Henry, C.H. 1986. Phase noise in semiconductor lasers. *J. Lightwave Technol.* LT-4: 298–311.
6. Yoshida, S., Tada, Y., and Nosu, K. 1994. High resolution optical spectrum analysis by coherent detection with multi-electrode DBR-LD's as local oscillators. Conference Proceedings. IMTC/94. Hamamatsu, Japan: Advanced Technologies in I & M. IEEE Instrumentation and Measurement Technology Conference.
7. Nazarathy, M., W.V. Sorin, D.M. Baney, and S.A. Newton. 1989. Spectral analysis of optical mixing measurements. *IEEE J. Lightwave Technol.* 7(7): 1083.
8. Baney, D.M. 1990. Modélization et caractérisation de la réponse FM des lasers à contre-réaction distribuée mono et multi-section. Doctoral Thesis, No. 90E015. Ecole Nationale Superiéure des Télécommunications, Paris, France.
9. Okoshi, T., Kikuchi, K., and Nakayama, A. 1980. Novel method for high frequency resolution measurement of laser output spectrum. *Electron. Lett.* 16: 630–631.
10. Mercer, L.B. 1991. 1/f frequency noise effects on self-heterodyne linewidth measurements. *Journal of Lightwave Technology* 9(4): 485–493.
11. Esman, R.D. and L. Goldberg. 1988. Simple measurement of laser diode spectral linewidth using modulation sidebands. *Electron. Lett.* 24(22): 1393–1395.
12. Constable, J.A. and I.H. White. 1994. Laser linewidth measurement using a Mach-Zehnder interferometer and an optical amplifier. *Electronics Lett.* 30(2): 140–142.
13. Baney, D.M. and W.V. Sorin. 1990. Linewidth and Power Spectral Measurements of Single-Frequency Lasers. *Hewlett-Packard Journal* 41(92): 92–96.
14. Gallion, P.B. and G. Debarge. 1984. Quantum phase noise and field correlation in single frequency laser systems. *IEEE J. Quantum Electron.* QE-20: 343–349.
15. Kruger, M.S., L.E. Richter, H.I. Mandelber, and P.A. McGrath. 1986. Linewidth determination from self-heterodyne measurements with sub-coherence delay times. *IEEE J. Quantum Electron.* 22: 2070–2074.

16. Sorin, W.V., S.A. Newton, and M. Nazarathy. 1988. Kilohertz laser linewidth measurements using fiber ring resonators. OFC/OFS '88, paper **WC5,** New Orleans, Louisiana. *Optical Fiber Communications Conference* p. 55.
17. Van Deventer, M.O., Spano, P., and Nielsen, S.K. 1990. Comparison of DFB laser linewidth measurement techniques results from COST 215 round robin. *Electronics Lett.* 26(24): 2018–2020.
18. Baney, D.M. and W.V. Sorin. 1988. Measurement of modulated DFB laser power spectrum using gated delayed self-homodyne technique. *Electron. Lett.* 24(4): 669.
19. Baney, D.M. and P.B. Gallion. 1989. Power spectrum measurement of a modulated semiconductor laser using an interferometric self-homodyne technique: influence of quantum phase noise and field correlation. *IEEE J. Quantum Electron.* 25(10): 2106.
20. Baney, D.M. and P.B. Gallion. 1991. Time domain measurement of chirp suppression for a multisection DFB laser, Optical Fiber Communications Conference, Optical Society of America. Paper WN7. San Diego, CA.
21. Vodhanel, R.S. and S. Tsuji. 1988. 12 Ghz FM bandwidth for a 1530 nm DFB laser. *Electron. Lett.* 24(22): 1359–1361.
22. Bergano, N.S. 1988. Wavelength discriminator method for measuring dynamic chirp in DFB lasers. *Electron. Lett.* 24(20): 1296–1297.
23. Sorin, W.V., K.W. Chang, G.A. Conrad, and P.R. Herndav, 1992. Frequency domain analysis of an optical FM discriminator. *J Lightwave Tech.* 10(6): 787–793.
24. Baney, D.M., P.B. Gallion, and C. Chabran. 1990. Measurement of the swept-frequency carrier-induced FM response of a semiconductor laser using an incoherent interferometric technique. *IEEE Photon. Technol. Lett.* 2(5): 325.
25. Kruger, U. and K. Kruger. 1995. Simultaneous measurement of the linewidth, linewidth enhancement factor and FM and AM response of a semiconductor laser, *J. Lightwave Tech.* 12(4): 592–597.

CHAPTER

6

Polarization Measurements

Paul Hernday

6.1 INTRODUCTION

The concept of lightwave polarization is less familiar to many of us than the concepts of modulation or optical spectra. Many early telecommunications applications did not specify the polarization properties of the signal or the polarization transforming properties of transmission media. A more fundamental reason for our relative unfamiliarity with polarization may be that humans do not have the biological equipment to differentiate between different polarization states. This is not the case with many other organisms. Reflection from surfaces often partially polarizes light, producing patterns which polarization-sensitive vision can detect. The ability of some creatures to see (image) polarization patterns enables them to orient themselves, to recognize elements in their environment, and perhaps to identify members of their own species. The pygmy octopus, the mantis shrimp, and the starfish are among the creatures that can detect polarization patterns.[1] Scarab beetles have the unusual property of converting unpolarized incident light into left-hand circularly polarized light.[2]

Just as some organisms have found an advantage in their ability to recognize polarization patterns, modern telecommunication system designers can benefit from recognizing and controlling the polarization properties of signal light and the polarization conditioning characteristics of transmission media and optical components. In fact, such mastery is critical for high-speed, long-distance fiber optic systems and for high channel-capacity CATV distribution systems. Unlike the conventional waveguides used in the microwave field, optical fiber transforms signal polarization in a random way. Fiber optic components exhibit polarization-dependent insertion loss or gain, and awareness of the polarization relationships within a lightwave system is key to successful design.

The aim of this chapter is to provide an introduction to the concepts and vocabulary of lightwave polarization and its measurement. It also explores several measurement applications. The emphasis is upon providing an interesting introduction to the field, and the reader is referred to other texts for thorough treatments of polarized light. Edward Collett's *Polarized Light: Fundamentals and Applications* provides an extremely interesting and authoritative explanation of polarization concepts and fundamental polarization measurements.[3] Some of Collett's mathematical conventions are followed in this chapter.

Beginning with an introduction to polarization in the context of optical fiber, this chapter will discuss the measurement of retardance and the measurement of polarization cross-talk in polarization-maintaining fiber.

6.2 POLARIZATION CONCEPTS

6.2.1 General Description of Polarized Light

A polarized lightwave signal that is propagating in fiber or in free space is represented by electric and magnetic field vectors that lie at right angles to one another in a transverse plane (a plane perpendicular to the direction of travel). Polarization is defined in terms of the pattern traced out in the transverse plane by the electric field vector as a function of time, as shown in Figure 6.1. These are snapshots in time, showing the electric field as a function of distance. As time passes, the patterns move toward the observer. The polarization ellipse, shown at the left in each example, provides a more convenient description of polarization. By convention, the ellipse is generated by propagating the three-dimensional pattern through a fixed *xy*-plane. The ellipse shows the locus and the direction of rotation—the handedness—of the electric field vector in the fixed plane. In general, fully polarized light is elliptically polarized; linear and circular polarization are simply extremes of ellipticity.

It is not always possible to describe light in terms of a predictable electric field vector. Naturally produced light—sunlight, firelight, light from fireflies—is unpolarized. Unpolarized light of a given intensity can be represented intuitively as an electric field vector that from moment to moment occupies random orientations in the *xy*-plane. The random reorientation need only be fast enough to be beyond observation within the physical context of a particular measurement or application. This qualifier is worth noting, because there are applications in telecommunications and optical sensors in which fully polarized light is polarization-scrambled at a sufficiently high rate for it to appear unpolarized within the lifetime of carriers in an optical amplifier or within the bandwidth of optical instrumentation. It is not possible to systematically predict the electric field orientation of unpolarized light, nor to manipulate the polarization state with retarders (polarization-transforming devices discussed later in this chapter).

The usefulness of a lightwave in a particular application can depend upon its degree of polarization. Light from an ordinary light bulb is entirely unpolarized and is generally adequate for the daily life of non-fiber optics engineers. Light from a diode laser is almost completely polarized, presenting both opportunities and challenges in sensor and telecommunications applications. The light produced by a light emitting diode (LED) may be 10

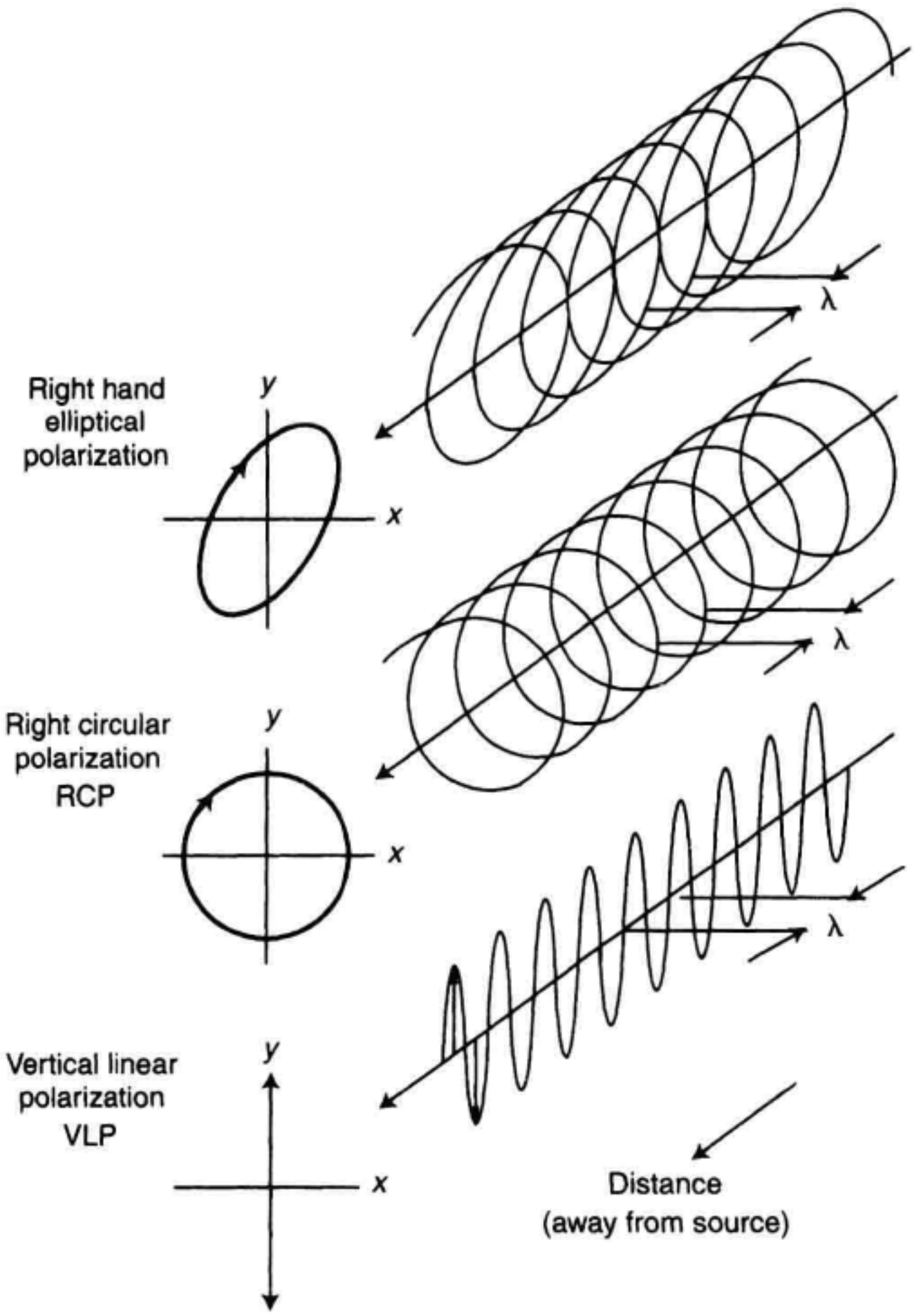

Figure 6.1 Three-dimensional and "polarization ellipse" representations of polarized light.

to 20% polarized. Partially polarized light can be modeled as the superposition of a fully polarized and a completely unpolarized lightwave. The degree of polarization (DOP) is described by

$$\text{DOP} = \frac{P_{\text{polarized}}}{P_{\text{polarized}} + P_{\text{unpolarized}}} \tag{6.1}$$

involving the amount of power, in linear terms, of the polarized and unpolarized components of the signal. A lightwave traveling through free space will maintain its degree of polarization indefinitely. However, a nonideal transmission medium or two-port optical component can change the degree of polarization of the signal in a relationship involving the spectral width of the signal and the dispersive properties of the transmission path. This relationship is discussed in Chapter 12, which deals with dispersion measurements.

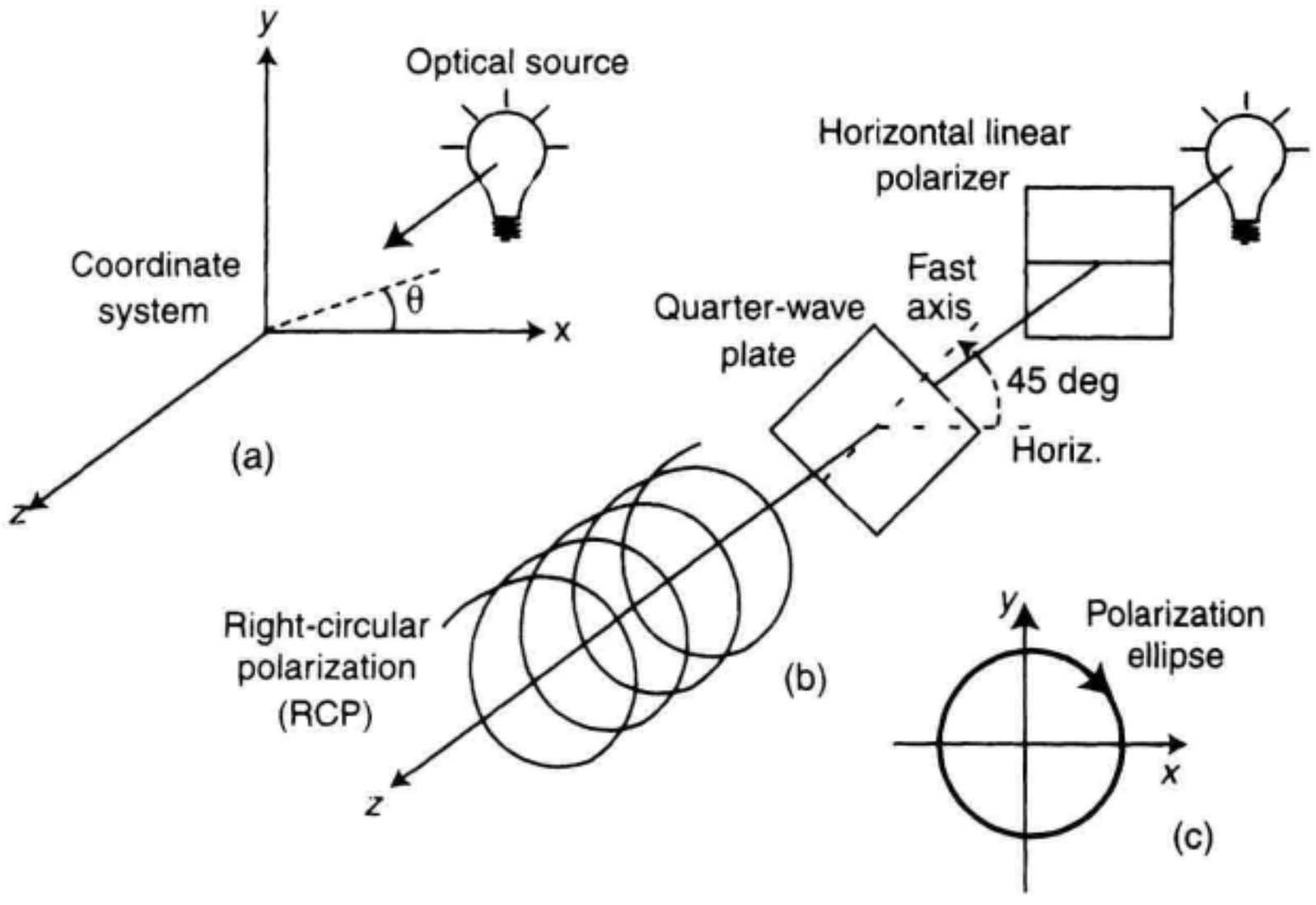

Figure 6.2 (a) A coordinate system for unambiguous description of the state of polarization. (b) Generation of right circular polarization. (c) Corresponding polarization ellipse.

6.2.2 A Polarization Coordinate System

An explicit coordinate system must be specified in order to unambiguously describe a state of polarization. A conventional coordinate system is shown in Figure 6.2a. The z-axis is horizontally oriented in the direction of propagation of the light. The y-axis is vertically oriented pointing up, and the x-axis is horizontally oriented to form a right-handed rectangular coordinate system. Angles are measured with reference to the x-axis, a positive angle indicating the sense of rotation from the x-axis toward the y-axis. In Figure 6.2b, unpolarized light is filtered by a polarizer to produce horizontal linear light. A quarter-wave retarder, which is discussed later in the chapter, is used to resolve the horizontally polarized light into two equal-intensity components that travel at slightly different speeds. For the retarder orientation shown, light emerging from the retarder is right-hand circularly polarized, illustrated in the polarization ellipse of Figure 6.2c.

6.2.3 The Polarization Ellipse

Polarized light can be represented mathematically in terms of the x- and y-axis projections of the electric field vector. Borrowing from Collett, the transverse components are given by [3]

$$E_x(z, t) = E_{0x} \cos(\tau + \delta_x) \tag{6.2}$$

$$E_y(z, t) = E_{0y} \cos(\tau + \delta_y) \tag{6.3}$$

where $\tau = \omega t - kz$ is the "propagator." Subscripts x and y indicate the directions of the axes, E_{Ox} and E_{Oy} are the maximum amplitudes, and δ_x and δ_y are the corresponding phases. The pattern traced out by the electric field in a fixed xy-plane is described by

$$\frac{E_x^2}{E_{0x}^2} + \frac{E_y^2}{E_{0y}^2} - 2\frac{E_x E_y}{E_{0x} E_{oy}} \cos\delta = \sin^2\delta \tag{6.4}$$

where $\delta = \delta_y - \delta_x$ is the difference in phase between the two components.

The relationships are illustrated in Figure 6.3 for arbitrarily selected amplitudes and phases. By convention, the ellipse is presented as it would appear looking through the xy-plane toward the source. The light is right-handed, which can be verified by inspection of the plots of E_x and E_y. By varying the magnitudes and phases, any polarization state can be described.

6.2.4 The Jones Calculus

Between 1941 and 1948, R. Clark Jones published a series of papers describing a new polarization calculus based upon optical fields rather than intensities.[4] This approach, although more removed from direct observation than previous methods, allowed calculation of interference effects and in some cases provided a simpler description of optical physics.

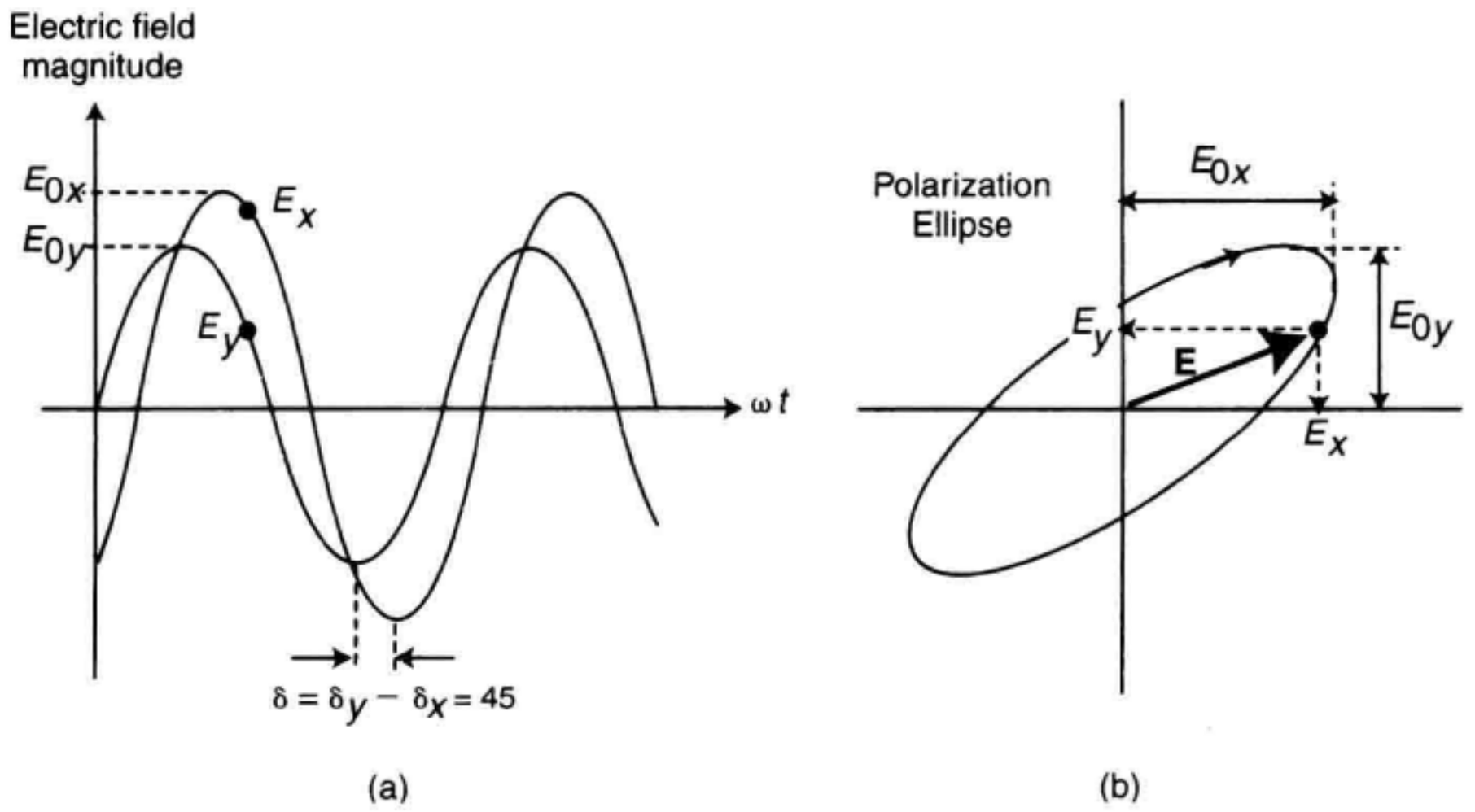

Figure 6.3 The polarization ellipse in relation to the x- and y- components of the electric field.

Polarized light can be represented by a two-element complex vector, the elements of which specify the magnitude and phase of the x- and y-components of the electric field at a particular point in space. The Jones vector has the form

$$\mathbf{E} = \begin{pmatrix} E_x \\ E_y \end{pmatrix} = \begin{pmatrix} E_{0x}\, e^{i\delta x} \\ E_{0y}\, e^{i\delta_y} \end{pmatrix} \tag{6.5}$$

where real quantities E_{Ox} and E_{Oy} represent the maximum amplitudes and δ_x and δ_y represent the phases. It is customary to use the Jones vector in normalized form and to simplify the representation of phase. The Jones vector for linear horizontal polarized light

$$\mathbf{E} = \begin{pmatrix} E_{0x} e^{i\delta x} \\ 0 \end{pmatrix} \text{ becomes } \mathbf{E} = \begin{pmatrix} 1 \\ 0 \end{pmatrix}. \tag{6.6}$$

The Jones vector for right-hand circularly polarized light is

$$\mathbf{E} = \frac{1}{\sqrt{2}} \begin{pmatrix} 1 \\ +i \end{pmatrix} \tag{6.7}$$

where the amplitude of the normalized Jones vector is unity and the imaginary bottom element represents the phase relationship $\delta_y - \delta_x = +90$ degrees. The Jones vector is limited to the description of fully polarized light.

The transmission properties of a two-port optical device can be described by the complex two-by-two Jones matrix, which relates the input and output Jones vectors. The Jones matrix representation of an unknown device can be found by measuring three output Jones vectors in response to three known stimulus polarizations, as shown in Figure 6.4. Calculation of the matrix is simplest when the stimuli are linear polarizations oriented at 0, 45, and 90 degrees, but any three distinct stimuli may be used. The matrix calculated in this manner is related to the true Jones matrix by a multiplicative complex con-

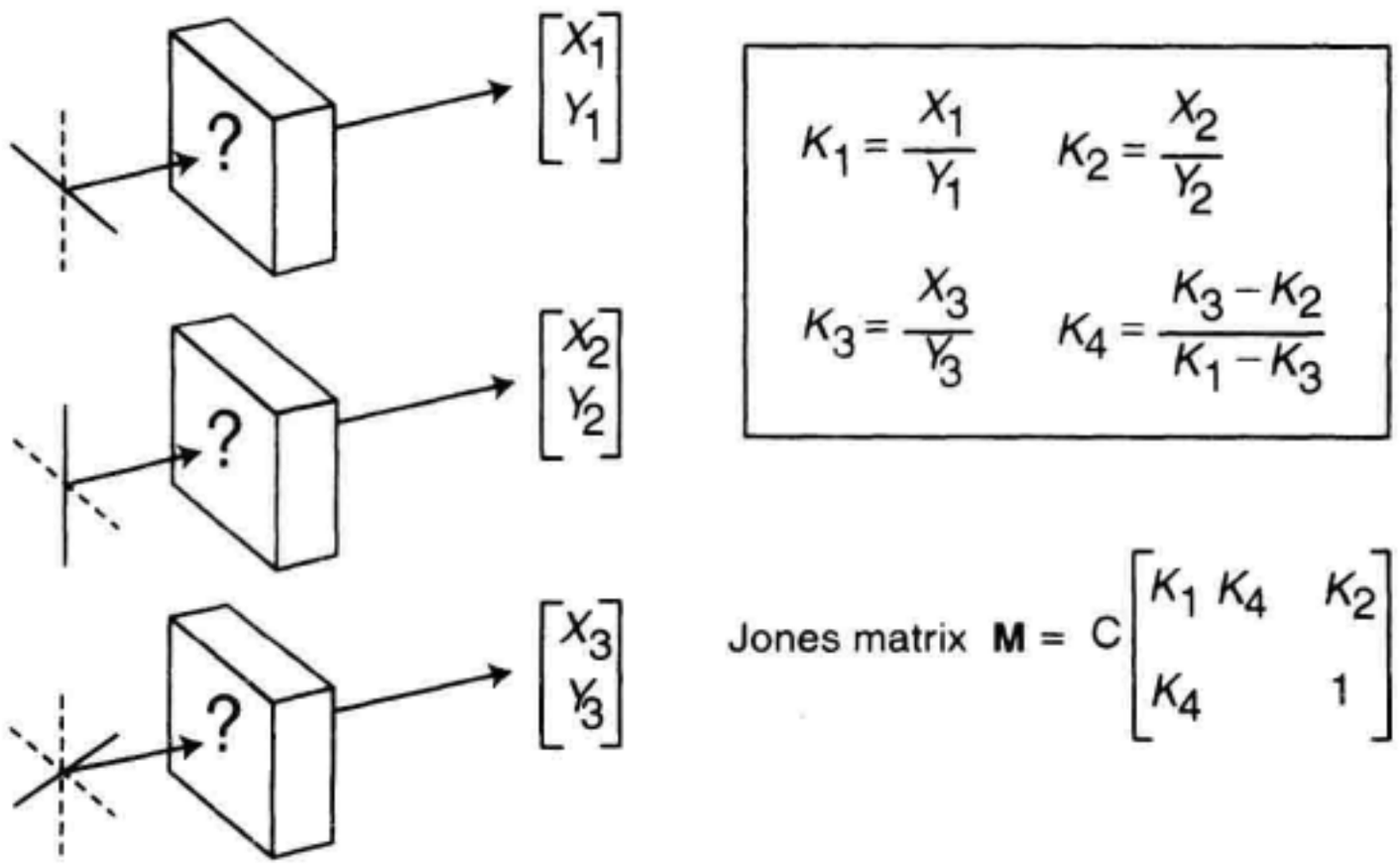

Figure 6.4 Measurement of the Jones matrix of an optical component.

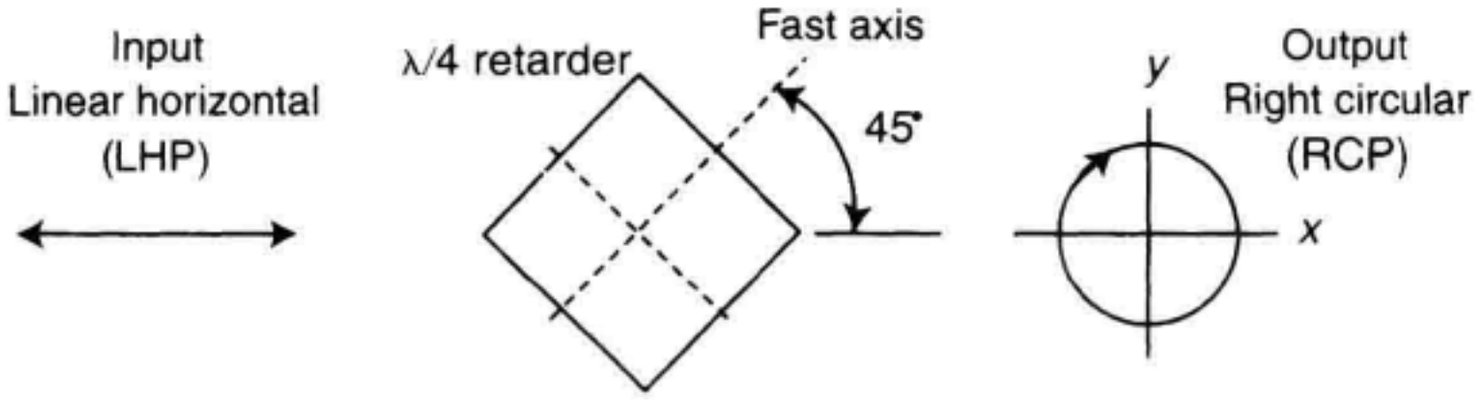

Figure 6.5 Jones calculus description of the effect of a rotated retarder on linear horizontally polarized light.

stant C. The magnitude of this constant can be calculated from intensities measured with the device removed from the optical path, but the phase is relatively difficult to calculate, requiring a stable interferometric measurement. Fortunately, most measurements do not require determination of this constant.

An example of the use of the Jones calculus is given in Figure 6.5. Linear horizontally polarized light (LHP) is passed through a retarder that is tilted to bring the fast axis +45 degrees from the horizontal. The output polarization is right circular (RCP).

6.2.5 The Stokes Parameters

It is not convenient to measure the electric field of a lightwave, and in any case it is problematic to deal with the case of partially polarized light. For these reasons, methods have been developed for expressing polarization in terms of easily measured optical powers. One widely used tool is the Stokes vector, an array of optical power values in which the elements describe the optical power in particular reference polarization states. The Stokes parameters uniquely represent the polarization state of the signal. The array has the form

$$\begin{bmatrix} S_0 \\ S_1 \\ S_2 \\ S_3 \end{bmatrix} \tag{6.8}$$

where each element caries the units of optical power and has the meaning given below. Abbreviations LH, LV, RC, and LC are introduced to denote linear horizontal, linear vertical, right circular, and left circular polarizations, respectively. A following P, for polarization, is often used. Linear polarized light at a particular angle is abbreviated as $L \pm\theta$.

S_0 = Total power (polarized + unpolarized)
S_1 = Power through LH polarizer – power through LV polarizer
S_2 = Power through L +45 polarizer – power through L –45 polarizer
S_3 = Power through RC polarizer – power through LC polarizer

Stokes parameters S_1, S_2, and S_3 can be assigned to an *xyz*-coordinate system as shown in Figure 6.6a. The amount of optical power contained in the polarized part of the lightwave is given by

$$P_{\text{polarized}} = \sqrt{S_1^2 + S_2^2 + S_3^2} \tag{6.9}$$

The *normalized* Stokes parameters are obtained by dividing the Stokes parameters by the total optical power:

$$s1 = \frac{S_1}{S_0} \quad s2 = \frac{S_2}{S_0} \quad s3 = \frac{S_3}{S_0} \tag{6.10}$$

The range of the normalized Stokes parameters is −1 to +1. For example, fully polarized horizontal linear light is expressed by $s1 = +1$, $s2 = s3 = 0$. The normalized Stokes parameters can be assigned to *xyz*-axes as shown in Figure 6.6b.

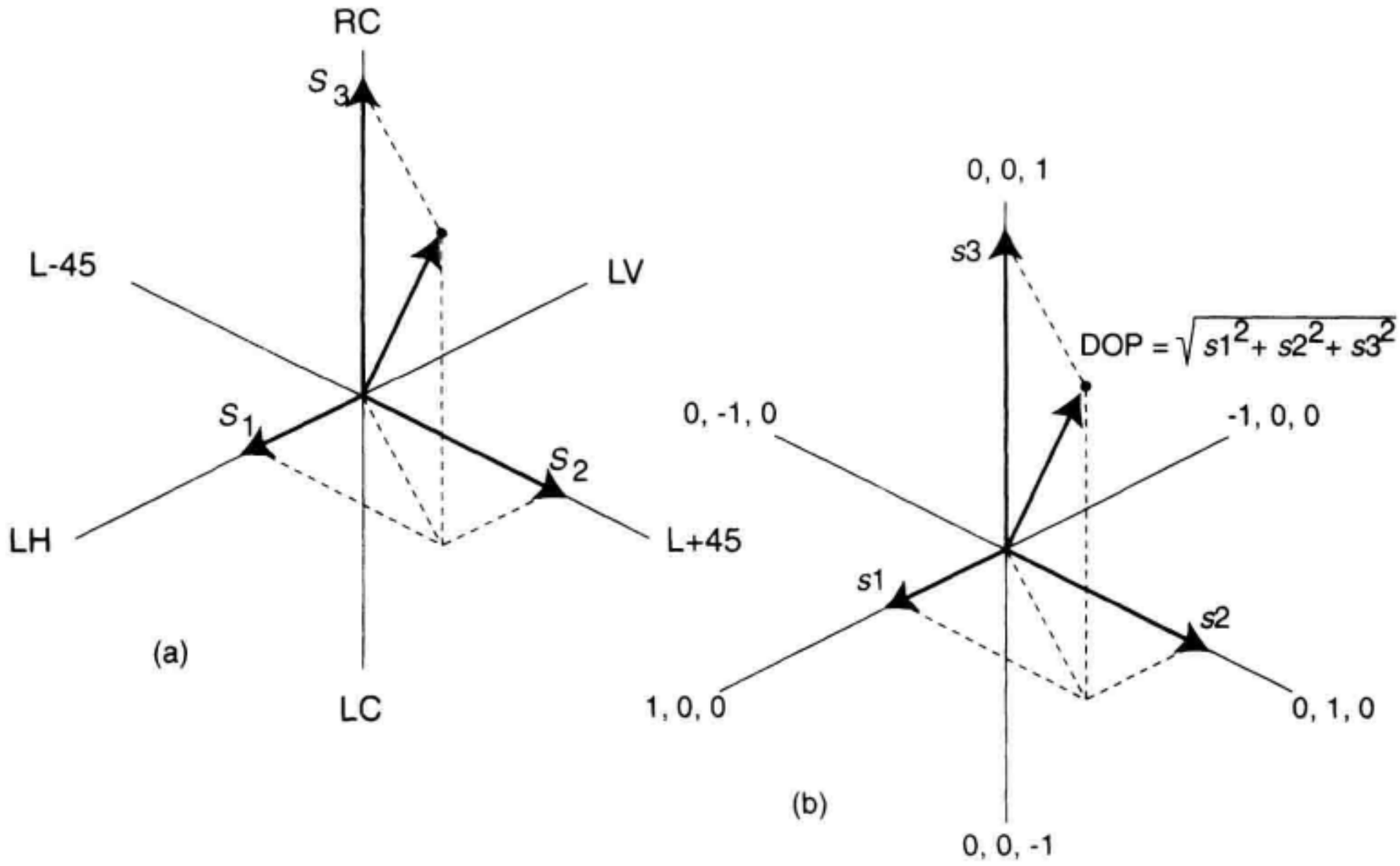

Figure 6.6 Orthogonal representations of (a) the Stokes parameters; (b) the normalized Stokes parameters.

6.2.6 Degree of Polarization

As discussed earlier, the degree to which a lightwave signal is polarized is given by the ratio of polarized light to total light:

$$\text{DOP} = \frac{P_{\text{polarized}}}{P_{\text{polarized}} + P_{\text{unpolarized}}} \tag{6.11}$$

The degree of polarization can be expressed in terms of the Stokes parameters

$$\text{DOP} = \frac{\sqrt{S_1^2 + S_2^2 + S_3^2}}{S_0} \tag{6.12}$$

or the normalized Stokes parameters

$$\text{DOP} = \sqrt{s1^2 + s2^2 + s3^2} \tag{6.13}$$

In the case of fully polarized light, DOP = 1, Equation 6.13 describes a sphere of unit radius. If the light is 50% polarized, Equation 6.13 defines a sphere of radius 1/2.

Depolarization of Lightwave Signals. Depolarization of lightwave signals may be a help or a hindrance. If the goal is to measure the polarization-mode dispersion of a fiber path, depolarization should be avoided. At the system level, the same is true in systems based on coherent detection, where depolarization causes the detected signal to fade. On the other hand, totally unpolarized light does not experience the effects of polarization-dependent loss or gain in fiber components or polarization-dependent sensitivity of photodiodes. In high-speed systems based on erbium-doped fiber amplifiers (EDFAs), polarized light produced by the transmitter laser may be scrambled using optical integrated circuits, effectively depolarizing the light to obtain best performance from the EDFAs.

Under some conditions, a fully polarized lightwave signal can depolarize simply by transmission through a fiber path. High-birefringence (hi-bi) fiber exhibits a significant difference in the index of refraction for orthogonal electric fields. A monochromatic (single-wavelength) optical signal coupled partially into each of these principal states of polarization splits into two wavefronts that experience an entire wave of differential delay in a distance of only a few millimeters (the "beat length" of the hi-bi fiber). If the signal has significant spectral width, the differential delay depolarizes the light. Depolarization becomes most severe when the fast and slow axes are equally illuminated and the differential delay exceeds the coherence time of the signal, given by

$$t_c = \frac{1}{\Delta f} = \frac{\lambda^2}{c\Delta\lambda} \tag{6.14}$$

where Δf is the source linewidth in Hz, $\Delta\lambda$ is the full-width, half-maximum (FWHM) spectral width of the source in meters, λ is the center wavelength of the source in meters, and c is the speed of light (3×10^8 m/s). Assuming a source with Gaussian spectrum of

width $\Delta\lambda$ centered at λ, the lowest degree of polarization which can result from a differential delay $\Delta\tau$ (seconds) is given by

$$\text{DOP} = e^{-\frac{1}{4\ln 2}\left(\frac{\pi c\,\Delta\tau\,\Delta\lambda}{\lambda^2}\right)^2} \tag{6.15}$$

Depolarization is most severe when fast and slow polarization modes are equally illuminated.

6.2.7 The Poincaré Sphere

The Poincaré sphere,[5] shown in Figure 6.7, is a graphical tool in real, three-dimensional space that allows convenient description of polarized signals and of polarization transformations caused by propagation through devices. Any state of polarization can be uniquely represented by a point on or within a unit sphere centered on a rectangular *xyz*-coordinate system. Circular states are located at the poles, with intermediate elliptical states continuously distributed between the equator and the poles. Right-hand and left-hand elliptical states occupy the northern and southern hemispheres, respectively. The coordinates of a point within or upon this sphere are the normalized Stokes parameters.

Fully polarized light is represented by a point on the surface of the Poincaré sphere. Partially polarized light, which can be considered a superposition of polarized and unpolarized light, is represented by a point within the volume of the Poincaré sphere. The distance of the point from the center of the sphere gives the degree of polarization of the signal, ranging from zero at the origin (unpolarized light) to unity at the sphere surface

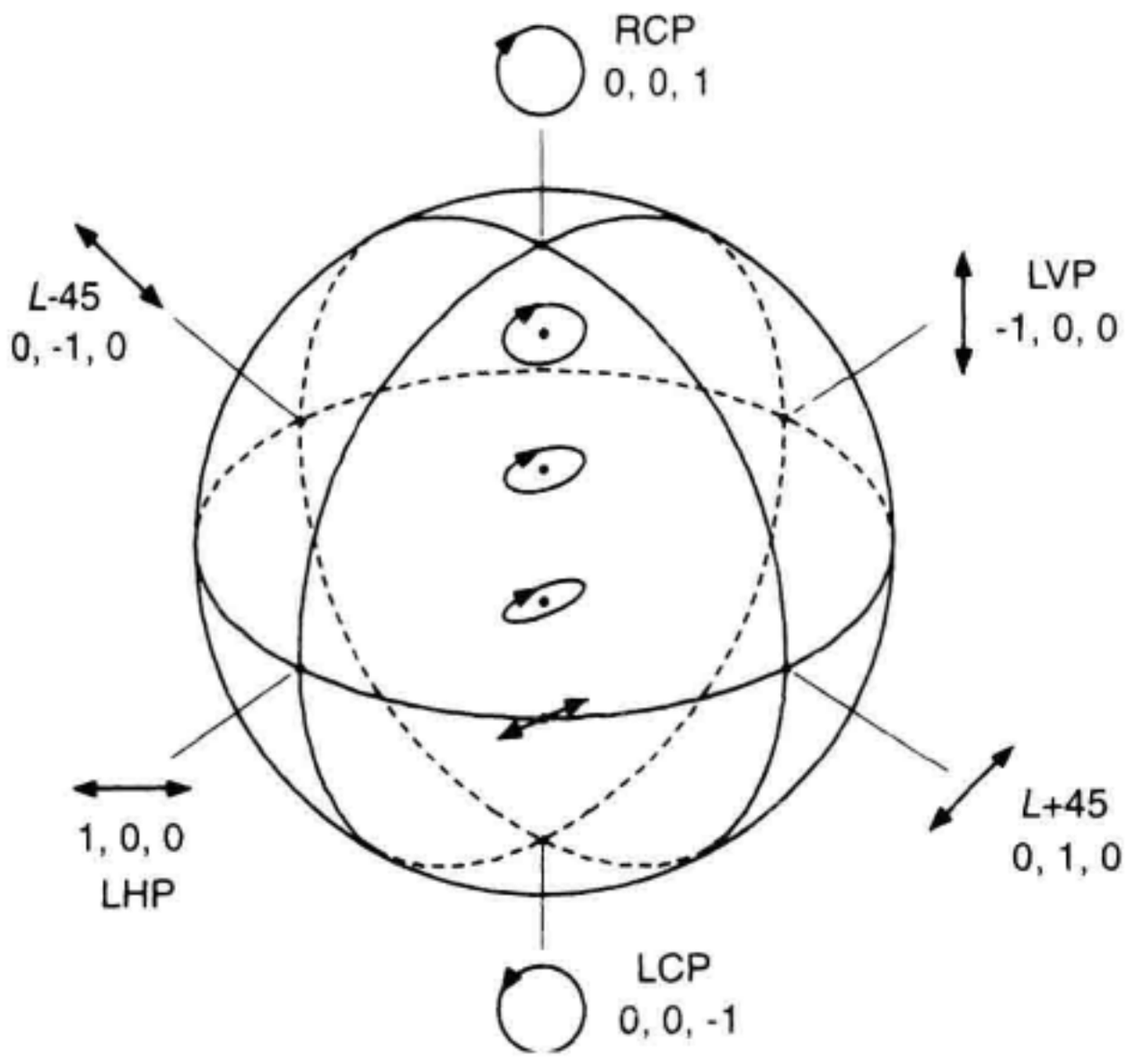

Figure 6.7 The Poincaré sphere representation of polarized light.

(completely polarized light). Points close together on the sphere represent polarizations that are similar, in the sense that the interferometric contrast between two polarizations is related to the distance between the corresponding two points on the sphere. Orthogonal polarizations with zero interferometric contrast are located diametrically opposite one another on the sphere.

As a display device for instrumentation, the Poincaré sphere is generally used to represent fully polarized light or the polarized part of a partially polarized lightwave. In the case of partially polarized light, a ray is extended from the center of the sphere along the normalized Stokes vector to locate a point on the surface of the unit sphere.

Because a state of polarization is represented on the Poincaré sphere as a single point, a continuous evolution of polarization is represented as a continuous path. For example, the evolution of polarization of light emerging from a birefringent device as wavelength is changed is represented by circular traces as illustrated in Figure 6.8. (Birefringence refers to a physical asymmetry in the index of refraction that allows different polarization modes to travel at different speeds.) The amount of rotation is proportional to the change in wavelenth. All of the circles are centered along a diameter of the sphere. The endpoints of the diameter locate the eigenmodes of the device. Eigenmodes are polarization states that propagate unchanged through a device. In linearly birefringent material,

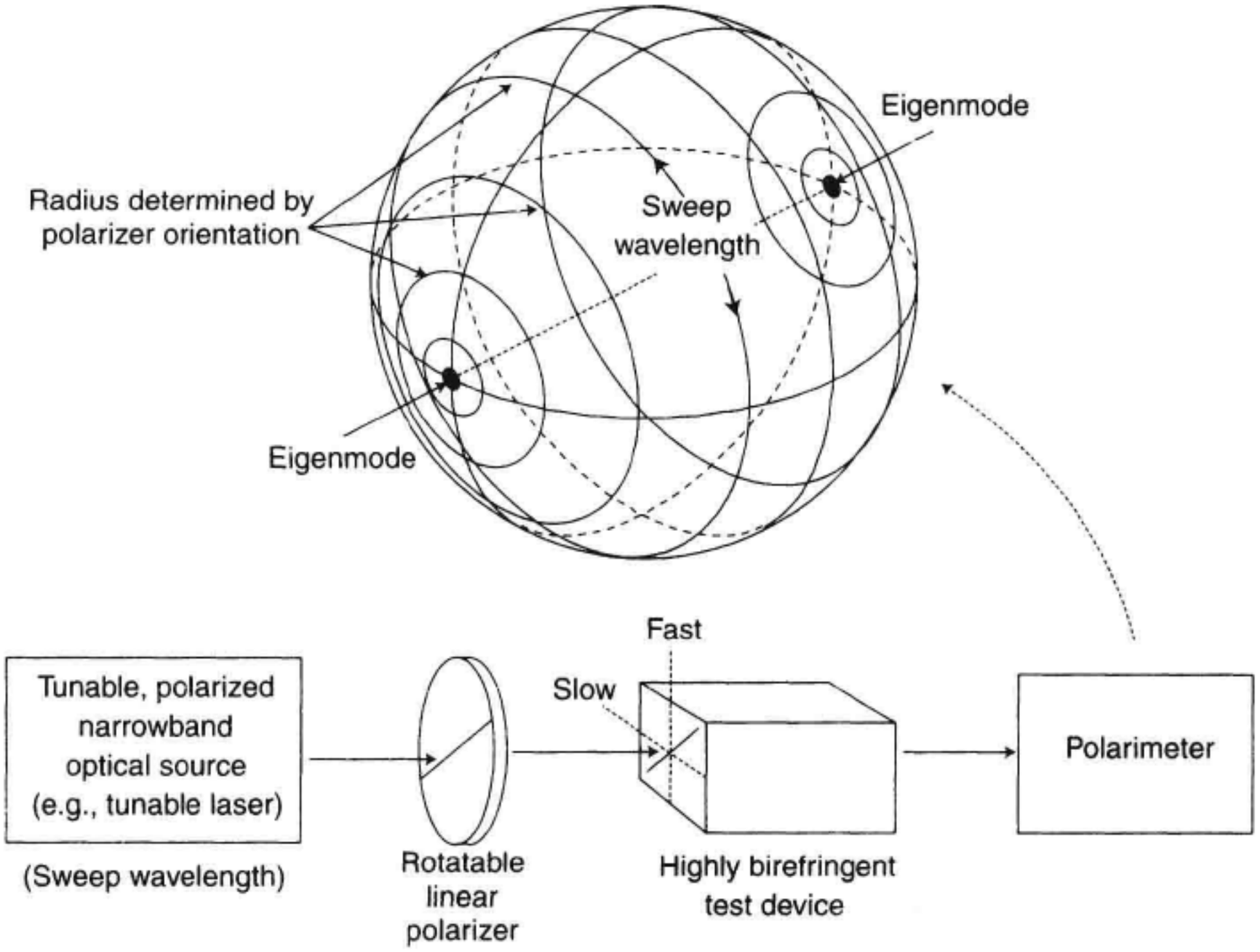

Figure 6.8 Poincaré sphere representation of the output polarization of a highly birefringent device as wavelength is changed.

the eigenmodes are linear and correspond to the fast and slow axes of the device. In Figure 6.8, each circle corresponds to a different rotational angle of the rotatable linear polarizer. The circle is largest when the electric field of the input light resolves equally into the eigenmodes.

A path on the sphere can also record the polarization history of a signal, allowing the operator to view the time-dependent behavior of polarization.

6.2.8 The Polarimeter and Polarization Analyzer

The polarization state of an optical signal can be determined by detecting the optical power transmitted through specially defined polarization filters. The measurement requires splitting the lightwave into samples in space or in time. In the space-division polarimeter, shown in Figure 6.9a, the beam is split into four and the resulting beams are processed in parallel.[6] One beam passes directly to a detector without polarization filtering, to provide a measurement that is proportional to total power. Another beam passes through a linear horizontal polarizer and provides a basis for the measurement of S_1. A third beam passes through a linear +45 degree polarizer and forms the basis for measurement of S_2. The final beam passes through a quarter-wave plate and a linear +45 degree polarizer. Circularly polarized input light is transformed to linear +45 degree by the waveplate and detected after passing through the polarizer.

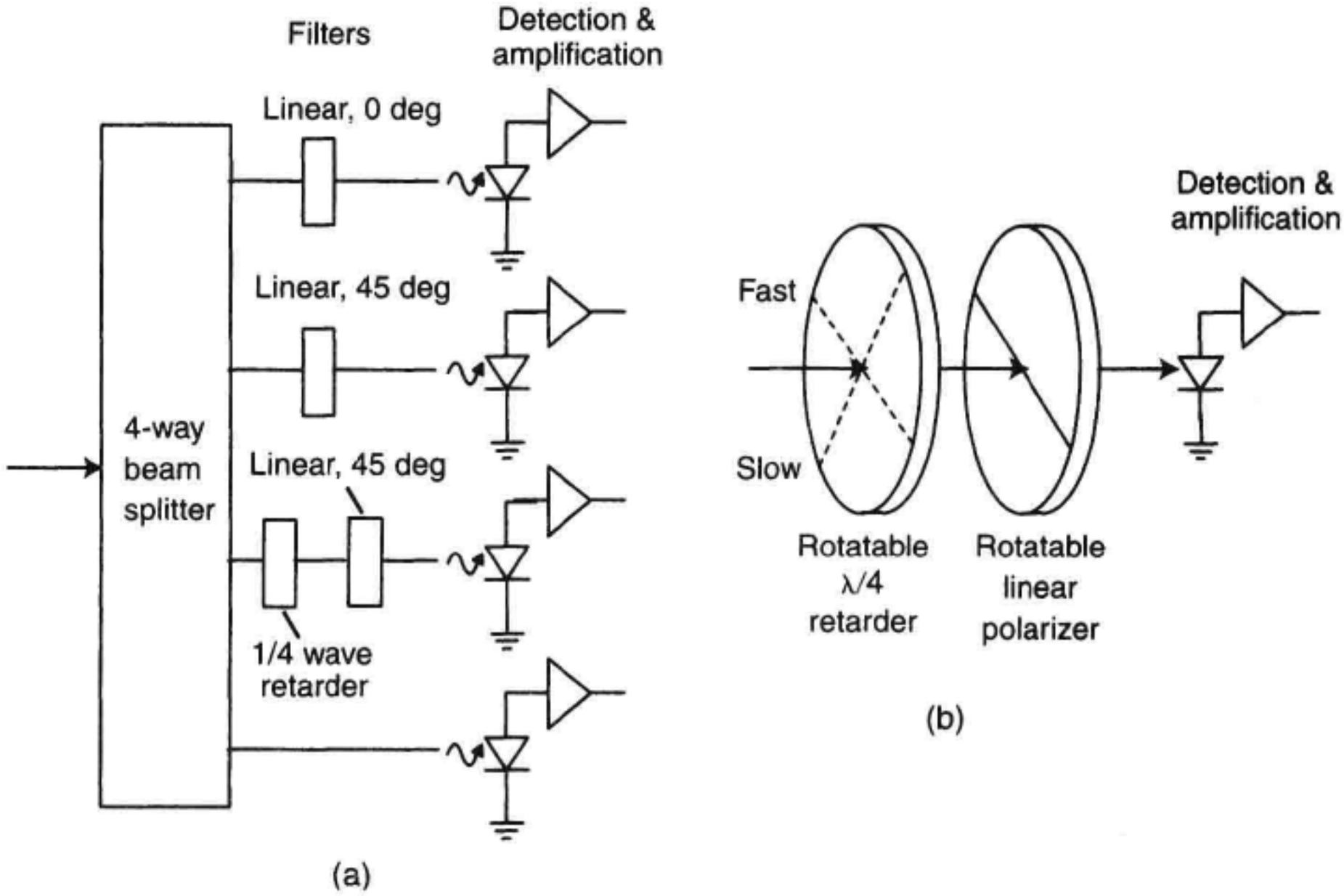

Figure 6.9 Examples of polarimeters based on (a) space division, and (b) time division of the optical beam.

In the time-division polarimeter, shown in Figure 6.9b, the signal passes through an independently rotatable quarter-wave retarder and a polarizer. Angular orientations are orchestrated by hand, or using motors, to sequentially detect the polarization components described above. Total power is determined by analysis of the resulting data.

Space- and time-division polarimeters can be built in a number of configurations. The time-division method is the simplest route for homemade setups and manual measurements. Higher speed measurements require motorization and computer control, and the speed advantage belongs to the space-division polarimeter with its parallel processing and lack of moving parts. All types of polarimeters require a calibration process to overcome such effects as differences in optical path losses and photodiode sensitivities, variations in coupling as optical elements rotate, and imperfections of the optical retarders. In addition, a calibration for total power is needed.

The functionality of a polarimeter can be expanded by adding external polarizers and mathematical algorithms. These enhancements allow the measurement of polarization within a physical reference frame removed from the polarimeter by an arbitrary length of singlemode optical fiber. They also allow the measurement of retardance, polarization-dependent loss, and polarization-mode dispersion in two-port optical devices. This type of instrument is typically referred to as a polarization analyzer.[6]

6.2.9 The Mueller Matrix

The polarization ellipse, Jones vector, Stokes vector, and Poincaré sphere are mathematical tools for representing the polarization state of a lightwave signal. The Jones matrix and the Mueller matrix represent the transmission characteristics of a device. The Jones vector completely describes fully polarized light but can represent only the polarized portion of partially polarized light. In addition, the elements of the Jones vector are not convenient to measure. In contrast, the Stokes parameters and the Mueller matrix provide a means of describing devices and signals for light of any degree of polarization, in terms that are easily measured using a retarder, polarizer, and optical power meter. The Mueller matrix relates the input and output Stokes vectors of an optical device in the following form:

$$\begin{pmatrix} S'_0 \\ S'_1 \\ S'_2 \\ S'_3 \end{pmatrix} = \begin{pmatrix} m_{00} & m_{01} & m_{02} & m_{03} \\ m_{10} & m_{11} & m_{12} & m_{13} \\ m_{20} & m_{21} & m_{22} & m_{23} \\ m_{30} & m_{31} & m_{32} & m_{33} \end{pmatrix} \begin{pmatrix} S_0 \\ S_1 \\ S_2 \\ S_3 \end{pmatrix} \tag{6.16}$$

where the column matrices S and S' are the input and output Stokes vectors, respectively, and the 4×4 array is the Mueller matrix. The standard rules of matrix multiplication apply. For example,

$$S'_0 = m_{00} S_0 + m_{01} S_1 + m_{02} S_2 + m_{03} S_3 \tag{6.17}$$

Mueller matrix relations for several important optical elements are described below. For simplicity, normalized Stokes parameters are used.

When unpolarized light is incident upon a horizontal linear polarizer, the output light is horizontal linearly polarized and contains half of the incident power. The vertically polarized portion of the light has been filtered out by the polarizer. This relationship is expressed as:

$$\frac{1}{2}\begin{pmatrix}1\\1\\0\\0\end{pmatrix} = \frac{1}{2}\begin{pmatrix}1&1&0&0\\1&1&0&0\\0&0&0&0\\0&0&0&0\end{pmatrix}\begin{pmatrix}1\\0\\0\\0\end{pmatrix} \tag{6.18}$$

Mueller matrices for several other common optical devices are shown below:

Linear vertical polarizer

$$\frac{1}{2}\begin{pmatrix}1&-1&0&0\\-1&1&0&0\\0&0&0&0\\0&0&0&0\end{pmatrix}$$

Linear +45 degree polarizer

$$\frac{1}{2}\begin{pmatrix}1&0&1&0\\0&0&0&0\\1&0&1&0\\0&0&0&0\end{pmatrix} \tag{6.19}$$

A neutral density filter, or broadband optical attenuator, of strength 1:1/*a* is represented by:

$$\frac{1}{a}\begin{pmatrix}1&0&0&0\\0&1&0&0\\0&0&1&0\\0&0&0&1\end{pmatrix} \tag{6.20}$$

The use of rotatable polarizers is common in experimental work. The Mueller matrix of an ideal linear polarizer with its transmission axis rotated by an arbitrary angle θ from the horizontal, as shown in Figure 6.10, is given by:

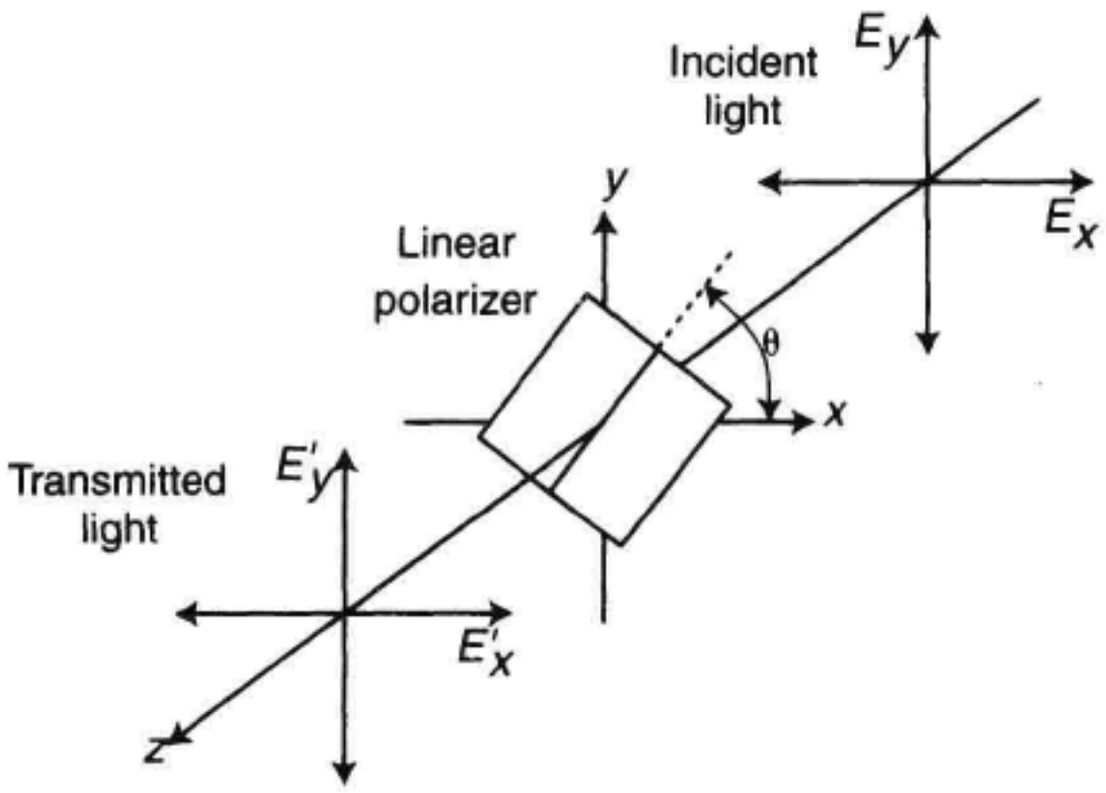

Figure 6.10 Coordinate system for describing the Mueller matrix of a linear polarizer rotated from the horizontal.

$$\frac{1}{2}\begin{pmatrix} 1 & \cos 2\theta & 0 & 0 \\ \cos 2\theta & 1 & 0 & 0 \\ 0 & 0 & \sin 2\theta & 0 \\ 0 & 0 & 0 & \sin 2\theta \end{pmatrix} \tag{6.21}$$

Chapter 9 describes a method for determining polarization-dependent loss (PDL) from measurements of the Mueller matrix.

6.3 RETARDANCE MEASUREMENT

6.3.1 Introduction

Most optical materials exhibit some degree of refractive index asymmetry that allows light in two orthogonal polarization states to travel at different speeds through the material. This property is called birefringence. The polarization states into which polarized incident light is resolved are defined by the internal structure of the material. For well-defined structures such as a quartz crystal, these states are maintained during transmission through the device and are called the eigenmodes. Birefringence can be linear or circular, although most applications of birefringent devices, and most concerns about birefringence in fiber-optic components, involve linear birefringence. Quartz is linearly birefringent.

Retardance is a measure of the differential phase shift of light in the eigenmodes, more commonly referred to as the fast and slow waves. An example is the retarder or wave plate, a device fabricated to provide a predictable amount of phase shift. Polarized light incident on a typical waveplate decomposes into linear fast and slow waves. In general, the output polarization is different from the input state, depending upon the relationship of the incident polarization to the internal structure, and corresponding eigenmodes, of the waveplate. Retardance is typically expressed in waves or in degrees of phase shift at a specified wavelength.

Polarization Controllers. Because polarization adjusters and controllers are widely used in fiber-optics laboratory work, we will use the topic to illustrate some applications of retardance. In the polarization controller shown in Figure 6.11a, light is transmitted through a polarizer and quarter- and half-wave plates. The input and output of the controller may be in open air or in fiber, as shown. When the linear input polarizer is aligned with either the fast or the slow axis of the quarter-wave plate, transmission through the quarter-wave plate leaves the signal polarization unchanged. When the linearly polarized input light is oriented midway between the fast and slow axes of the wave plate, it is decomposed equally into the fast and slow polarization modes or eigenmodes. The two waves experience a 90 degree phase shift and produce circularly polarized light at the output of the wave plate. At all other input orientations, the quarter-wave plate transforms linear input light to elliptical output states. The half-wave plate in Figure 6.11a allows additional polarization control. Coordinating the rotations of the quarter- and half-wave plates allows the generation of any desired output polarization state.

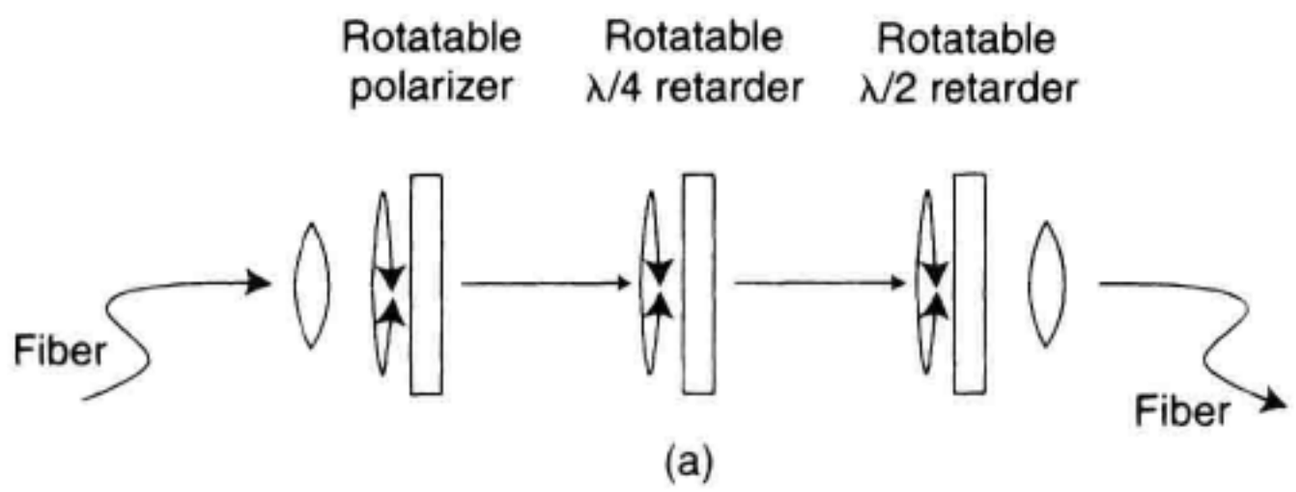

Figure 6.11 Examples of polarization manipulators. (a) Polarization controller using polarizer and wave plates. (b) Polarization adjuster based on fiber coils.

Although retarders are typically implemented in the form of discrete optical waveplates, retarders can also be made from short lengths of highly birefringent fiber (hi-bi, or polarization-maintaining fiber) or from coils of singlemode fiber.[7] A 4-coil polarization controller is depicted in Figure 6.11b. Bending produces an asymmetric stress field which induces a difference in index of refraction between the stressed and nonstressed axes. Retardance increases with the number of turns. The fiber coils are typically arranged so that they can rotate about a common tangent, along which the interconnecting fiber is routed. Rotation of a coil changes the way the input electric field decomposes into the fast and slow axes of the coil, changing the polarization transformation produced by the coil. Several combinations of quarter- and half-wave fiber coils are commercially available and the devices are readily constructed in the laboratory.

6.3.2 Measurement of Retardance

Over the years, many retardance measurement methods have been developed. Some of this work has achieved great accuracy.[8] The two methods described here are not the most accurate, but they do give insight into measurement technique and the concept of birefringence, and they are quite convenient. Both methods make use of a polarimeter or polarization analyzer. The Poincaré sphere method is most intuitive, although the second method, based on the Jones matrix measurement, is faster and more easily automated. The setup for both measurements is shown in Figure 6.12. We will assume that the retarder under test is a quartz fractional waveplate. The fiber path between the output lens and the polarimeter must be fixed in position to prevent spurious polarization shifts during the measurement.

Both measurement methods require the establishment of a physical reference frame, that is, a set of axes within which polarization can be defined. For polarimeters with fiber inputs, this involves fixing the fiber in position to stabilize the polarization transformation it produces. A rotatable linear polarizer is coupled into the fiber end through a lens. Using the

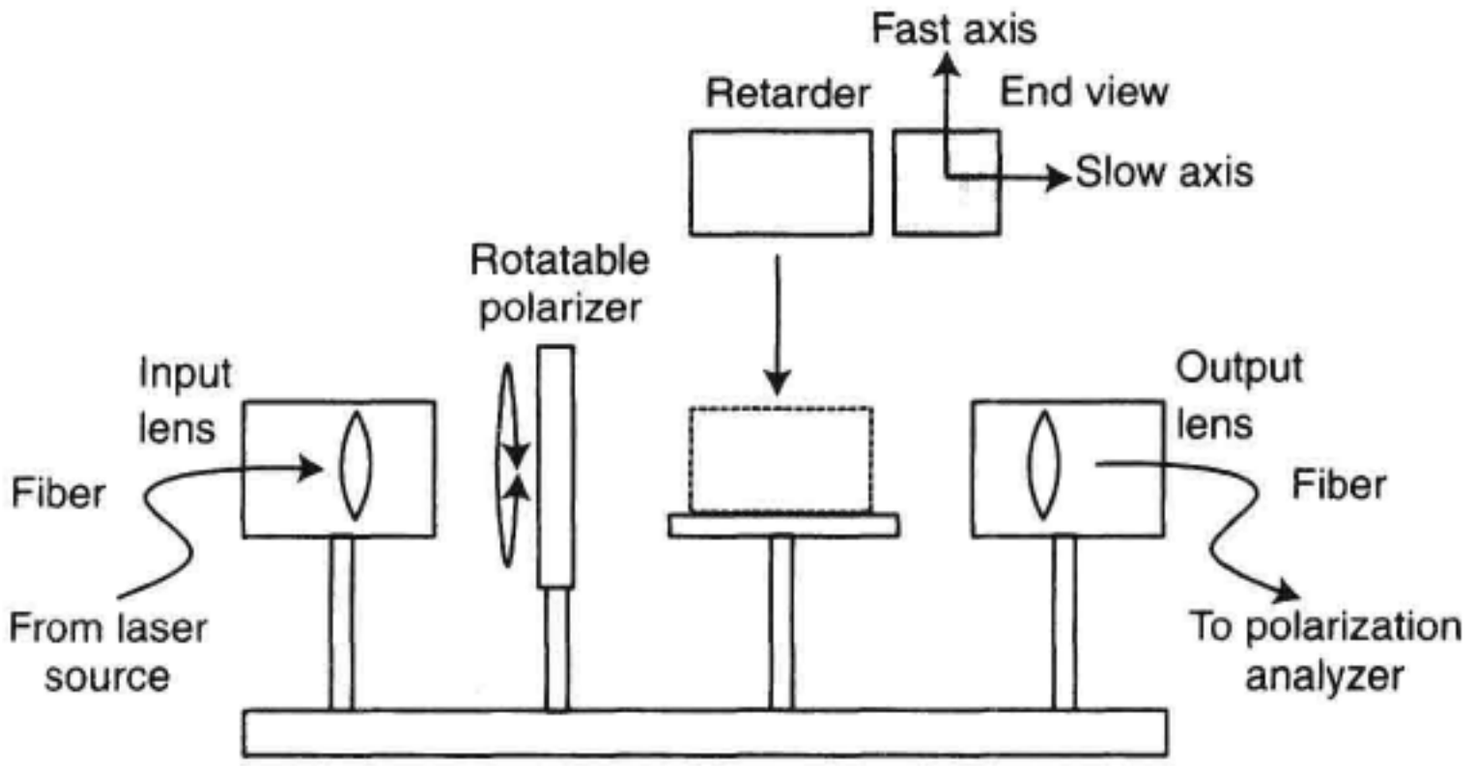

Figure 6.12 Setup for measurement of retardance using the Poincare sphere and Jones matrix methods.

polarizer and an algorithm based on the Jones matrix, the birefringence and polarization-dependent loss of the path connecting the setup to the polarimeter is measured and removed. Polarizer angles of 0, 60, and 120 degrees are commonly used. The first state is typically assumed by the instrument to represent horizontal linear polarization. Once the resulting reference frame is activated, rotation of the polarizer to the 0 degree or horizontal orientation causes a point to appear at 1, 0, 0 (LHP) on the Poincaré sphere, and rotation of the polarizer by 180 degrees traces out the entire equator.

6.3.3 The Poincaré Sphere Method

This method determines retardance from the pattern traced out on the Poincaré sphere when the retarder under test is rotated in a linearly polarized beam. The retarder may be supported in a rotatable mount. The polarization reference frame is not strictly necessary for this method, but it can simplify interpretation of the graphical results. After the reference frame is created and activated, the polarizer is returned to horizontal and the retarder is placed in the beam following the polarizer. The retarder is rotated about its optical axis until the Poincaré display again indicates horizontal linearly polarized light. In this condition, the stimulus polarization is coupled entirely into one of the eigenmodes. Because the electric-field vector is ideally aligned with one of the crystalline axes and experiences only the index of refraction associated with that axis, no polarization transformation occurs. The corresponding polarization state is marked on the Poincaré sphere. Next, the retarder is rotated +45 degrees to allow the input polarization to decompose equally into the two eigenmodes. This condition produces the greatest polarization shift, and the corresponding state is marked on the sphere. The angle formed at the center of the sphere by rays to the two marked points is the retardance of the waveplate. The pattern traced out on the Poincaré sphere for a slightly less-than-quarter-wave retarder is shown in Figure 6.13. If it is known that the retarder exhibits linear birefringence, the retarder may be measured without a reference frame. The figure-8 pattern will appear in an arbitrary orientation on the sphere and the retardance is again determined by marking the central intersection and one extreme of the pattern.

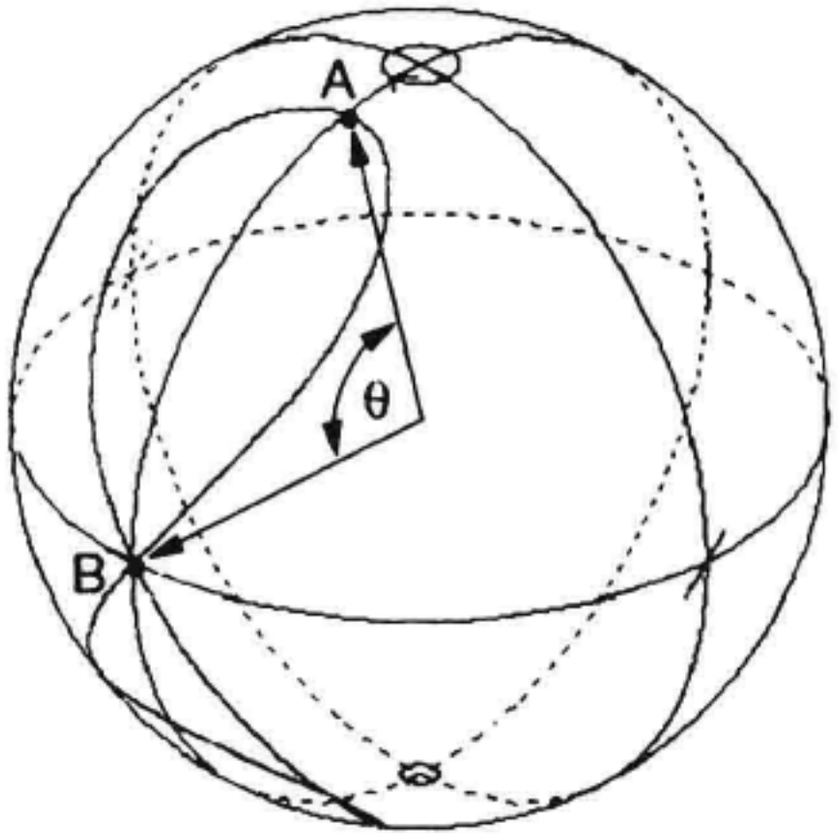

Figure 6.13 Measurement of the retardance θ of a near-quarter-wave retarder using a polarimeter with Poincaré sphere display.

6.3.4 The Jones Matrix Method

The retardance of a two-port device can be determined from the Jones matrix. The measurement setup is identical to that of the Poincaré sphere method, shown in Figure 6.12, and generally involves the use of a polarization analyzer.[6] A reference frame is established at the polarizer, as described above. The polarizer is returned to horizontal orientation and the retarder is placed in the beam following the polarizer. The retarder is rotated about its optical axis until the state of polarization of light emerging from the retarder is linear horizontal. In this orientation, linearly polarized light is propagating solely in one eigenmode. The polarization state of the emerging light is measured at polarizer orientations of 0 degrees (LHP), +45 degrees (L + 45), and +90 degrees (LVP). The Jones matrix is computed from these three measurements. For a quarter-wave plate with its fast axis oriented horizontally,

$$\mathbf{J}\left(\frac{\lambda}{4}\right) = \begin{pmatrix} e^{i\frac{\pi}{4}} & 0 \\ 0 & e^{-i\frac{\pi}{4}} \end{pmatrix} \tag{6.22}$$

The retardance is found by comparing the arguments of the exponentials as follows

$$\frac{\pi}{4} - \left(-\frac{\pi}{4}\right) = \frac{\pi}{2} \tag{6.23}$$

resulting in a retardance of 90 degrees.

6.4 MEASUREMENT OF CROSS-TALK IN POLARIZATION-MAINTAINING FIBER

6.4.1 Introduction

The term polarization-maintaining (PM) refers to a class of highly linearly birefringent singlemode fiber. PM fiber is typically used to guide linearly polarized light from point to

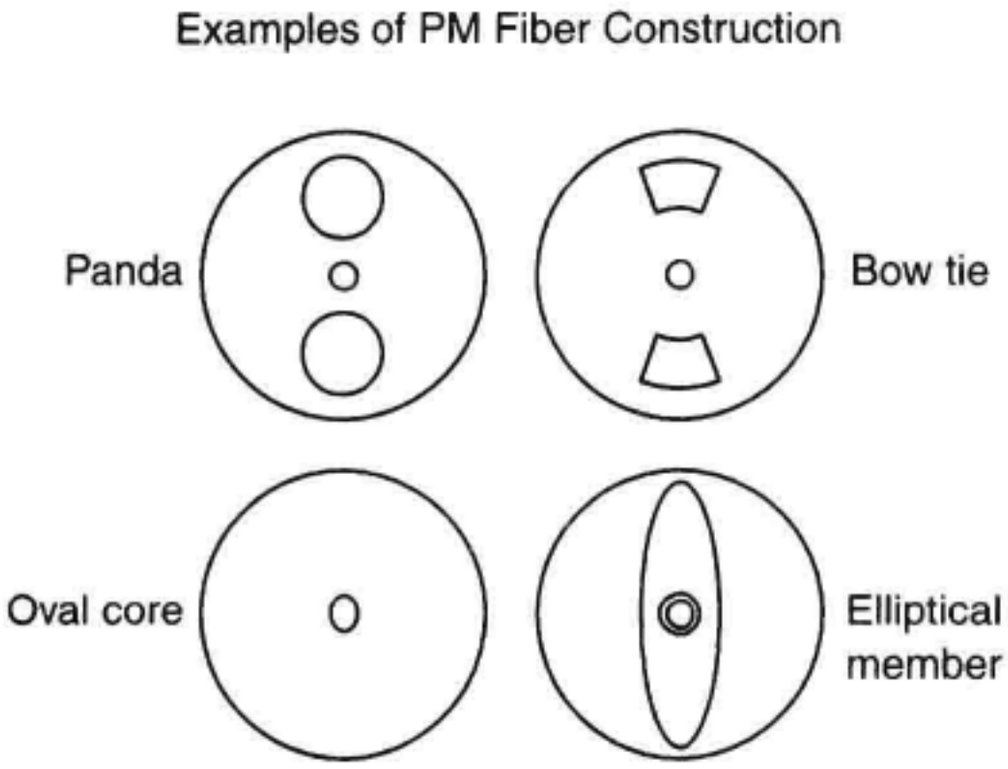

Figure 6.14 Examples of polarization maintaining (PM) fiber. Physical asymmetry induces a difference in refractive index between orthogonal axes.

point, for example between a DFB laser diode and a lithium-niobate modulator in a high-speed telecommunication system. It also finds many specialized applications in lightwave communication and optical sensor research. Birefringence may stress-induced by placing the core between or within glass elements of different physical composition, or may originate with a purposeful asymmetry in the core geometry (form birefringence). In all cases, the result is a difference in the index of refraction between orthogonal axes. Several examples of PM fiber are shown in Figure 6.14.

The birefringence of PM fiber is much larger and more uniform than the residual birefringence of ordinary singlemode fiber. Because the birefringence is associated with a systematic, physical asymmetry of the fiber cross-section, PM fiber exhibits distinct fast and slow principal optical axes. Light coupled into a length of PM fiber resolves into two orthogonal, linearly polarized modes, or waves, according to how the input electric field projects onto the fast and slow axes of the fiber. In most applications, linearly polarized light is aligned with one of the axes, commonly the slow axis.

Only when the electric field of the light is entirely aligned with the slow or fast axis is PM fiber actually polarization maintaining, as indicated in Figure 6.15. Because of the difference in index of refraction between the fast and slow axes, electric fields in the two

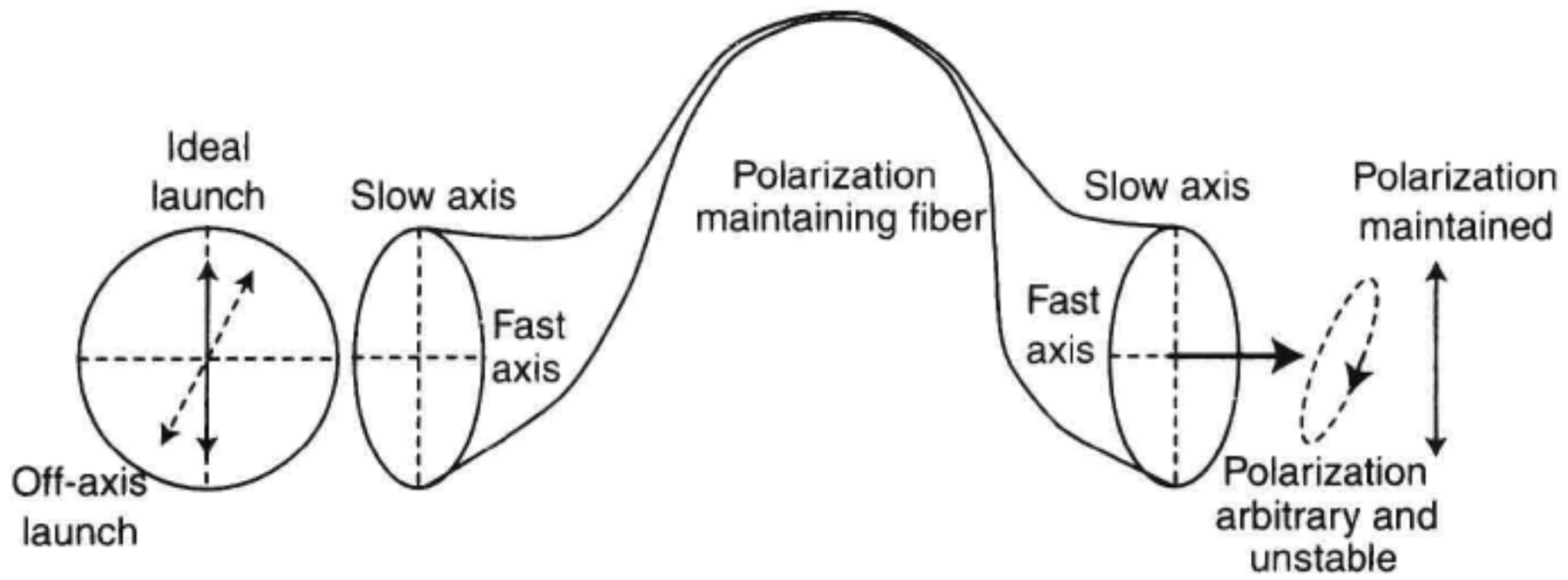

Figure 6.15 Polarization-maintaining (PM) fiber maintains polarization only if the launch polarization is aligned with the fast or slow axis.

axes are phase-shifted relative to one another in proportion to the distance traveled. If electric field components exist in both axes, the polarization state of the propagating light evolves as it travels along the fiber's length and exits at an arbitrary polarization state. Under these conditions, the output polarization of the fiber is readily influenced by temperature and fiber movement.

There are several requirements for guiding linearly polarized light in PM fiber. Light must be linearly polarized to a high extinction before coupling to the core, and birefringence in lenses or optical connectors must be minimized. Light can be scattered between principal axes by impurities and structural flaws, and can also couple between axes where the fiber is sharply stressed by outside forces. In a path made up of several connected PM fibers, light can couple between fast and slow axes at fiber interfaces. This section presents two methods for measuring polarization cross-talk, the figure of merit for the confinement of light to a single axis of PM fiber.

6.4.2 The Crossed-Polarizer Cross-Talk Measurement

The setup for this method is shown in Figure 6.16. To avoid interferometric effects, a spectrally broad optical source is used. As a guide, the coherence time of the source should be much shorter than the differential propagation time along the fast and slow axes of the test fiber. An unpolarized source gives the advantage that coupling to the input of the test fiber is independent of rotation of the input polarizer. The output of the test fiber is detected by a power meter, through a second rotatable polarizer. Input and output optics should be strain-free to avoid influencing the measurement with their own birefringence. Following adjustment of the coupling optics, the two polarizers are iteratively adjusted to minimize the detected signal. In this state, the input polarizer is aligned with one of the principal axes and the output polarizer with the other. The resulting power level P_{min} indicates the amount of light that has coupled into the unintended axis of the PM fiber. Next, the output polarizer is rotated by +90 degrees. The corresponding power level P_{max} indicates the amount of light in the intended axis. Polarization cross-talk is computed according to

$$\text{Polarization cross-talk} = 10 \log(P_{min}/P_{max}) \tag{6.24}$$

Measurement results can be affected by source instability and by variation of the optical coupling with rotation of the polarizers. Iterative adjustment of the coupling and the polarizers can overcome the coupling variation. Polarizers must be strong enough that

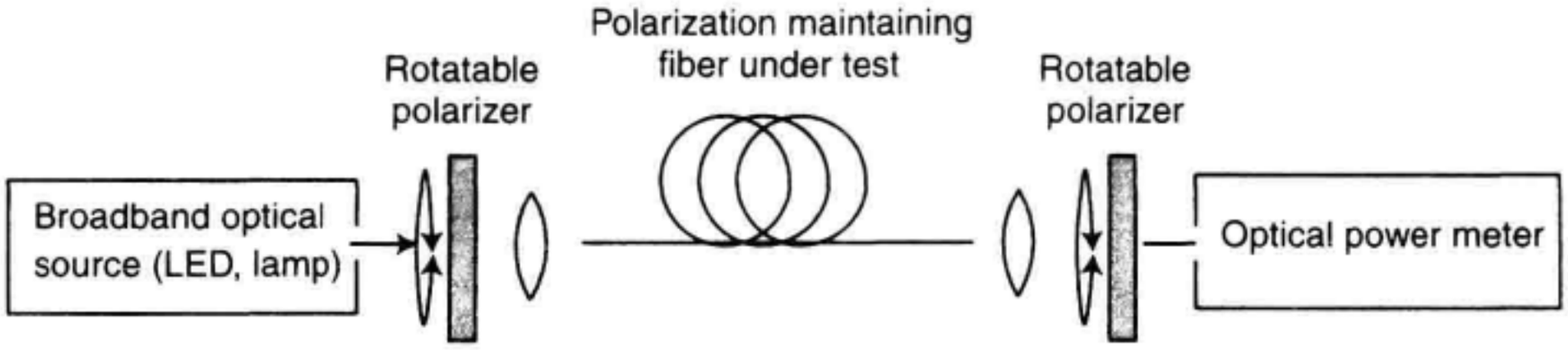

Figure 6.16 Setup for measuring cross-talk in polarization maintaining fiber by the crossed-polarizer method.

with the test fiber removed and the polarizers crossed, the attenuation is at least 10dB greater than the cross-talk to be measured. The strength of a polarizer is given by the extinction ratio

$$\text{Polarization extinction ratio} = 10 \log \frac{P_{\text{block axis}}}{P_{\text{pass axis}}} \tag{6.25}$$

where the numerator and denominator represent the optical power transmitted with the electric field of linearly polarized input light aligned with the block axis and the pass axis, respectively, of the polarizer under test. For example, in order to measure a polarization cross-talk value of −30 dB, the polarizers should have an extinction ratio of at least −40 dB.

6.4.3 The Polarimetric Cross-Talk Measurement

As indicated earlier, PM fiber maintains linear polarization only if the electric field is confined to a single principal axis. If the field has components along both axes, the polarization state within the PM fiber evolves with distance along the fiber. For the same physical reasons, the output polarization of the fiber evolves as the wavelength of a narrowband source is tuned. In the discussion of the Poincaré sphere, it was shown that this polarization evolution traces out circular arcs on the sphere. Polarization cross-talk can be calculated from the diameter of these circular arcs.

The polarimeter-based cross-talk measurement is an example of a *relative* polarization measurement. The cross-talk information is taken from the diameter of the circle, and the specific position of the circle on the sphere is not significant. The PM fiber under test may even be connected to the polarimeter through other sections of fiber.

A setup for measurement of cross-talk is shown in Figure 6.17. The optical source must be highly polarized, exceeding the cross-talk to be measured by at least 10 dB.

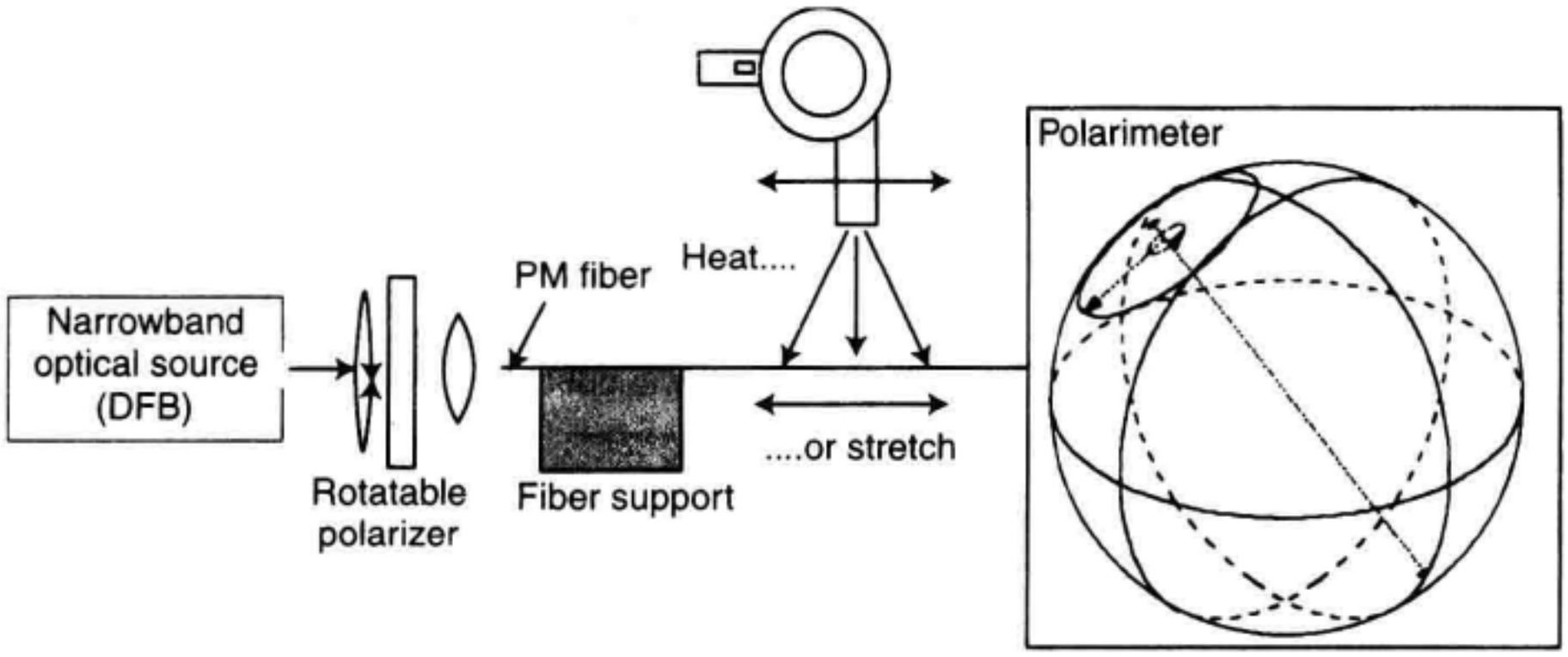

Figure 6.17 Setup for measuring cross-talk in polarization maintaining fiber by the polarimetric method.

In addition, the source spectrum must be narrow enough that the source coherence time is much larger than the difference in propagation time between the fast and slow axes of the fiber under test. This assures that light propagating in the orthogonal fiber axes can interfere at the output. The differential propagation delay of the transmission path can be estimated from the beat length and the overall physical length of the PM fiber. A beat length of 2 mm means that the fast and slow modes experience a 360 degree phase shift in each 2 mm of fiber length. At 1550 nm, a cycle of phase shift corresponds to a differential time delay of about 0.005 ps, so a 2 m segment of PM fiber would have a differential group delay of 5 ps. Assuming a Gaussian spectral shape, the source coherence time is given by

$$t_c = \frac{\lambda^2}{c\,\Delta\lambda} \tag{6.26}$$

where λ is the center wavelength of the optical source and $\Delta\lambda$ is its spectral width. Wavelengths are in meters and c is the velocity of light in free space in m/s. For example, at 1550 nm, an optical source with 0.1 nm spectral width has a coherence time of about 80 ps, sufficiently long to be used in testing the 2 m length of PM fiber. The spectral width of FP lasers and unfiltered LED sources are generally too broad to support this method.

The method makes use of the fact that as polarization-maintaining fiber is stretched or heated, the resulting change in length causes a phase shift between the fast and slow polarization modes of the fiber. A change of phase between orthogonal polarization states always describes a circle on the Poincaré sphere. From the diameter of this circle, the polarization cross-talk can be calculated. To see why this its true, consider the front and side-cutaway views of the Poincaré sphere shown in Figure 6.18. Points A and B correspond to the orthogonal fast and slow polarization modes of the polarization-maintaining fiber. The circular data trace of radius r is shown in cross section as a vertical line of length $2r$. The angle between the AB axis and a ray to a point on the circular trace is given by θ.

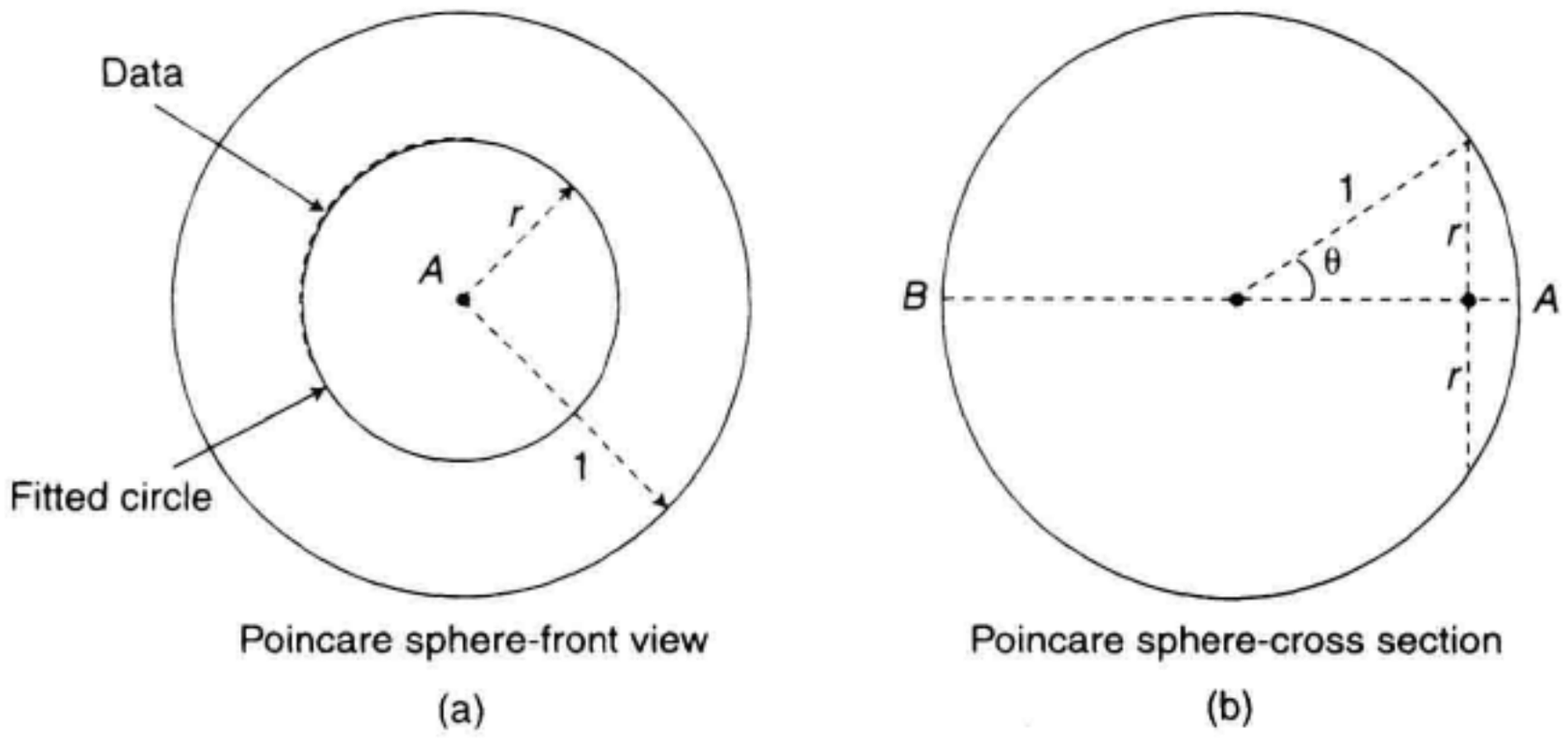

Figure 6.18 Basis for the calculation of polarization crosstalk from the circular data trace. (a) Poincaré sphere front view. (b) Side-cutaway view.

As discussed earlier, any polarization state can be decomposed into orthogonal pairs of polarization states. In this application, the projection of the data point onto the principal states axis divides the line AB into segments of length $1 + \cos\theta$ and $1 - \cos\theta$. The ratio of optical power in states B and A is given by

$$\frac{P_B}{P_A} = \frac{1 - \cos\theta}{1 + \cos\theta} \tag{6.27}$$

and the polarization cross-talk is given by

$$\text{Polarization cross-talk} = 10 \log\left(\frac{1 - \cos\theta}{1 + \cos\theta}\right). \tag{6.28}$$

To express the cross-talk in terms of the radius of the data trace, note that

$$\theta = \sin^{-1} r \quad \text{and} \quad \cos\theta = \sqrt{1 - r^2} \tag{6.29}$$

leading to the relationship

$$\text{Polarization cross-talk} = 10 \log\left[\frac{1 - \sqrt{1 - r^2}}{1 + \sqrt{1 - r^2}}\right] \tag{6.30}$$

The largest possible circle has unity radius, corresponding to 50% of the light propagating in each of the polarization modes. In the case in which light is very well confined to a single principal axis, the circle shrinks, converging toward a point on the Poincaré sphere that represents, in a relative way, the output eigenmode of the fiber. (The representation is relative because a polarization reference frame has not been set up at the output of the PM fiber).

At the time of writing, careful comparisons of the two measurement methods described above have been undertaken in the measurement community. In an initial, limited interlab comparison, the two methods were found to agree to within a few dB up to a cross-talk level of 20 dB. A divergence of the measurements for larger cross-talk values is under study. In the author's experience, clean circular traces indicating cross-talk values of –50 dB have been observed on certain types of PM fiber with input polarization adjusted to overcome the effects of connectors. Observation of effects of this level requires careful adjustment of the launch polarization and gentle heating of the fiber sample to avoid increasing the coupling between modes. Such observations may eventually provide insight into the structure of the PM fiber, but a clear view of the relationships and the causes of divergence for values beyond –20 dB will emerge from work now underway. Following are several applications of the polarimeter-based polarization cross-talk measurement.

6.4.4 Measurement of Cross-Talk Along a PM Fiber

In the case of very long PM fibers, polarization cross-talk can be measured at points along the fiber using the polarimeter-based method. When the PM fiber under test is stretched or heated, the circle on the Poincaré reveals the polarization cross-talk *in the region of the fiber that is stretched or heated.* The following fiber can be viewed as a fixed birefringence which affects the position of the circle on the sphere but does not affect its diameter. For example,

consider a 100 m length of PM fiber. Light is linearly polarized and coupled into the fiber at an initial orientation. The cross-talk is measured by gently heating a short length of fiber immediately following the launch. The polarizer or fiber is rotated as needed to optimize the launch. Once the launch is established (and physically protected from movement of the rest of the fiber), the cross-talk at other points can be measured by simply applying the heat at the point of interest. In each case, about 1/2 m of fiber is heated or carefully stretched to produce an arc and a corresponding cross-talk value. When stretching the fiber, it is important to avoid bending the fiber at the point where it is being gripped, for these bends can cause light to couple between polarization modes.

6.4.5 Cross-Talk Measurement of PM Fiber Interfaces

PM fibers are interconnected by fusion splicing, by proximity coupling with or without index-matching fluid, and by means of various commercial connectors. In each case, maintenance of linear polarization across the fiber interfaces requires that the fiber axes are well aligned and that the fiber ends are prepared and supported in such a way as to avoid cross-talk between polarization modes.

Degradation of cross-talk due to a PM fiber interconnection is best determined by launching linearly polarized light into a single polarization mode of the first segment and then measuring the cross-talk on either side of the interconnection by heating the corresponding fiber.

6.4.6 Measurement of the Polarization Stability of Cascaded PM Fibers

As discussed earlier, if polarized light is not perfectly confined to a single axis, slight changes in fiber length caused by heating or movement can cause the output state to wander. This problem is compounded when several PM fibers are cascaded. Consider the case of a connectorized, linearly polarized source driving a cascade of three connectorized PM fiber jumpers. Typically, the launch into the first fiber is imperfect and the interconnections are slightly misaligned. We are interested in the stability of the final output polarization. The Poincaré sphere measurement in Figure 6.19a shows the pattern resulting from gentle stretches of each of the PM fiber jumpers; each circle indicates the polarization cross-talk in the jumper being stretched. Figure 6.19b was generated for a two-section cascade by slowly stretching one fiber while rapidly stretching and releasing the second. The shaded pattern indicates the range of possible output polarization states. The worst-case cross-talk for the combination of fibers is computed from the diameter of the outer perimeter of the pattern.

6.5 SUMMARY

Polarization measurements play a major role in the design and characterization of modern telecommunication systems, and familiarity with the concepts and vocabulary is extremely useful. In this chapter, we have examined several representations of polarized light:

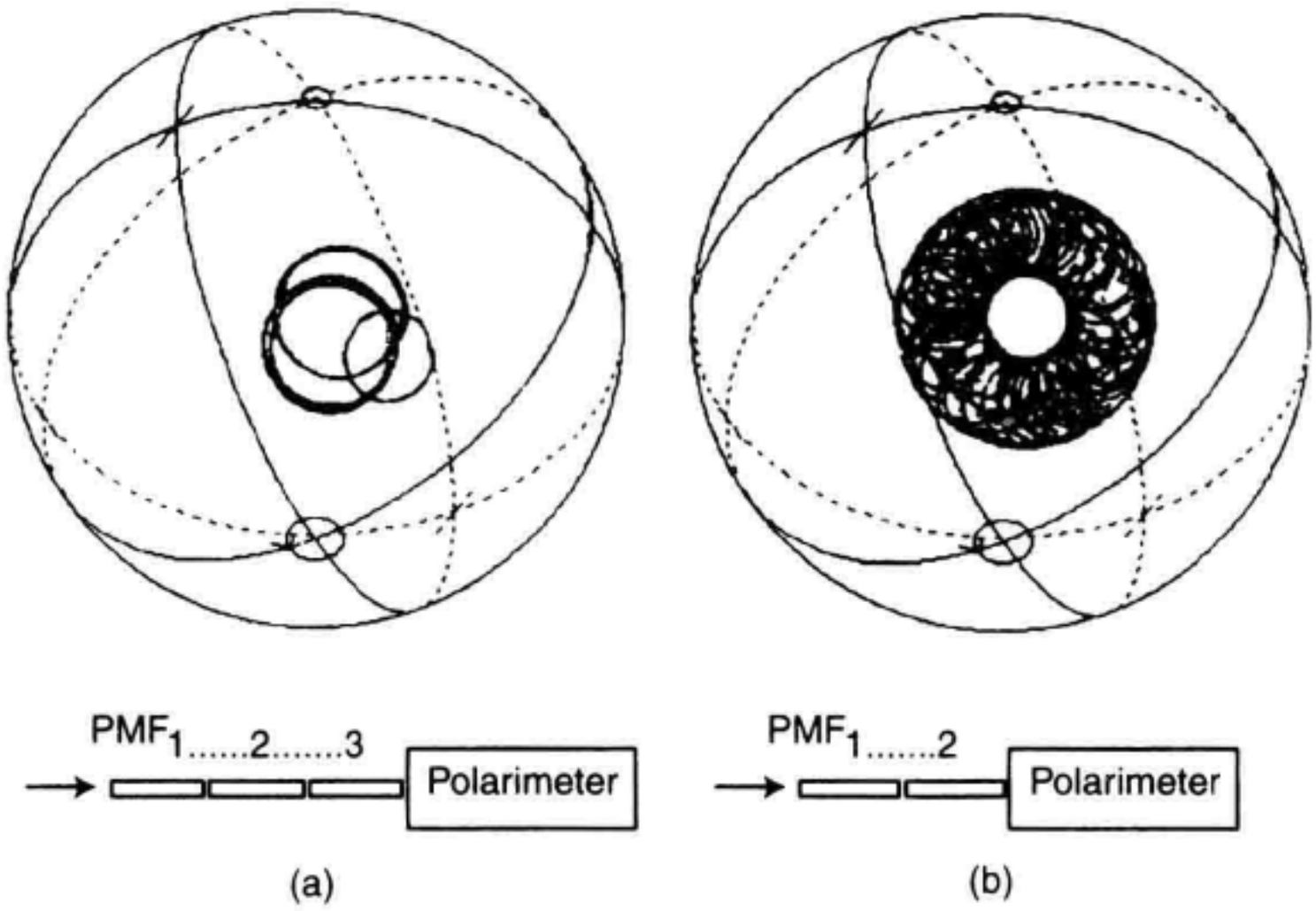

Figure 6.19 Output polarization of (a) three cascaded PM fibers stretched individually, and (b) two cascaded PM fibers stretched simultaneously but randomly.

- The polarization ellipse;
- The Jones vector;
- The Stokes vector;
- The Poincaré sphere.

Partially polarized light can be modeled as the superposition of polarized and unpolarized light. The polarization ellipse, the surface of the Jones vector and Poincaré sphere are used to represent polarized light. The Stokes vector and the interior of the Poincaré sphere represent light of any degree of polarization.

In addition, we have introduced tools for description of the polarization-transforming behavior of two-port devices and fibers:

- The Jones matrix;
- The Mueller matrix.

The Jones matrix is useful for describing the effect of a device on a fully polarized signal. The Mueller matrix is capable of describing the effect of a device on a signal of any degree of polarization.

Several measurements were described, mainly involving the polarimeter, a tool that supports fast and intuitive analysis of polarization behavior. A polarization analyzer extends the functionality of the polarimeter with the addition of insertable polarizers and algorithms that measure and extract information from the Jones matrix. The polarization an-

alyzer allows the creation of a polarization reference frame removed from the polarimeter by a length of singlemode fiber.

Two retardance measurement methods were considered, the Poincaré sphere and Jones matrix measurements. The first offers the advantage of speed and intuitiveness, and the second the benefit of speed. Measurements of polarization cross-talk on polarization-maintaining fiber were also discussed. Numerical agreement of the crossed polarizer and polarimetric methods is under study at the time of this writing.

The reader is referred to Edward Collett's *Polarized Light: Fundamentals and Applications* for an extremely interesting, in-depth discussion of polarization concepts and fundamental polarization movements.[3]

REFERENCES

Polarization in the Biosphere

1. Cronin, T.W., N. Shashar, L. Wolff. 1995. Imaging technology reveals the polarized light fields that exist in nature. *Biophotonics International,* March/April: 38–41.
2. Kattawar, G.W. 1994. A search for circular polarization in nature. *Optics and Photonics News,* September: 42–43.

Polarization References

3. Collett, Edward. 1993. *Polarized light: fundamentals and applications.* New York, NY: Marcel Dekker, Inc.
4. Jones, R.C. 1947. A new calculus for the treatment of optical systems. VI: Experimental determination of the matrix. *Journal of the Optical Society of America,* 37: 110–112.
5. Born, M. and E. Wolf. 1980. *Principles of optics.* 6th ed. Pergamon.

A Polarization Analyzer

6. Heffner, B.L. and P.R. Herndday. 1995. Measurement of polarization-mode dispersion. *Hewlett-Packard Journal.* February: 27–33.

Polarization Controllers

7. Lefevre, H.C. 1980. Singlemode fibre fractional wave devices and polarization contollers. *Electronics Letters* Sept., 16 (20): 778–780.

Retardance Measurement

8. Rochford, K.B., P.A. Williams, A.H. Rose, I.G. Clarke, P.D. Hale, and G.W. Day. 1994. Standard polarization components: progress toward an optical retardance standard, SPIE 2265. *Polarization Analysis and Measurement II:*2–8.

CHAPTER

7

Intensity Modulation and Noise Characterization of Optical Signals

Christopher M. Miller

7.1 MODULATION DOMAIN ANALYSIS

The low propagation loss and extremely broad bandwidth of singlemode optical fiber have contributed to the emergence of high-capacity lightwave digital transmission systems and analog-modulated RF and microwave-frequency optical systems. New lightwave components have been developed to meet the performance requirements of these systems. Most notable among these components are high-power single-frequency lasers such as distributed-feedback (DFB) semiconductor lasers, optical intensity modulators, erbium-doped fiber amplifiers (EDFAs), and broad bandwidth p-i-n photodetectors. Modulation frequency domain characterization of these lightwave components, as well as the systems they go into, is required to achieve the desired performance requirements of transmission bandwidth, signal fidelity, and signal-to-noise ratio (SNR).

This chapter starts with an explanation of intensity modulation, how it is used in optical transmission systems, and how it can be characterized. It is important to have a clear understanding of the differences between measurements on the optical carrier signal (as studied in Chapters 3 and 4) and measurements involving the modulation on the optical carrier. Section 7.2 discusses the measurement of the modulation transfer function for components such as DFB lasers and p-i-n photodetectors. Modulation transfer function measurements are made using instrumentation based on an electrical vector network analyzer in conjunction with calibrated optical to electrical (O/E) and electrical to optical (E/O) converters. Section 7.3 describes measurements made on the modulated optical signal. Parameters such as optical modulation index and distortion can be made with instru-

mentation consisting of a calibrated O/E converter in conjunction with an electrical spectrum analyzer. Section 7.4 deals with the measurement of intensity noise on optical signals. Finally, Section 7.5 reviews the topic of modulation domain calibration techniques. All of the measurements discussed in this chapter require accurate characterization of reference optical transmitters and reference optical receivers, at times in conjunction with the appropriate measurement instrumentation. It is the accuracy of these calibrations that ultimately determines the quality of the measurements described in this chapter.

7.1.1 Simplified Transmission Systems

A basic intensity-modulated transmission system is shown in simplified form in Figure 7.1. Information is transmitted by varying the power of the optical carrier by means of an electrical drive signal. This simplified system can either model a digital or analog lightwave transmission system depending on the type of electrical modulation applied to the optical carrier, and the characteristics of the electrical and optical components used. In a digital lightwave system, a binary electrical-data waveform is used to modulate the optical carrier. In these types of systems, described in detail in Chapter 8, the bit-error ratio as well as the characteristics of the modulated optical waveform are important. In an analog lightwave system, an electrical signal is used to linearly modulate the optical carrier. This is typical of routing radio frequency (RF) or microwave signals using fiber optics such as in the case of satellite antenna remoting, radars, or in various shipboard or avionics systems. Analog fiber-optic links are very attractive because of their light weight and low loss over long distances. Because fiber is a dielectric, these optical links are free from the effects of electromagnetic interference (EMI). Many electrical signals can be multiplexed simultaneously, as in the distribution of cable television (CATV) signals using fiber optics, where 60 or more analog-modulated, cable-television-frequency subcarriers are placed on the optical carrier.

7.1.2 Lightwave Transmission Components

Measurement examples will be given throughout this chapter to illustrate some of the measurement concepts. Three lightwave components will be used as devices under test for these measurements: a directly modulated DFB laser, a Mach-Zehnder optical modu-

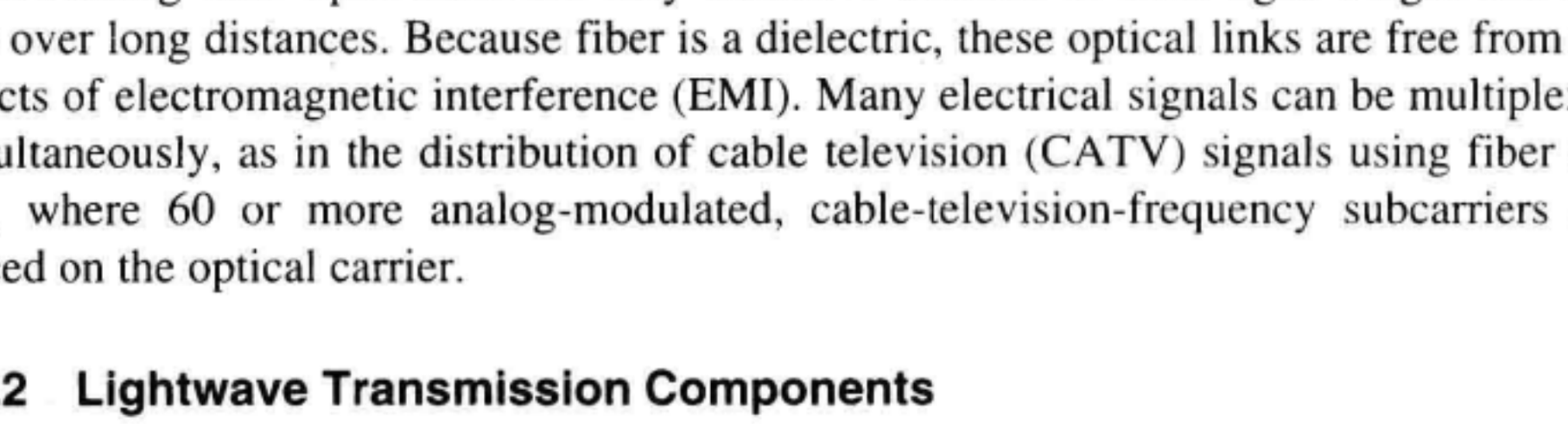

Figure 7.1 Simplified intensity-modulated fiber-optic transmission link.

lator, and a p-i-n photodetector. This section will describe these three components in some detail to make the measurement examples more informative.

Direct and External Modulation. There are two basic approaches to modulating the laser transmitter in intensity-modulated transmission systems. The first technique is to directly modulate the bias current to the laser which causes a corresponding change in the optical output power of the laser. The second approach is to operate the laser at a constant optical output power and externally modulate the optical signal. Mach-Zehnder modulators fabricated in either lithium niobate or gallium arsenide are often used for this purpose. In many lightwave systems, the modulation bandwidth of the laser or the external modulator will limit the maximum transmitted data rate or modulation frequency.

DFB Semiconductor Laser. A common type of laser deployed in direct modulated systems is the distributed feedback (DFB) semiconductor laser as shown in Figure 7.2. This laser uses a double-heterostructure design, in which the active region is placed between layers of larger bandgap material. This bandgap difference confines the electrons and holes to a narrow region and provides the high carrier density necessary for laser gain. The InGaAsP/InP material system is used for semiconductor lasers designed to lase at a wavelength of 1300 nm or 1550 nm. The narrower band gap InGaAsP material has a higher refractive index than InP, forming an optical waveguide for the laser in the plane perpendicular to the wafer surface. The optical waveguide for the plane parallel to the wafer surface is provided in this case by a regrown InP layer. This regrown InP layer is often made semi-insulating to increase lateral current confinement and to reduce parasitic capacitance, which can limit the laser's modulation bandwidth.

A periodic Bragg grating is etched near the InGaAsP guiding region to provide frequency selective feedback to allow oscillation at one dominant mode in the laser cavity. When the bias current to the laser is modulated above the lasing threshold, a proportional modulation of the output optical power is induced.

Mach-Zehnder Modulator. Externally modulated laser transmitters are often deployed where high power, wavelength stability, and a large modulation bandwidth are required. An optical intensity modulator based on the Mach-Zehnder interferometer configuration is shown in Figure 7.3. An optical waveguide is formed in $LiNbO_3$ by diffusing a

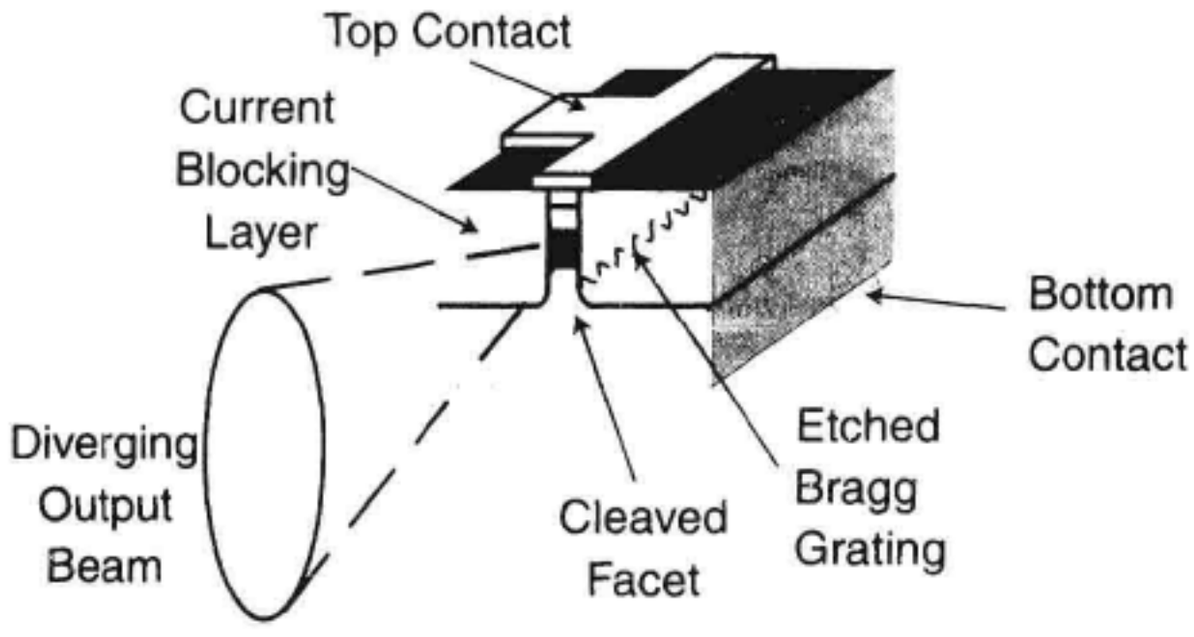

Figure 7.2 Simplified buried-heterostructure DFB laser structure.

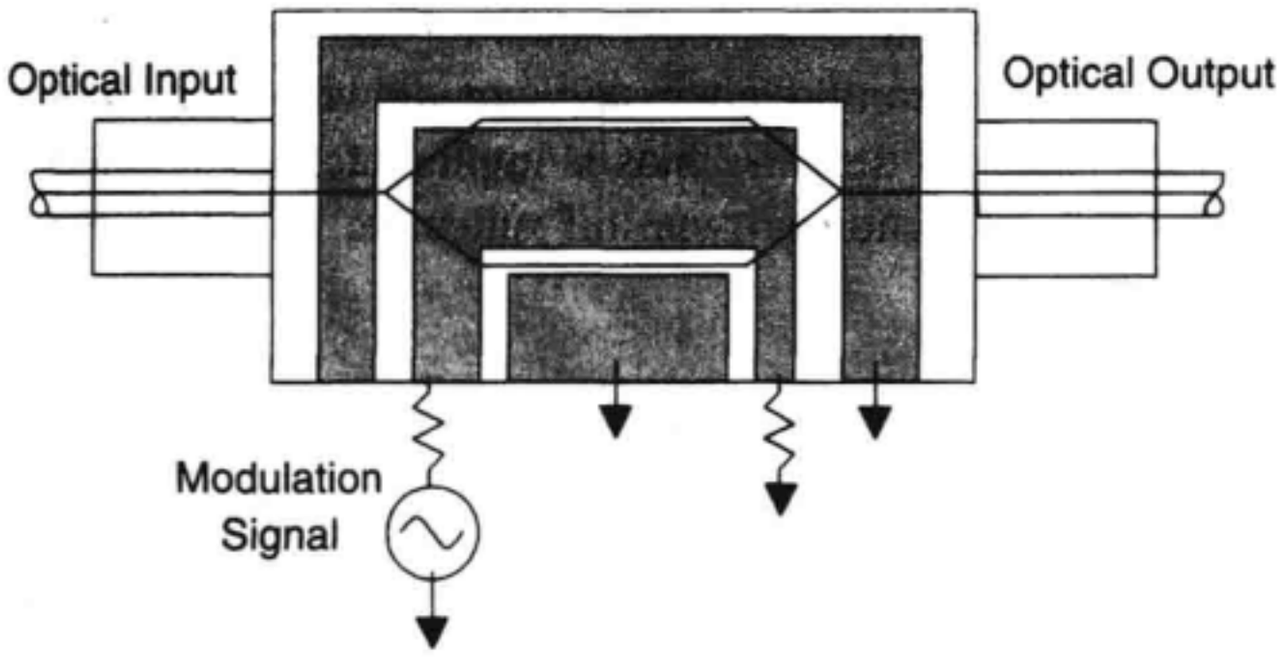

Figure 7.3 Integrated Ti:$LiNbO_3$ Mach-Zehnder interferometer optical modulator.

strip of titanium into the wafer at an elevated temperature. Electrodes are deposited onto the substrate to form a coplanar microwave waveguide. The input light is split in a Y branch. The two parallel optical waveguide arms form two phase modulators, which operate in a push-pull fashion. The phase modulation is made possible by the electro-optic effect in $LiNbO_3$ in which the velocity of light is proportional to the applied electric field. The light from the upper and lower waveguide arms are recombined in the output Y branch. If the two optical waves arrive in phase, the light will be guided on the output waveguide. If the two signals arrive out of phase, then the optical wave will not be guided and will slowly be dispersed into the substrate. Thus, the Mach-Zehnder modulator can produce a transmission loss that is dependent on the electrical modulation signal. This transmission loss through the device is polarization dependent, so the polarization of the optical signal at the input of the device must be well controlled.

p-i-n Photodetector. Receivers deployed in many high-performance lightwave transmission systems employ p-i-n photodetectors because of their broad detection bandwidth, excellent linearity, and temperature stability. A cross-section of a mesa p-i-n photodetector is shown in Figure 7.4. InP/InGaAs/InP heterojunction p-i-n photodetectors operate by absorbing infrared light in the 1.0 to 1.6 μm wavelength range and converting

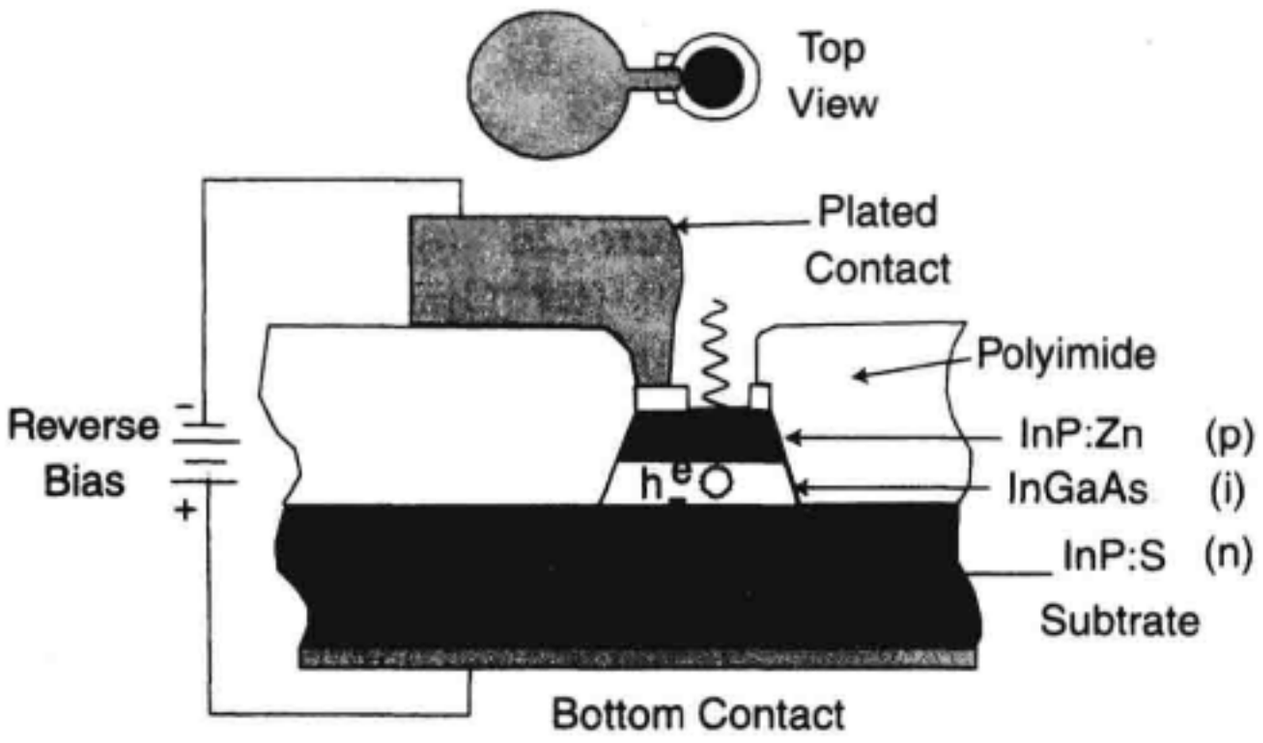

Figure 7.4 Mesa p-i-n photodetector cross-section and top view.

it to a photocurrent. Light enters through the antireflection-coated top surface, and passes through the transparent InP p-type layer. Electron/hole pairs are created when the photons are absorbed in the intrinsic (i) InGaAs layer. Reverse bias is applied across the device, which sweeps the electrons out through the bottom n-type InP substrate, while the holes are collected by the p-type top contact.

7.1.3 Intensity-Modulated Waveform and Spectrum

If one could observe the optical spectrum with sufficient resolution as an optical carrier is being intensity modulated, a pair of modulation sidebands would be seen on either side of the optical carrier, offset from the carrier by the modulation frequency. This is shown in Figure 7.5a for the case of an optical carrier at 193 THz being modulated at 1 GHz. Unfortunately, the resolution of commercial diffraction-grating based OSA is approximately 0.1 nm, which roughly corresponds to 12 GHz at a carrier wavelength of 1550 nm. This makes observation of modulation sidebands difficult. However, heterodyne signal analysis techniques described in Chapter 5 could make this measurement. It is impossible to directly observe an optical carrier waveform being modulated in the time domain, as such measurement instrumentation does not exist. In principle, it would look like the waveform

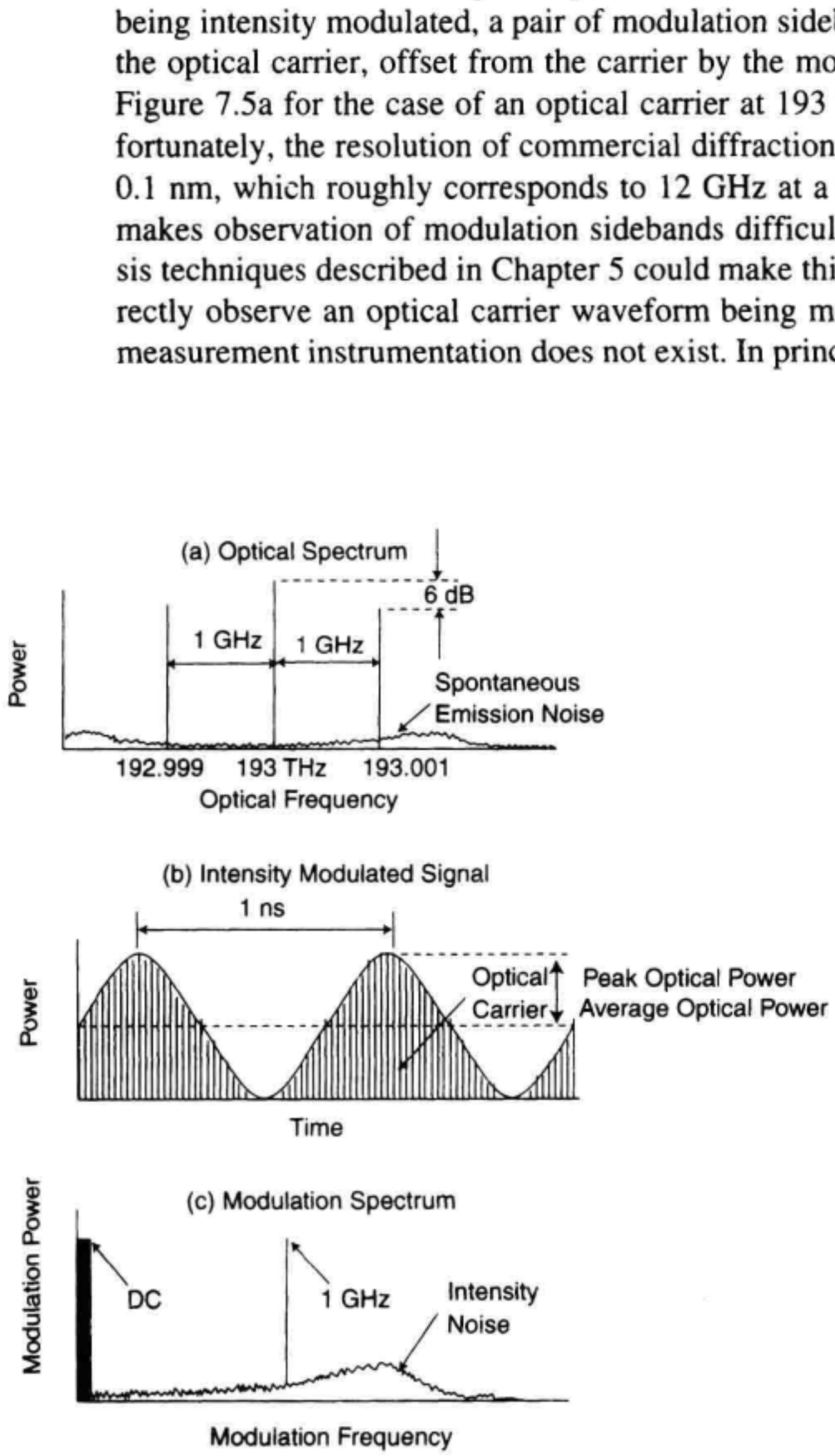

Figure 7.5 (a) Power spectrum of a 193 THz (1554.4 nm) optical carrier being intensity modulated at 1 GHz. (b) Power waveform versus time for the same signal. Both the power envelope and a representation of the optical carrier are shown. (c) Modulation power spectrum for the same signal.

in Figure 7.5b. The vertical lines under the modulation envelope are only symbolic of the optical carrier in this illustration. A laser with a center frequency of 193 THz being modulated at 1 GHz would have 193,000 optical cycles for each 1 ns modulation period.

Because the optical carrier cannot be observed directly in the time domain, nor the modulated optical spectrum be easily resolved, direct detection of the modulation envelope is used to make measurements. A photodetector such as a p-i-n photodiode is used to convert photons of light into an output current. The resulting signal consists of both a modulated component and a time-averaged or dc component of the lightwave signal. This process is essentially baseband demodulation of the optical signal. Assuming the photodetection process is a linear one, the spectrum or waveform of the modulation on the optical carrier can now be measured using conventional electronic measurement instrumentation such as oscilloscopes and RF spectrum analyzers. Notice also in Figure 7.5b, the lightwave waveform is truly being intensity modulated, as there will always be some optical power at the optical carrier frequency which in direct detection corresponds to the time-averaged optical power.

The example in Figure 7.5 corresponds to sinusoidal amplitude modulation with a 100%-modulation depth. In Figure 7.5a, the optical power in each modulated sideband is one-half that of the optical carrier. In Figure 7.5b, the peak modulated power is equal in amplitude to the average optical power. Figure 7.5c, shows the direct-detected optical modulation spectrum, where both amplitude-modulated sidebands fall on one another and sum to a peak-modulated optical power equal to the optical power in the optical carrier, which appears as the dc component.

It is also possible to frequency modulate an optical carrier although this is not typically done. However, frequency modulation or chirping of a semiconductor laser is a common artifact of direct current modulation. This amplitude-phase coupling is often referred as to the alpha- or linewidth-enhancement factor. At low modulation frequencies, this effect is dominated by thermal heating inside the laser cavity changing the effective cavity length and thus the lasing frequency. At higher modulation frequencies, the optical index of the laser cavity varies due to its dependence on the carrier density. This changes the optical transit time in the cavity, causing the lasing frequency to fluctuate.[1] This chirping or spectral broadening of the optical carrier is an important consideration when transmitting signals over long distances where chromatic dispersion in the fiber can cause the signal to become distorted. Chirp and its measurement is discussed more fully in Chapter 5.

7.1.4 Modulation-Frequency-Domain Measurements

In order to optimize the performance of any high-speed transmission system, a number of modulation-frequency-domain measurements must be made on the components and devices that are integrated into the system. Generally, these frequency domain measurements can be grouped into three general categories:

- Modulation transfer function (Section 7.2)
- Modulation signal analysis (Section 7.3)
- Intensity noise characterization (Section 7.4)

Modulation transfer function measurements are necessary to determine if the optical components have the required modulation bandwidth, with appropriate amplitude and phase characteristics, to allow adequate transmission and reception. Modulation signal analysis is useful to analyze the modulation spectrum, to determine the linearity of the modulation function, or conversely to measure any distortion. Maintaining a minimum SNR is a requirement of any transmission system. Typical noise sources include shot noise, receiver noise, and intensity noise. The intensity noise of the semiconductor laser is often the primary limiting factor in the noise performance of many analog lightwave transmission systems, making its measurement extremely important. See Appendix A for a detailed theoretical description of these various noise sources.

Each of these measurement categories will be examined in greater detail in the following sections.

7.2 MODULATION TRANSFER FUNCTION

A fundamental requirement of any component or device in a transmission system is that it have sufficient modulation bandwidth to allow the transmission and reception of the intended information. For digital systems using a non-return-to-zero (NRZ) binary format, the modulation bandwidth needs to be greater than one-half the bit rate. For example, at least 500 MHz of bandwidth is required for a 1 Gbit/s NRZ transmission rate. In addition, the phase response over this bandwidth should vary linearly with modulation frequency in order to avoid the effects of intersymbol interference (ISI). For a return-to-zero (RZ) binary format, the modulation bandwidth needs to be at least greater than the bit rate. In analog systems, such as those used in fiber-optic CATV transmission, a modulation bandwidth approaching 1 GHz is required to carry the multiple television subcarriers.

This modulation transfer function of the component or system as a function of the radian frequency, w, can be expressed simply as

$$H(jw) = \frac{O(jw)}{I(jw)} \tag{7.1}$$

where $H(jw)$ is the modulation transfer function, $O(jw)$ is the output response, and $I(jw)$ is the input stimulus.

The most common technique to measure the modulation transfer function is to use a lightwave component analyzer. The complex frequency notation, jw, is used to indicate that both the magnitude and the phase function of the transfer function are being measured. Figure 7.6 illustrates the modulation transfer functions that will be examined in this section. A brief description of each is given here:

- E/O measurement: A small signal electrical current is applied to an optical source such as a laser and the resulting output optical-modulation power is measured.
- O/E measurement: A small modulation-depth optical signal is applied to a receiver such as a photodetector and the resulting output electrical current is measured.

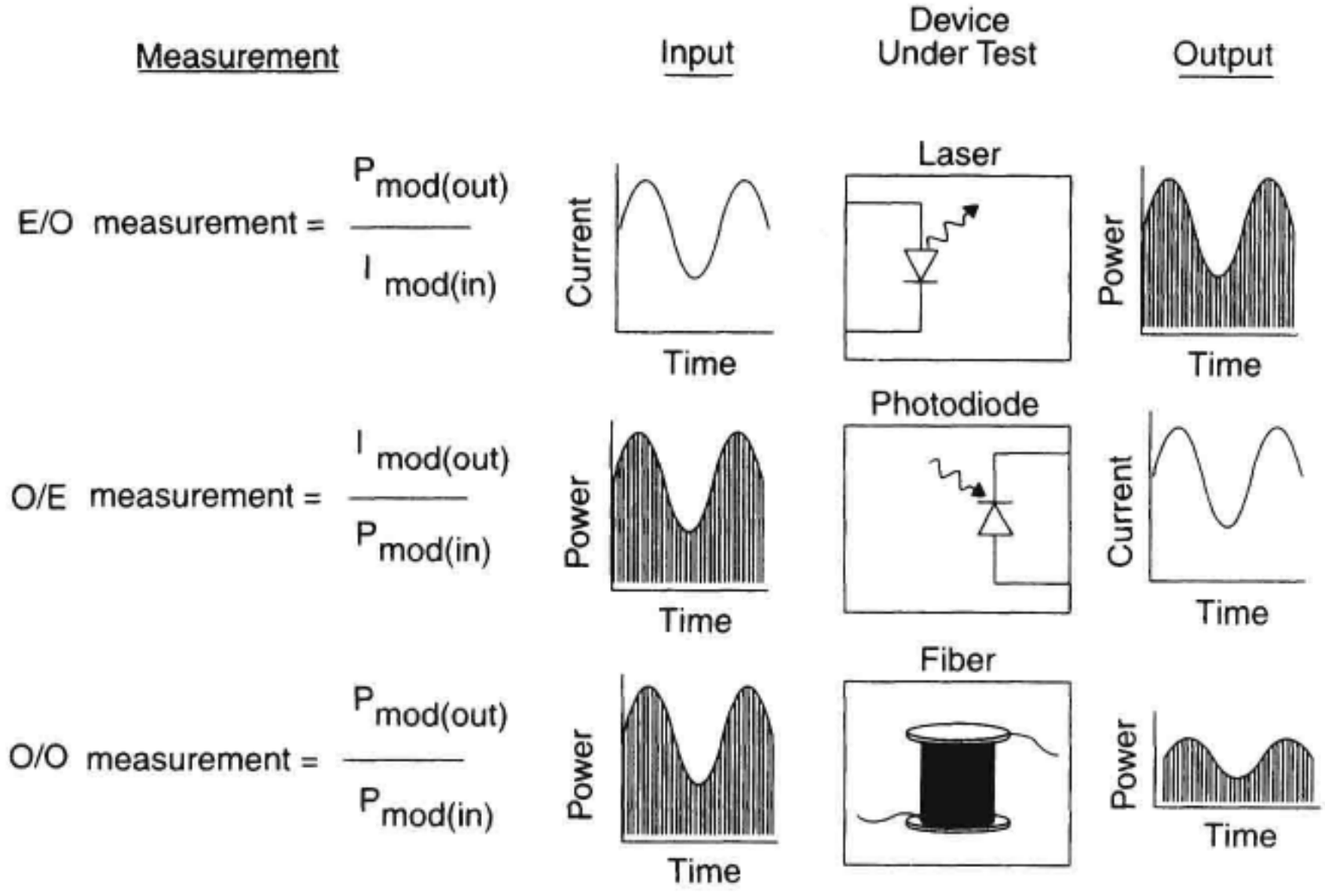

Figure 7.6 Modulation transfer functions for optical components. (a) E/O measurements. (b) O/E measurements. (c) O/O measurements.

- O/O measurement: A small modulation-depth optical signal is applied to a two-port optical device such as optical fiber and the resulting output optical modulation is measured.
- E/E measurement: The modulation response of the entire link of Figure 7.1 from the electrical input to the electrical output can also be characterized. This measurement is not illustrated in Figure 7.6. Since it is strictly an electrical measurement, it will not be further discussed in this section.

7.2.1 Lightwave Component Analyzer

A lightwave component analyzer is used primarily to measure the small-signal linear transmission and reflection characteristics of a lightwave component or system as a function of modulation frequency. It is a measurement system that operates by injecting a modulated signal into a test device and comparing the modulated input signal to the signal that is transmitted or reflected by the test device. This comparison of the transmitted signal to the incident signal results in a ratio measurement. The concept of making ratio measurements to test the response of electrical devices and systems has traditionally been used in the RF and microwave industries. The instrument used to make these types of transmission measurements for high-frequency electrical networks is called a vector-network analyzer.

Electrical vector-network analyzers use a swept-RF frequency source as a stimulus signal to the device under test (DUT). This incident sinewave signal is also used as a

"known" reference signal. Both the magnitude and phase of the signal that is transmitted through the DUT is routed to the analyzer's receiver and compared to the reference signal. If a reflection measurement is made, an electrical test set is used to separate the incident signal from the reflected signal. The result of this process is a ratio measurement comparing an incident signal to a transmitted or reflected signal.

In the microwave world, this type of measurement is called an S-parameter (scattering parameter) measurement. It is an OUT/IN ratio. For example, S_{21} means that the scattering parameter is a ratio of the signal OUT of port 2 (device output) compared to the signal IN to port 1 (device input). S_{11} would be a reflection measurement, where 11 represents the signal coming OUT of (reflected from) port 1 of a device compared to the signal (incident) going IN to port 1 (same port) of the device.

A lightwave component analyzer is based on a vector network analyzer platform and includes an optical test set that includes a calibrated lightwave source and receiver. An electrical signal is provided to modulate the lightwave source. The lightwave receiver detects the RF modulation imposed on the optical carrier and passes the detected electrical signal to the analyzer for signal processing. With the two calibrated converters, the lightwave component analyzer can measure four types of components categorized by their input and output ports as shown in Figure 7.7.[2,3] This figure illustrates the transmission-modulation transfer functions that can be performed. Optical reflection measurements can also be made with the addition of optical directional couplers.

7.2.2 E/O Transfer Function Measurements

The modulation transfer function for an E/O transducer such as a semiconductor laser can be measured in the following manner. The lightwave component analyzer measures the input modulating current to the laser as well as the laser's output optical modulation power. The lightwave component analyzer then displays the ratio of the two measurements in watts/amp. Although responsivity is often used to describe a static or dc parame-

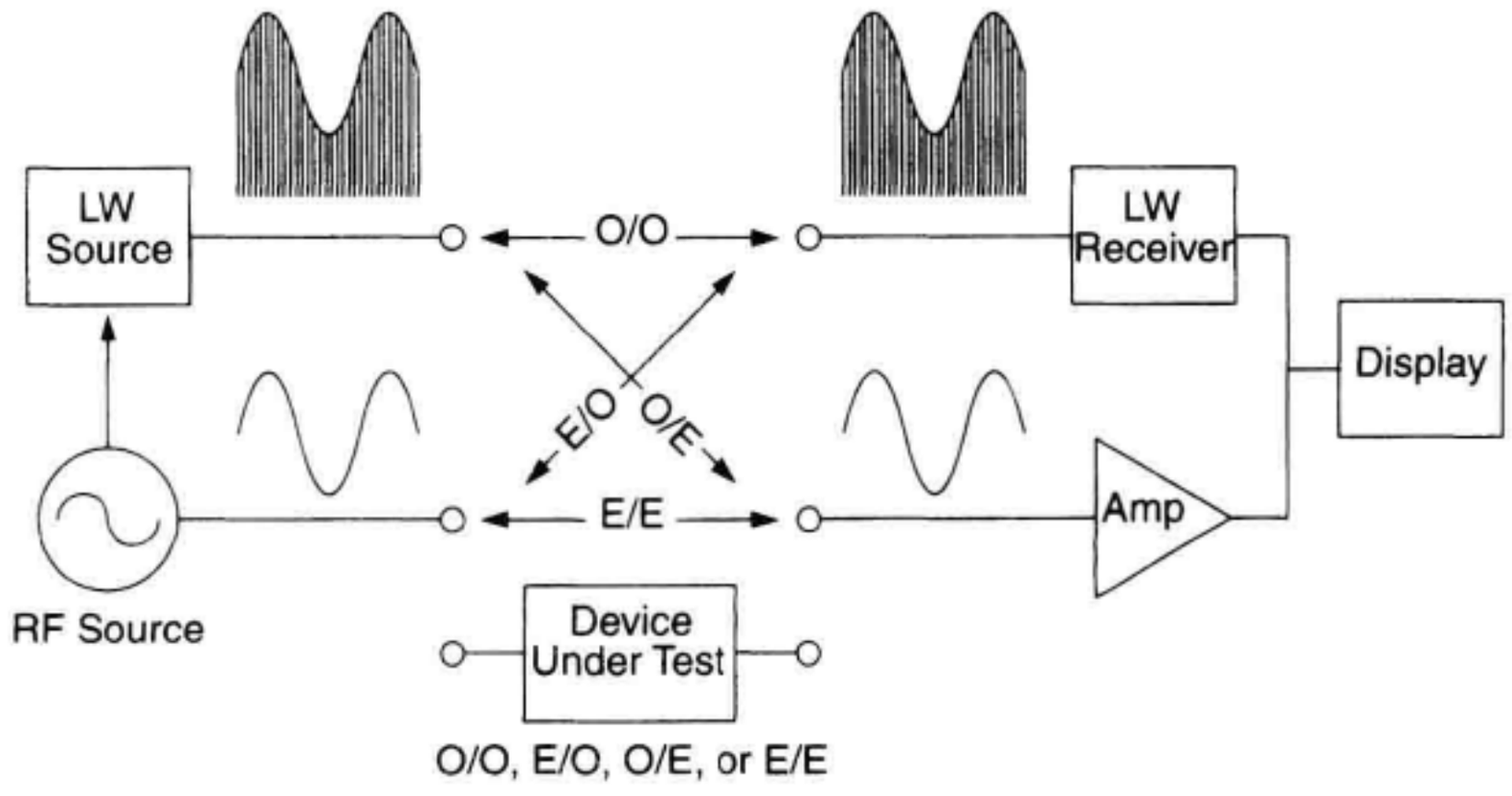

Figure 7.7 Lightwave component analyzer block diagram and measurement modes.

ter, the conversion efficiency of an optical source is a dynamic characteristic and can be referred to as "slope responsivity," R_s. (For lasers this is often referred to as the laser efficiency.) Slope responsivity is used to describe how a change in input current produces a change in optical power. Graphically, this is shown in Figure 7.8. As one may expect, the slope responsivity is a function of the frequency of the modulating current. As the frequency of modulation increases, the conversion efficiency will eventually degrade or "roll off." The frequency at which the conversion efficiency drops to one-half of the maximum value is the "−3 dB point" when displayed logarithmically, and indicates a laser's modulation bandwidth.

Example: DFB-Semiconductor-Laser Intensity-Modulation Response

The frequency response of a laser is dependent on biasing conditions. As the dc bias current of the laser is increased, the bandwidth generally increases. This is caused by a shift in the "relaxation oscillation" characteristic, which is a natural resonance frequency of the laser. This relaxation oscillation phenomenon creates an observable resonance in the intensity modulation response of the laser.

Measurement Procedure

This is basically an E/O transfer measurement well-suited for the lightwave component analyzer. First, an initial calibration is required to perform an accurate measurement. This calibration allows the lightwave component analyzer to remove the response of the test system, including the electrical cables, optical fiber, and the instrument itself. Prior to the calibration of the instrument, the following instrument settings need to be made:

- start and stop frequencies,
- sweep type (linear or logarithmic),
- number of measurement points,
- measurement sweep time,
- source power level.

To perform a simple frequency-response calibration, the connections shown in Figure 7.9 must be made. The analyzer measures the appropriate paths so the frequency and phase response of the "unknown" paths are characterized. The analyzer then uses this information in conjunction with the internal calibration data to generate an error matrix. The lightwave source and receiver characteristics are predetermined during a factory calibration and stored

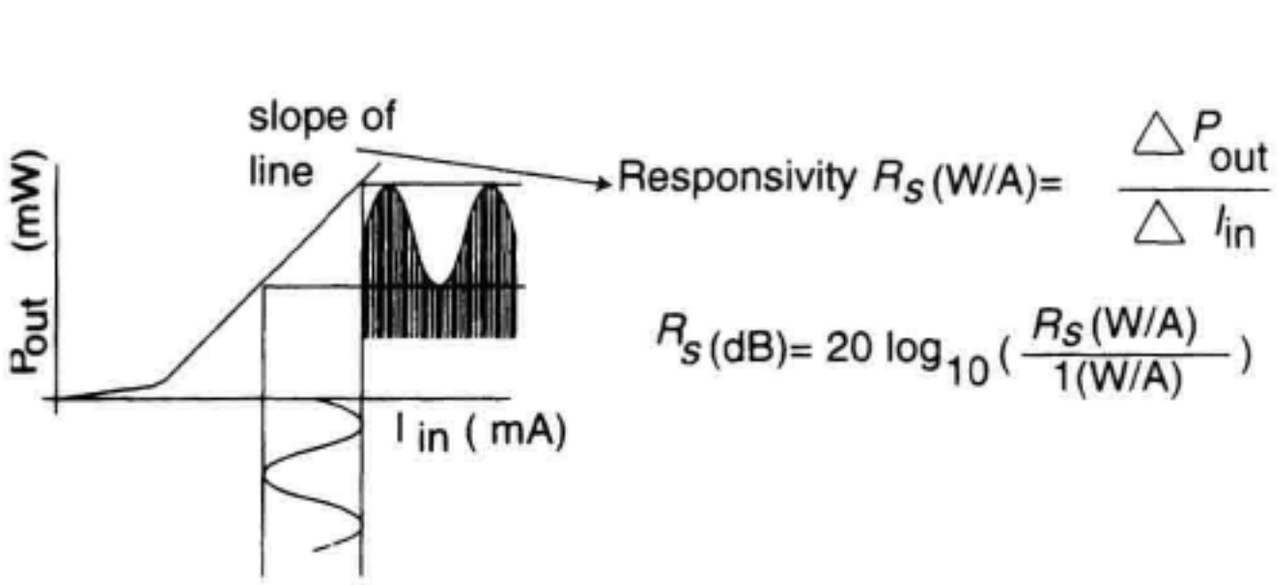

Figure 7.8 E/O slope responsivity.

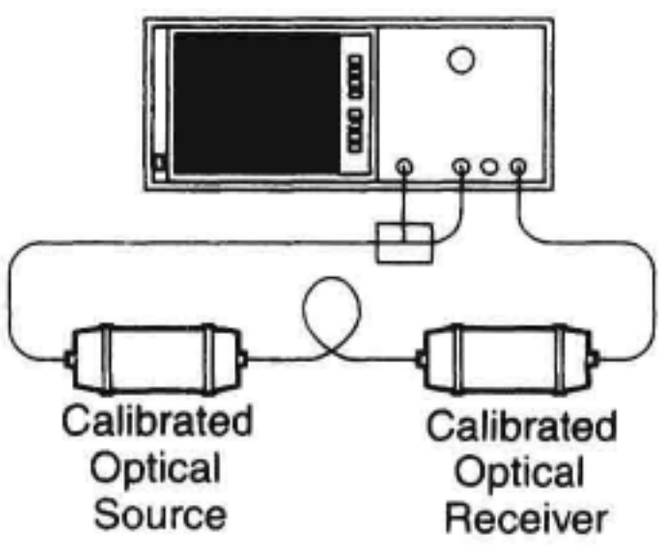

Figure 7.9 E/O calibration configuration.

in memory. The accuracy of this measurement is dependent on accurate calibration of the magnitude and phase response of the lightwave source and receiver used with the vector network analyzer. Section 7.5 discusses how this calibration may be performed. Once the setup and calibration have been completed, the laser under test is connected between the electrical and optical measurement interface connections, substituting for the calibrated lightwave source.

Figure 7.10 shows a measurement of the conversion efficiency of a DFB semiconductor laser as a function of modulation frequency. The horizontal axis in this case covers the frequency range from 130 MHz to 10 GHz. The vertical axis is in units of watts/amp, displayed logarithmically where O dB represents 1 W/A. This particular laser has a −3 dB modulation bandwidth of approximately 3.5 GHz. By varying the external bias supply to the laser, one can make a number of measurements at different bias conditions to determine the optimum bias for maximum frequency response. Typically, as the bias is increased, both the responsivity and bandwidth will increase until the bias reaches a certain point where the high-end frequency response begins to degrade.

Figure 7.11 shows the measured phase response of the laser. A laser's modulation response would ideally exhibit a linear phase response versus modulation frequency. The derivative of the phase response with respect to modulation frequency is referred to as the group delay. A linear phase response is equivalent to a constant group delay. If the group delay is not constant with the modulation frequency, the modulated waveform will be dis-

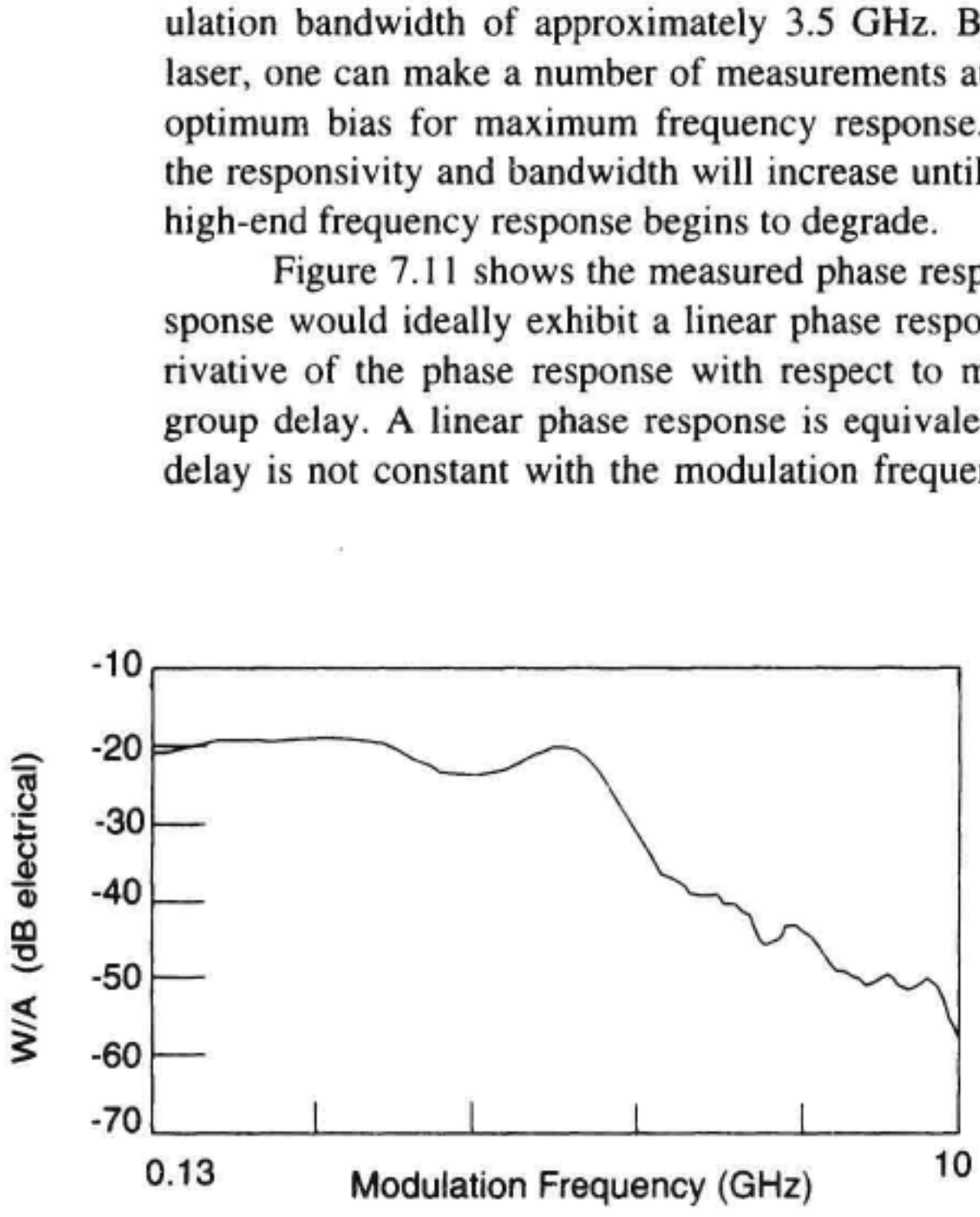

Figure 7.10 Modulation transfer-function magnitude-response for a DFB laser.

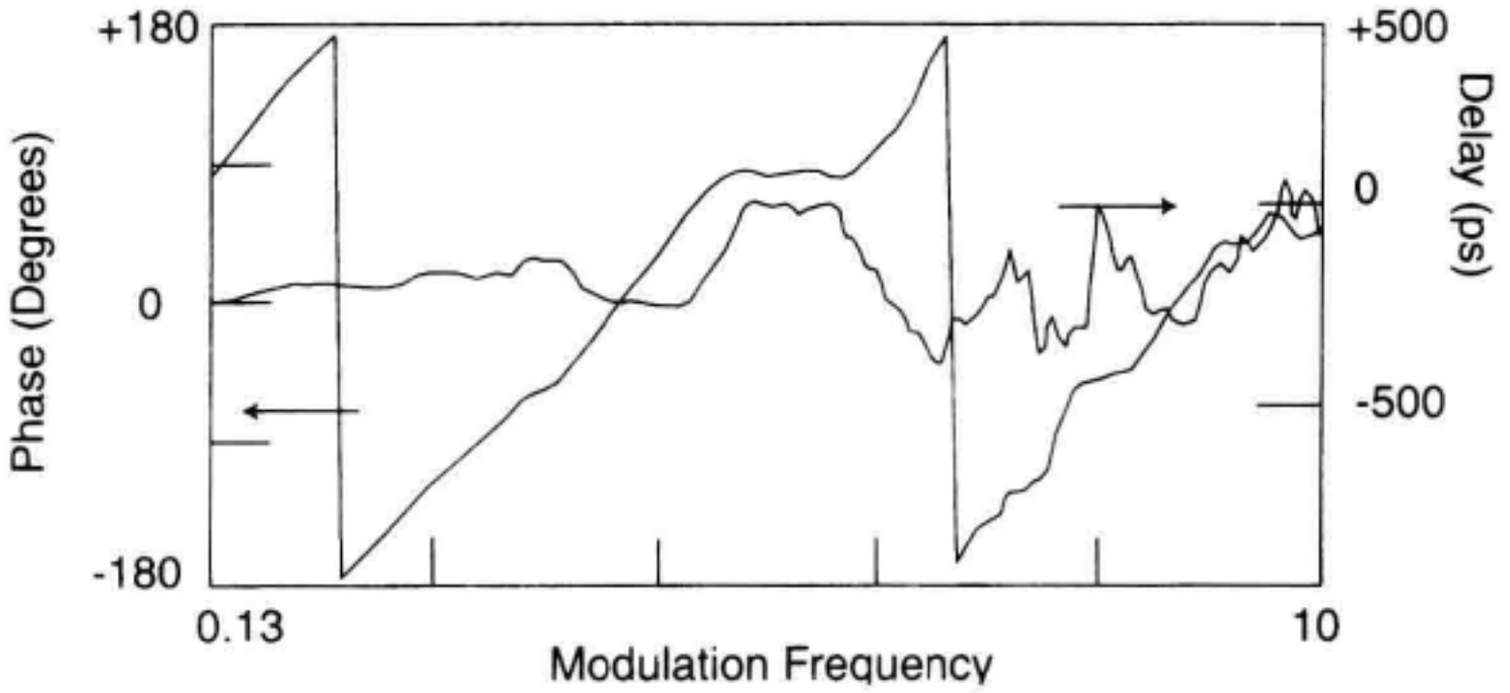

Figure 7.11 Modulation transfer-function phase-response for the DFB laser of Figure 7.10.

torted. The frequency range where the phase response begins to deviate from linear often occurs near the frequency where the magnitude of the modulation response begins to roll off.

Measurement Interpretation

The measurement of a semiconductor laser's modulation response conveys a significant amount of information. There are several factors that limit the modulation bandwidth of semiconductor lasers. The measured modulation response can be compared to the predicted theoretical response based on semiconductor laser dynamics. An analysis utilizing the rate equations can be used to determine the intrinsic intensity modulation response. The rate equations comprise a set of coupled equations that describe the relationship between the laser's bias current, I, electron density, N, and photon density, S. A simplified version of these equations for single longitudinal mode operation is shown:

$$\frac{dN}{dt} = -g(N - N_t)S + \frac{I}{qV} - \frac{N}{\tau_n} \tag{7.2}$$

$$\frac{dS}{dt} = \Gamma g(N - N_t)S - \frac{S}{\tau_p} + \frac{\Gamma \beta N}{\tau_n} \tag{7.3}$$

where N_t is the carrier density for transparency, g is the differential gain, q is the electron charge, V is the volume of the active region, τ_n is the photon lifetime, Γ is the optical confinement factor (which is the fraction of the optical power in the active region), and β is the fraction of spontaneous emission coupled into the active region.[4]

Analyzing the rate equations illustrates four points:

- Electron density increases because of the injection of a current I, into a volume V.
- Electron density decreases because of both spontaneous emission with a lifetime τ_n and stimulated emission, whose rate is dependent on the differential gain, g.
- Photon density increases because of stimulated and spontaneous emissions confined inside the active layer.

- Photon density decreases because of internal and mirror losses, which cause a photon decay with lifetime τ_p.

An analytical expression relating the intensity modulation response to the modulating current can be obtained for the nonlinear differential rate equations. By assuming small signal sinusoidal variation of the current, carrier density, and photon density; such that $I = I_0 + ie^{jwt}$, $S = S_0 + se^{jwt}$, and $N = N_0 + ne^{jwt}$, and solving the rate equations, the following transfer function results:

$$\frac{s(f)}{i(f)} = \frac{s(0)}{i(0)} \times \frac{f_0^2}{f_0^2 - f^2 + jff_d} \tag{7.4}$$

The key result shown here is the second-order nature of the denominator term, which predicts a damped resonance in the laser's modulation frequency response. Two important terms, f_0 and f_d, appear in the equation. f_0 results from a resonance between the electrons and photons in the active region and is related to the geometric mean of the stimulated electron lifetime and photon lifetime.[5,6] f_d is the damping frequency and is dependent on the photon lifetime and ϵ, which characterizes several nonlinear mechanisms in the differential gain. The relaxation oscillation frequency, f_p, can be calculated from f_0 and f_d as shown:

$$f_0 = \frac{1}{2\pi\sqrt{\tau_n \tau_p}} \tag{7.5}$$

$$f_d = \frac{\epsilon S}{2\pi\tau_p} \tag{7.6}$$

$$f_p^2 = f_0^2 - \frac{f_d^2}{4} \tag{7.7}$$

Theory predicts that the intensity modulation response of semiconductor lasers is peaked at f_p, the relaxation oscillation frequency.[7] The amount of peaking or, conversely, damping is a strong function of ϵ. Beyond the relaxation oscillation frequency, a roll off of 12 dB per octave increase in modulation frequency is predicted. In addition, theory predicts that the relaxation oscillation frequency increases with the square root of the bias current, and that the peaking in the response becomes more damped until it is critically damped.

Unfortunately, achieving a high relaxation oscillation frequency does not guarantee a wide modulation bandwidth. Both device structure and package parasitics can dramatically alter the drive current passing through the active region. Parasitics requiring consideration include the bond wire inductance, the bonding pad capacitance, any device capacitance, and contact resistance.

Example: External Modulator Intensity Modulation Response

The optical transmission response of a Mach-Zehnder modulator is a function of the applied dc bias voltage as shown in Figure 7.12. The transfer curve highlights four parameters:

1. The insertion loss, which is the optical loss at the maximum transmission point of the curve.

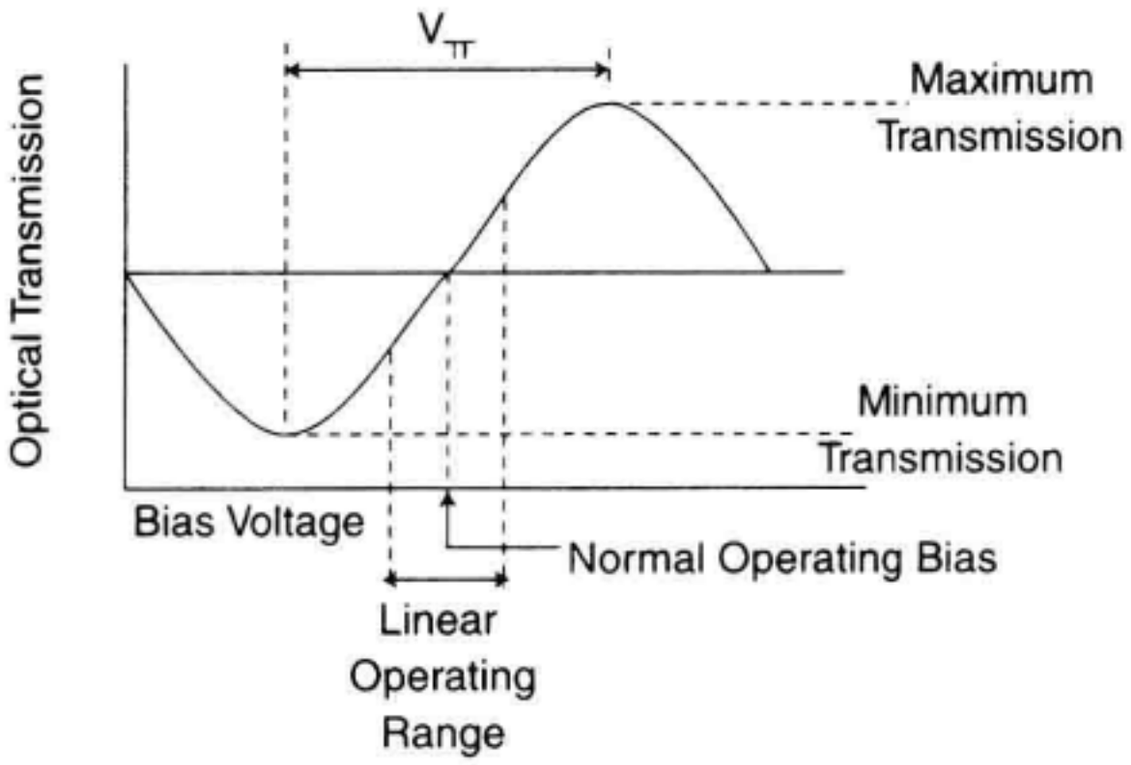

Figure 7.12 Mach-Zehnder interferometer transmission transfer curve versus bias.

2. The switching voltage, V_{π}, which is the difference in bias voltages at the minimum and maximum transmission points.
3. The extinction ratio, which is the ratio of the maximum to the minimum optical transmission levels.
4. The nominal operating point, which is the bias voltage that results in optical transmission halfway between the minimum and maximum transmission levels.

The modulator response is linear for small deviations from the nominal operating bias point. When a sinusoid with radian frequency w is applied, the transmitted light power $I(t)$ can be written as:

$$I(t) = \frac{I_0}{2}\left[1 + \cos\left(\pi \frac{V_b + E(w)V_p\cos(wt)}{V_{\pi}}\right)\right] \tag{7.8}$$

where I_0 is the maximum transmitted light power, $E(w)$ is the frequency-dependent modulation efficiency, V_p is the peak signal voltage applied to the modulator, and V_{π} is the modulator's characteristic switching voltage. The operating point on the modulator's transfer curve can be adjusted by varying the dc bias, V_b.[8]

Measurement Procedure

The modulation response of external intensity modulators can be characterized using a lightwave component analyzer in much the same way as laser sources. This is another class of E/O measurements where the stimulus is a swept-frequency electrical signal and the response out of the modulator is intensity-modulated light. The modulation bandwidth and phase measurements of external intensity modulators are made with the lightwave component analyzer in the same configuration that is used for laser measurements. However, a significant difference exists in this measurement because the modulator is a three-port device. While the frequency response of a modulator is often independent of input optical power, the responsivity is not. The conversion efficiency of the modulator is not only a function of the electrical input, but also the optical input level.

To compute the responsivity of the modulator in watts/amp, the lightwave component analyzer compares the output modulation power to the input modulation current. If the input optical power to the modulator is increased, the output optical modulation typically will increase also. Thus, the lightwave component analyzer will measure an apparent increase in responsivity. This means that the responsivity measurement of the modulator is valid only for the specific optical input power that existed when the measurement was performed. However, the frequency response of the modulator is typically valid over a wide range of input optical powers.

Though lasers are typically described by an input current versus output power relationship, the preferred description for a modulator is often an input voltage versus output power relationship. Because lightwave component analyzer measurements assume a 50 ohm measurement environment, the modulator measurement in watts/amp can be converted to watts/volt by scaling (dividing) by 50. Figure 7.13 shows a measurement of a wide-bandwidth $LiNbO_3$ Mach-Zehnder external modulator. The unusual response in the low frequency range is caused by electrical impedence matching circuitry in the modulator. This is caused by the high dielectric constant of $LiNbO_3$ which results in a low characteristic impedance of 22 ohms for the coplanar microwave transmission line.

Measurement Interpretation

Several factors limit the modulation efficiency of optical-intensity modulators at high-modulation frequencies. The main limitation is a mismatch of the velocities of the copropagating optical and microwave traveling waves as shown in Figure 7.14. The optical signal travels about twice as fast as the modulating microwave signal. If the difference in time of propagation through the modulator is great enough, the microwave signal will get out of phase with the modulation impressed on the optical signal and begin to reverse the effect. Velocity mismatch can be reduced and broad bandwidth operation achieved by keeping the device length short. Microwave losses in the coplanar electrodes also contribute to a reduced modulation efficiency at high frequencies. If the electrodes are sufficiently thick, the loss will be mainly due to the skin effect and will increase as the square root of frequency.

7.2.3 O/E Transfer Function Measurements

The measurement process for O/E devices, such as lightwave receivers and photodiodes, is similar to that for E/O devices. The slope responsivity, R_r, for these O/E devices describes how a change in input optical-modulation power produces a change in output

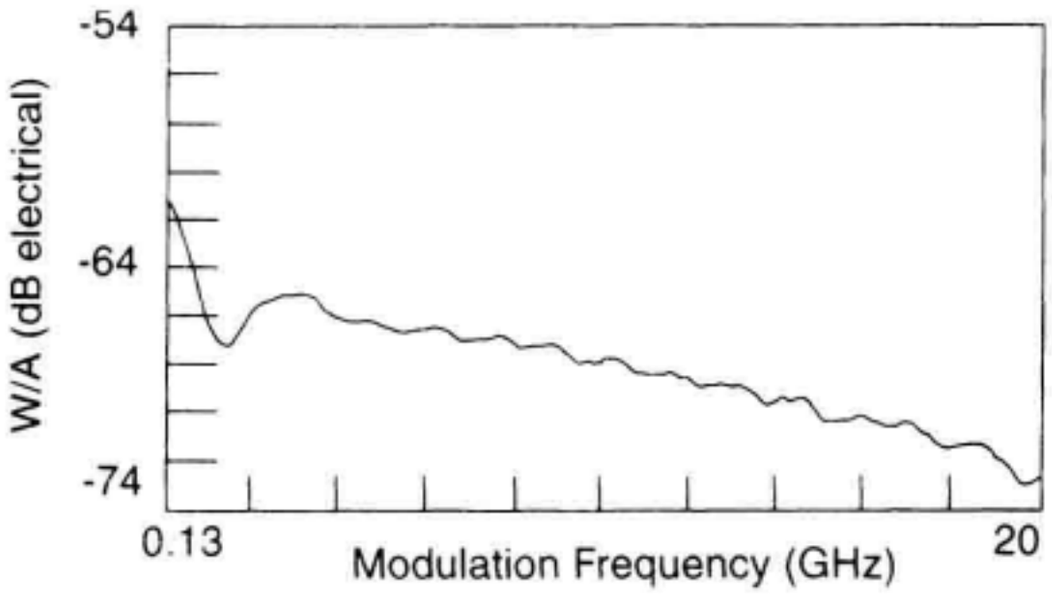

Figure 7.13 Measurement of a Mach-Zehnder modulator modulation bandwidth.

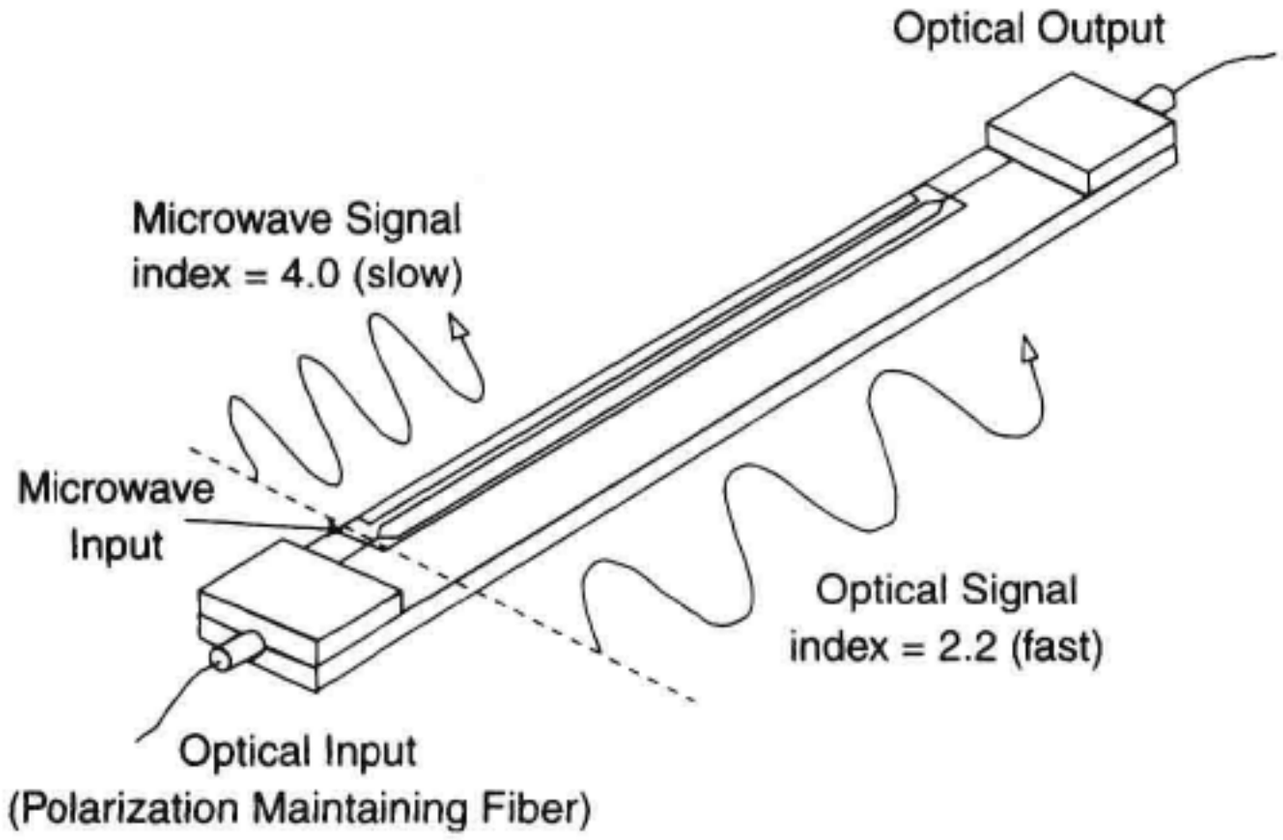

Figure 7.14 Velocity mismatch between the microwave modulation and the optical carrier.

electrical-modulation current. Graphically this is shown in Figure 7.15. The lightwave component analyzer measures the input optical-modulation power and output modulation current. It then displays the ratio of the two in amps/watt.

Example: p-i-n Photodetector Frequency Response

The frequency response of a p-i-n photodetector is determined by a combination of the RC time constant of the photodiode and the transit time for the generated electrical carriers to travel through the i-region. Both a low capacitance and a short transit time are desirable. However, these two parameters are interconnected. A thin i-region can result in a short transit time, but it also increases the capacitance. Therefore, both parameters must be optimized in relation to one another in the design of high-speed p-i-n photodetectors.[9]

Measurement Procedure

The measurement process for a p-i-n photodetector is virtually identical to the laser measurement. The configuration and user calibration of the lightwave-component analyzer is the

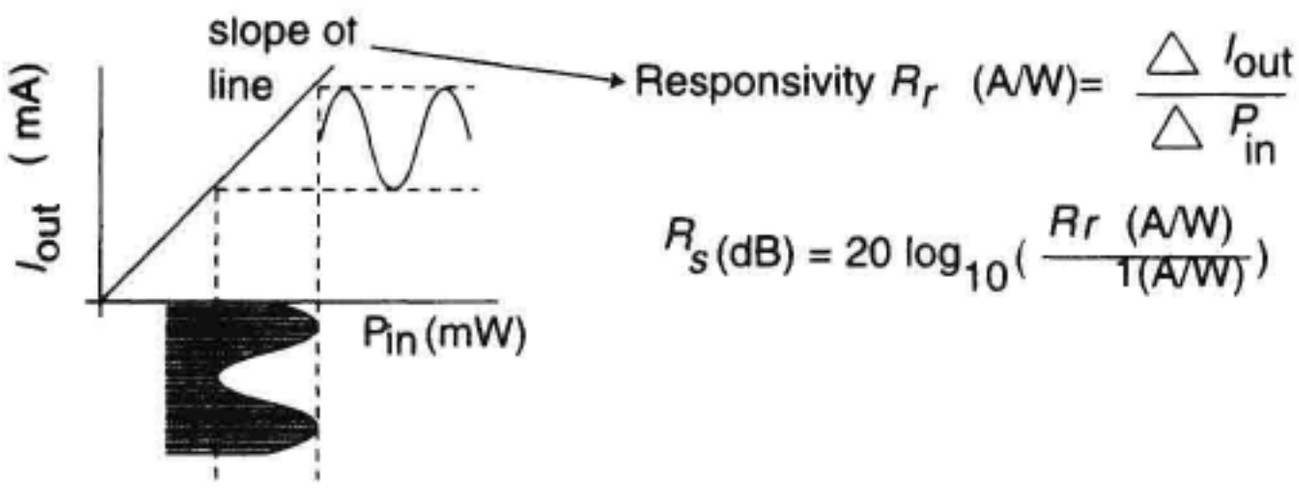

Figure 7.15 O/E slope responsivity.

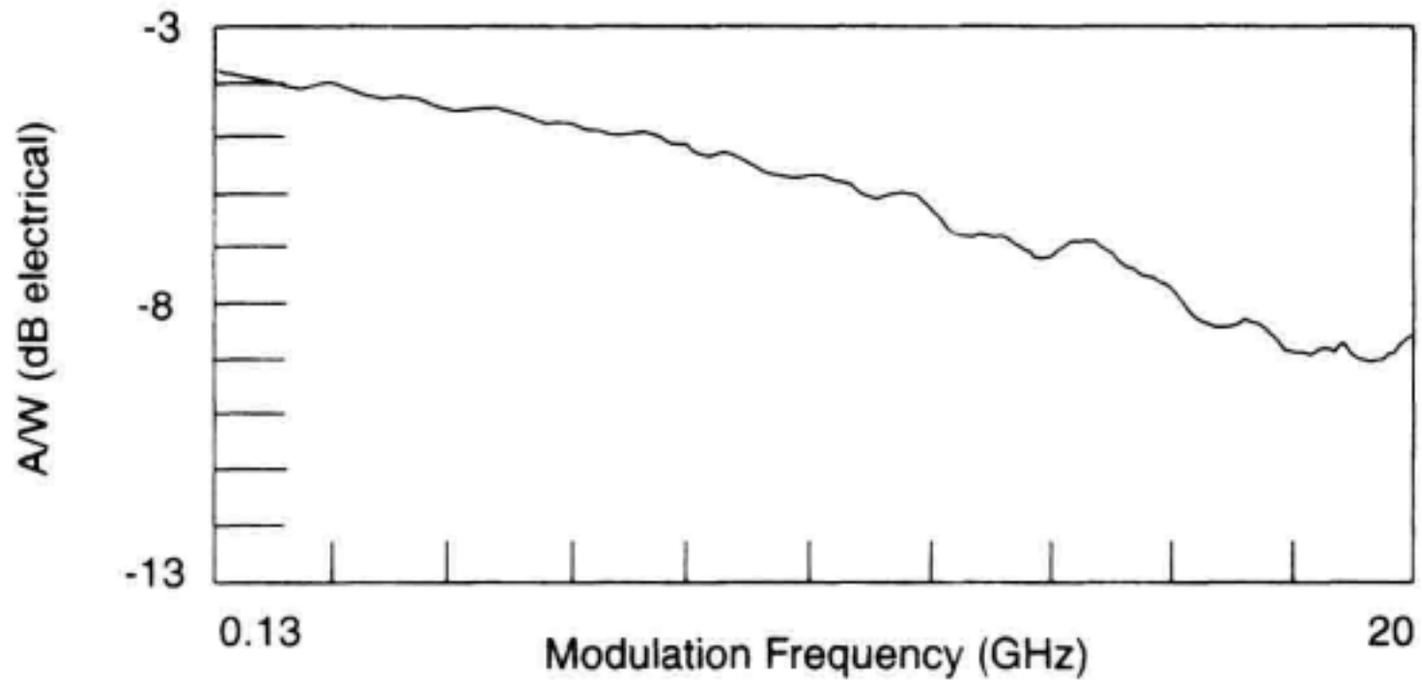

Figure 7.16 Measurement of the frequency response magnitude of a p-i-n photodetector.

same. Once the setup and calibration have been completed, the p-i-n photodetector is placed in the measurement path.

Figure 7.16 shows a measurement of the conversion efficiency of a high-speed p-i-n photodetector as a function of modulation frequency. The vertical axis display units are in amps/watt and the horizontal axis is the modulation frequency. In this case, the vertical axis is in a logarithmic format where 0 db represents 1 A/W. This photodiode under test has a modulation bandwidth of approximately 15 GHz.

Measurement Interpretation

The frequency response of lightwave receivers can show some distinct resonances that will impact the time-domain performance. There can be several reasons for this behavior. Once the photodiode has converted the modulated light to a proportional electrical current, the next task is to efficiently transfer the demodulated signal to a following electrical circuit such as a preamplifier. High-speed systems usually require this transfer over 50 or 75 ohm transmission lines. However the output impedance of a photodiode is usually much higher than 50 or 75 ohms. This can result in signals being reflected and a degradation in conversion efficiency if the signal transmitted from the photodiode encounters another impedance mismatch along the transmission path. Reflections can occur resulting in "mismatch loss" and ripple in the measured frequency response.

The phase response of a lightwave receiver is also an important parameter. If the phase response of the receiver is not linear, the detected waveform will be distorted. Figure 7.17 shows the phase response of a p-i-n photodetector assembly. When components have significant length in either the optical or electrical paths, the relative phase will have a large variation. This is not caused by the detection process. For example, if a transmission line following the photodiode is one-half of a wavelength long at the modulation frequency of 10 GHz, this will result in a 180 degree phase deviation. More important is the deviation from linear phase. To view this, the effects of path length must be removed by mathematically adding delay to the analyzer reference path. In this case the delay required is approximately 630 ps. Also shown is the variation in delay versus modulation frequency. Ideally, all frequency components would require the same amount of time to propagate through the device in both the optical and electrical domains. If this is not true, waveform distortion results.

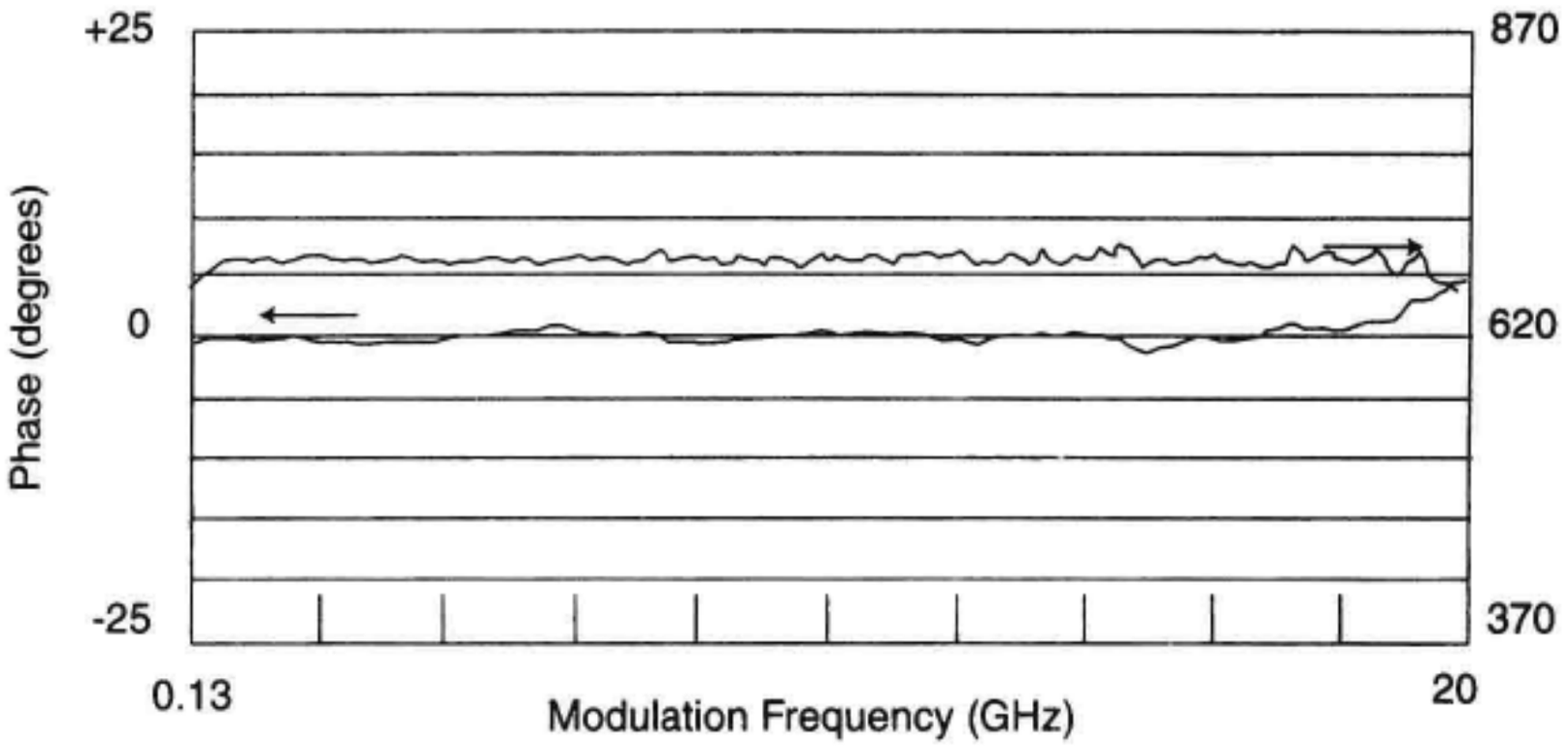

Figure 7.17 Measurement of the phase response of a p-i-n photodetector.

7.2.4 O/O Transfer Function Measurements

The modulation response for two-port optical measurements can also be made. One of the major applications of this mode is in the measurement of chromatic dispersion of optical fiber. The group delay of the fiber is calculated from the measured phase response. If the optical frequency for the measurement is adjusted and the group delay recalculated, the dispersion of the optical fiber can be determined. Chapter 12 covers this measurement area in detail.

7.3 MODULATION SIGNAL ANALYSIS

As lightwave transmission systems and their components have evolved, designers have become interested in the measurement and characterization of the optical modulation depth, signal strength, distortion, and intensity noise of optical signals. Optical modulation depth and distortion are very important in analog systems employing multiple microwave subcarriers such as CATV optical-distribution systems and microwave links for antenna remoting. These CATV systems typically employ high-power DFB lasers or linearized external modulators. They can transmit 60 or more subcarriers spaced in a bandwidth of up to 750 MHz or higher. In antenna-remoting applications, the microwave subcarrier frequencies modulating the optical carrier can reach 15 GHz or more. A recent development is fiber optic links designed for expanding coverage in cellular networks to microcells. These employ subcarriers in the 800 MHz to 1 GHz frequency range.

The most common technique to make these measurements utilizes a lightwave signal analyzer.

7.3.1 Lightwave Signal Analyzer

A lightwave signal analyzer is used for a variety of signal analysis measurements on the modulation present on the optical carrier. In the simplest terms it can be described as a calibrated optical receiver system that can display the modulated spectrum on an optical carrier. A simplified block diagram of a lightwave signal analyzer is shown in Figure 7.18. The lightwave signal analyzer essentially consists of two elements: a wide-bandwidth, high-conversion gain optical converter, and an RF spectrum analyzer. Light from the input fiber is collimated by a lens and focused onto a high-speed p-i-n photodetector. The variable optical attenuator in the collimated beam is used to prevent signal overload. The optical attenuator can also be used to examine if distortion products are generated by the incoming lightwave signal or from nonlinearities within the measurement instrument itself. The time-varying component of the photocurrent, which represents the demodulated signal, is fed through a preamplifier and then to the input of the RF spectrum analyzer. The optical converter in front of the RF spectrum analyzer must have high-conversion gain to overcome the relatively high-noise figure of the RF spectrum analyzer. RF spectrum analyzers are swept-tuned heterodyne electrical receivers employing RF mixers to down-convert the electrical signal to an intermediate frequency (IF) so it can be further processed and detected. The DC portion of the photocurrent is fed to a power meter circuit to allow the display of the average optical power. A major contribution of a lightwave signal analyzer is its optical calibration. It is calibrated in both absolute and relative optical power.[10] Various calibration techniques are described in Section 7.5

Electrical dB and Optical dB Displays. In this section, the lightwave signal analyzer examples will be displayed in either electrical dB or optical dB units. Since the photodetector is a power-to-current converter, a 1 dB change in optical power corresponds to a 2 dB change in electrical power, thus the dB optical and dB electrical terminology. For some measurements such as modulation-depth characterization, it is useful to use dB optical displays on the lightwave signal analyzer. This allows an easy comparison of the average optical power to the modulated optical power. In other applications such as relative intensity noise characterization, it is more useful to have a display in dB electrical units.

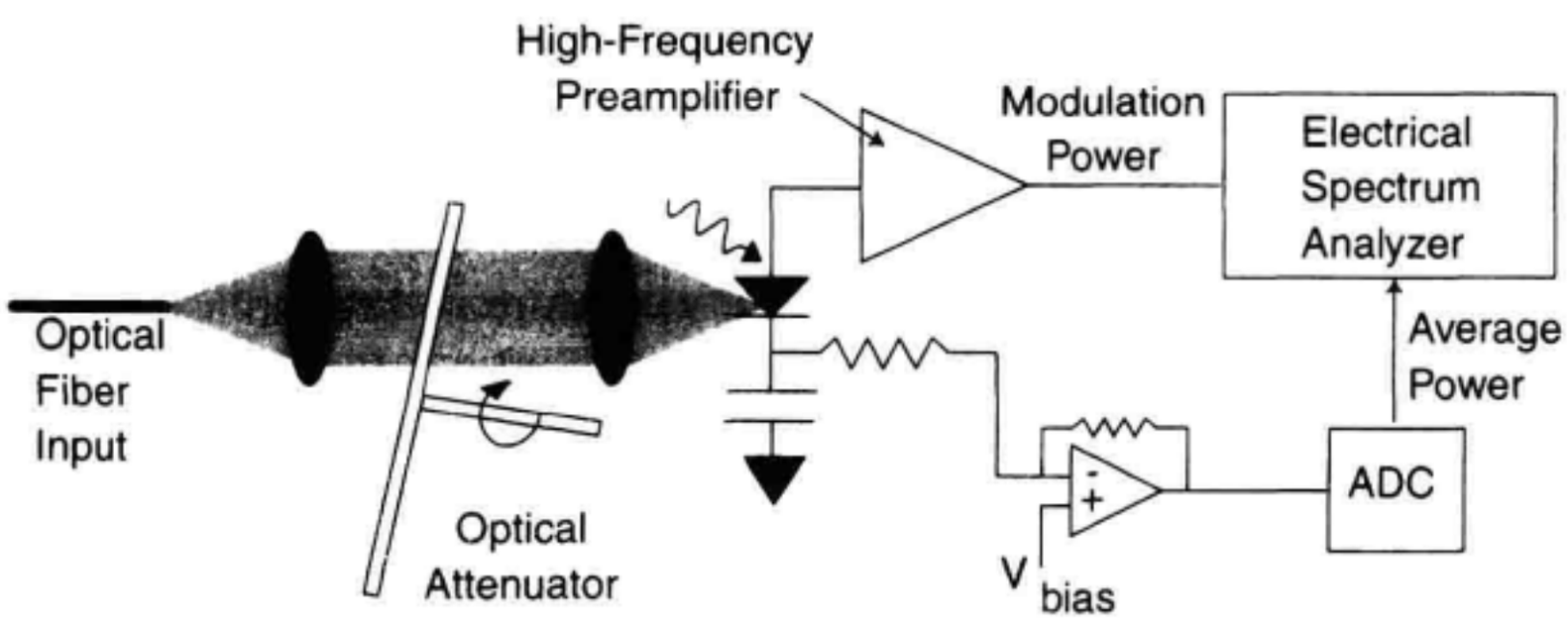

Figure 7.18 Block diagram of lightwave signal analyzer.

The lightwave signal analyzer is often confused with an OSA which is discussed in Chapter 3. Although both instruments have frequency-domain displays, the information they provide is quite different. The OSA shows the spectral distribution of average optical power as a function of optical wavelength. It is suitable for observing the modes of a multimode laser or the sidelobe rejection of a single-frequency laser. The measurement resolution is typically about 0.1 nm or approximately 18 GHz at a wavelength of 1300 nm. The lightwave signal analyzer displays the total average optical power as well as the power of the intensity modulation on the optical carrier. It does not provide any information about the wavelength of the optical signal. This distinction was shown in Figures 7.5a and 7.5c.

7.3.2 Intensity Modulation and Modulation Depth

The measurement of intensity modulation on an optical carrier requires some type of analyzer. If there is only one modulating signal such as in a digital transmission system, the intensity modulation can be measured on a digital communications analyzer, which is based on an oscilloscope platform, as described in Chapter 8. However, if there are multiple modulating signals, it is much more convenient to use a lightwave signal analyzer. Figure 7.19 shows multiple modulating signals that are present on an optical carrier. The horizontal axis is the modulation frequency, indicating the measurement is being made over a wide range of frequencies. The vertical axis is displayed logarithmically in units of dBm where 0 dBm is equal to 1 mW. The amplitude and frequency of each modulating signal can be easily measured using built-in marker functions common in lightwave signal analyzers and spectrum analyzers.

An important parameter in optical CATV and other analog-modulated optical transmission systems is the optical modulation depth (OMD). Sometimes it is referred to as the optical modulation index (OMI). They represent the same ratio which is defined as:

$$\text{OMD} = \frac{P(f_{\text{mod}})}{P_{\text{AVG}}} \tag{7.9}$$

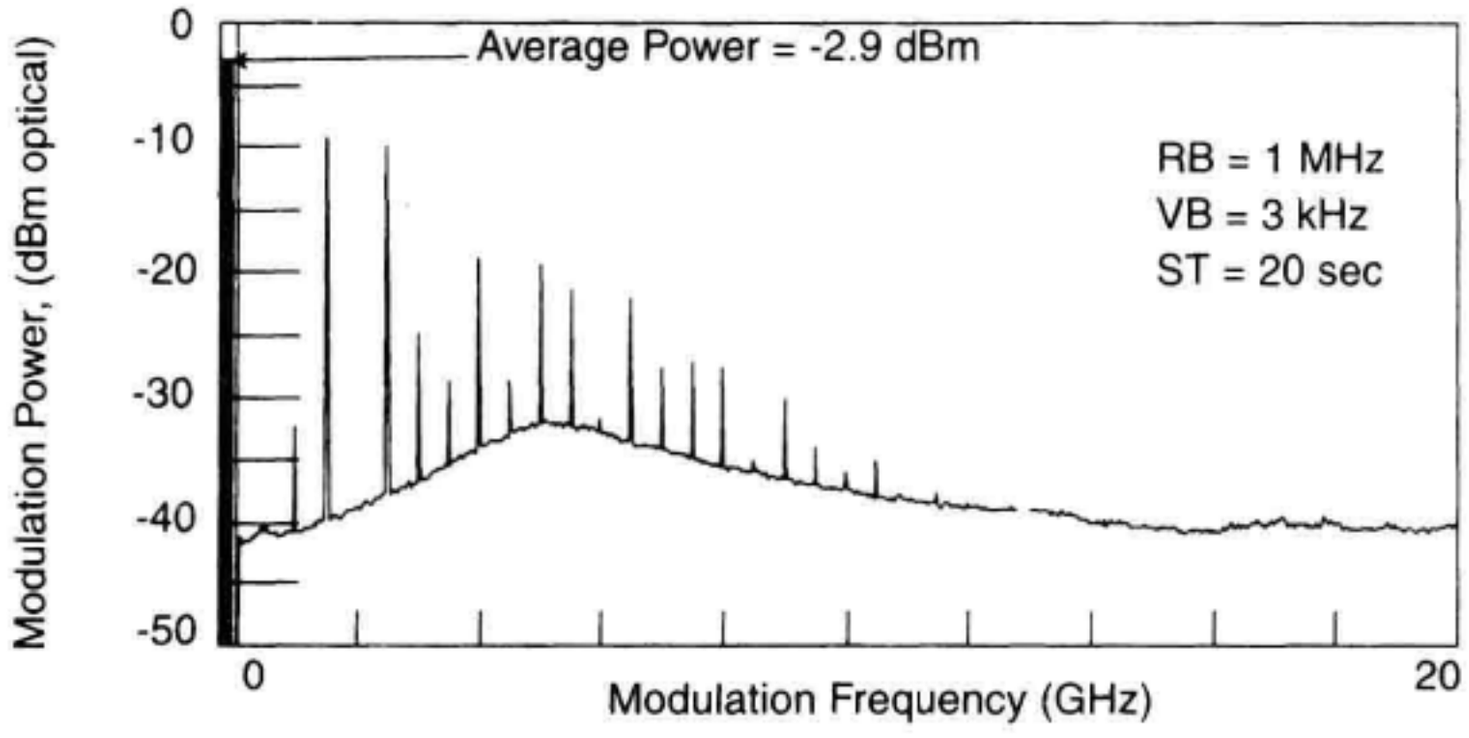

Figure 7.19 Lightwave signal analyzer display of multiple-modulating signals.

where OMD is the optical modulation depth, $P(f_{mod})$ is the peak optical modulated signal power as shown in Figure 7.5b, and P_{AVG} is the average optical power.

In many CATV systems, the OMD of each modulated subcarrier is only a couple of percent. This is because there are typically many subcarriers (TV channels) being modulated simultaneously on the optical carrier, and the cumulative modulation depth is much higher. If the modulation depth becomes too large, signal distortion or clipping can result. This measurement can be made on the lightwave signal analyzer using a specific marker function that determines the ratio of the modulated signal power at a given frequency to the average optical power.

7.3.3 Distortion

The goal of any transmission system is to transfer information as accurately as possible. To the first order, both lasers and p-i-n photodetectors are linear devices. A laser translates an electrical current into a proportional optical power. A p-i-n photodetector translates optical power into a proportional electrical current. This is equivalent to saying their slope responsivities, which were discussed in Section 7.2, are close to being linear. However, neither device is perfectly linear, particularly when large modulation levels are involved. Several different types of distortion products are common from these components such as harmonic distortion and intermodulation distortion.

When a device such as a laser is intensity modulated there will be modulated signal power at the modulating frequency; and depending on the linearity of the device, there will also be some modulating power at harmonics of the modulating frequency. Some modulated power at the second harmonic and third harmonic of the modulating frequency is very common. Harmonic distortion is defined as the ratio of modulated power in a harmonic of the modulating frequency to the power at the modulating frequency. For example:

$$\mathrm{HD}_2 = \frac{P(2f_{mod})}{P(f_{mod})} \tag{7.10}$$

$$\mathrm{HD}_3 = \frac{P(3f_{mod})}{P(f_{mod})} \tag{7.11}$$

$$\mathrm{THD} = \frac{P(2f_{mod}) + P(3f_{mod}) + \ldots + P(nf_{mod})}{P(f_{mod})} \tag{7.12}$$

where HD_2 is the second harmonic distortion, HD_3 is the third harmonic distortion, and THD is the total harmonic distortion.

Figure 7.20 shows a measurement of second harmonic distortion. Also shown are the third and higher harmonics. It is common to express the distortion in decibels (dB) as shown. In this case, the harmonic distortion is expressed as:

$$\mathrm{HD}_x = 10 \log \left(\frac{P(xf_{mod})}{P(f_{mod})} \right) \tag{7.13}$$

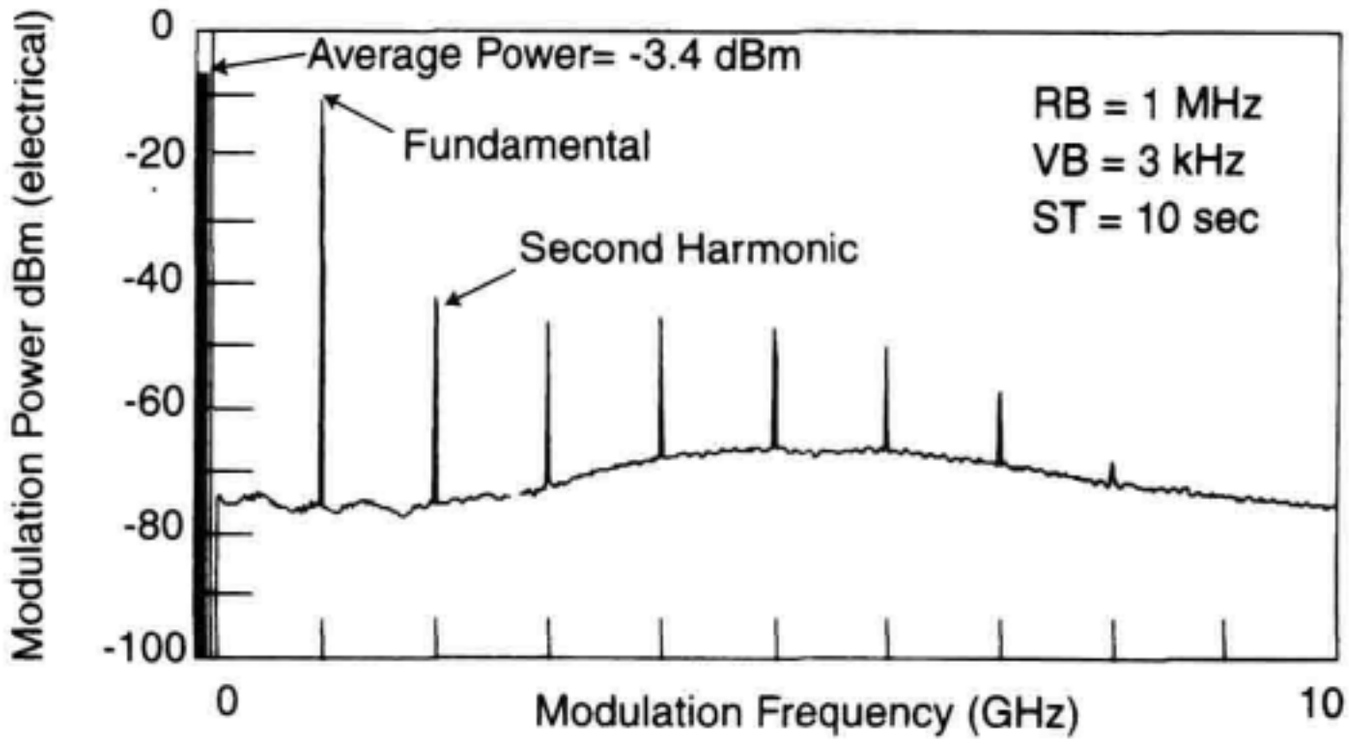

Figure 7.20 Measurement of harmonic distortion.

Intermodulation distortion (ID) occurs when two or more modulating signals are present. In this case, device nonlinearities cause the two modulating signals to interact, producing new signals at the sum and difference frequencies. Second-order intermodulation distortion for two signals can be measured as:

$$ID2(f_i \pm f_j) = \frac{P(f_i \pm f_j)}{P(f_i)} \tag{7.14}$$

where $P(f_i) = P(f_j)$.

For three modulating signals, third-order intermodulation can be expressed as:

$$ID3(f_i \pm f_j \pm f_k) = \frac{P(f_i \pm f_j \pm f_k)}{P(f_i)} \tag{7.15}$$

where $P(f_i) = P(f_j) = P(f_k)$.

A particularly distressing form of intermodulation distortion is third-order intermodulation (IMD) for two closely spaced signals. This is because the IMD signals fall close to the original modulating frequencies.

$$\text{IMD}(2f_i - f_j) = \frac{P(2f_i - f_j)}{P(f_i)} \tag{7.16}$$

Figure 7.21 shows an intermodulation distortion measurement.

Care must be taken to make accurate distortion measurements. A measurement system consisting of a lightwave signal analyzer or RF spectrum analyzer can contribute its own distortion. Usually, the instrument distortion is specified either in terms of harmonic distortion at a given input power level or in terms of a second-order intercept (SOI) or a third-order intercept (TOI). The intercept refers to the power level at which the distortion term, either second order or third order, is equal in amplitude to the power of the fundamental signal. Both SOI and TOI are extrapolated quantities used as figures of merit, since equal levels of signal power and harmonics are not likely to occur in practice. How-

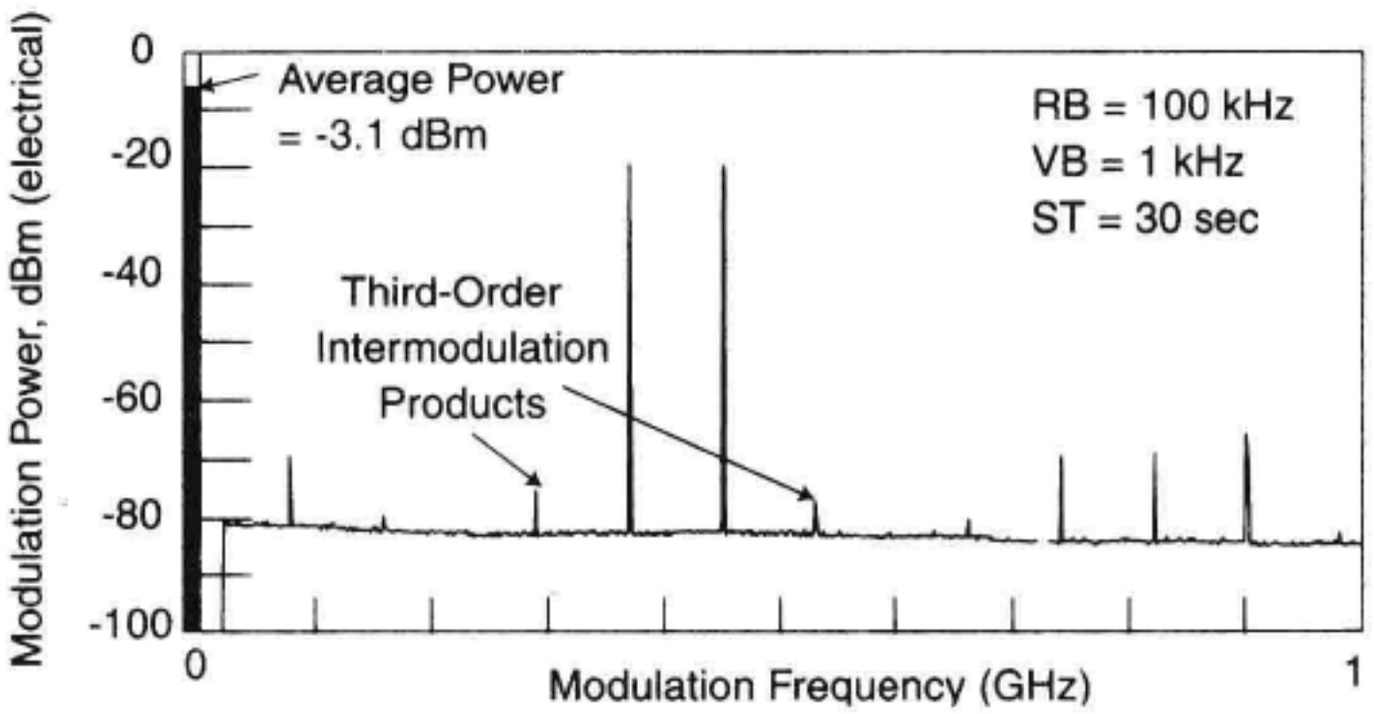

Figure 7.21 Measurement of intermodulation distortion.

ever, modest ratios of peak power to average power can cause measurement distortion by overdriving the input to the instrumentation. This is common with pulse waveforms with low-duty cycles or when a number of modulated subcarriers are present. A technique to check for instrumentation linearity is to vary the input optical attenuation value and observe if any change in the displayed spectrum shape or amplitude occurs. If an optical attenuator change does not affect the harmonic distortion level, then the displayed distortion is generated outside of the measurement instrumentation.

Distortion in Lightwave CATV Systems. As previously stated, lightwave CATV systems employ subcarrier modulation. The video information is vestigial-sideband amplitude-modulated (AM-VSB) on a TV frequency channel or carrier. These TV signals are combined and are used to modulate the optical carrier. Typically, there will be a number of second-order and third-order distortion products generated. For N TV signals or subcarriers there will be the following second-order products: N harmonics at $2 f_i$, and approximately N^2 order terms at $f_i \pm f_j$. The latter tends to dominate the second-order distortion performance of these systems. The summation of the second-order distortion terms is referred to as the composite second-order (CSO) distortion. For N-subcarriers there are the following third-order products: N harmonics at $3 f_i$, approximately N^2 two-tone intermodulation terms at $2 f_i \pm f_j$, and approximately N^3 three-tone intermodulation terms at $f_i \pm f_j \pm f_k$. The last term tends to dominate the third-order distortion performance of these systems. The summation of the third-order distortion terms is referred to as the composite triple-beat (CTB) distortion. When 60 CATV subcarriers are placed in the 50 MHz to the 450 MHz frequency band, it can be shown that the CSO distortion is worse at the low-band edge where approximately 50 terms contribute, whereas it is at a minimum in the middle of the frequency band. However, the CTB peaks in around 200 MHz where over 1100 third-order terms fall on one another.

Distortion in lightwave CATV systems can come from many sources including the laser transmitter and the receiver. DFB semiconductor lasers have several distortion

mechanisms including a frequency-dependent distortion related to the relaxation oscillation,[11,12] and frequency-independent distortion caused by gain saturation[13] and spatial hole burning.[14] In addition, the frequency chirp inherent in the direct modulation of DFB lasers causes distortions due to the nonflat gain profile of fiber amplifiers and the chromatic dispersion of optical fiber. External intensity modulators have low or zero chirp, however these devices are only linear for small-signal modulation. This is because the optical intensity transfer function is sinusoidal with applied voltage as was discussed in Section 7.2.2. When the modulator is biased at the half-power point, second-order distortions are suppressed, however third-order distortions must be reduced through some type of linearization. In addition, p-i-n-based photoreceivers have linearity limitations at high power levels and operating frequencies due to internal electric field perturbations that impact the carrier velocity and generate harmonics and intermodulation products in the output current.[15,16]

7.4 INTENSITY NOISE CHARACTERIZATION

In many applications, the intensity noise spectrum is very important. First and foremost, the intensity noise spectrum affects the SNR in a transmission system. Many CATV systems employ low-noise Nd:YAG lasers with external Mach-Zehnder intensity modulators to achieve both high-power and low-noise transmission. However, much work has been done to improve both the output power and noise performance of DFB semiconductor lasers to make them an attractive lower-cost alternative in these applications. In addition, the noise spectrum can provide valuable information about a semiconductor laser's relaxation oscillation frequency.

7.4.1 Intensity Noise Measurement Techniques

The intensity noise from an optical source can be measured in a number of ways. A lightwave signal analyzer described in Section 7.3.1 is the most convenient measurement tool. Both the intensity modulation and the intensity noise are displayed simultaneously. In principle, a broad-bandwidth photoreceiver in conjunction with an electrical spectrum analyzer with the appropriate calibrations can also serve the purpose.

Alternative approaches to measure laser intensity noise would be to use a photoreceiver with a noise figure meter or electrical power meter. Noise figure meters typically offer good noise figures (6 to 8 dB) because of a built-in preamplifier, and can automatically correct for their internally generated thermal noise when a 50 ohm termination is placed at the input. However, there can be significant measurement uncertainty due to mismatch loss if the photoreceiver is not reverse terminated in 50 ohms. Electrical power meters offer good sensitivity over a very wide bandwidth. To use them effectively, a bandpass filter is required to select the noise measurement range of interest. Also, the noise power is effectively integrated over this bandwidth, which in some cases can be desirable. However the spectral characteristics of the noise are not measured.

Example: DFB Semiconductor Laser Intensity Noise

Intensity fluctuations, as well as phase fluctuations, are inherent characteristics of semiconductor laser devices. These fluctuations are due to the quantum nature of the transitions of the lasing process, which gives rise to the intensity noise. Dependent on the structural parameters of the device, the intensity noise is attributed to both the spontaneous emission and carrier-recombination processes.

Measurement Procedure

Prior to measurement, the following lightwave signal analyzer instrument settings need to be made:

- start and stop frequencies,
- resolution bandwidth,
- video bandwidth,
- reference level,
- noise marker.

The start and stop frequencies are set for the desired measurement frequency range. A wide span is useful for observing the full laser-intensity noise spectrum. The resolution bandwidth sets the effective measurement resolution and should be set to a value approximately one-hundredth of the measurement span to maintain a reasonably fast measurement sweep time. The video bandwidth which serves the same function as trace averaging is also set at a value low enough to maintain reasonable sweep time. The reference level should nominally be placed high enough to allow the display of any modulated signals. However, in the case of measuring noise, the reference level can be set to a sufficiently low level such that the internal attenuator auto-sets itself to zero attenuation. This value results in the best instrument sensitivity setting.

The intensity noise spectrum of a DFB semiconductor laser at several bias settings is shown in Figure 7.22. Typically, analyses and measurements have shown that the intensity noise increases with rising current and optical power, reaches a maximum at threshold, and then decreases above threshold.

Measurement Interpretation

The frequency dependence of the intensity noise can be analyzed by adding Langevin sources to the rate equations as described in Section 7.2.2. These Langevin terms mathematically model the spontaneous emission and the carrier shot noise. The photonic shot noise caused by the particulate nature of photons is not included in the rate equations. The small signal solution below shows that the frequency dependence of the intensity noise, $n(f)$, has exactly the same denominator term as the intrinsic modulation response (Equation 7.4):[17,18,19]

$$n(f) = \frac{f_0^2}{a} \times \frac{1 + b^2 f^2}{f_0^2 - f^2 + jff_d} \tag{7.17}$$

where a and b are terms dependent on the Langevin noise sources. Once again, the denominator term generates the damped resonance at the relaxation oscillation frequency. The intensity noise spectrum has the same general shape as the intrinsic intensity modulation response, except for the frequency-squared term in the numerator that indicates an increased noise con-

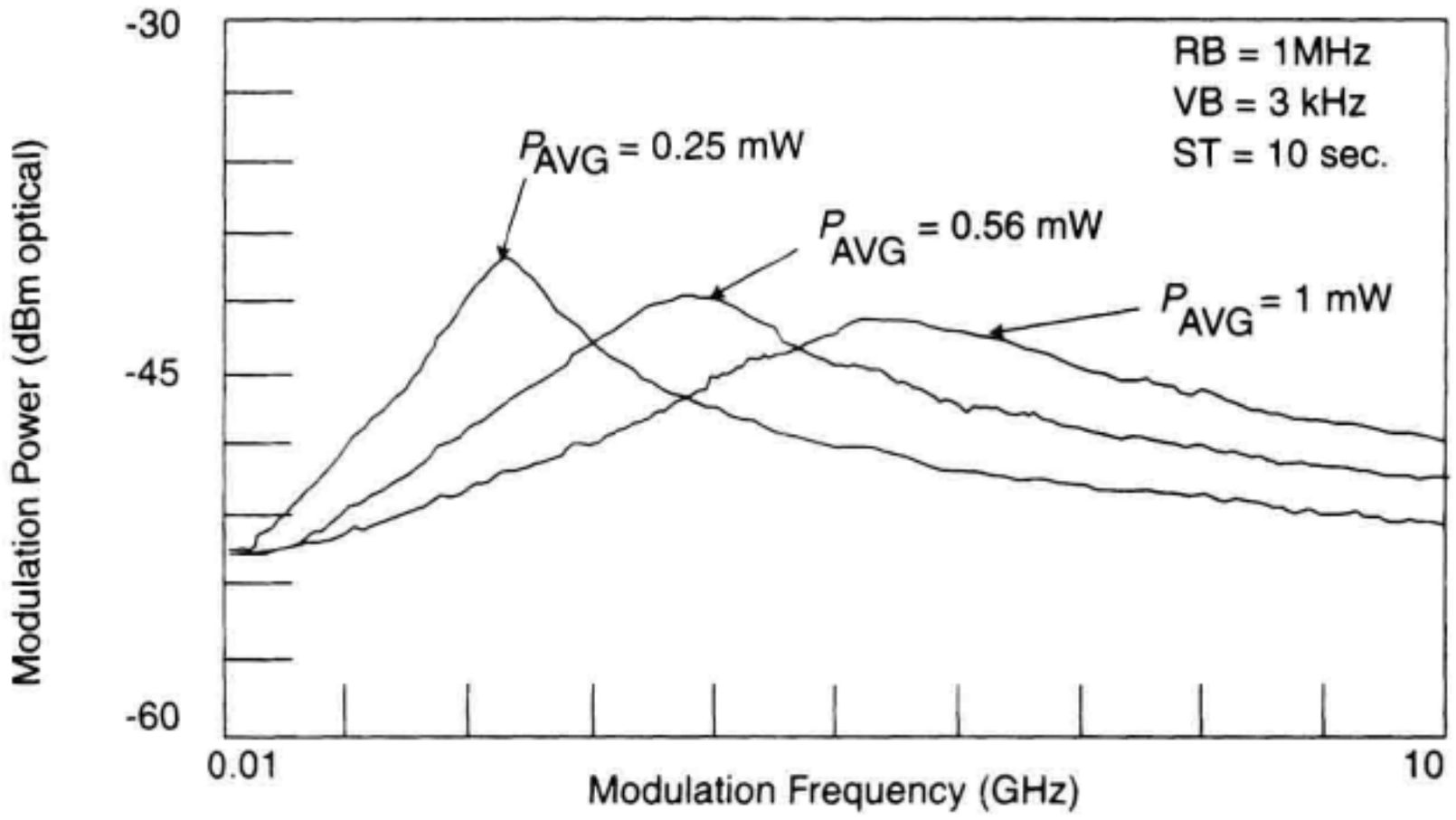

Figure 7.22 Measurement of a DFB laser intensity noise at several bias settings.

tribution at high frequencies. Theoretically, the SNR is relatively constant out to the relaxation oscillation frequency and decreases monotonically at higher frequencies. Typically, as the bias current increases, the resonance peaks of both the intensity-modulation response and intensity-noise spectrum track one another until the modulation response becomes limited by parasitics. Since the relaxation oscillation peak in the intensity-noise response is not affected by device capacitance, it is often used as an indicator of the intrinsic laser modulation response.

Example: Effect of Reflections on DFB Semiconductor Laser Intensity Noise

The laser intensity noise spectrum can be affected by both the magnitude and polarization of optical power that is reflected back to the laser. Reflections from connectors or splices can have a dramatic effect on laser intensity noise.[20]

Measurement Procedure

The measurement settings for the lightwave signal analyzer are basically the same as before. Two intensity-noise traces of the DFB semiconductor laser are shown in Figure 7.23. One is with the reflections minimized indicating the nominal intensity noise spectrum. The other trace is with reflections present showing their effect in enhancing the noise level. Markers can be used to determine the frequency separation between the noise peaks. This frequency separation, Δf, can be used to determine the distance, D, between the reflections by using the following relationship:

$$D = \frac{c}{2n\Delta f} \tag{7.18}$$

where c is the speed of light in a vacuum, 3×10^8 m/s, and n is the index of refraction in glass (approximately 1.5).

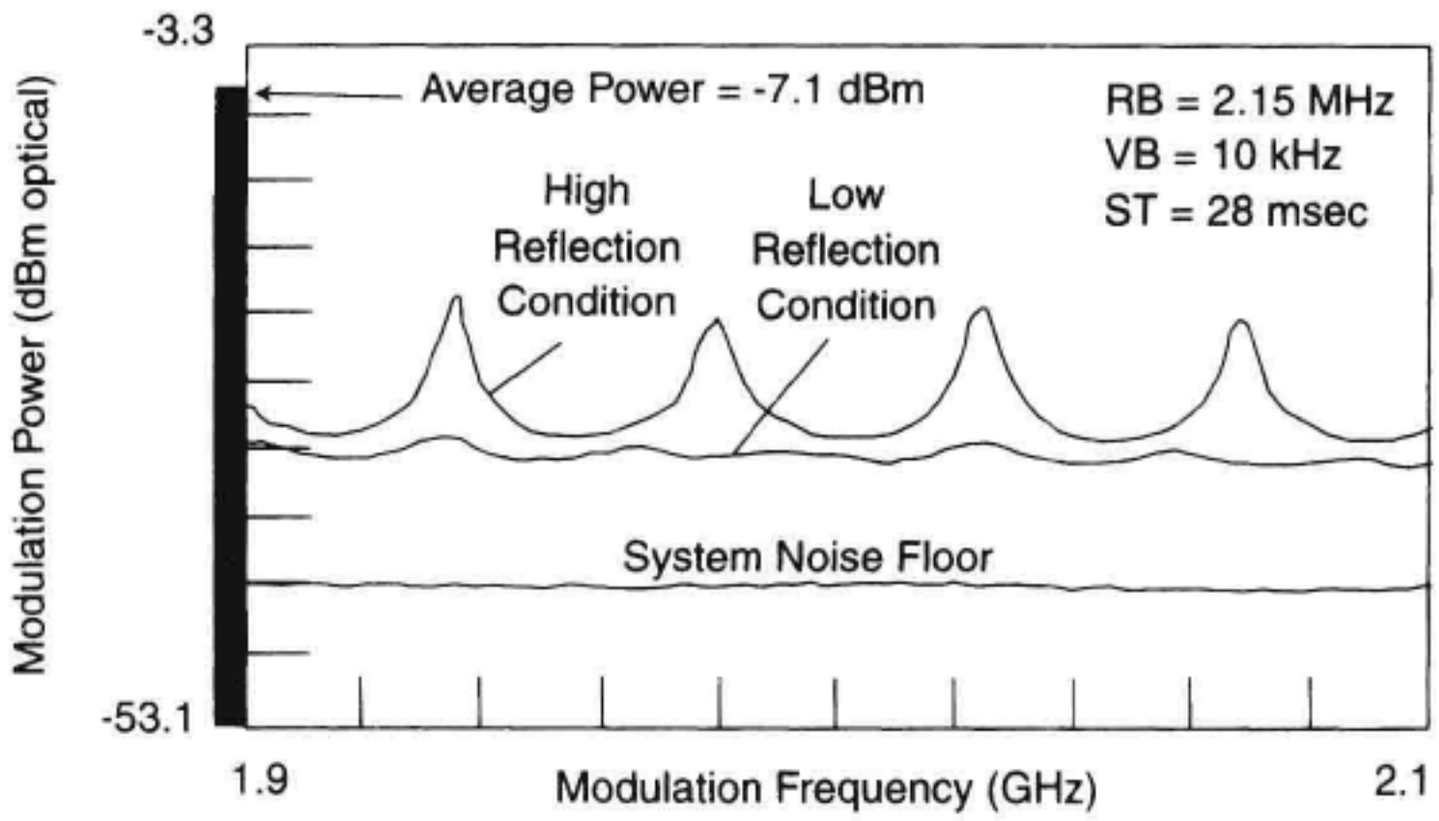

Figure 7.23 Effect of reflections on the intensity noise of a DFB laser.

Measurement Interpretation

An optical resonant cavity formed between the reflection and the back-facet mirror of the laser can enhance the noise of the laser diode. Interference between the forward transmitted wave and the reflected wave in the laser cavity offsets the gain of the laser, producing a sinusoidal variation of the noise spectrum that is dependent on the resonance path length. The reflected power upsets the dynamic equilibrium of the lasing process and typically increases the amplitude of the intensity noise particularly around the relaxation oscillation frequency. It can also induce a ripple on the noise spectrum with a frequency that is inversely proportional to the round-trip time from the laser to the reflection. To avoid this noise increase caused by reflected power, isolators are often employed. It has been reported that from 30 to 60 dB or more, isolation may be required to eliminate this effect. In addition, an increase in the intensity-noise spectrum can be observed at low frequencies in system measurements using DFB lasers. This effect has been attributed to interferometric conversion of the laser phase noise or linewidth-to-intensity noise because of reflections at connectors and splices. See Appendix A for a more detailed discussion on the phase-noise to intensity-noise conversion process.

7.4.2 Relative Intensity Noise

Relative intensity noise (RIN) is an important quantity related to SNR. RIN is defined as:[6,18,21]

$$\text{RIN} = \frac{(\Delta P)^2}{(P_{\text{AVG}})^2} \tag{7.19}$$

where $(\Delta P)^2$ is the mean square intensity-fluctuation spectral-density of an optical signal and P_{AVG} is the average optical power. A very low value of RIN is desirable. The quantity can be used to determine the maximum realizable SNR in a lightwave transmission system where the dominant noise source is laser intensity noise. The following relationship shows the theoretical relationship between the signal-to-noise level and the RIN:

$$\frac{S}{N} = \frac{m^2}{2B \times \text{RIN}} \tag{7.20}$$

where m is the optical modulation index and B is the noise bandwidth. A rate equation analysis shows that over a large operating range, the RIN of semiconductor lasers decreases (improves) with increasing laser power.[19]

Traditionally, RIN has been measured by using a photodetector to detect the laser output power. The electrical output of the photodetector is often amplified, and then displayed, on an electrical spectrum analyzer. The measurement on the electrical spectrum analyzer is intended to correspond to an amplified electrical equivalent of $(\Delta P)^2$ in the equation defining RIN. Simultaneously, the dc photocurrent must be monitored. This dc photocurrent, when squared and multiplied by 50 ohms and the amplifier gain, results in the corresponding electrical-equivalent term for $(P_{\text{AVG}})^2$. Here 50 ohm impedances are assumed for the amplifier and the spectrum analyzer input.

Care must be used in this measurement technique to obtain accurate results. The photodetector, amplifier, and spectrum analyzer frequency responses, as well as the mismatch losses between them, must all be well characterized. In addition, the amplifier gain must be large enough, and its noise figure low enough in relation to the spectrum analyzer noise figure to provide adequate sensitivity to make RIN measurements.

Unfortunately, the spectrum analyzer measures other noise components in addition to the laser RIN. These include the shot noise power caused by the quantum nature of the photodetection process and the receiver's total measured thermal noise power. By dividing by the calibrated amplifier gain, the noise power contributions can be conveniently referenced to the photodetector output and expressed as:

$$P_n(\text{measured}) = P_n(\text{laser}) + P_n(\text{shot}) + P_n(\text{thermal}) \tag{7.21}$$

P_n(laser) is the detected laser intensity noise. P_n(shot) is the detected shot noise power, which can be expressed as:

$$P_n(\text{shot}) = (i_n)^2 \times 50\Omega \tag{7.22}$$

where i_n is the shot noise current, and $(i_n)^2 = 2qI_{\text{dc}}$ for a 1 Hz bandwidth. q is the electronic charge equal to 1.60×10^{-19} coulomb. P_n(thermal) is the receiver noise, which can be expressed as:

$$P_n(\text{thermal}) = \frac{(F_A G_A + F_{SA} - 1)kT_0 B}{G_A} \tag{7.23}$$

where F_A is the amplifier noise figure, F_{SA} is the spectrum analyzer noise figure, and G_A is the amplifier gain, all expressed in linear power units. k is Boltzman's constant and B is the noise bandwidth. For a 1 Hz bandwidth, $kT_0 = 4.00 \times 10^{-21}$ at the standard reference temperature of 290 K. By dividing by the detected average power, $P_{\text{AVG}}(\text{electrical}) = (I_{DC})^2 \times 50\Omega$, one can determine the RIN:

$$\text{RIN(measured)} = \text{RIN} + \frac{2q}{I_{dc}} + \frac{P_n(\text{thermal})}{P_{AVG}(\text{electrical})} \tag{7.24}$$

For shot noise limited detection, the measurable RIN can be shown to be equal to $2q/I_{dc}$, which indicates the minimum measurable RIN decreases linearly as the detected photocurrent increases. RIN is often expressed in dB. Thus, RIN decreases 10 dB per decade increase in detected photocurrent. If the responsivity of the photodetector is 1mA/mW, then a minimum RIN of −155 dB/Hz could be measured at 1 mW of average optical signal power, but only −145 dB/Hz could be measured at 100 μW of average optical power. This relationship is shown in Figure 7.24. Also shown for comparison are the thermal noise contributions of the electrical spectrum analyzer, with and without a low-noise preamplifier, relative to the room temperature 1 Hz kT_oB noise floor of approximately −174 dBm. Both the receiver thermal noise and shot-noise contributions can limit the accuracy of RIN measurements.

RIN can also be measured on a lightwave signal analyzer, which has the capability to measure both the average optical signal power as well as the detected intensity noise fluctuations. In addition, the lightwave signal analyzer has the ability to measure both the detected shot noise and thermal noise levels, and correct for these contributions to make RIN measurements below the shot-noise limit.[22] A measurement of a low-noise DFB semiconductor laser is shown in Figure 7.25. RIN (system) is the value that the lightwave signal analyzer directly measures with all noise terms included. RIN (laser) refers to the desired laser intensity noise value with the thermal and shot-noise contributions removed. The typical RIN measurement range of the lightwave signal analyzer as a function of input optical power is shown in Figure 7.26. Subtraction of the thermal noise and shot noise from RIN (system) provides approximately an additional 16 dB measurement range for the determination of RIN (laser).

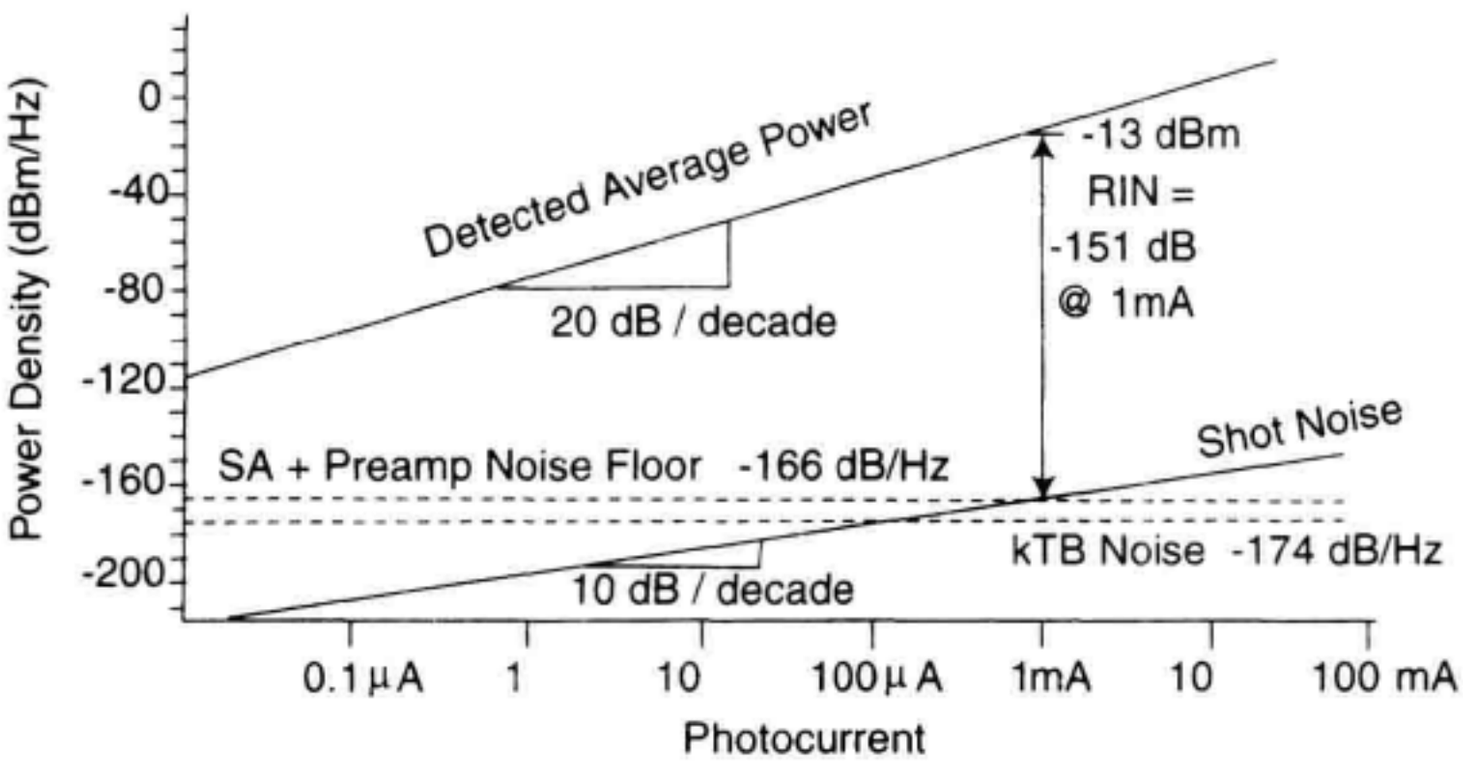

Figure 7.24 Noise considerations when making an RIN measurement on an electrical spectrum analyzer.

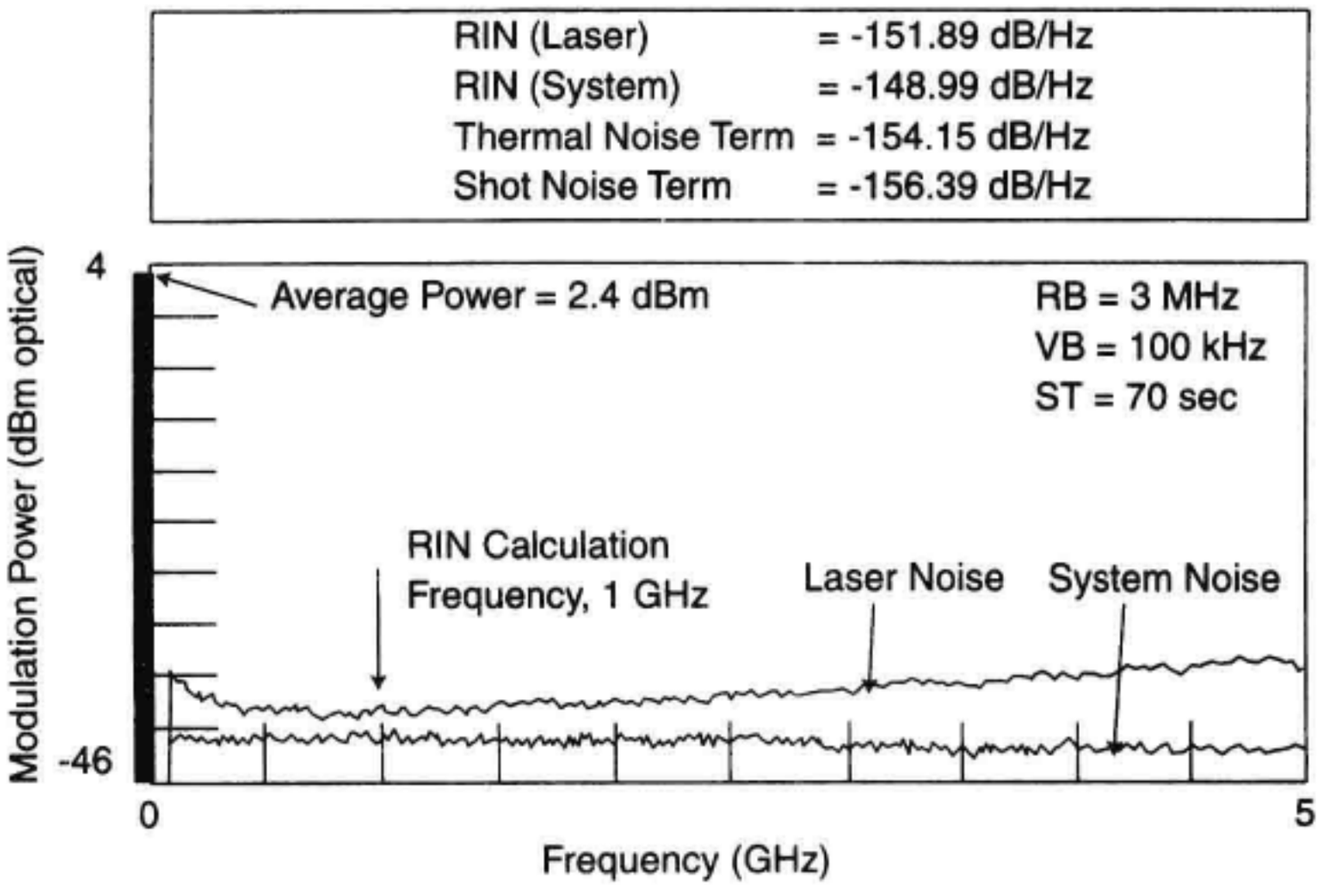

Figure 7.25 RIN measurement on a lightwave signal analyzer.

7.5 MODULATION DOMAIN CALIBRATION TECHNIQUES

Optical frequency response calibration is required in order to make accurate measurements of the modulation transfer function of optical devices as well as intensity modulation and intensity noise measurements. There are several techniques that employ a variety of optical sources that can be used to calibrate the frequency response of measurement instrumentation:

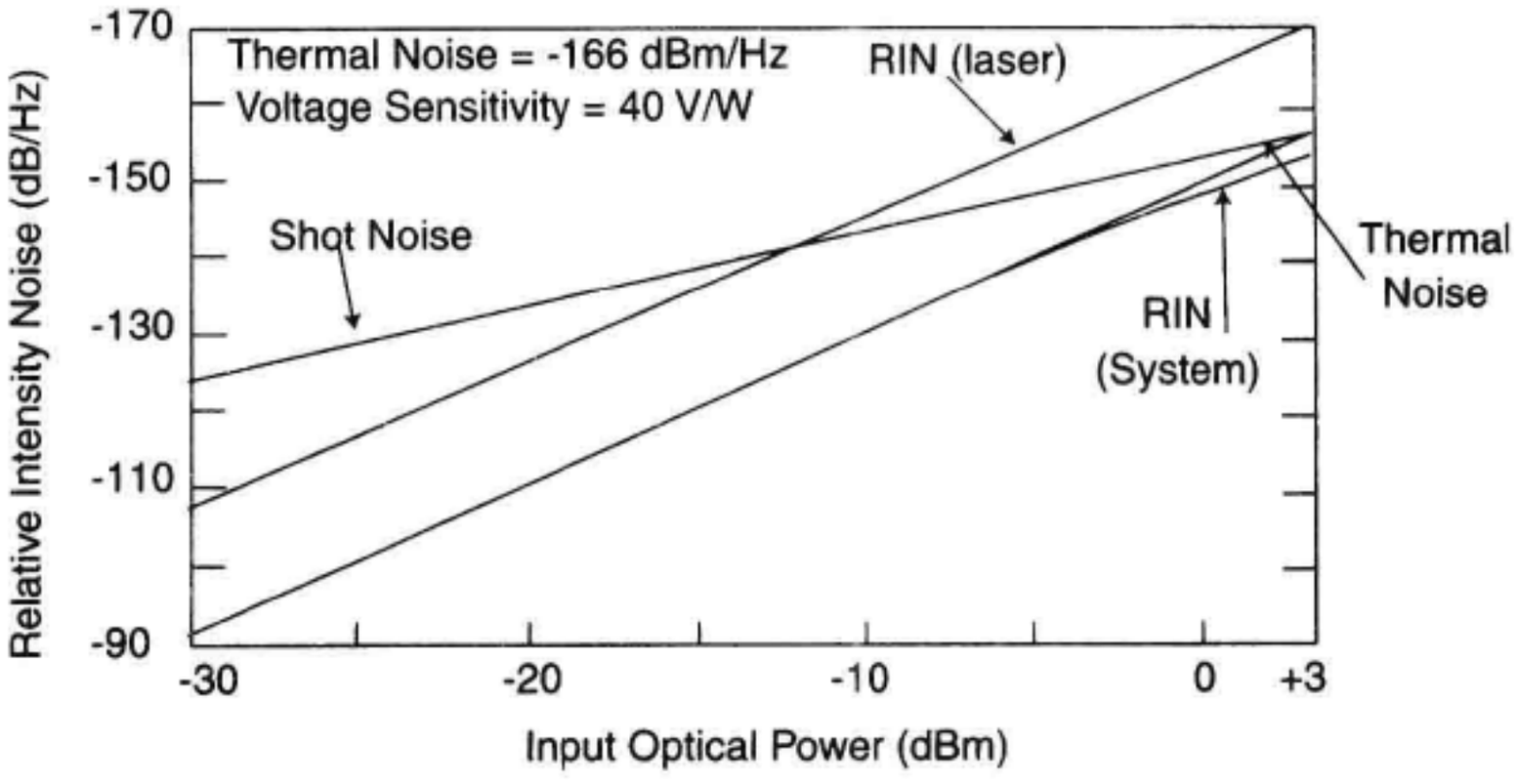

Figure 7.26 RIN measurement range on a lightwave signal analyzer.

- Use an optical impulse source to determine the impulse response of an optical receiver. This is the only method discussed that gives both magnitude and phase information directly.
- Optically heterodyne two stable single-frequency lasers whose beat frequency can be adjusted and used to calibrate the frequency response of an optical receiver.
- Use an optical modulator whose frequency response is calibrated by a two-tone measurement technique.
- Use the amplified spontaneous emission noise of an optical amplifier as a broadbandwidth white noise generator.

Each of these "primary" calibration techniques can be used to calibrate the frequency response of a photoreceiver as a "secondary" standard. The photoreceiver can then use used to transfer the calibration from the primary standard to the measurement system.[23] These calibration techniques: optical impulse response, optical heterodyning, modulator two-tone, and optical intensity noise will now be reviewed in greater detail.

7.5.1 Optical Impulse Response

The frequency response of a measurement system can be computed from the Fourier transform of the time-domain impulse response. This approach has the advantage that it provides both amplitude and phase information about the measurement system which is important for lightwave component analysis and other vector-network-analysis-based measurements. An optical impulse generator can be approximated by a sufficiently narrow laser pulse with a low repetition rate. When viewed in the frequency domain, this type of optical signal generates a frequency domain spectrum consisting of a comb of discrete signals, at harmonics of the pulse repetition frequency, whose amplitude follows the response:

$$P(w) = \frac{\sin\left(\frac{nw_0\tau}{2}\right)}{\frac{nw_0\tau}{2}} \tag{7.25}$$

where w_0 is the radian pulse repetition frequency, τ is the pulse width, and n is the harmonic number. If the pulse width is sufficiently narrow and the period is much longer than the pulse width, then the amplitude of the discrete signals is considered flat with frequency over the desired measurement bandwidth.

Picosecond (ps) pulses can be generated by several techniques. One technique is to use a system consisting of an actively mode-locked Nd:YAG laser and a fiber-grating pulse compressor as shown in Figure 7.27. This particular laser can produce 80 ps pulses at an 80 MHz rate, with an average power of 20 W, at a wavelength of 1.06 μm. The pulse compressor uses self-phase modulation for spectral broadening and positive group velocity dispersion in singlemode fiber to separate out the pulse in time as it propagates through the fiber.[24] When this chirped and spectrally broadened pulse is passed through the diffraction grating pair, a time delay proportional to wavelength is introduced, which

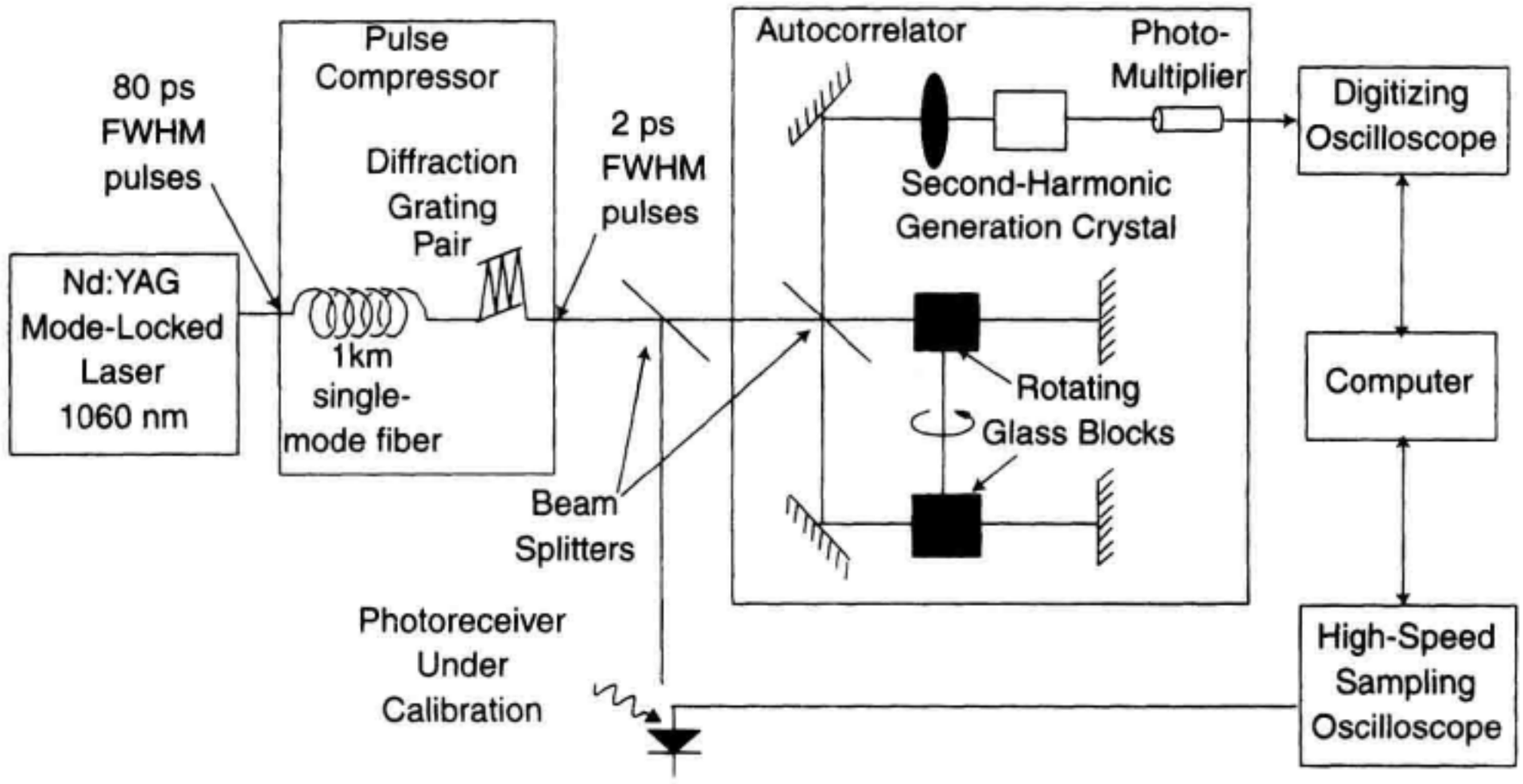

Figure 7.27 Optical impulse response measurement system.

compresses the pulse to about 2 ps full-width at half-maximum (FWHM). Other solid-state lasers such as Ti:Sapphire lasers are available to cover wavelengths shorter than 1 μm. Also shown in Figure 7.27 is an autocorrelator which is often used to characterize the width of very short pulses.

Another technique to generate short optical pulses is to use a colliding-pulse passively mode-locked erbium-doped fiber ring laser as shown in Figure 7.28. This source is convenient because it can be easily packaged and does not require the use of a large optical table with operator adjustments.[25] The key to the operation of the laser is the saturable absorber. The leading edge of the incoming pulse is absorbed. After absorbing a set number of photons, the absorber becomes transparent. This causes a narrowing of the pulse on each pass through the absorber. The absorption is quickly reset to a high absorption value

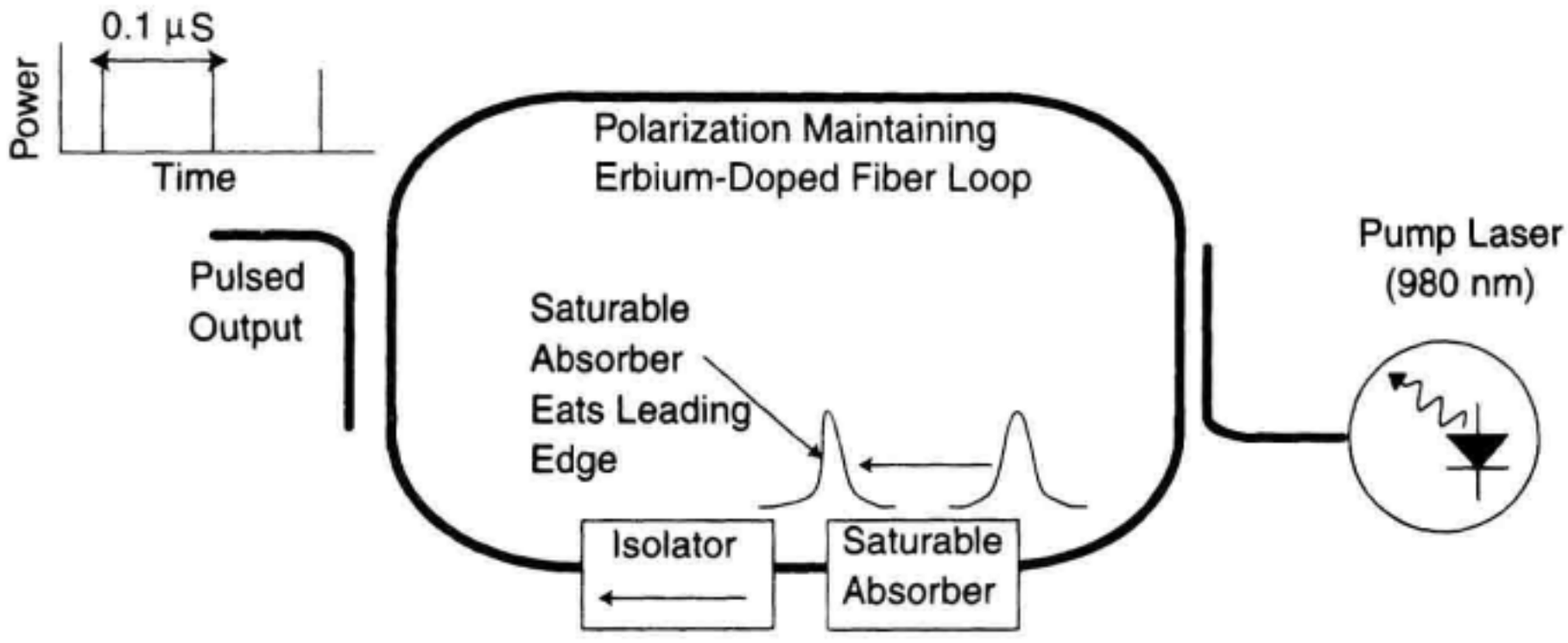

Figure 7.28 Erbium-doped fiber ring laser.

after the passage of the optical pulse because the saturable absorber has been proton-bombarded to reduce the carrier-recombination lifetime in the material. After many round-trips in the laser, the pulse width narrows to a width that is consistent with the available optical bandwidth in the erbium optical amplifier. Pulse widths of less than 1 ps are easily achievable. This ring laser is said to be passively mode locked. The laser starts up into the repetitively pulsed mode of operation without any external stimulus. The use of polarization-preserving erbium-doped fiber has made this design very easy to use and can be designed into a very compact package.

Similar results can be obtained using a semiconductor optical amplifier with a semiconductor saturable absorber.[26] This allows the generation of pulses at a wide range of wavelengths. Semiconductor lasers can be actively mode-locked to produce very low timing jitter. An alternate pulsing technique for semiconductor lasers is gain-switching.[26] In this method, the repetition rate of the optical pulse does not need to be perfectly repetitive as it does for mode-locked laser techniques.

It is difficult to measure the shape of short laser pulses directly. A 2 ps pulse would require a photodetector and oscilloscope to have a combined bandwidth of 250 GHz. Therefore, the autocorrelation function is often measured, from which the power spectral density and width of the pulse can be inferred. The autocorrelator shown in Figure 7.29 operates in the following manner. First, the input beam is split into two paths, one of which is varied in length via a moveable corner cube to introduce a swept differential delay. The two beams are then combined in a crystal with nonlinear characteristics, which generates a second harmonic with an amplitude proportional to the product of the intensities of the two beams overlapped in the crystal. The second harmonic light is detected by the photomultiplier tube. The output signal can then be displayed on an oscilloscope to trace out the optical pulse's autocorrelation function as the corner cube is swept. The Fourier transform of this time record is the power spectral density of the optical pulse.[27] Once the optical impulse has been characterized, it can be used to determine the frequency response of the measurement instrumentation. Depending on the bandwidth of the instrumentation, it may be necessary to deconvolve the contribution of the optical impulse.

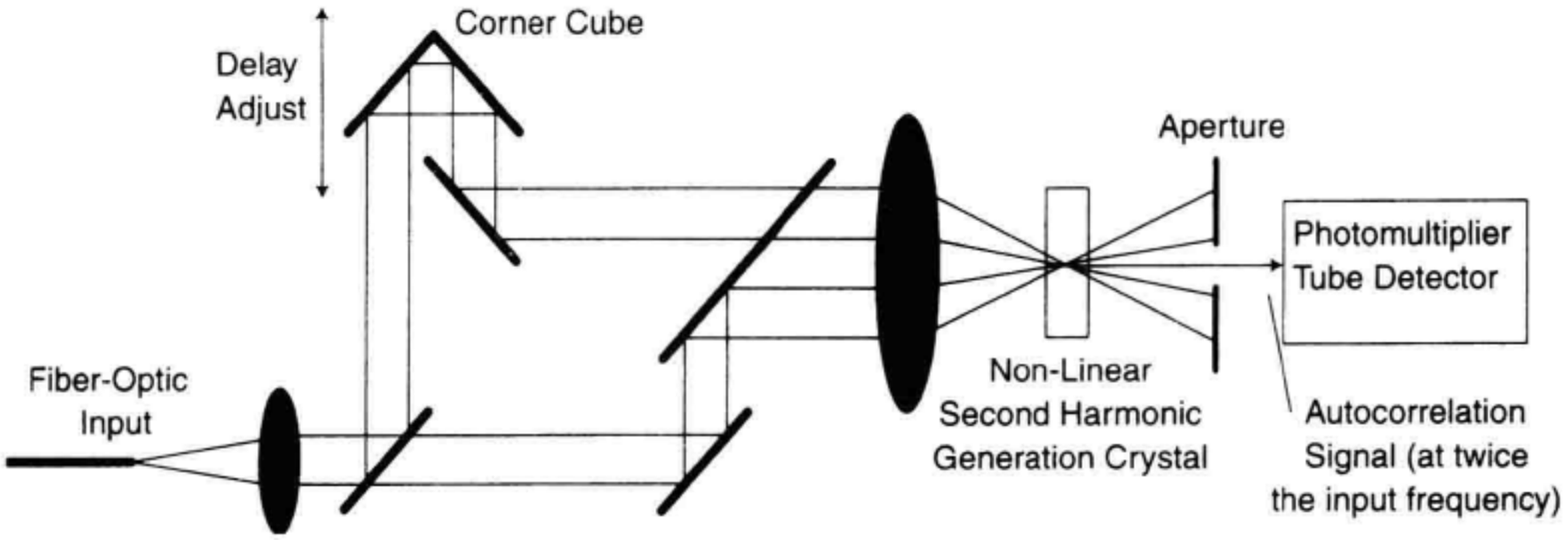

Figure 7.29 Autocorrelator.

The autocorrelation technique gives information on the magnitude of the modulation spectrum from the optical impulse source. It does not directly give information about the optical phase of the source. An alternate measurement technique is based on a nose-to-nose high-frequency oscilloscope measurement.[28] In this method, the magnitude and phase response of a high frequency sampling oscilloscope is made. After the oscilloscope is calibrated, the magnitude and phase of an optical receiver under test can be made with the impulse response method.

7.5.2 Optical Heterodyning

An optical heterodyne source can be built using diode-pumped Nd:YAG ring cavity lasers whose nominal wavelength of 1.32 μm can be varied by changing the laser crystal temperature. Figure 7.30 shows an example of such a calibration source. Three lasers are shown. One acts as a master laser oscillator and the other two as slave laser oscillators. The frequency of each of the slave lasers is temperature-adjusted to a known frequency away from the master laser with a synthesizer/phase-locked loop. The short term optical linewidth of either the master or slave oscillators is less than 10 kHz. By adjusting the frequencies of the slave lasers, a beat frequency between dc and approximately 50 GHz can be produced.[29] This beat frequency can be varied by adjusting the temperature of one slave laser relative to the other. The master-slave configuration is used because it allows small difference frequencies, or a beat frequency near dc, but avoids the problem of the slave lasers injection-locking one another. The use of open-beam combiners in this optical heterodyne source is preferable to fiber-coupled versions.

Let the difference between the laser slave frequencies be f, and the individual output powers be P_1 and P_2. If the laser outputs are linearly polarized and aligned, the signal at the combined output is:

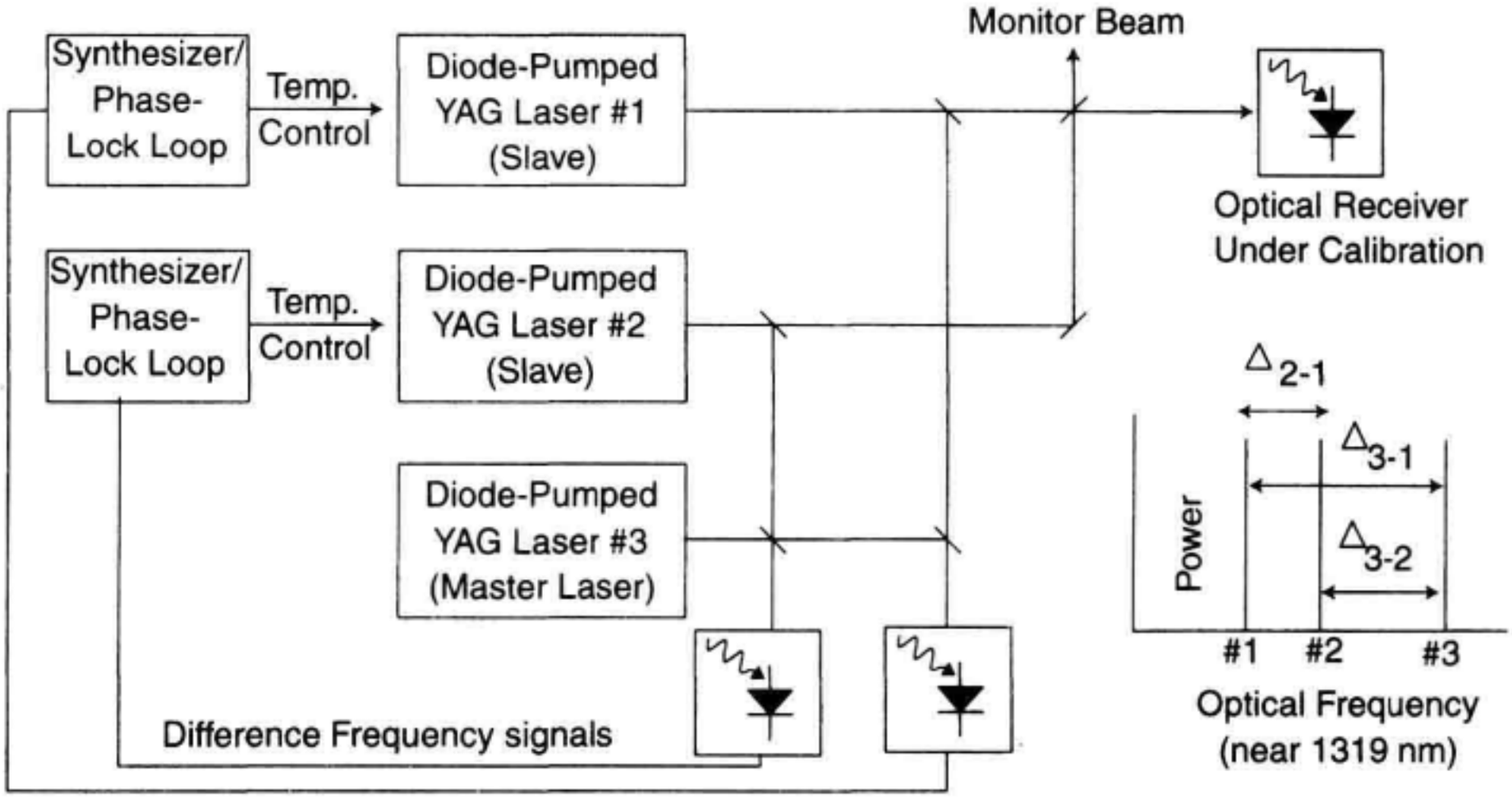

Figure 7.30 Dual YAG heterodyne frequency response measurement system.

$$P_O = P_1 + P_2 + 2\sqrt{P_1 P_2}\cos(2\pi ft) \tag{7.26}$$

If $P_1 = P_2$, the resulting output signal is 100% modulated at the difference frequency. In a test system one of the coupler/splitter's outputs is connected to the DUT or measurement system to be calibrated. The other output is used for monitoring the laser power. Optical receiver calibrations accurate to within 0.06 dB have been performed using this configuration.[23,27] Additional information on heterodyne theory is found in Chapter 5.

7.5.3 Two-Tone Technique

A Mach-Zehnder interferometer, whose use as an optical intensity modulator has already been described in Section 7.2.2, can be used as a calibrated source. To be used as a calibrated source, the modulator is biased for minimum signal transmission. When two modulation signals are applied with radian frequencies w_1 and w_2, having peak voltages V_{p1} and V_{p2}, one of the signals present at the modulator output will be a difference frequency component:

$$I(\Delta f) = I_0 J_1\left(\pi \frac{E(w_1)V_{p1}}{V_\pi}\right) J_1\left(\pi \frac{E(w_2)V_{p2}}{V_\pi}\right) \tag{7.27}$$

This expression can be used to measure the modulator's frequency-dependent modulation efficiency. If the two modulation signals are very close in frequency, then $E(w_1)$ is essentially the same as $E(w_2)$. By measuring I_0, V_π, the applied voltages V_{p1} and V_{p2}, and the optical power at the difference frequency, $I(\Delta f)$, the expression can be solved numerically for $E(w)$. By keeping the difference frequency small and constant, $E(w)$ can be determined by stepping w_1 and w_2 over the range of modulation frequencies. Once $E(w)$ has been determined, the modulator can be used as a calibrated optical source to measure other optical components or measurement systems.[27]

7.5.4 Optical Intensity Noise

Intensity-noise techniques take advantage of the beating between various optical spectral components of a broad-bandwidth spontaneous emission source. Any two spectral lines will beat, or mix, to create an intensity fluctuation with a frequency equal to the frequency difference between the two lines. This concept is shown graphically in Figure 7.31. Since the optical bandwidth of spontaneous emission sources can easily exceed thousands of gigahertz, the intensity beat noise will have a similar frequency content. These fluctuations in optical intensity are referred to as spontaneous-spontaneous beat noise. This technique permits very rapid optical calibration since the noise exists at all frequencies simultaneously. Additionally, intensity noise sources tend to be both unpolarized and have short-coherence lengths, which makes the measurements immune to polarization drifts and time-varying interference effects from multiple optical reflections, thereby allowing stable, repeatable measurements.

There are many sources of broad-bandwidth spontaneous emission. Hot surfaces (such as tungsten light bulbs) can emit optical radiation ranging from the visible to the far

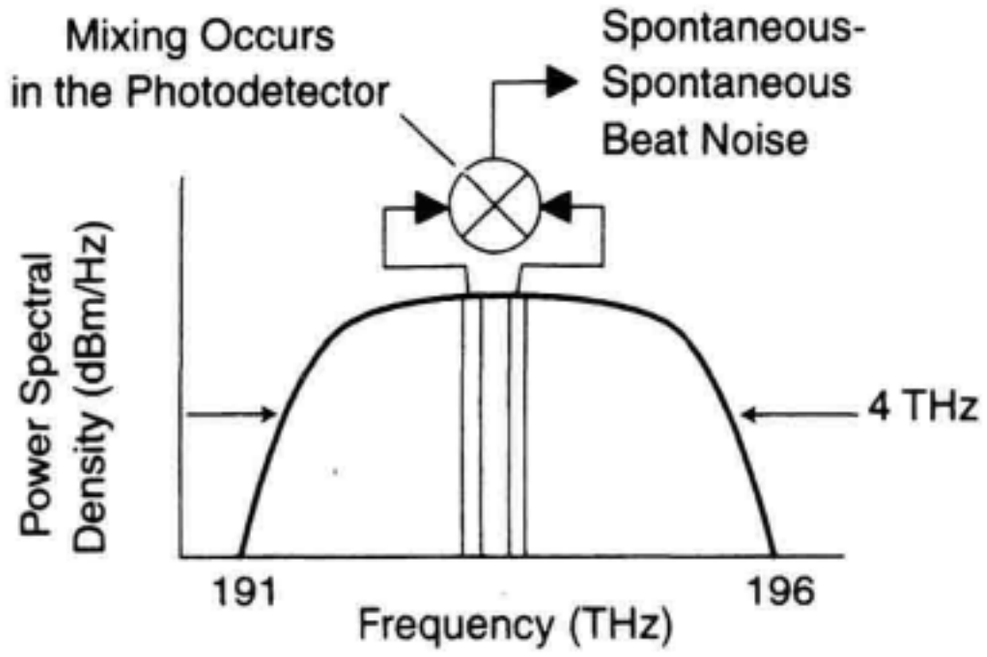

Figure 7.31 Spontaneous-spontaneous beat noise arising from an optical noise source.

infrared. Semiconductor sources such as edge emitting light-emitting diodes (EELEDs) provide increased power densities and a wavelength range of about 100 nm. Still higher power densities can be obtained from solid-state sources such as fiber optic amplifiers.

The ability to couple these sources of broad-bandwidth light efficiently into single-mode fiber is also important. Coupled-power densities can range from about 500 pW/nm for a light bulb to greater than 1 mW/nm for amplified spontaneous emission (ASE) from a fiber optic amplifier. The high-power densities from fiber optic amplifiers are particularly well-suited for intensity noise generation.[30] One must be careful in this method not to use power levels high enough to cause nonlinear responses in the optical receiver.

7.5.5 Comparison of Calibration Techniques

Table 7.1 shows a comparison of the calibration techniques for modulation domain measurements. Each of these calibration techniques have advantages and disadvantages. The optical impulse response technique allows direct measurement of the impulse response of photoreceiver-oscilloscope system. The measurement can be fast. However, depending on

Table 7.1 Comparison of the Calibration Techniques for Modulation Domain Measurements

Calibration Method	Wavelength Range	Phase Determined?	Modulation Frequencies	Comments
Optical impulse	1060 nm with Nd:YAG 1550 nm with EDFA Many other types	Yes	MHz- >50 GHz	Need autocorrelator, may require deconvolution of optical pulse
Optical heterodyne	1320 nm with YAG, others with DFBs	No	kHz- 50 GHz	Requires an optical bench setup
Two-tone technique with modulator	1300 or 1550 nm	No	kHz- 30 GHz	Relies on accurate electrical power measurements
ASE detection	1550 nm with EDFA	No	kHz- >50 GHz	Detector saturation issues

the pulse width of the optical pulse, the source effects may need to be deconvolved from the measurement. The heterodyne system is easy to extend to very high frequencies and very useful for performing calibration directly in the frequency domain. It is the technique that is most easily referenced to U.S. NIST standards. Measurement time can be long because of the thermal tuning of the laser wavelength. The optical modulator technique has very fine frequency resolution provided by synthesized microwave sources, but requires careful calibration in order to be used to calibrate the frequency response of devices or measurement systems. Any errors or uncertainties in the modulator calibration are transferred to the system being calibrated. The intensity noise technique also offers high resolution as well as fast measurement time. However, the noise power generated may not be always sufficiently high to calibrate low sensitivity systems.

REFERENCES

1. Henry, C.H. 1986. Phase noise in semiconductor lasers. *J. Lightwave Tech.* LT-4: 298–311.
2. Wong, R.W., P.R. Herndday, M.G. Hart, and G.A. Conrad 1989. High-speed lightwave component analysis. *Hewlett-Packard J.* 40 (3): 35–51.
3. Wong, R.W., P.R. Herndday, and D.R. Harkins. 1991. High-speed lightwave component analysis to 20 GHz. *Hewlett-Packard J.* 43 (1): 6–12.
4. Ikegami, T. and Y. Suematsu. 1968. Direct modulation of semiconductor junction laser. *Elect. Comm. Japan* 51-B: 51–58.
5. Lau, K.Y., C. Harder, and A. Yariv. 1981. Ultimate frequency response of GaAs injection laser. *Optics Comm.* 36: 472–474.
6. Lau, K.Y. and A. Yariv. 1985. Ultra high-speed semiconductor lasers. *IEEE J. Quantun Elect.* QE-21: 121–138.
7. Bowers, J.E. 1986. High-speed semiconductor laser design and performance. *Solid State Elect.* 30: 1–11.
8. Jungerman, R.L. et al. 1990. High-speed optical modulator for application in instrumentation. *J. Lightwave Tech.* 8: 1363–1370.
9. Bowers, J.E. et al. 1986. Millimetre-waveguide-mounted InGaAs photodetectors. *Elect. Lett.* 22: 633.
10. Miller, C.M. 1990. High-speed lightwave signal analysis. *Hewlett-Packard J.* 41 (1): 80–91.
11. Lau, K.Y. and A. Yariv. 1984. Intermodulation distortion in a directly modulated semiconductor injection laser. *Appl. Phys. Lett.* 45: 1034–1036.
12. Darcie, T.E., R.S. Tucker, and G.J. Sullivan. 1985. Intermodulation and harmonic distortion in InGaAsP lasers. *Electron. Lett.* 21: 665–666.
13. Tucker, R.S. and D.J. Pope. 1983. Circuit modeling of the effect of diffusion on damping in a narrow-stripe semiconductor. *IEEE J. Quantum Elect.* QE-19: 1179.
14. Takemoto, A. et al. 1990. Distributed feedback laser diode and module for CATV systems. *IEEE J. Selected Areas in Commun.* 8: 1365.
15. Dentan, M. and B. De Cremoux. 1990. Numerical simulation of the nonlinear response of a p-i-n photodiode under high illumination. *J. Lightwave Tech.* 8: 1137–1144.
16. Hayes, R.R. and D.L. Persechini. 1993. Nonlinearity of p-i-n photodetectors. *IEEE Photonics Tech. Lett.* 5: 70–72.

17. Bowers, J.E. and M.A. Pollack. 1988. Semiconductor lasers for telecommunications. In *Optical Fiber Telecommunication II,* ch. 13, eds. S.E. Miller and I.P. Kaminow, San Diego, CA: Academic Press.
18. Huag, M. 1969. Quantum mechanical rate equations for semiconductor lasers. *Phys. Rev.*184: 338–348.
19. Agrawal, G.P. and N.K. Dutta. 1986. *Long-wavelength semiconductor lasers,* ch. 6, New York: Van Nostrand Reinhold.
20. Gimlett, J.L. and N.K. Cheung. 1989. Effects of phase-to-intensity noise conversion by multiple reflections on gigabit-per-second DFB laser transmission systems. *J. Lightwave Tech.* 7: 888–895.
21. Yamamoto, Y. 1983. AM and FM quantum noise in semiconductor lasers—Part I: Theoretical analysis. *IEEE J. Quantum Elect.* QE-19: 34–36.
22. Miller, C.M. and L.F. Stokes. 1990. Measurement of laser diode intensity noise below the shot noise limit. Boulder, CO: *NIST Symp. on Optical Fiber Measurements.*
23. Hale, P.D., C.M. Wang, R. Park, and W.Y. Lau. 1996. Photoreceiver frequency response transfer standard: Calibration using a swept heterodyne method. *J. Lightwave Tech.* 14 (11): 2457–2466.
24. Sieman, A.E. 1986. *Lasers.* Mill Valley, CA: University Science Books.
25. Lin, H., D.K. Donald, K.W. Chang, and S.A. Newton. 1995. *Colliding pulse mode-locked lasers using erbium-doped fiber and a semiconductor saturable absorber.* Baltimore, MD: 1995 Conference on Lasers and Electrooptics, Optical Society of America, paper JTuE1.
26. Derickson, D.J., R.J. Helkey, A. Mar, J. Karin, J. Wasserbauer, and J. Bowers. 1992. Short pulse generation using multisegment mode-locked lasers. *IEEE J. Quant. Elect.* 28 (10): 2186–2201.
27. McQuate, D.J., K.W. Chang, C.J. Madden. 1993. Calibration of lightwave detectors to 50 GHz. *Hewlett-Packard J.* 44 (1): 87–92
28. Verspecht, J. and K. Rush. 1994. Individual characterization of broadband sampling oscilloscopes with a nose-to-nose calibration procedure. *IEEE Trans on Instrumentation and Measurement* 43 (2): 347–354.
29. Tan, T.S., R.L. Jungerman, and S.S. Elliot. 1988. Calibration of optical receivers and modulators using an optical heterodyne technique. *IEEE-MTT-S International Microwave Symp. Digest:* 1067–1070.
30. Baney, D.M. and W.V. Sorin. 1995. Broadband frequency characterization of optical receivers using intensity noise. *Hewlett-Packard J.* 46 (1): 6–12.